UNIVERSITAT DE BARCELONA

Liposome Study of Baricitinib as a Novel Formula for Topical Treatment of Autoimmune Diseases

Núria Garrós Aristizábal

UNIVERSITAT DE BARCELONA

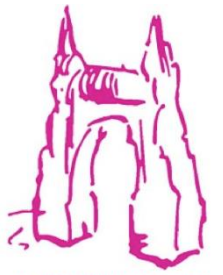

LIPOSOME STUDY OF BARICITINIB AS A NOVEL FORMULA FOR TOPICAL TREATMENT OF AUTOIMMUNE DISEASES

ESTUDI DE LIPOSOMES DE BARICITINIB COM A NOVA FÓRMULA PEL TRACTAMENT TÒPIC DE MALALTIES AUTOIMMUNES

DOCTORAL THESIS

Núria Garrós Aristizábal

Departament de Farmàcia i Tecnologia Farmacèutica, i Fisicoquímica

Universitat de Barcelona

2024

UNIVERSITAT DE BARCELONA

FACULTAT DE FARMÀCIA I CIÈNCIES DE L'ALIMENTACIÓ

PROGRAMA DE DOCTORAT DE BIOTECNOLOGIA

LIPOSOME STUDY OF BARICITINIB AS A NOVEL FORMULA FOR TOPICAL TREATMENT OF AUTOIMMUNE DISEASES

ESTUDI DE LIPOSOMES DE BARICITINIB COM A NOVA FÓRMULA PEL TRACTAMENT TÒPIC DE MALALTIES AUTOIMMUNES

Memòria presentada per

Núria Garrós Aristizábal

Per optar al títol de

Doctora en Biotecnologia

Tesis realitzada sota la direcció de

Dra. Helena Colom Codina **Mireia Mallandrich Miret**

Tutora acadèmica:

Dra. Ana Cristina Calpena Campmany

AGRAÏMENTS

Avui, en arribar al final d'aquest ardu i apassionant viatge acadèmic, em sento profundament agraïda i emocionada en dirigir-me a tots vosaltres. La culminació de la meva tesi marca no només el final de tres anys intensos de recerca, sinó també l'inici d'un nou capítol en la meva vida acadèmica i professional.

En primer lloc, vull expressar la meva gratitud als meus pares i germans, que han estat el meu suport imprescindible al llarg d'aquest camí. El seu suport econòmic i emocional ha estat fonamental per permetre dedicar temps i energia a aquest projecte i la força motriu que em va impulsar a perseverar en els moments desafiants. Sense el seu suport, aquest camí hauria estat molt més ardu, i estic eternament agraïda pel seu sacrifici i amor.

A més, vull reconèixer els meus col·legues i amics de la Unitat de Biofarmàcia, la col·laboració i la companyonia dels quals han enriquit la meva experiència doctoral. Junts hem enfrontat reptes, celebrat èxits i construït una comunitat d'aprenentatge remarcable.

A la meva tutora, Dra. Ana C. Calpena, i directores de tesi, Dra. Mireia Mallandrich i Dra. Helena Colom, no tinc prou paraules per expressar el meu agraïment per la seva guia experta i la seva paciència constant. El seu compromís amb el meu desenvolupament acadèmic ha estat fonamental per assolir aquesta fita. A més, he d'expressar el meu profund agraïment a la Dra. Majella Lane i al Dr. David Limón de la School of Pharmacy de la UCL a Londres. L'oportunitat de fer una estada a la seva prestigiosa institució va ser un privilegi que va enriquir enormement la meva experiència acadèmica i professional.

Tanco aquest capítol amb el cor ple de gratitud i la certesa que cada contribució, sigui gran o petita, ha deixat una empremta inesborrable en el meu viatge acadèmic. Estic agraïda per la xarxa de suport que m'envolta i haver tingut l'oportunitat d'aprendre i créixer en aquest entorn tan enriquidor. Aquest èxit no és només meu, sinó de tots els que han contribuït a la meva formació i desenvolupament al llarg d'aquests anys, i estic emocionada pel que el futur ens ofereix.

Amb gratitud i afecte,

Núria Garrós Aristizábal

ABSTRACT

Liposome Study of Baricitinib as a Novel Formula for Topical Treatment of Autoimmune Diseases

Autoimmune diseases are a diverse group of conditions characterized by an unknown origin, where the immune system becomes dysregulated and attacks the individual's organs. More than 110 of these diseases are recognized, and they affect over 10% of the population, primarily women at working age and during their fertile years.

These diseases can target various organs, with some exclusively affecting the skin and mucous membranes, or involve multiple organs. Autoimmune diseases vary in their chronic nature and severity, requiring tailored treatments. Generally, treatment often involves the use of immunosuppressive or immunomodulatory drugs to reduce or mitigate their effects.

Given their prevalence and impact on patients' lives, ongoing research to enhance treatment methods is essential. Improving drug administration, pharmacokinetics, adherence, and bioavailability can significantly benefit those affected. This is the focus of the thesis project, which explores biopharmaceutical and pharmacokinetic studies of an immunomodulatory drug to advance the treatment of autoimmune diseases.

In this research, liposomes were selected as the primary formulation of interest. Liposomes are small spherical vesicles made of natural or synthetic biodegradable phospholipids. They have the unique property of spontaneously forming in aqueous environments, allowing for the encapsulation of both hydrophobic and hydrophilic drugs. Liposomes possess several advantages, such as biocompatibility, biodegradability, and non-toxicity. Their versatile formulation capabilities enable the creation of different liposome sizes suitable for various applications, from ophthalmic drops to direct skin application. This versatility is particularly valuable when dealing with drugs like baricitinib (BNB), known for their poor solubility.

BNB, the study drug in this thesis, is an oral immunosuppressant that selectively inhibits specific molecules, including Janus kinase 1 and 2, leading to a reduction in inflammation, cell activation, and immune cell proliferation. BNB is currently employed to treat a range of conditions, including moderate to severe atopic dermatitis (AD), rheumatoid arthritis, and COVID-19 with recommended oral doses ranging from 2 to 4 mg per day. Notably, its effectiveness in improving skin symptoms is often noticeable from the first day of treatment.

Liposome Study of Baricitinib as a Novel Formula for Topical Treatment of Autoimmune Diseases

The thesis project involves the development of five different liposomes using the inverted evaporation method, also known as "inverted micelles." Among these liposomes, three are tailored for topical applications, specifically targeted for the treatment or co-adjuvant therapy of AD. The remaining two liposomes are designed for ophthalmological applications, intended to address the treatment or co-adjuvant therapy for Sjögren's Syndrome (SS). The liposomes inquired about are the following:

Atopic Dermatitis Application	**Sjögren's Syndrome Application**
POPC	Lα – PC
POPC:CHOL	POPE:POPG
POPC:CHOL:CER	

To achieve our objectives, we have started investigating the skin as a potential route for drug administration, both locally and systemically. Given the skin's protective barrier, drug diffusion is typically limited, necessitating the use of permeation enhancers, the impact of physical enhancers (solid titanium microneedles) and chemical enhancers on BNB permeation was explored. Two analytical HPLC methods were validated for BNB determination and quantification: UV-HPLC and Fluorescens-HPLC. And Confocal Raman Spectroscopy was used for the first time to obtain the BNB spectrum.

Once we had identified the potential for percutaneous BNB delivery as an alternative to oral administration, and we had validated two different methods for its detection and quantification, we began the studies with BNB-loaded liposomes.

The BNB-loaded liposomes for the treatment of SS, a chronic autoimmune disease affecting a 0,2-3% of the population, were studied. The liposomes were physiochemically characterized for ocular administration, a novel approach for this condition. In vitro drug release, ex vivo permeation through ocular tissues, and tolerance assessments were conducted, showing no irritant effects on the ocular membrane. Both liposomes displayed promising results.

The BNB-loaded liposomes for the treatment of AD, a prevalent autoimmune skin condition were physiochemically characterizatied and in vitro release studies, ex vivo permeation, and tolerance assessments were conducted All liposomes showed good physicochemical properties and promising results.

RESUM

Les malalties autoimmunes són un grup especial amb causa desconeguda en què el sistema immunitari es veu alterat i ataca òrgans del mateix individu. Actualment, es coneixen més de 110 d'aquestes malalties i alguns estudis epidemiològics estimen que més del 10% de la població en pateix alguna, principalment dones en edat laboral i durant els anys fèrtils.

Entre les moltes malalties autoimmunes existents, algunes poden tenir afectació de pell i/o mucoses, sent aquestes les úniques dianes, o per contra, poden afectar diversos òrgans. Totes però són generalment cròniques i varien molt depenent de la susceptibilitat individual de cada persona, necessitant tractaments personalitzats. En general, cal intentar reduir o minimitzar els sues efectes amb fàrmacs immunosupressors o immunomodulador.

A més, l'alta prevalença de malalties autoimmunes i l'impacte que tenen en la qualitat de vida dels pacients, fa necessària la investigació en aquesta àrea; la millora mitjançant una nova via d'administració que proporcioni una millor adherència al tractament, millors perfils farmacocinètics, una formulació que millori la biodisponibilitat del fàrmac, etc. tindrà un impacte positiu pels pacients. És per això que el projecte de tesi s'emmarca dins dels estudis biofarmacèutics i farmacocinètics d'un fàrmac immunomodulador.

La formulació escollida per treballar-hi ha estat els liposomes, vesícules esfèriques de mida nano a micro composats per fosfolípids biodegradables naturals o sintètics, es formen de manera espontània en un medi aquos pel que en l'interior de les vesícules es poden encapsular fàrmacs tan hidrofòbics com hidrofílics, resolent un problema comú que és la dificultat de vehiculitzar fàrmacs insolubles com el baricitinib (BNB), el fàrmac d'estudi en aquesta tesi. La composició dels liposomes és biocompatible, biodegradable i no tòxica, i la seva flexibilitat en la formulació permet crear diferents mides de liposoma per diferents aplicacions des de gotes oftàlmiques fins l'aplicació directa en la pell.

El BNB és un immunosupressor oral que actua inhibint selectivament la janus quinasa 1 i 2 entre altres molècules, reduint així signes i símptomes de malalties disminuint la inflamació, l'activació cel·lular i la proliferació de cèl·lules immunes clau. En el moment

el BNB s'utilitza pel tractament de dermatitis atòpica (AD) moderada a severa, l'artritis reumatoide i el COVID-19, en dosis entre 2 i 4 mg al dia. Fins el moment ha esta demostrat que millora des del primer dia de dosis els símptomes cutani.

Aquest projecte de tesi inclou l'elaboració d'un total de 5 liposomes diferents per mètode d'evaporació invertida o "micel·les invertides": tres per la seva aplicació tòpica enfocats en el tractament o coadjuvant d'aquest de la AD i, els dos liposomes restants, per la seva aplicació oftalmològica pel tractament o coadjuvant d'aquest del Síndrome de Sjögren (SS):

Aplicació Dermatitis Atòpica	**Aplicació Síndrome de Sjögren**
POPC	Lα – PC
POPC:CHOL	POPE:POPG
POPC:CHOL:CER	

Per aconseguir els nostres objectius primer vam estudiar la pell com a ruta potencial per l'administració del fàrmac BNB, per aconseguir tan efecte local com sistèmic. A causa de la funció protectora de la pell, la difusió de fàrmacs a través d'aquesta sol requerir l'ús de potenciadors de la permeació. Els potenciadors usats van ser físics (microagulles de titani sòlid) i químics. A més, es van validar dos mètodes analítics HPLC per a la determinació i quantificació de BNB i es va estudiar per primera vegada l'espectre del BNB a traves de la tècnica d'espectrofotometria confocal de Raman.

La SS és una malaltia autoimmune sistèmica crònica que afecta entre el 0,2 i el 3% dels la població general. Dues formulacions liposòmiques es van caracteritzar fisicoquímicament per la seva aplicació ocular, junt amb estudis d'alliberació del fàrmac in vitro, la permeació i retenció ex vivo i estudis de tolerància. Tots dos liposomes van donar resultats prometedors.

Finalment els tres liposomes restants pensats per la seva aplicació en brots de la AD, una malaltia inflamatòria de la pell autoimmune crònica important per la seva prevalença, van caracteritzats fisioquímicament, junt amb estudis d'alliberació del fàrmac in vitro, la permeació i retenció ex vivo i estudis de tolerància. Tots els liposomes van mostrar bones propietats fisicoquímiques i resultats prometedors.

TABLE OF CONTENTS

TABLE OF CONTENTS

ABBREVIATION AND ACRONYMS

Abbreviature /Acronym	Definition
ACD	Allergic Contact Dermatitis
AD	Atopic Dermatitis
AHS	Altered Human Skin
AMPs	Antimicrobial peptides
ARS	Altered Rabbit Skin
AUC	Area under the depth profile curves
BAFF	B-cell Activating Factor
BLyS	B-Lymphocyte Stimulator
BNB	Baricitinib
CAM	Chorioallantoic Membrane
CDS	Chromatography Data System
CER	Ceramides
CHOL	Cholesterol
CRS	Confocal Raman Spectroscopy
Css	Predicted plasma concentration of BNB at the steady state in humans
DCMS	Decylmethyl Sulfoxide
DMSO	Dimethyl sulfoxide
E	Efficiency
EE	Encapsulation Efficency
EF	Enhancer Factor
EM	Emission Wavelength
EMA	European Medicines Agency

EPR	Permeability and retention effect
EX	Excitation Wavelength
FDA	United States Food and Drug Administration
FP	Fingerprint Region
HET-CAM	Hen's Egg Test-Chorioallantoic Membrane
HPLC	High-Performance Liquid Chromatography
HPLC-F	HPLC System with a Fluorescence Detector
HPLC-UV	HPLC System with a UV Detector
HWN	High Wavenumber Region
ICH	International Conference on Harmonization
IFN	Interferons
Ig	Immunoglobulin
IL	Interleukins
IQ	Installation Qualification
IS	Irritation Score
J	Flux of the active ingredient
JAK	Janus kinase
Kp	Permeation or Penetration Constant
Log P	Octanol/Water Partition Coefficient Logarithm
LVET	Low Volume Eye Test
Lα-PC	Lα-Phosphatidylcholine
MAS	Maximum Average Score
MRT	Mean Release Time
MTT	Mean Transit Time
NIST	National Institute of Standards and Technology

NK	Natural Killer
NPs	Nanoparticles
OECD	Organisation for Economic Co-operation and Development
OQ	Operational Qualification
PDI	Polydispersity Index
POPC	1-Palmitoyl-2-Oleoyl-Glycero-3-Phosphocholine
POPE	1-Palmitoyl-2-Oleoyl-Phosphatidylethanolamine
POPG	1-Palmitoyl-2-oleoyl-sn-glycerol-3-phosphoglycerol
PQ	Performance Qualification
R	Recovery constant
SC	Stratum corneum
SS	Sjögren's Syndrome
STAT	Signal transducers and activators of transcription
TDCMS	Tetradecylmethyl Sulfoxide
TEM	Transmission Electron Microscopy
TEWL	Transepidemal water loss
Th	T helper cells
Tl	Lag time
TSLP	Thymic stromal lymphopoietin
TYK2	Non-receptor tyrosine-protein kinase
UV/Vis	Ultraviolet-Visible
ZP	Zeta Potential

1. INTRODUCTION

1.1. SKIN – STRUCTURE, PROPERTIES, AND FUNCTIONS

The skin is one of the most important organs in our body; a loss of 40% of our skin tissue would be incompatible with life. Furthermore, the skin is the largest organ we have. It weighs between 3 and 5 kg, and when completely stretched, it can cover an area of up to 18 m^2. In general terms, the skin performs functions such as mechanical protection, thermal regulation, water balance, excretion, sensory input, and immune response. Additionally, it is now known that the skin actively participates in the synthesis, utilization, and metabolism of proteins, lipids, and cellular signalling molecules.

1.1.1. Structure

The skin consists of three well-differentiated layers: the epidermis, dermis, and hypodermis or subcutaneous tissue. Additionally, it contains sebaceous glands, sweat glands, and hair follicles. The surface of the skin is typically covered by an epicutaneous emulsion or hydrolipidic mantle, which forms from the fatty acids of the sebaceous secretions of keratinocytes and water from sweat glands. This contributes to the maintenance of its protective function and cutaneous microbial flora (Montagna & Parakkal, 1974). In Figure 1, which we'll see below, we can observe a brief outline of the skin's structure.

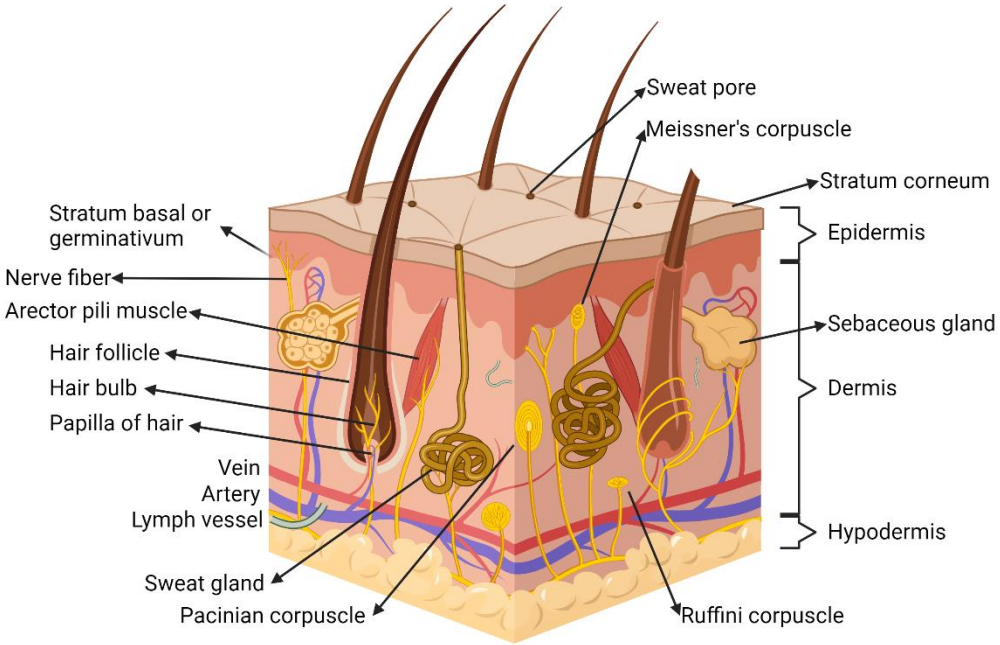

Figure 1. Skin structure.

- Epidermis:

It is the outermost layer. It has a thickness of one millimeter, although on the palms of the hands and soles of the feet, it can measure a bit more, and less on the eyelids, between 0.02 and 0.2 mm depending on the anatomical area (Wertz, 1996).

It is composed of several layers of cells called keratinocytes, arranged one above the other, forming an impermeable barrier to almost all substances. It regenerates every two months, and its function is to keep the skin hydrated, as well as protect us from solar radiation. The epidermis is made up of different layers, each with distinct names; from a deeper level to a more superficial one, we find:

- Basal or germinative layer: It is formed by a row of living cells that exhibit high activity and constantly regenerate the epidermis. In this layer, melanocytes are present — star-shaped cells with projections called dendrites. These cells are responsible for producing melanin, a pigment that contributes to the colour of the skin and protects us from the potential negative effects of sunlight. Additionally, immune system cells known as Langerhans cells are also found in this layer. They are responsible for presenting antigens to lymphocytes, initiating the immune defence response.
- Spinous layer: Situated above the basal layer, it consists of several rows of cells representing another stage of evolution from basal cells. The cells in the spinous layer unite with each other and with those in the basal layer, forming a solid armor.
- Granular layer: Composed of flattened cells containing granules of keratohyalin, a characteristic cornified substance. These cells lack the ability to divide, as they are exclusively dedicated to the synthesis and formation of keratin.
- Cornified layer or stratum corneum (SC): Comprising layers of dead cells called corneocytes, this layer represents the final stage in the evolution of keratinocytes from their origin in the basal layer. It is in constant shedding, although under normal conditions, this phenomenon is imperceptible. Thus, the skin is constantly renewing itself. This layer is present throughout the skin, except in mucous membranes.

Between the epidermis and the dermis lies the basement membrane, which is a folded plasma membrane with a large surface area. This membrane facilitates the exchange of

nutrients between the dermis and the epidermis since the epidermis lacks blood vessels. Additionally, it prevents displacement between the two layers.

- *Dermis:*

It forms the largest proportion of the skin and constitutes the true support of this organ. It has a thickness of 4 millimetres. It is divided into three zones which, from a more superficial to a deeper level, are called the papillary dermis, reticular dermis, and deep dermis. Unlike the epidermis, these are not layers of superimposed cells but a complex system of interlaced fibres surrounded by a substance called the ground substance, where a wide variety of cell types are located. The dermis also contains cutaneous appendages of two types: horny (hair and nails) and glandular (sebaceous glands and sweat glands). Blood vessels that irrigate the skin and nerve endings are also found in the dermis.

The types of fibres that make up the framework of the dermis and contribute to the fineness, flexibility, and elasticity of the skin are:

- Collagen fibres: They are the primary component of the dermis and provide resistance to tension and flexibility.
- Elastic fibres: Less abundant than collagen fibres, but important because they are responsible for the skin's elasticity.
- Reticular fibres: The least abundant, arranged around appendages (hair, nails, and glands) and blood vessels. These are small, fine fibres with a diameter of 30 to 40 nm that associate to form networks. These networks act as a supporting tissue.

The cells that primarily form the dermis are called fibroblasts. They are responsible for producing collagen and elastic fibres, as well as the ground substance. In the dermis, we also find various cells of the immune system (lymphocytes, macrophages, eosinophils, and mast cells), present in variable numbers depending on the circumstances of the skin, increasing during inflammation. In this scenario, we also find cells that have extravasated from blood vessels, including red blood cells and white blood cells. The ground substance is located between the fibres and is composed of proteins, electrolytes (such as sodium and potassium), glucose, and water.

- *Hypodermis or subcutaneous tissue:*

It is the deepest layer of the skin, also known as subcutaneous cellular tissue. It is composed of a large number of adipocytes arranged in lobules and separated by collagen and elastic fibres called trabeculae. Fat forms a highly active metabolic tissue that also protects the organism by providing cushioning and thermal insulation (Cassel, 1982).

1.1.2. Properties and Functions

The skin is essentially the outer covering of the organism, functioning continuously and fulfilling two important missions: connecting us with the external world and protecting us from external aggressions.

Regarding the function of connection, one of our most developed senses, touch, is involved. The skin is responsible for receiving stimuli from the external environment, and through the nerve endings located in it, directing them to the brain, which tells us how to react. Every square centimetre of skin contains about 5,000 sensory receptors. The skin is responsible for us feeling a caress or sensing the heat produced by fire or the cold of the snow. However, the skin also reflects feelings and emotions. Blushing due to embarrassment, experiencing "goosebumps", or sweating out of fear are some of the emotional responses that manifest through the skin. For this reason, it is not surprising that this organ plays a key role in a person's outward appearance.

The skin has other basic functions for the proper functioning of the organism. It has a protective function, as it can select what is harmful to the organism and what, on the contrary, is beneficial to us. This occurs thanks to its barrier disposition that prevents the entry of harmful substances (millions of bacteria that live on it, foreign bodies, and partly harmful solar radiation) and contains its own immune system. It also has a regulatory function of metabolism: it prevents the exit of essential substances (liquids, cells) for the organism, regulates body temperature protecting us from changes in environmental temperature, and transforms sunlight into vitamin D, a necessary vitamin for the proper functioning of our bones, among many other functions (Fleischer et al., 2001).

1.2. EYES – STRUCTURE, PROPERTIES, AND FUNCTIONS

The human eye is the anatomical organ that houses the sensitive structure that enables the initiation of the complex process of vision. Due to its shape, it is called the eyeball or ocular globe. It is a paired organ located on either side of the sagittal plane, protected by fat and soft tissues, as well as the bony walls that make up the orbital cavities. In addition to the eyeball, the orbital cavities house the optic nerve, ocular muscles, lacrimal gland, blood vessels, and nerves. Eyelids, eyelashes, and tears serve as protectors for the eye.

1.2.1. Ocular structure

The human eye consists of several layers that work together to enable the visual function. The main layers of the eye include:

1. *Fibrous Tunic or Sclerocorneal*:

As its name suggests, it is composed of collagen fibers, providing it with great strength to fulfill the function of protecting the contents of the eyeball. The fibrous tunic consists of two spherical segments: the anterior is the **cornea**, the smaller and more prominent portion, and the posterior segment is the **sclera**, which are continuous with each other.

The cornea is the clear and transparent anterior portion of the outer layer of the eyeball, formed by collagen fibres arranged in an orderly parallel fashion to allow the passage of light through them. It is the largest refracting surface of the eye and the most sensitive in the body due to the abundance of nerve fibres it contains. Its primary physiological function is to maintain the eye's surface smooth and transparent while protecting the intraocular contents. It is bathed by fluids both in front and behind, providing the necessary nutrients for corneal metabolism since it lacks blood vessels; tears moisten the corneal epithelium or anterior surface, and aqueous humour enables nutrition from the posterior or endothelial surface (Martín & Bueno, 1994).

The cornea is stratified into 3 cellular layers and two interfaces: epithelium, Bowman's membrane, stroma, Descemet's membrane, and endothelium. Its structure is relatively simple compared to other parts of the body (Oyster, 1999). The types of cells that constitute it are epithelial cells, corneal fibroblasts known as keratocytes, and

endothelial cells. These components interact with each other to maintain the integrity and functionality of the tissue.

The sclera forms the skeleton of the eyeball. It is composed of bundles of connective tissue and elastic fibres arranged in a disorderly manner, forming a more opaque and stronger structure, allowing it to maintain the shape of the eye while achieving a maximum thickness of 1 mm. At the front, it has the insertions of the extrinsic muscles of the eye, and at the posterior pole, the exit of the optic nerve, the central vein of the retina, and the central artery of the retina.

2. *Vascular Tunic:*

The **iris** forms the anterior part, and the posterior part is the **choroid**; the junction of the two parts is a thickening known as the ciliary body. It is a delicate, thin, and pigmented membrane that separates the anterior and posterior chambers of the eyeball.

The iris is a membrane located behind the cornea and immediately in front of the lens. It is noticeable to the observer as the part that imparts the colour that characterizes our eyes. It is of variable colour, circular in shape, and perforated at the centre by an also circular opening (pupil), the size of which varies due to the action of the sphincter and dilator muscles of the pupil that control the amount of light entering the eye.

The choroid constitutes a major part of the uveal region. It is situated between the sclera and the retina. It is mainly composed of blood vessels, giving it an earthy colour. Its primary function is to nourish the retina, vitreous body, and lens, as well as to collect waste products.

The choroid continues forward with the ciliary body, which contains the ciliary muscle responsible for the accommodation or focusing of the lens. It presents protrusions called ciliary processes, highly vascularized structures specialized in the production of aqueous humour necessary for maintaining the anatomy and physiology of the anterior segment of the eye (cornea, iris, and lens). Aqueous humour is a liquid whose composition resembles that of plasma with almost all proteins removed. It contributes to maintaining intraocular pressure and facilitates the metabolism of the lens and cornea, which lack blood vessels. Secreted by the ciliary body, it flows into the posterior chamber between

the iris and the lens, then passes to the anterior chamber through the pupil. It is eliminated from the eye through the trabecular meshwork to reach Schlemm's canal.

3. *Neurosensory or Retinal Tunic:*

Formed by the **retina**, which continues forward with the deep layer of the ciliary body and the iris. The retina is the innermost layer of the eye, situated between the choroid and the vitreous body. It is a complex structure, with numerous types of cells and an anatomical arrangement of ten layers or strata. The outermost layers contain cellular elements responsible for transforming light energy into bio-electric energy (photoreceptors), while the innermost layers are responsible for transmitting this energy, conducting the visual stimulus to the brain, and representing the first step in the optic pathway.

The retina features a central avascular extension, the **macula lutea**, in the centre of which is a small depression, the central fovea. With a high concentration of cones and nearly devoid of rods, it constitutes the area of maximum visual acuity. About 3 mm on the inner side of the posterior pole of the eye is the head of the optic nerve (optic disc or papilla), an area composed of nerve fibres without visual power, hence also known as the blind spot.

The lens is a lenticular-shaped, transparent, biconvex organ encapsulated by a series of concentric layers. Suspended from the ciliary processes by filaments, it is a hollow sphere of epithelial cells. The function of the lens, along with the cornea, is to focus the rays on such a way that they form an image on the macula.

The vitreous body is a transparent, colourless, soft-consistency mass that occupies the posterior cavity of the eyeball. Positioned between the lens, the ciliary body, and the retina, it constitutes the most extensive volume of the eye. Devoid of blood vessels, it is nourished by the adjacent tissues: the choroid, ciliary body, and retina (Martín & Bueno, 1994).

Everything explained can be schematically appreciated in Figure 2, where we will be able to see the structure of the eye with all its parts.

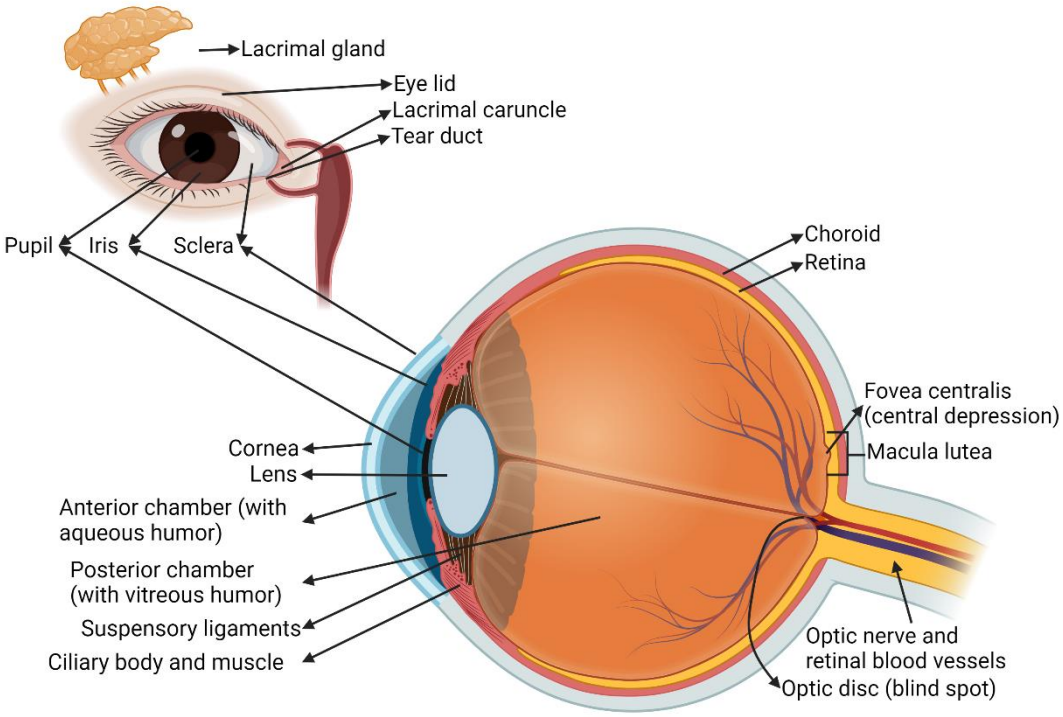

Figure 2. Eye Structure.

1.2.2. Properties and functions

The primary function of the eye is to see the external world to facilitate easier and clearer interaction with it. Humans and other primates continually move their eyes to gather visual information and to guide their hands and body toward interesting objects. Vision is a complex process involving many different parts of the eye. Light first passes through the outermost layer called the cornea, then through the opening known as the pupil, allowing it to reach the lens, the crystalline lens. The amount of light reaching this lens depends on the aperture set by the iris muscle for the pupil. Finally, the lens acts like a camera lens, helping to focus the amount of light entering the eye and ultimately illuminating the retina. The retina, located on the inner wall of the eyeball, has light-sensitive cells where images begin to be detected and developed. The information from the retina is sent to the brain, where it will be processed and understood (Muth, 2017).

The ability to visualize the external world not only informs us about where to move and where the objects we need are located but technological advances and the availability of affordable eye-tracking and manual tracking technology have made it clear that, in motor tasks, eye movements actively guide hand movements. Eye movements enhance the precision of goal-directed movements and facilitate the learning of new motor skills

and the adaptation of familiar movements. Eye movements can also be sensitive indicators of limb motor processes and performance, and they may be influenced by concurrent hand movement (de Brouwer et al., 2021).

1.3. MUCOUS MEMBRANES AND SKIN PERMEABILITY

Drugs pass through the skin and/or mucous membranes through the mechanism of passive diffusion. It is necessary to distinguish three different routes: transcellular or intracellular, paracellular or intercellular, and transappendageal. The transcellular and paracellular routes can be grouped as transepidermal routes. Figure 3 shows the three routes mentioned:

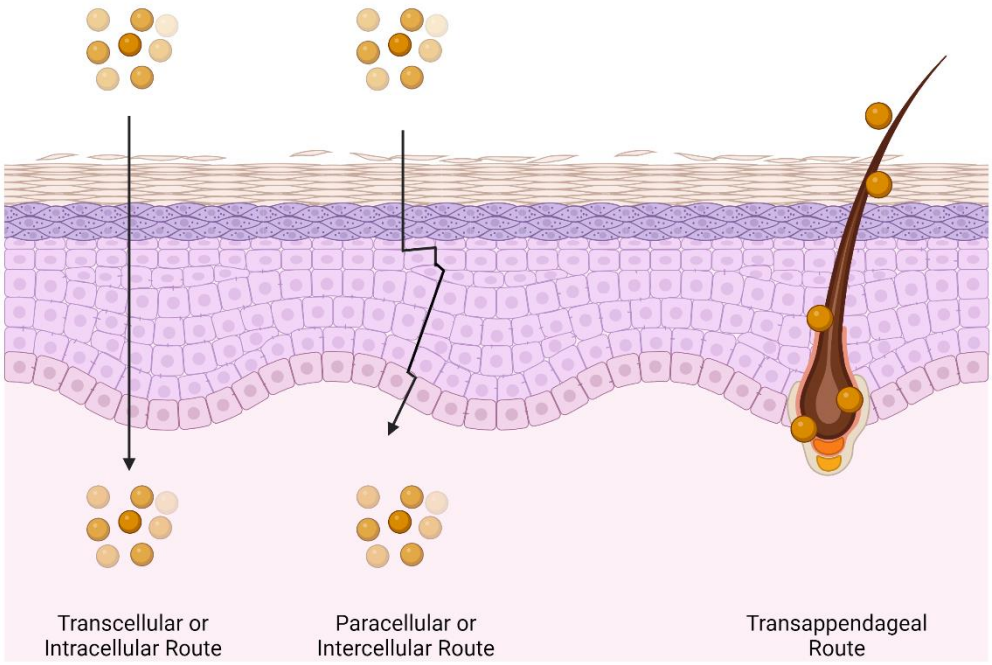

Figure 3. Scheme of the main routes followed by drugs when permeating the skin and/or mucous membranes.

The transcellular or intracellular route results from crossing the entire SC and includes the transport of molecules through phospholipid membranes, such as the matrix (cytoplasm) of dead keratinocytes. Therefore, the penetrating agents diffuse through the SC corneocytes containing highly hydrated keratin and surrounded by lipids that connect the cells. This route creates an aqueous hydrophilic pathway suitable for transferring hydrophilic molecules. This path is the shortest, but penetrating agents encounter significant resistance to permeation, as molecules must pass through the

lipophilic membrane of each cell, then the hydrophilic cellular content containing keratin, and finally the phospholipid bilayer of the cell. These steps are repeated numerous times for molecules to traverse the entire thickness of the SC. Additionally, drugs undergo successive partitioning between the hydrophilic (keratin) and lipophilic (lipid matrix) portions of the SC. Consequently, the physicochemical properties of the drug molecule particularly affect the importance of this route. Hydrophilic drugs may favour this route in a pseudo permanent state. However, lipid bilayers are considered the rate-determining step for transcutaneous penetration through this route (Elmowafy, 2021). The transcellular route is important when using a penetration enhancer such as urea to increase the permeability of corneocytes by altering the structure of keratin (Nafisi & Maibach, 2018).

The paracellular or intercellular route involves the drug passing only through the continuous lipid matrix of the spaces between the cells of the SC. The limited space hinders the penetration of macromolecules. On the other hand, since this route occurs through lipid bilayers (covering up to 1% of the diffusion area of the SC), it is essential for drug molecules penetrating through this route to exhibit a balanced solubility between lipids and water (Elmowafy, 2021), Small molecules can reach the intercellular spaces with diffusion rates largely influenced by their lipophilicity and other physicochemical properties such as solubility, molecular weight, and hydrogen bonding capacity. The intercellular route is the appropriate penetration pathway for most permeants and is primarily suitable for lipophilic, uncharged molecules (Nafisi & Maibach, 2018). The paracellular routes were described some years ago in rabbits using polyethylene glycols of different molecular weights (from 200 to 1000 Da). These agents were chosen because their characteristics are common to peptides and oligonucleotides (hydrophilicity, hydrogen bonding capacity, and molecular size) (Andrés-Guerrero & Herrero-Vanrell, 2008).

Finally, we have the transappendageal route where drug molecules diffuse through the skin appendages such as the ducts of sweat glands or hair follicles. Among the two, hair follicles are considered the most significant appendages due to their surface. In the literature, this route is believed to play a secondary role, representing 0.1% to 1% of

cutaneous absorption (Patzelt & Lademann, 2020). Currently, however, its significance is under discussion (Lai et al., 2020).

The administration of drugs through the skin and/or mucous membranes to achieve a systemic therapeutic effect is currently under intense research. These tissues offer unique advantages and limitations for drug entry into the body (Guy et al., 1987). Here are the main advantages and disadvantages of transdermal and transmucosal drug administration.

Benefits:

- Avoidance of first-pass metabolism and other variables associated with the gastrointestinal tract, such as pH and gastric emptying time.
- Sustained and controlled release over an extended period.
- Reduction of side effects associated with systemic toxicity, i.e., minimizing peaks and valleys in drug concentration in the blood.
- Direct access to the target site, facilitating dose termination in case of adverse reactions, whether systemic or local.
- Convenient, simple, and painless administration, making it user-friendly and reducing overall healthcare costs.
- Providing an alternative to oral dosing contraindication (in unconscious or nauseated patients).

Limitations:

- A molecular weight below 500 Da is essential to ensure easy diffusion through the SC, as solute diffusivity is inversely related to its size.
- Adequate aqueous and lipid solubility. A partition coefficient (Log P) (octanol/water) between 1 and 3 is necessary for the active ingredient to successfully traverse the SC and the underlying aqueous layers for systemic administration.
- Intra- and inter-individual variability associated with the permeability of intact and diseased human skin, implying rapid, slow, and normal cutaneous absorption profiles leading to variable biological responses.

- Presystemic metabolism; skin enzymes, such as peptidases and esterases, may metabolize the drug into a therapeutically inactive form, thereby reducing drug efficacy.
- Irritation and sensitization of the skin and mucous membranes. The skin, as an immunological barrier, can be triggered by exposure to certain stimuli, including drugs, excipients, or components of administration devices, resulting in erythema, edema, etc. (Brown et al., 2006).

1.3.1. Percutaneous Absorption

Percutaneous absorption of drugs can be defined as the absorption of drugs through intact skin to enrich the circulatory system. The choice of the skin as a route for drug administration is based on the advantages it provides. Sometimes, cutaneous treatment is the only way to address a pathology; in other instances, it serves as a strategy in conjunction with the systemic route, and in certain cases, it offers a viable alternative to the limitations of systemic administration.

Stages of Percutaneous Absorption:

The skin constitutes a highly selective barrier to the passage of substances. The epidermis, and within the epidermis, the SC, is primarily responsible for this control (Barry, 1983b). Moreover, the flow of molecules through the skin depends on the nature of the substance, the vehicle-skin partition coefficient, and the diffusion coefficient of the diffusing substance through the skin (Morimoto et al., 1994). Drug absorption occurs in three stages:

1. Adsorption: The process by which the drug is retained on the skin's surface, typically through physicochemical interactions with high molecular weight cutaneous components (keratin, melanin, etc.). For this step to occur, the active ingredient must first be released from the containing vehicle, requiring dissolution (if not already dissolved) and diffusion to the vehicle-SC interface. In this initial phase, the pharmaceutical formulation is crucial as it modulates the release of the contained active ingredient.

2. Permeation: This stage is governed by a process of passive drug diffusion through the different layers of the skin. The main barrier drugs encounter in crossing the skin is the SC.
3. Absorption: It is the passage of the substance into the circulatory system (blood vessels or lymphatics). The processes that the drug undergoes in the body after absorption are like those found in other routes of administration.

Advancements in pharmaceutical technology now allow for the modulation of transdermal permeation of drugs according to the desired objective. In the case of transdermal administration systems, the dosage form aims to maximize the flow through the skin into systemic circulation while simultaneously minimizing drug retention and metabolism in the skin. In contrast, in topical application forms, the general goal is to minimize drug flow through the skin, maximizing the retention time on the skin (Dean, 1994). However, both in transdermal and topical systems, the drug must penetrate through the SC, the outermost layer of the skin and the main responsible for its barrier function.

Factors influencing percutaneous absorption:

Biological factors:

- Age: Due to the interindividual variability in permeation parameters, study results are inconclusive. It can only be stated that the skin of children and infants, as well as that of the elderly, is more permeable than that of adults (Bonina et al., 1993).
- Body region: There are significant intra-individual variations depending on the body region (Wester & Maibach, 1999). The least permeable area for the passage of substances is the sole of the foot (thickness of the SC: 600 µm), followed by the ankles and the palm of the hand (thickness of the SC: 400 µm). The forearm and back exhibit greater permeability, followed by the scalp, armpits, and forehead. The most permeable areas were found to be the angle of the jaw and the skin of the scrotum (thickness of the SC: 5 µm) (Scheuplein & Blank, 1971).
- Skin condition: There are certain pathologies that affect the state of the skin, potentially altering its barrier function and increasing its permeability to xenobiotics, drugs, and microorganisms. Permeability increases in cases of skin peeling, chemical or physical aggression, and inflammation.

- Degree of hydration of the SC: If the water content increases, the permeability of drugs also increases (Idson, 1975). When the hydration level is less than 10%, it is considered that keratin is dehydrated, leading to desquamation of the SC, and affecting absorption.
- Blood flow: Increasing blood flow reduces the drug residence time in the dermis, thereby increasing the concentration gradient and promoting the passage of the drug from the skin surface to the dermis. If the blood flow in the area is low or decreases, the substance cannot diffuse as it penetrates, becoming a limiting factor for drug absorption (Barry, 1983a).
- Environmental factors: Related to blood flow, the vasoconstrictor effect of decreasing ambient temperature on the skin surface could be mentioned, leading to a consequent decrease in permeability. Since topical forms are usually applied with a gentle massage, this increases local blood flow and promotes drug absorption.

Physicochemical factors:

- Criteria related to the drug:

- Partition coefficient: The octanol/water Log P is one of the most important factors for drug penetration through the epithelium and can be used to predict the drug's distribution in the skin. The Log P and skin distribution maintain a parabolic relationship (M.-K. Kim et al., 2010). Therefore, compounds with a low Log P exhibit low permeability due to their low distribution with the skin lipids (tending to stay in the vehicle). However, drugs with a high Log P (facilitating the drug's exit from the vehicle to the skin) also have low permeability due to their inability to distribute outside the SC (where it would be retained). It is accepted that maximum permeation is achieved with a Log P between 1 and 3 (Thomas & Finnin, 2004). The Fick's law establishes a proportionality between the drug flux through the skin and the partition coefficient between the vehicle and the skin.
- Diffusion coefficient: Expresses the rate of diffusion of a compound in a specific medium. If it is assumed that drug molecules are spherical, the diffusion coefficient can be calculated using the Stokes-Einstein equation:

$$D = \frac{K \cdot T}{6 \cdot \pi \cdot r \cdot \eta} \ (cm^2 \cdot s^{-1}) \quad (1)$$

Where K is the Boltzmann constant (Joules/Kelvin (1.380649×10^{-23} $J\cdot k^{-1}$)), T is the absolute temperature (kelvin), r is the molecule's radius (cm), and η is the viscosity of the medium (Joules·s^{-1}). The diffusion coefficient is inversely proportional to the size of the molecule. Therefore, drugs with a low molecular weight are more likely to penetrate the epithelium. The degree of dispersion significantly influences the penetration of poorly soluble drugs into vehicles because it affects the diffusion coefficient. Increasing the degree of dispersion in the vehicle increases the diffusion coefficient and consequently penetration.

- Drug solubility: The solubility of the drug will affect release since increasing the concentration of the dissolved drug in the vehicle creates a larger concentration gradient between the drug and the skin surface, resulting in a greater amount of released drug. Thermodynamic activity depends on the concentration and solubility of the drug, as well as drug-drug and drug-vehicle interactions. The thermodynamic activity of the drug in the vehicle will be maximum when saturated solutions are used. This parameter indicates the drug's tendency to escape from the vehicle (Carelli et al., 1992). To prevent a decrease in the concentration of dissolved drug during the release process, some authors recommend using supersaturated solutions or suspensions (Lippold, 1992; Valenta et al., 2000). In this case, the dissolution rate of the drug must be considered. On the other hand, there must be a balance between the drug-vehicle affinity and the drug-skin/mucosa affinity since an extreme affinity towards either of them would mean that the drug will predominantly stay in the more favourable site. Therefore, lipophilic drugs dissolved in aqueous media will be absorbed faster than if they are in a lipophilic solvent at the same concentration (Jacobi et al., 2006). Most drugs are weak acids or bases, and at physiological pH, they are partially ionized, exhibiting pH-dependent solubility. Ionized drugs diffuse less readily than those in the molecular form.

Taking all these factors into account, it could be stated that the ideal characteristics of a drug allowing it to penetrate through the skin are an aqueous solubility of 1 mg/ml, a

molecular weight below 500 Daltons, and a melting point below 200 °C. As a general rule, it is estimated that if the drug does not have the ability to form more than two hydrogen bonds, it can be considered to have good diffusion (Du Plessis et al., 2002).

- Criteria related to the vehicle:

- Drug concentration: According to Fick's law of diffusion, the transfer rate of a substance from areas of high concentration to low concentration is proportional to the concentration gradient. Moreover, a higher drug solubilized in the vehicle without selectivity for it will exhibit greater thermodynamic activity to decrease the drug's solubility in it (Thomas & Finnin, 2004).
- pH: pH influences the proportion in which drugs are ionized, depending on both the compound's pKa and the pH of the formulation that carries the drug. It has been observed that the non-ionized form of a drug has a higher lipid-water partition coefficient than the corresponding ionized form. Therefore, a higher permeability in the SC could be expected for the non-ionized fraction. (Tsai & Maibach, 1999).
- Occlusion: occlusion (of transdermal systems, occlusive dressings, and lipophilic bases) has been shown to increase the permeability of certain drugs (Feldmann, 1965). Therefore, as the aqueous phase increases in the formulation, its occlusive power decreases. The mechanisms involved in this process are thought to be due to the accumulation of water within the skin, swelling the corneocytes, and increasing the water content in the intercellular matrix (Tsai & Maibach, 1999); On the other hand, it also increases the skin's temperature and reduces the loss of co-solvents through evaporation (Taylor et al., 2002). However, in some cases, occlusion can lead to irritation and promote microbial growth (Tanner & Marks, 2008).
- Viscosity: The smaller the viscosity of the vehicle, the greater the drug release will be since it will have a higher diffusion coefficient (Al-Khamis et al., 1986). The choice of formulation and its appropriate rheological behaviour will determine the residence time and local exposure of the drug to the required site.
- Dosage and application frequency: To understand the effect of excipients on transdermal penetration, it is advisable to apply infinite doses to the donor compartment (>100 mg of formulation per cm^2). The application of infinite doses

results in a relatively constant drug input force through the skin, allowing for the achievement of steady-state plasma levels. However, in daily practice, such high doses are not applied; typically, doses of approximately 2-5 mg/cm² are used, resulting in a thin layer of the formulation (10-30 μm), which is less than needed to saturate the SC with the drug. This leads to a finite dose model. On the other hand, the effects of excipients on the skin can impact transdermal penetration differently when applied as a single dose or following a multiple-dose regimen. To study the effect of dosing frequency, it is more advisable to conduct a study with multiple finite doses (Lu & Gao, 2010).

- Absorption enhancers: Absorption enhancers are molecules of different chemical nature that act reversibly at the SC level, disrupting and facilitating the drug's faster penetration into viable tissues and systemic circulation. There is a general theory (Lipid-Protein-Partition) based on possible molecular-scale alterations that the SC undergoes due to the action of enhancers. This theory postulates that the enhancer's action on various epidermal histological structures will occur through one or more of the following actions (Barry, 1987, 1988; Potts et al., 1991):
  - Interaction with cellular proteins, promoting permeation through corneocytes (intracellular route).
  - Interaction with the lipid structure surrounding corneocytes, increasing intercellular diffusion (intercellular route). This action can occur through the interaction of enhancers with the polar groups of lipids, by inserting them between lipid structures, or by changes in polarity in certain areas, altering the Log P of the drug between the vehicle and the skin.

Types of chemical absorption enhancers:

- Alcohols and fatty acids: The promoting effect of this group of substances depends significantly on the size of the structures. It seems that the promoting effect is due to the fluidization of cutaneous lipids and the increase in the level of surface hydration that these substances can induce (Cevc et al., 1996). Saturated fatty acids generally increase the Log P of the drug between the vehicle and the skin. Their effectiveness is related to the length of the hydrocarbon chain. Chains with 10 or 12 carbon atoms are those that exhibit optimal lipophilicity (C. K. Kim et al., 1993;

Tanojo et al., 1997). Unsaturated fatty acids alter the structure of extracellular lipids and reduce the resistance to the diffusion of compounds, thereby increasing absorption. Generally, unsaturated fatty acids are more effective than their saturated counterparts because the double bond introduces greater disorder in the lipid bilayers due to its flexion (Aungst et al., 1990). Regarding the optimal degree of unsaturation, studies are inconclusive. While some authors indicate that the promoting effect increases with the number of unsaturation, others suggest that unsaturated fatty acids have similar or even lesser effects when compared to saturated ones (Carelli et al., 1992; K et al., 1999; Santoyo et al., 1996). It has been suggested that oleic acid is arranged heterogeneously in lipid bilayers, resulting in the formation of fluid channels within the SC (Walker & Hadgraft, 1991). Oleic acid acts on the nonpolar route, increasing both the diffusion and distribution of the drug, but on the polar route, it only increases distribution, indicating an increase in the hydration of the SC (Koyama et al., 1994; Yamashita et al., 1995). On the other hand, it is worth noting that fatty acids can form ionic pairs with cationic drugs, thereby increasing their partition coefficient and, consequently, their absorption (Aungst et al., 1990). It is also important to note that oleic acid must be used with caution because its application causes morphological changes in Langerhans cells of the epidermis. These cells play a crucial role in initiating and coordinating the immune response involving T lymphocytes. Therefore, it can lead to immunosuppression on the skin at high concentrations (Kogan & Garti, 2006). The promoting effect of fatty acids appears to be concentration dependent. As the concentration of the fatty acid increases, the promoting effect also increases until it reaches a maximum, beyond which its effect decreases (S. K. Singh et al., 1996). Fatty alcohols have the same promoting mechanism as their corresponding fatty acids, but weaker, as the interactions with the SC are milder. Among them, lauryl alcohol is the most effective, being as potent as oleic acid (Yamada & Uda, 1987).

- Fatty Alcohol Esters: Isopropyl myristate stands out among them. It acts on extracellular lipids by fluidizing them and reducing their resistance to drug penetration and/or by increasing the partition coefficient between the drug, the formulation, and the SC (Leopold & Lippold, 1995a; Sato et al., 1988).

- Alcohols Ethanol has been widely used as a co-solvent in topical formulations because it can increase the solubility of certain drugs. It appears that with hydrophobic compounds, which penetrate by dissolving into the fluid lipid regions of the SC, ethanol dissolves in these regions, thereby increasing the solubility of the drug in them (Berner et al., 1989). In the case of hydrophilic drugs, ethanol extracts lipid and peptide substances, achieving an increase in the porosity of the SC. As in other cases, the promoting effect of ethanol depends on the concentration introduced into the formulation. Therefore, at low concentrations, ethanol increases the solubility of the drug in the SC, at high concentrations, ethanol alters the structure of the SC, increasing the diffusion of substances (Jiang et al., 1998; Yum et al., 1994). The mechanism of action is not entirely clear; it seems to induce dehydration of the SC and a shrinkage of keratin, leading to subsequent conformational changes (Berner et al., 1989; Megrab et al., 1995). Increasing the number of carbon atoms in the alcohol chain enhances the promoting effect (about four times for each methyl group introduced), with n-propanol being more potent than isopropanol (Y. H. Kim et al., 1992).
- Lactones: Azona (1-dodecylazacycloheptan-2-one) is an example, acting by disrupting lipid organization and increasing the water content of SC proteins (Goodman & Barry, 2011). The insertion of the large azona ring into lamellar regions prevents lipid packing and crystallization in the structure, reducing resistance to diffusion. Additionally, its twelve-carbon chain coincides with the dimensions of cholesterol, potentially altering cholesterol-ceramide or cholesterol-cholesterol interactions (Allan, 1995). The promoting action of azona depends on the concentration used and the lipophilicity of the drug (Díez-Sales et al., 1996). It is typically used at low concentrations (1-5%), and its activity is enhanced using co-solvents such as propylene glycol. In these cases, the role of the co-solvent is to modify the distribution of the enhancer on the skin (Beastall et al., 1988). Additionally, there is a potentiation of the promoting effect when both are combined, as azona increases drug passage through the intercellular route, and propylene glycol does so through the intracellular route (Takeuchi et al., 1995).
- Surfactants: Above the critical micellar concentration, surfactants form micelles, reducing thermodynamic activity. The observed promoting effect is due to the

ability of these compounds to penetrate the skin and disrupt its structure. Surfactants appear to alter both lipid structures and proteins in the SC (Goodman & Barry, 1989). Cationic surfactants cause more irritation and damage to the skin, followed by anionic surfactants, and finally non-ionic surfactants. Moreover, non-ionic surfactants have a more immediate promoting effect as they penetrate the membrane more easily than those that are charged. The promoting effect of surfactants greatly depends on their affinity for the SC and the solubility of the drug in the vehicle (Ashton et al., 1992).

- Terpenes: they are constituents of essential oils consisting of isoprene units (C5H8), and may include various heteroatoms in their structure. They are classified based on the number of isoprene units in their structure as monoterpenes (C10), sesquiterpenes (C15), and diterpenes (C20). Their physicochemical characteristics vary, but they generally exhibit high lipophilicity. Some authors have found a linear relationship between the promoting effect of the terpene and the logarithm of the octanol-water partition coefficient, while others found a parabolic relationship (Takanashi et al., 1999; Williams & Barry, 1991). Terpenes act in part by disrupting intercellular lipid packing, thereby increasing drug diffusion (Barry, 1991). In the case of lipophilic drugs, the use of these enhancers also increases the drug distribution due to their solubilizing effect. An example is menthol, which distributes among the intercellular spaces of the SC, causing reversible disorganization of lipids (Kunta et al., 1997; Williams & Barry, 1991).
- Sulfoxides: Dimethyl sulfoxide (DMSO) is a polar solvent that penetrates quickly, exerting its promoting effect, which is concentration dependent. The promoting effect of DMSO is due, on the one hand, to its drug solubilization properties, which increases drug distribution to the skin. On the other hand, it also affects the SC, reducing resistance to diffusion (Barry, 1991; Kai et al., 1993). At low concentrations, DMSO is initially distributed within the corneocytes, displaces water bound to proteins, and creates a larger solvation layer. As the concentration increases (above 60%), it displaces water surrounding the polar heads of intercellular lipids, mainly favoring the diffusion of polar compounds. Finally, it also seems to distort the packing of hydrocarbon chains. Due to the high concentrations required, the skin irritation it causes, as well as the unpleasant odor of its DMSO

degradation compounds, derivatives such as tetradecylmethyl sulfoxide (TDCMS) and decylmethyl sulfoxide (DCMS) have been studied (A. N. C. Anigbogu et al., 1995).

- Pyrrolidone group: Pyrrolidone group are derivatives of amino acids. The solubilizing capacity of a pyrrolidone is partly due to the formation of lipophilic ion pairs with anionic drugs. 2-pyrrolidone is a hygroscopic solvent like DMSO. At low concentrations, it is distributed to proteins, denaturing alpha-keratin, and at high concentrations, it interacts with lipids, increasing their fluidity. Additionally, it increases the water content within the SC. 2-pyrrolidone appears to enhance the penetration and diffusion of drugs through the polar route while reducing those of the non-polar route (Southwell & Barry, 1983). In order to enhance the promoting effect, derivatives of pyrrolidone have been developed, such as N-methyl-2-pyrrolidone, among others. This derivative acts by partially extracting sphingolipids from the SC and by hydrating the skin due to its humectant capacity (Bhatia & Singh, 2008; Ogiso et al., 1995). N-dodecyl-2-pyrrolidone, on the other hand, intercalates into the ceramide matrix through electrostatic repulsions (Fuhrman et al., 1997).
- Propylene Glycol: It is generally a good solubilizer for lipophilic drugs in aqueous vehicles. This is one of the promoting mechanisms of the compound. On the other hand, similar to ethanol, it dissolves in the aqueous layers found between the lipid bilayers and alters their composition. Therefore, it increases the affinity of this phase for lipophilic substances and promotes the distribution of these compounds between the vehicle and the skin. However, large amounts of propylene glycol in formulations can reduce the partition coefficient between the vehicle and the skin, potentially counteracting the benefit of increasing the concentration gradient due to the overall reduction in drug activity in the vehicle and, therefore, decreasing transdermal flux (Turi et al., 1979). It has also been observed it intercalates with the polar heads of lipids and produces solvation of the alpha keratin in corneocytes, thereby favoring the penetration of drugs through intracellular pathways (Bouwstra et al., 1991; Takeuchi et al., 1993).
- Nanoemulsions and microemulsions: Emulsions, both micro- and nano-, are composed of small droplets, measuring 100-400 nm and 1-100 nm, respectively. Both systems are vehicles capable of acting as enhancers for permeation and

penetration of drugs through the skin due to the characteristics they possess, allowing them to overcome the barrier of the SC. They also stand out for their ability to solubilize molecules that are difficult to incorporate into traditional formulations (Souto et al., 2022).

Finally, the following points should be considered:

- Application surface area: Generally defined by the cm^2 of exposed skin to the medication.
- Application frequency: As a general rule, one or two daily applications are assumed to be sufficient for most formulations, among other reasons because the kinetic processes through the skin are slow; it should be noted that the SC acts as a reservoir, allowing a gradual penetration of the medication into the deeper layers. On the other hand, multiple applications increase absorption and bioavailability.
- Application method: Occlusive dressing, friction, and hydration through immersion in water accelerate the penetration of certain drugs, increasing their absorption up to 10 times, although adverse effects can also be increased.

1.3.1. Ocular Permeation

The penetration of drugs into the interior of the eye after topical ocular administration is one of the most interesting challenges faced by pharmaceutical research. The goal is to traverse the protective barriers of the eye without causing damage to ocular structures. Unlike other tissues, the epithelia on the ocular surface are not well-suited for absorption, resulting in the residence time of a conventional formulation being reduced to less than two minutes. This is compounded by losses due to systemic absorption of the drug through the conjunctiva and nasolacrimal duct. It is estimated that the percentage of active substance capable of reaching the anterior segment of the eye is between 1-5% of the total administered dose. For this reason, even if the drug reaches the aqueous humor, its diffusion to the posterior segment is generally insignificant in most cases (Andrés-Guerrero & Herrero-Vanrell, 2008).

There are different routes to reach ocular tissues, which can be selected based on the target tissue. Generally, for the anterior segment, the ocular topical route is preferably used, while for the posterior segment, the intravitreal route is commonly employed

(Lorenzo et al., 2008). The penetration of drugs when administered topically to the eye can occur through the cornea (transcorneal route) or through the conjunctiva and sclera (conjunctival/scleral route). It is known that most active substances administered topically are absorbed using the transcorneal route. This explains why, for a long time, the conjunctiva was only considered an elimination route. Nowadays, it is known that there are substances capable of crossing the conjunctiva, reaching, on certain occasions, the posterior segment. Figure 4 is an example of the different routes drugs can use to get in or out the ocular tissues.

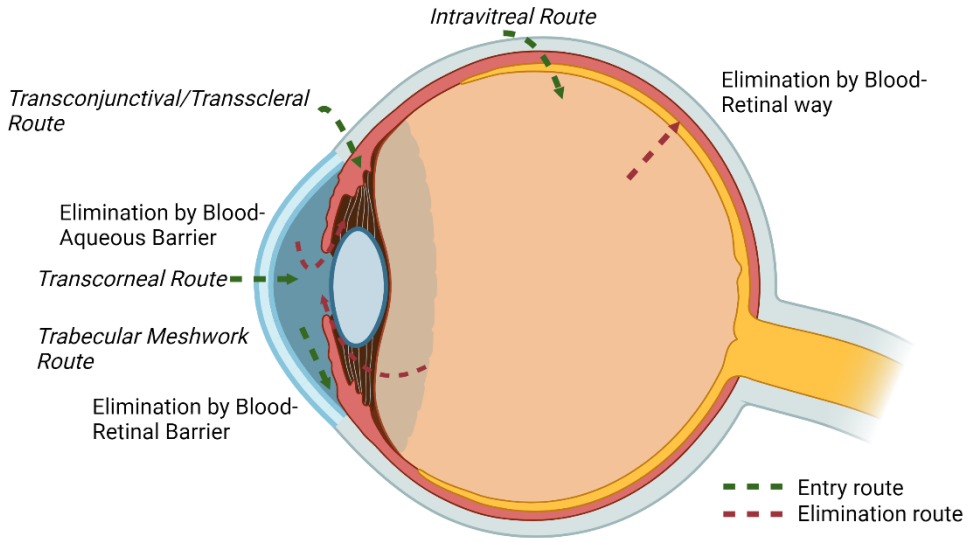

Figure 4. Entry and elimination routes for drugs in ocular tissues.

- <u>Transcorneal Route:</u>

The passage of the drug through the cornea depends not only on the structure and integrity of the cornea but also on the physicochemical properties of the drug and its formulation. Essentially, it is influenced by the octanol/water partition coefficient (Log P), which is related to the lipophilicity of the active ingredient, and the molecular weight, which provides information about the size of the molecule (Schoenwald & Ward, 1978). Considering the histological characteristics of the cornea, which, for practical purposes, can be equated to a structure formed by three zones of different polarity—lipophilic (epithelium and endothelium) and hydrophilic (stroma)—the penetration of any locally administered drug will be conditioned by its Log P. The Log P not only evaluates the amount of the drug distributed between the two phases but also determines the contribution of each layer of the cornea in the resistance posed by this structure to the

transcorneal penetration of drugs. The corneal epithelium provides the maximum resistance to the passage of drugs, acting as a barrier for 90% of hydrophilic drugs and 10% for lipophilic drugs. The main active ingredients penetrate this layer either through diffusion through the cells (transcellular route) or through the spaces between them in what is known as the paracellular route. The paracellular route predominates for hydrophilic drugs or low molecular weight ions, while the intercellular route predominates for lipophilic drugs (Prausnitz & Noonan, 1998; Schoenwald & Stewart, 1980).

- Transconjunctival/Transscleral Route:

The conjunctiva is a mucous membrane that covers approximately 80% of the ocular surface. It consists of a bulbar portion that covers the anterior part of the eyeball, except the cornea, and two palpebral portions on the posterior surfaces of the upper and lower eyelids. The conjunctival epithelium is composed of several layers of stratified epithelial cells (5 to 15 layers) and is covered by microvilli. The bulbar conjunctiva is covered by the tear film and contributes to its formation by secreting electrolytes, mucus, and glycoproteins. Similar to the cornea, the passage through the conjunctiva can occur through the transcellular or paracellular route. If we focus on the general properties of active substances, molecular size is the limiting factor for the paracellular route in both the cornea and the conjunctiva. On the other hand, the epithelial cells of the conjunctiva have the same intercellular junctions as the corneal epithelium known as "tight junctions", although the conjunctiva is more permeable to the passage of hydrophilic molecules. The subconjunctival route also presents itself as an alternative to intravitreal injections, which are more aggressive for the patient. This route aims to increase the intraocular concentration of the drug by reducing its administration frequency. For this purpose, subconjunctival implants and nano- and microparticles have been developed. Iontophoresis is a technique in which drugs penetrate the membrane in an ionized form through the application of an electric current, restricting it to active substances capable of ionizing. Nowadays, the access routes offered by the conjunctiva are under study (paracellular route, transcellular, active transport, or endocytosis) (Andrés-Guerrero & Herrero-Vanrell, 2008).

- Intravitreal Route:

The administration of drugs directly into the vitreous humor through an injection is carried out to ensure the drug reaches the interior of the eye with the appropriate concentration.

- Trabecular Meshwork Route:

Through the trabecular meshwork route, approximately 90% of the aqueous humor is drained. This traverses the trabecular meshwork and the Schlemm's canal before draining into the venous system. The contraction/relaxation of trabecular cells or changes in cellular volume modify the drainage of aqueous humor. Drugs that use this route usually target improving the functionality of this pathway due to its deterioration (Gasull, 2003).

1.4. PHARMACEUTICAL EVALUATION OF TOPICAL ADMINISTRATION DRUGS

Topically administered drugs are generally designed to exert a local effect on the skin or mucous membranes upon superficial application. The goal is to maximize the drug concentration at the site of action with minimal systemic absorption. The assessment of topical bioavailability is essential to evaluate its toxicity and effectiveness.

1.4.1. Methods for Release and Permeation Studies

To determine if the transdermal route can be an alternative to the oral route, and if the drug meets the basic requirements for formulating a transdermal administration system, two types of study methods are employed: in vivo and in vitro methods.

The most common in vitro studies involve the use of diffusion cells, which allow determining the amount of drug that has diffused through the selected barrier, as well as studying the amount of drug that has penetrated it. In these methods, both animal or human skin/mucosa and artificial membranes (artificial skin) are used for permeation studies, and different types of membranes are used for release studies. The diffusion cells used can be vertical diffusion cells (Franz diffusion cell or flow-through diffusion cell) and horizontal side-by-side diffusion cells (Ussing diffusion cell or Sweetana-Grass diffusion cell) (S. Wang et al., 2021).

The Franz diffusion cell is a static single-chamber diffusion chamber, consisting of the half upper part named donor chamber and the half lower part named receiver chamber, with the selected barrier in between. In the donor chamber, the formulation with the concentration of the drug under study is applied, and the receiver chamber is filled with a receptor medium capable of dissolving up to 10 times the amount of drug present in the donor compartment; this characteristic is known as the Sink condition. The receptor medium will vary according to the physicochemical characteristics of the drug and the characteristics of the tissue used in the study. Magnetic stirrers are incorporated into the receiver chamber to constantly homogenize the medium. In Figure 5 we can see all the named parts from the Franz cell.

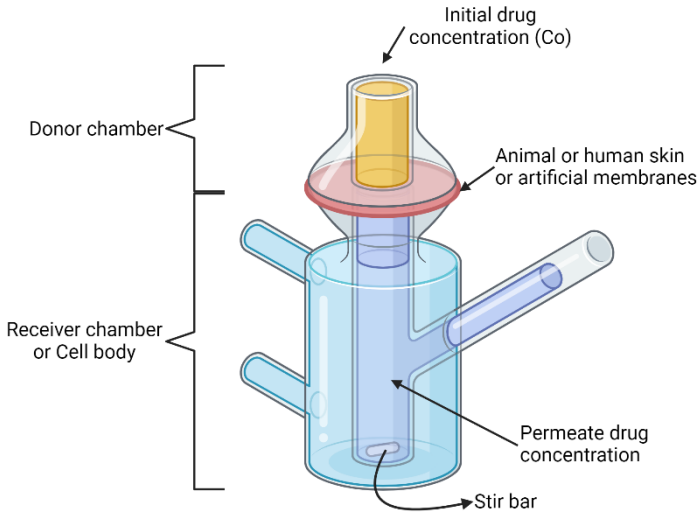

Figure 5. Franz cell diagram.

Finally, this system is coupled to a temperature-controlled jacket connected to a water or air circuit that allows controlling the assay's temperature, or in the absence of a jacket, the cells are immersed in a water bath. The cells are made of materials that react minimally with many chemical substances (glass or Teflon) to minimize interference with the substance under study (Hopf et al., 2020).

The Organisation for Economic Co-operation and Development (OECD) with the guidelines for in vitro skin absorption studies: Guidance Document 28 (GD28), Test Guideline 428 (TGD428) and Guidance Notes 156 (GN156). As well as the United States Food and Drug Administration (FDA), and the European Medicines Agency (EMA) have published various guidelines providing some recommendations for the evaluation of

topical products in in vitro release studies and in vitro permeation studies (European Medicines Agency, n.d.; Food and Drug Administration, 1997; Hopf et al., 2020; Zsikó et al., 2019).

Furthermore, with the values obtained in both release and permeation studies, various mathematical models can be used to describe the kinetics of drug absorption and release. The aim of these models is to accurately represent the processes associated with absorption/release, be able to describe and summarize experimental data with parametric equations and predict kinetics under variable conditions (Elmas et al., 2020).

Release studies are an important tool for the development of semi-solid pharmaceutical forms. This study allows evaluating the speed and degree of release of an active substance in the proposed formulation, thus determining the available quantity capable of reaching the skin and/or mucosa (Siepmann, 2001). For its execution, synthetic membranes and a receptor medium compatible with the formulation and the active substances under study are used, avoiding any significant degradation or binding phenomena during the assay (Zsikó et al., 2019).

On the other hand, in vitro permeation studies can have different objectives, ranging from studying the amount of drug that permeates the skin or mucosa and reaches the systemic circulation to evaluating the amount of drug retained in the tissue and/or determining its distribution in its different layers. In this case, guidelines recommend the use of human tissue; however, animal models are widely accepted during the research and development stages, where porcine skin has been suggested as an alternative due to its similar physiological characteristics.

The permeability can be performed at finite or infinite doses, as analytical limitations may require lower flux rates producing higher concentrations or longer time intervals. The selection of the dose also conditions the different treatment of the data from the samples obtained during the study and the usefulness of the data obtained. In infinite doses, a very high dose of drug/formulation is applied to the donor behavior, so that at the end of the permeation experiment, the concentration gradient between compartments is still maximum and constant.

In this thesis, we have worked with infinite doses to study the transdermal permeation of our drug. In this case, the variation in the concentration of the active ingredient in the receptor compartment is studied as a function of time. Data are obtained by withdrawing through the sampling arm at different time intervals according to the release/permeation rate of the substance of interest (with the recommended range being 6 to 12 points over 24 hours) (Hopf et al., 2020). By constructing a curve with these variations, it is possible to apply Fick's laws and obtain parameters reflecting penetration, such as the flux of the active ingredient (J) and the permeation or penetration constant (Kp). Figure 6 shows an example of Fick's law application.

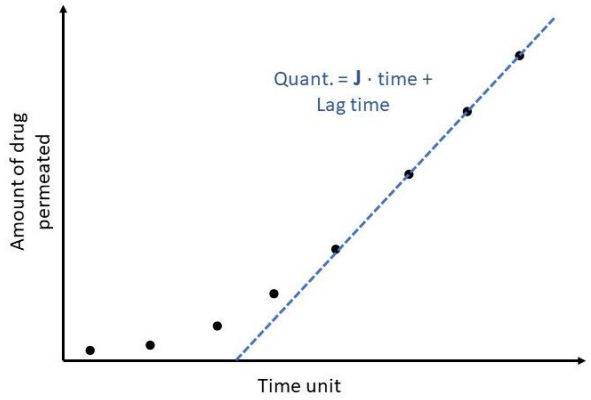

Figure 6. Example of a permeation study graph.

The slope of the line relating the quantity of permeated active ingredient to time is equivalent to J (mg/cm^2/h). The characteristics of the active ingredient that mostly influence the permeation rate are the distribution (K) and diffusion (D) through the membrane. The product of the two coefficients quantifying these properties (K and D) per unit of space traversed (L) of the membrane is defined as Kp (cm/h). The direct calculation of Kp as a function of D, K, and L is hardly viable, so with some substitutions and knowing the value of J, the value of Kp can be estimated, knowing the concentration of the active ingredient in the donor compartment (C_0) (mg/cm^3) with equation 2:

$$J = K_p C_0 \quad (2)$$

In the early stages of the release process, the curve formed will be convex and then transform into a straight line. This is because in the early stages, it is not in a steady-

state equilibrium. Over time, the permeation rate is constant, the curve is practically linear, and it reaches a steady-state equilibrium (points forming a straight line).

If the representative line of permeation in a steady-state equilibrium is extrapolated to the x-axis, the value of the accumulated active ingredient is zero, and the time at which this occurs is equal to the lag time (Tl) (point of intersection of the line with the x-axis). Consequently, Tl indicates the time it takes, from the start of the experiment, to reach a steady-state equilibrium.

Tl helps us subsequently calculate the Laplace transform coefficients to find the Mean Transit Time (MTT), which indicates the average time it takes for the drug to cross the skin. In equation 3, we can see the calculation:

$$MTT = \frac{V}{P_1 \times P_2 \times Ae} + \frac{1}{2 \times P_2} \quad (3)$$

Where V is the volume of the dose we put in the donor compartment, P_1 is the partition coefficient, P_2 is the diffusion coefficient, and A is the diffusion area of the membrane. P_1 and P_2 are calculated as expressed in equations 4 and 5:

$$Kp = P_1 \cdot P_2 \quad \text{and} \quad Tl = \frac{1}{6} \cdot P_2 \quad (4) \text{ and } (5)$$

In all types of tissues or artificial membranes, the equations to calculate the mentioned parameters will be the same.

In in vivo methods, the penetration capacity of locally applied formulations or drugs is estimated by evaluating the concentrations achieved in the systemic circulation or urine. Cutaneous biopsy represents another method that allows assessing the amount of drug that penetrates through the different structures of the skin over time. Both these and other in vivo methods have advantages and disadvantages in terms of quantification that can be resolved with the combination of one or more techniques for a more comprehensive study.

1.4.2. Techniques for Determining Drug Retention in Tissue

When the goal of our study is to achieve a local action, determining the drug retained in the different layers of the skin or mucous membranes is especially important, as it allows us to assess whether effective concentrations are reached at the therapeutic target.

There are numerous techniques, both qualitative and quantitative, for their determination.

Quantitative techniques include: (1) tissue homogenization and subsequent extraction and quantification of the drug. It is a quick and simple technique that allows the detection of low levels of drug penetration, although it does not provide specific localization. Therefore, separate extraction from the dermis and epidermis should be performed. Different methods of dermoepidermal separation exist, including chemical separation, enzymatic digestion, thermal separation, and mechanical separation (Touitou et al., 1998; Zou & Maibach, 2018). (2) *Tape stripping* involves estimating the amount of drug retained in the SC of the skin by applying adhesive tape on it, applying slight pressure to ensure good contact with the skin, and sequentially removing horizontal fractions of skin (0.5-1 mm) at increasing time intervals. The strips undergo subsequent extraction to recover the retained drug. The technique can be applied in vitro and in vivo, on human or animal skin. Additionally, estimating drug in the SC allows extrapolating by difference the quantity retained in the rest of the skin layers, or by determining the content in each layer, the mass balance can be established to verify the adequacy of the assay (Escobar-Chavez et al., 2008; European Medicines Agency, n.d.; Supe & Takudage, 2021; Zsikó et al., 2019). (3) Performing specific micrometer-thick tissue sections using a cryostat and subsequent analysis by imaging techniques such as confocal Raman microscopy or matrix-assisted laser desorption/ionization mass spectrometry (MALDI-TOF) (Bonnel et al., 2018; Franzen et al., 2013).

Qualitative techniques allow determining the bio-distribution of active ingredients and excipients in different regions of the skin and mucous membranes. Most of these techniques involve an initial tissue sectioning in different sections, marking, and subsequent analysis using spectroscopic techniques such as fluorescent microscopy or immunofluorescence.

1.4.3. Toxicity and Safety

The assessment of local effects must be carried out to understand the impact on the target tissue before the approval of a new product. In the case of topical administration, one of the most common adverse effects is irritation. Traditionally, the potential to

cause skin and mucous membrane irritation/corrosion has been evaluated through in vivo tests on the skin and mucous membranes of animals, mainly rabbits. Additionally, alternative in vivo methods have been described to identify the risk of irritation in human volunteers through the Patch test, where irritation is assessed at 24, 48, and 72 hours after the removal of the patch with the product of interest (Basketter et al., 2004; Draize et al., 1944).

In 1944, John H. Draize and his team, toxicologists at the FDA, developed the rabbit irritation tests to identify and evaluate toxic reactions when test materials come into contact with the skin, penis, or eyes. The Draize test was initially used to assess the safety of cosmetics and later extended to insecticides, sunscreens, and antiseptics. As the Draize test has been employed for various types of chemicals, it remained a reliable, standardized, and internationally accepted method for eye and skin irritation for a long time (Lee et al., 2017).

The Draize eye irritation test observed changes in the cornea, conjunctiva, and iris of the rabbit's eye due to exposure to test substances. The New Zealand White rabbit is commonly used as the preferred test variety because of its large eyes, ease of handling, and relatively low cost. For a test substance, a maximum of 6 rabbits is required, but this can be reduced to 3 when severe eye damage occurs. Depending on the physical state of the test substances (liquid, ointment, paste, or solid), 0.1 ml or 0.1 g of the chemical product is applied to the cornea and conjunctival sac of a conscious rabbit eye, while the other eye remains untreated to serve as the negative and paired control. Signs of eye irritation, including redness, swelling, cloudiness, edema, and hemorrhage, are recorded, and scored to assess ocular irritation at specified time intervals, and once the study is completed, the rabbits are humanely sacrificed. Although there are various scoring systems for the Draize test, the Maximum Average Score (MAS) is the most used. The eye is examined at selected time intervals after exposure, and lesions and changes in the cornea, conjunctiva, and iris are scored (Lee et al., 2017).

The skin irritation test is performed on albino rabbits one day after shaving their backs. The test substance (0.5 g solid or 0.5 ml liquid) is applied to a small area (~6 cm^2), and the treated site is covered with a patch. The patch is removed after 4 hours, and the signs of erythema and edema are scored at 1, 24, 48, and 72 hours. For the initial test,

one animal is used, and the test site is examined immediately after removing the patch. If the test substance is not corrosive, the confirmation test is carried out with 2 additional animals. Erythema and edema are scored on a scale of 0 to 4 based on severity. Histopathological examination should be considered to clarify equivocal responses (Lee et al., 2017).

The Draize skin and eye irritation test has been criticized for a significant variation in test results and the species difference between humans and rabbits. Additionally, this test imposes intense pain on the rabbit during the testing procedure. To reduce animal suffering from test chemicals in ocular irritation, the Low Volume Eye Test (LVET) was developed, a refined version of the Draize test. LVET applies a lower volume (0.01 ml/0.01 g) of test substances only to the cornea without forced eyelid closure. In fact, LVET shows a higher correlation with human eye responses than the original test. For skin irritation, alternative parameters to erythema and edema have also been developed, such as assessing cutaneous blood flow, measuring skin temperature, and skin thickness evaluation (Lee et al., 2017).

The Hen's Egg Test-Chorioallantoic Membrane (HET-CAM) is an example of non-ocular ex vivo organotypic models. These methods use the chorioallantoic membrane (CAM), which resembles the vascular mucosal tissues of human eyes, and can examine the effects of test substances on the conjunctiva. HET-CAM assesses hemorrhage (bleeding), vascular lysis (blood vessel disintegration), and coagulation (protein denaturation intra- and extravascular) on the CAM on the 9th day of fertilization when nervous tissue and pain perception have not yet developed. The reaction time method is commonly used, determining the time to each of the 3 endpoints. Another approach is the irritation threshold method, which estimates the threshold concentration of the test material for these parameters.

The process involves the removal of the shell from the air cell and extraction of inner membranes to expose the chorionallantoic membrane. Subsequently, test chemicals are applied to this membrane and left in contact for 5 minutes. The evaluation focuses on observing vascular damage and recording the time it takes for injury to manifest. The severity and speed of damage determine the irritancy score. The 5-minute exposure

period has been established as sufficient to detect irritant or toxic effects, with longer exposures not providing additional insights (Spielmann, 1995a).

It's important to consider whether the hen's egg test qualifies as an animal experiment, as it is often viewed as borderline. Nevertheless, there is potential for its use to reduce the number of mammals used in traditional testing, thus contributing to a decrease in associated suffering (Spielmann, 1995a).

To quantify the results, the time taken for each reaction is measured in seconds, and an irritation score (IS) is calculated as expressed in equation 6.

$$IS = [\frac{301 - \sec H}{300}] * 5 + [\frac{301 - \sec L}{300}] * 7 + [(\frac{301 - \sec C}{300}] * 9 \quad (6)$$

The determination of the threshold involves recording the severity of each reaction based on a scale: 0 for no reaction, 1 for slight reaction, 2 for moderate reaction, and 3 for severe reaction (Spielmann, 1995a).

HET-CAM shows a good correlation with the Draize eye test for mild and non-irritating test materials, including surfactants. However, solid and insoluble or adhesive materials may pose challenges for reproducibility. Additionally, pigments and dyes can cause interference (Lee et al., 2017). In Figure 7 we can see the diagram from both tests.

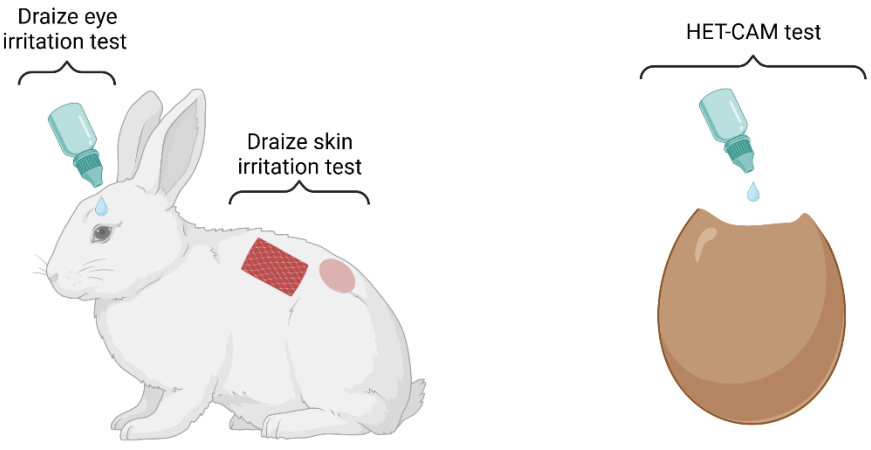

Figure 7. Graphic example of the different tests mentioned above: Draize eye irritation test, Draize topical irritation test, and HET-CAM test.

1.5. AUTOIMMUNE DISEASES – DESCRIPTION, CLINICAL FEATURES, DIAGNOSIS AND TREATMENTS

1.5.1. Immune System

The immune system has evolved over millions of years and serves as the body's defense against viruses, bacteria, other invaders, and malignant cells (Cardona Villa & Serrano Reyes, 2010).

It's important to note that the immune system, as we understand it, constitutes the second and third lines of defense for the body. The first line of defense consists of various physical barriers such as the skin and mucous membranes, the acidic pH of the stomach, enzymes, and microbicidal molecules secreted by various cell types, as well as some microorganisms residing in the body.

The skin acts as the first line of defense through the SC, providing mechanical protection to the underlying epidermis and acting as a barrier to prevent water loss and the invasion of foreign substances. Continuous desquamation, along with the dermis's ability to produce chemical substances such as defensins (peptides), protects the skin from microbial entry. Additionally, the SC harbors most of the cutaneous microbiota, which is necessary for homeostasis and the maintenance of healthy skin, playing a significant role in the development and regulation of the immune system. Alterations in the structure of the SC are associated with the onset of diseases such as AD, psoriasis, or congenital disorders like ichthyosis.

When microorganisms breach the barriers of the first line of defense, they encounter the second line, the innate immune system, and if that is insufficient, the third line, the adaptive immune system (Grammer & Greenberger, 2011).

The innate immune system is represented by phagocytic cells: monocytes/macrophages, granulocytes, specifically neutrophils, and the so called Natural Killer (NK) cells. The humoral component or complement consists of acute-phase proteins capable of directing lysis and opsonization on biological membranes of invaders but not the body's own due to strict control by soluble proteins and membranes (Paola, 2012).

The adaptive immune system includes the lymphocytic cell lines (T and B cells) and the humoral component with specific antibodies. There are at least five characteristics that define the adaptive immune response. First, the responses are specific to different antigens or pathogens; second, the responses are diverse; third, after the initial exposure to an antigen, the responses retain a memory, so upon a new exposure to the antigen, a stronger, longer, and more effective immune response is generated; fourth, most immune responses are self-limiting after the elimination of the antigen. Finally, the immune response allows distinguishing between the same organism and different organisms (Cardona Villa & Serrano Reyes, 2010).

In a healthy individual, the immune system can differentiate between what is self and what is not, attacking only what does not belong directly to our body in the right intensity. Malfunction of the immune system can lead to an overly intense reaction that results in the destruction of the body's own tissues and cells or, conversely, an insufficient reaction that fails to solve the problem. These situations are referred to as autoimmune disorders (Ganapathy et al., 2017).

Autoimmune disorders are a group of conditions in which structural or functional damage to cells/tissues/organs/organ systems caused by immune cells or antibodies against normal components of the body. This situation can arise from the interaction of various genetic, environmental, and endocrine factors in our immune system through the following mechanisms (Ganapathy et al., 2017):

1. Release of tissue-specific antibodies through complement initiation leading to the lysis of target cells.
2. Binding of antibodies to soluble mediators resulting in the deposition of immune complexes.
3. Attack mediated by autoantibodies in the natural immune system resulting in phagocytosis, cytotoxicity, and cellular immunity.
4. Autoantibodies directed against a foreign antigen and epitopes of autoantigens mimicking the foreign antigen, causing tissue damage.
5. Action of autoantibodies on the surface of cellular structures resulting in the stimulation/obstruction of the target structure.

Examples of autoimmune diseases or disorders include Pemphigus Vulgaris, ***Sjögren's Syndrome (SS)***, Behcet's Disease, Psoriasis, Systemic Lupus Erythematosus, Rheumatoid Arthritis, and ***Atopic Dermatitis (AD)***. Figure 8 shows an example of four the six just mentioned pathogenesis.

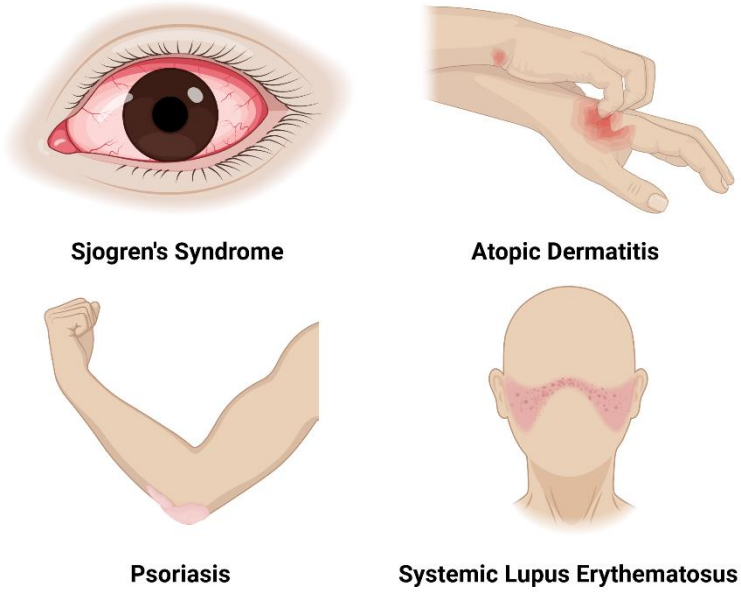

Figure 8. Examples of symptomatology of different topical autoimmune diseases.

1.5.2. Atopic Dermatitis (AD)

AD is the most common inflammatory skin condition in the pediatric population. Its prevalence has consistently increased over the past 200 years, reaching 12% in children and 7.2% in adults, leading to a high healthcare burden. AD typically begins in childhood, with 60% of patients developing AD before the age of one and 90% before the age of five (Sroka-Tomaszewska & Trzeciak, 2021a). A complex set of risk factors, including irritants, contact and inhalation of allergens, stress, and infections, contribute to the development and persistence of AD. Clinically, AD is characterized by itching, skin inflammation, abnormalities in the skin barrier, and an increased susceptibility to skin infections. This condition negatively impacts the quality of life of affected children and their caregivers, leading to a decrease in their self-esteem as well as an increase in depression, anxiety, and suicidal thoughts (Adler-Neal et al., 2019).

AD is a complex disease with a heterogeneous clinical picture, involving a multitude of overlapping factors in its pathogenesis. Data suggest that extrinsic environmental

factors work together with intrinsic mechanisms such as mutations in epidermal genes, dysfunction of the skin barrier, immune disorders, changes in lipid composition, and skin microbiome imbalance. It has been observed that children with a family history of allergic diseases are at a higher risk of developing AD. In the case of parents with asthma, allergic rhinitis, or food allergies, the risk of the child developing AD increases up to 1.5 times. When one parent has AD, the probabilities for the child triple, and if both parents are affected, these probabilities quintuple. Moreover, it is not a Mendelian inherited disease; genes related to AD are also subject to different inheritance phenomena such as epigenetic changes, incomplete gene penetrance, and genomic imprinting (Sroka-Tomaszewska & Trzeciak, 2021b).

The diagnosis of AD is made clinically and is based on historical features, morphology, and distribution of skin lesions, as well as associated clinical signs. A consensus conference in 2003 led by the American Academy of Dermatology suggested the "Hanifin and Rajka" revised diagnostic criteria as the guidelines to follow at all ages. In Table 1, an array of distinct criteria employed for the diagnosis of AD is delineated.

Table 1. Adapted from the "Guidelines for the Treatment of AD" (Eichenfield et al., 2014).

Essential features; they must be present:
Itching Eczema (acute, subacute, chronic): - Typical morphology and age-specific patterns. - Chronic or relapse history Patterns include: 1) Face, neck and extensors in infants and children. 2) Current or previous injuries in flexion zones in any age group. 3) The groin and armpit areas are affected.
Important features; Seen in most cases, they provide support to the diagnosis
Age of onset. Atopy: - Personal and/or family history. - Reactive IgE Xerosis
Associate features; they help suggest the diagnosis of AD but are not enough to define or detect AD in search or epidemiological studies.**:**
Atypical vascular responses (ex: facial paleness, white dermographism, delayed paleness response) Keratosis pilaris/ Pityriasis alba/ Palmar hyperlinearity/ Ichthyosis Ocular/periorbital changes Other regional meetings (ex: perioral changes/periauricular lesions) Perifollicular accentuation lesions/lichenification/prurigo
Exclusion features; they must not be present:
Scabies Seborrheic dermatitis Contact dermatitis (irritant or allergic) Ichthyosis Cutaneous T cell lymphoma Psoriasis Photosensitivity dermatosis Immune deficiency diseases Erythroderma of other causes

Looking at the pathogenesis of the disease, AD involves the disruption of the protein and lipid barrier in the outer layers of the epidermis, reflecting primarily a decrease in the expression of epidermal differentiation proteins (e.g., filaggrin) and tight junctions (the main barrier against transepidemal water loss (TEWL); e.g., claudins), as well as a decreased concentration of long-chain fatty acids and ceramides. The dysfunctional barrier leads to increased susceptibility to external aggressions, such as proinflammatory microbes and allergens, toxins, and irritants. In adults, the reduced production of antimicrobial peptides (AMPs) in response to stimuli alters the normal defensive response to environmental pathogens, and the reduction of type 1 cytokines from T helper cells (Th1) may diminish the antimicrobial response in affected children.

Antigen-presenting cells capture antigens to present them mainly to CD4+ T cells, and keratinocytes directly release chemokines and cytokines such as interleukins (IL): IL-1β, IL-25, and IL-33. The initiation of chemokines and cytokines induces the release of additional cytokines, and their contribution to heightened oxidative stress underscores their significance in chronic inflammation. This inflammatory environment results in an immune response predominantly skewed towards Th2 cells, leading to increased amounts of characteristic Th2 cytokines such as IL-4, IL-5, IL-13, and IL-31. Th2 cytokines, especially IL-4 and IL-13, contribute to further polarization of Th2 cells, promote the switch of antibody isotype towards Immunoglobulin E (IgE), a specific class of mammal antibodies IgE, and recruit eosinophils that continue to impair the epidermal barrier function by inhibiting its differentiation, lipid production, and AMP expression. Although Th2 skewing is universal among patients with AD, the activation of other T helper cell-driven pathways (e.g., Th1 in adults, Th17 in children and Asians) is more heterogeneous and may be related to other patient factors, such as age and race. Many of the same exogenous signals (allergens, irritants, pathogens) and endogenous signals (cytokines, neuropeptides, lipids) act as pruritogens and directly modulate and/or sensitize the itching sensation. Activation of cytokine receptors (e.g., IL-4, IL-13, IL-31, IL-33, TSLP), G protein-coupled receptors, and transient receptor potential channels results in action potentials, which propagate sensory information to the central nervous system and stimulate the local production of inflammatory mediators such as calcitonin gene-related peptide and substance P.

Janus kinase (JAK) proteins and signal transducers and activators of transcription (STAT) factors bind to the intracellular part of type I/II cytokine receptors that are responsible for recognizing soluble inflammatory mediators such as IL and INF. Upon binding an extracellular ligand to the cytokine receptor, JAK proteins become activated and phosphorylate STAT proteins, which in turn dimerize and translocate to the nucleus. There, they activate gene transcription. There are four members of the JAK family (JAK1, JAK2, JAK3, and non-receptor tyrosine-protein kinase (TYK2)) and seven additional members of the STAT family that selectively associate with different cytokine receptors in various combinations. The JAK-STAT signaling pathway is crucial for measuring the effect of various key cytokines that bind to immune cells, keratinocytes, and peripheral sensory neurons to propagate inflammation and itching, including IL-4, IL-5, IL-13, IL-31, IL-22, and thymic stromal lymphopoietin (TSLP) (Chovatiya & Paller, 2021).

The treatment of this disease will depend on the degree of manifestations present in the patient. It is crucial to be aware of the causative factors to avoid them and reduce relapses (Wollenberg et al., 2018). The European Academy of Dermatology and Venerology classifies different treatments based on the severity of symptoms: erythema, exudation, excoriation, dryness, fissures, and lichenification. Both in children and adults, it begins with proper skin care education, and depending on the signs, topical or oral glucocorticoids, systemic immunosuppressants, and progressively more intensive therapies are added (Oranje, 2011).

1.5.3. Sjögren's syndrome (SS)

The SS is a chronic autoimmune systemic rheumatic disease that can occur alone, known as primary SS, or in the context of another underlying connective tissue disease, most commonly rheumatoid arthritis or systemic lupus erythematosus, referred to as secondary SS. It has a clear preference for the female gender (ratio 9:1), with a prevalence rate ranging from 0.1 to 4.8% of the total female population. It can start at any age but more frequently affects women between the fourth and fifth decades of life.

SS involves a lymphocytic infiltration of the salivary and lacrimal glands leading to secretory dysfunction mediated by the immune system. It is characterized by symptoms

of dry mouth (xerostomia) and dry eyes (dry keratoconjunctiva), dysfunction of lacrimal and salivary secretory glands, ocular surface staining, autoantibodies, and focal infiltration of lymphocytes in salivary and lacrimal glands. Dry eye, a very common condition, may or may not be related to the syndrome. The distinctive feature of dry eye due to SS is the alteration of the corneal barrier clinically measured as increased uptake of fluorescent dyes like fluorescein (de Paiva & Rocha, 2015). In both primary and secondary SS, symptoms can be diffuse and misleading, leading to incorrect diagnoses. Approximately half of those affected may not receive a diagnosis, and the subtle symptomatic presentation, especially in the early stages, results in a significant delay in diagnosis and underreporting, with an average time elapsed from the onset of symptoms to diagnosis of three and a half years (Nair & Singh, 2017).

The classification criteria for primary SS include clinical manifestations and objective tests related to dry eyes and dry mouth, characteristic serological abnormalities (presence of Anti-Ro/SSA and/or Anti-La/SSB antibodies), and compatible histopathology (focal lymphocytic sialadenitis) of the minor salivary gland. Currently, the most used classification criteria are the European-American consensus criteria of 2002 (López-Pintor et al., 2015).

Nowadays, the burden of this disease is substantial due to the lack of effective therapeutic options. The pathogenesis is multifactorial and involves dysregulation of various immune pathways. Patients with primary SS have shown higher expression of B-cell activating factor (BAFF), also known as B-lymphocyte stimulator (BLyS), in serum and salivary glands compared to controls. This factor stimulates the growth and hyperactivity of B cells, suggesting an important role of these cells in the pathogenesis of this disease with lymphoproliferative complications (López-Pintor et al., 2015).

The mechanism by which SS develops is not clear, and various factors seem to contribute to the progression of the condition. Essentially, in the presence of a genetic predisposition and an environmental or hormonal trigger, glandular epithelial cells become dysregulated and release chemokines and adhesion molecules. This triggers the migration of dendritic cells and lymphocytes (T cells and B cells) to the glands. Dendritic cells in the glands produce high levels of interferons (IFN), leading to increased retention of lymphocytes in the tissues and their subsequent activation. IFNs stimulate the

production of BAFF by epithelial cells, dendritic cells, and T cells. BAFF promotes the irregular maturation of B cells, leading to the formation of autoimmune B cells that secrete local autoantibodies (Voulgarelis & Tzioufas, 2010).

Despite continuous advances in our understanding of the mechanisms involved in the pathogenesis of the disease, there is currently no targeted treatment for SS, as mentioned earlier. Treatment is decided on an individual basis depending on the activity of the disease and the presence and extent of extraglandular manifestations. In patients with secondary SS, the indication for treatment is based on the underlying disease. In general, a multidisciplinary team, including family doctors, rheumatologists, ophthalmologists, and specialists in chronic diseases, as well as dentists, should be involved in the treatment. Depending on the affected organ or organs and the symptoms presented, consultation with other specialists (gynecologists, pulmonologists, neurologists, etc.) may be necessary. To measure the activity of systemic disease, the EULAR SS disease activity index (ESSDAI) was developed and validated (Stefanski et al., 2017).

In most patients, the primary goal of therapy is to improve the quality of life by addressing the symptoms. At the same time, this is a challenging task for physicians, as evidence-based treatment options are limited, and most therapeutic approaches are only symptomatic. Patient education plays an important role, focusing on compliance with daily behavioral rules, addressing environmental factors (e.g., air humidification), prevention (e.g., sleep hygiene), as well as physical condition (aerobic resistance training to combat fatigue) (Stefanski et al., 2017).

There are several tears substitutes available to treat keratoconjunctivitis sicca. The composition of tear substitutes varies according to the complex physiology of the preocular three-layer tear film (lipid layer, aqueous layer, and mucin layer). Since immunity-mediated mechanisms play a central role in the pathogenesis of dry eyes, anti-inflammatory treatment with cyclosporine A eye drops has gained significant importance. Its efficacy has been demonstrated in randomized controlled trials (RCTs), and based on the data from these studies, the 0.1% cyclosporine A cationic emulsion received marketing authorization from the EMA. Additional measures that significantly enhance the quality of life for these patients include the use of punctal plugs in the tear

drainage area to retain tears and the placement of extra-large contact lenses ("scleral lenses") with water storage function (Stefanski et al., 2017).

In Figure 9, we can see two of the mentioned examples for the treatment of SS.

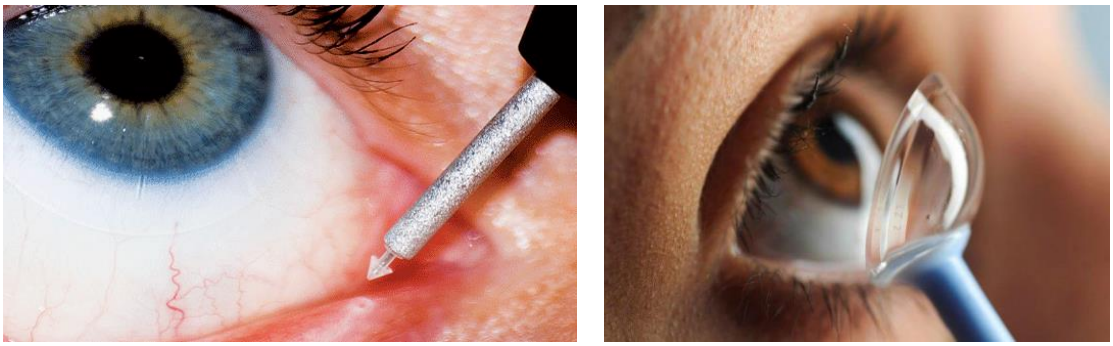

(a) (b)

Figure 9. (a) Punctual plugs for ocular drainage. (b) Scleral lenses. Image (a) has been obtained from the Online Patient Community for Dry Eye (Nguyen & Maharaj, 2020) and image (b) has been acquired from the Weston Contact Lens Institute (Kramer, 2022).

Xerostomia is treated jointly by dentists and otolaryngologists. The surface of the oral mucosa is relatively large, and it is necessary to moisten different structures of the oral cavity (tongue, teeth, gums, oral mucosa). Additionally, the composition of saliva varies according to function and time of day. Optimal therapeutic compensation for the complex functions of saliva cannot be achieved. Two systematic reviews on topical/non-pharmacological treatments conclude that, although symptoms can be relieved, saliva flow cannot be increased. Dental care for patients with xerostomia is particularly challenging as the lack of saliva reduces the tolerability of removable dental restorations. In contrast, patients with SS achieve good results with dental implant treatment (Stefanski et al., 2017).

Treatment for advanced stages of SS may require surgeries to improve ocular hydration or systemic treatments such as hydroxychloroquine, sodium mycophenolate, pilocarpine, and/or omega-6 (Bjordal et al., 2020).

1.5.4. Immunosuppressants and Baricitinib (BNB)

Immunosuppressive drugs help inhibit or decrease the intensity of the immune response in the body. They are most commonly used in organ transplants, where it is necessary to prevent the activation and rejection of the newly transplanted organ.

Advanced knowledge of signal transduction pathways has led to the development of drugs like small molecule inhibitors that target intracellular cytokine pathways, providing a pharmacological alternative to biologic products. Although biologic products have been a significant advancement in immunotherapy due to their high selectivity and therapeutic efficacy, they do not elicit the same response in all patients. BNB, whose structure is shown in Figure 10, is an example of an alternative proposed to biologic products.

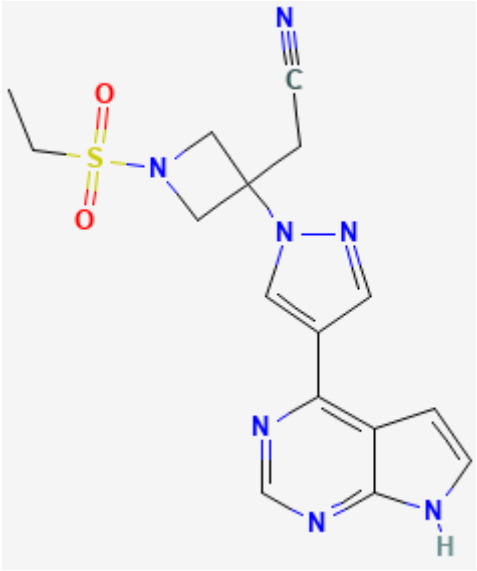

Figure 10. Structure of BNB obtained from the PubChem open database belonging to the National Institutes of Health of the United States (NIH).

The JAK-STAT pathway operates under the influence of more than 50 cytokines and growth factors and is considered a central communication point for the immune system. There are 4 JAKs: JAK1, JAK2, JAK3, and the TYK2. It is the specific combination of JAK and STAT that determines the functional outcomes of cytokine receptor stimulation (Bechman et al., 2019).

The JAKs, more specifically, are enzymes that transduce intracellular signals from cell surface receptors to produce a series of cytokines and growth factors involved in

hematopoiesis, inflammation, and immune function. The presence of BNB decreases, therefore, these three mentioned actions.

In Figure 11, we have a diagram where we can see the different reactions that occur in a cell in the presence or absence of BNB.

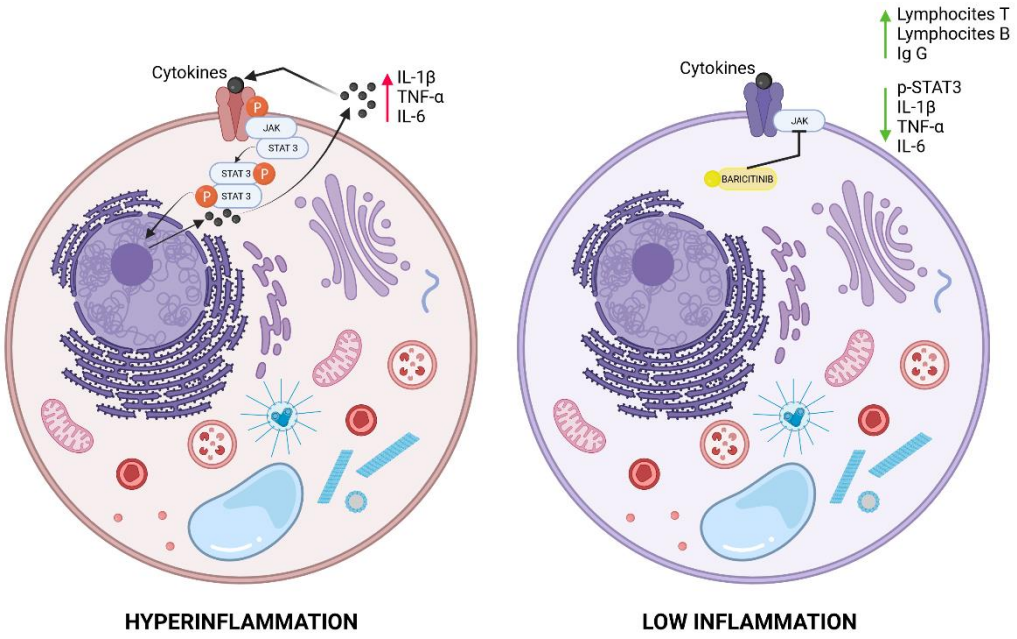

Figure 11. Scheme of the mechanism of action of BNB.

BNB dose-dependently inhibits the phosphorylation of IL-6-induced STAT3 throughout the bloodstream of healthy volunteers, with a maximum inhibition observed 2 hours after administration, returning to a near-baseline state at 24 hours (Committee for Medicinal Products for Human Use (CHMP), 2020).

BNB is characterized by its low water solubility (0.357 mg/mL), making it challenging to develop various formulations containing it; however, it has high solubility in organic solvents such as DMSO and polyethylene glycol-400 (PEG-400) (Alshetaili, 2019; Anwer et al., 2021).

Currently, BNB is used orally for the treatment of moderate to severe AD, rheumatoid arthritis, COVID-19, and has recently been approved for the treatment of alopecia areata in adults. It is also being studied for the treatment of Systemic Lupus Erythematosus (Committee for Medicinal Products for Human Use (CHMP), 2020; Markham, 2017; Wishart et al., 2023). Its oral administration is performed using tablets of 2 to 4 mg concentration.

1.6. NANOSYSTEMS

Various methods have been developed to enhance drug permeation through the skin: physical methods, manipulation of the SC, release systems, optimization of the drug or the vehicle, and the combination of strategies. Within release systems, one of the most commonly used strategies today is the development of nanoscopic systems: nanovesicular and nanoparticulate systems as dermal and transdermal administration systems. Their dermal and transdermal administration is justified by different factors. On the one hand, they have the advantage of protecting the substance they contain, increasing the drug's shelf life. On the other hand, these systems could act as penetration enhancers and also function as reservoirs for sustained release.

These systems have shown an increase in drug absorption, penetration, half-life, bioavailability, and stability. Thanks to their size, which is not perceptible by the immune system, they can release the drug into the target tissue using lower doses.

Nanomedicine is an emerging field that combines nanotechnology with pharmaceutical and biomedical sciences. One of the goals is to develop nanoparticles (NPs) for biomedical applications, such as drug delivery vehicles and imaging agents with higher efficacy and improved safety and toxicology profiles. Due to their submicrometer size and high surface-to-volume ratio, NPs exhibit key differences compared to bulk materials, including changes in biochemical, magnetic, optical, and electronic properties(Albanese et al., 2012; Barenholz, 2012a; Flühmann et al., 2019; Khodabandehloo et al., 2016; Tenzer et al., 2011). NPs are colloidal systems with sizes ranging from 10 to 1000 nm (Zimmer & Kreuter, 1995).

NPs can be made from a wide variety of materials, including proteins, peptides, polymers, lipids, metals and metal oxides, and carbon. The most relevant NP structures include drug conjugates and complexes, viruses, dendrimers, vesicles, micelles, core-shell structures, virus-like particles, and carbon nanotubes, among others (Janib et al., 2010; Kewal K., 2008). Typically, NPs are classified based on their composition and materials. Thus, NPs can be categorized as inorganic NPs, polymer-based NPs, lipid-based NPs, and protein-based NPs (Gu et al., 2011; B. Kim et al., 2019; Wicki et al., 2015).

- Inorganic NPs are primarily composed of metals or metal oxides and have generated considerable interest due to the ability to adjust their size and modify their surface (Qin et al., 2019). Their production is highly controllable, allowing for a wide variety of inorganic NPs with different properties (Qin et al., 2019).
- Protein-based NPs are composed of proteins or modified proteins, which can self-assemble into larger structures (Unzueta et al., 2015). This provides an advantage over other NPs, as the protein's own structure can act as both the targeting unit and the vehicle.
- Polymer-based NPs are utilized in biomedical applications due to the biocompatibility and biodegradability of their main components, the polymers(Qin et al., 2019). These NPs are solid structures whose surface can be easily functionalized with desired molecules to alter their properties (Gu et al., 2011; Qin et al., 2019).
- Lipid-based NPs are composed of natural or synthetic lipids (Grimaldi et al., 2016). This type of NP can be easily functionalized with certain ligands or molecules to acquire new properties (Puri et al., 2009).

1.6.1. Nanovesicles

Within lipid-based NPs, we find nanovesicles. Nanovesicles are primarily composed of amphiphilic molecules that self-assemble into closed bilayer structures, enclosing an aqueous core inside (Grimaldi et al., 2016; Immordino et al., 2006; Qin et al., 2019). Nanovesicles can be divided depending on the nature of the membrane components. Liposomes are one of the main types of vesicles, whose amphiphilic molecules are mainly phospholipids (Bulbake et al., 2017a; Cabrera et al., 2016; Immordino et al., 2006). They can carry hydrophobic or hydrophilic molecules (Elizondo et al., 2011; Grimaldi et al., 2016).

Nanovesicles are one of the types of NPs that are gaining attention for drug administration via intravenous and for the development of fluorescent organic NPs (FONs) for optical imaging. As explained before, nanovesicles are lipid-based NPs that are spherical complexes formed by amphiphilic molecules. When amphiphilic molecules are dispersed in water, they self-organize to form a closed bilayer, encircling a liquid compartment inside (lumen) (Islam Shishir et al., 2019; Lipowsky & Sackmann, 1995;

Whitesides & Grzybowski, 2002). Amphiphilic molecules have at least two parts, one that is soluble in a solvent (the hydrophilic part) and one that is insoluble (the hydrophobic part). When the solvent is water, it is usually referred to as the hydrophilic (water-soluble) and hydrophobic (water-insoluble) parts. Generally, the hydrophobic region consists of one or two hydrocarbon tails, and the hydrophilic region is typically a polar head, which may be ionized or not. When in contact with water, these types of molecules orient themselves, protecting the hydrophobic tails from water and exposing their polar head towards water, forming closed bilayers (Elizondo et al., 2011; Lipowsky & Sackmann, 1995).

Depending on their size and the number of bilayers (lamellarity), as we can see in Figure 12, vesicles can be classified as: small unilamellar vesicles (SUVs, size <200 nm and a single bilayer), large unilamellar vesicles (LUVs, size ranging from 200 to 1000 nm and a single bilayer), giant unilamellar vesicles (GUVs, size >1000 nm and a single bilayer), multilamellar vesicles (MLVs, consisting of several concentric bilayers), and multivesicular vesicles (MVVs, composed of several small vesicles trapped inside larger ones). Size and lamellarity are crucial factors determining the performance of vesicles as drug carriers (Guida, 2010; Malam et al., 2009; Sawant & Torchilin, 2010).

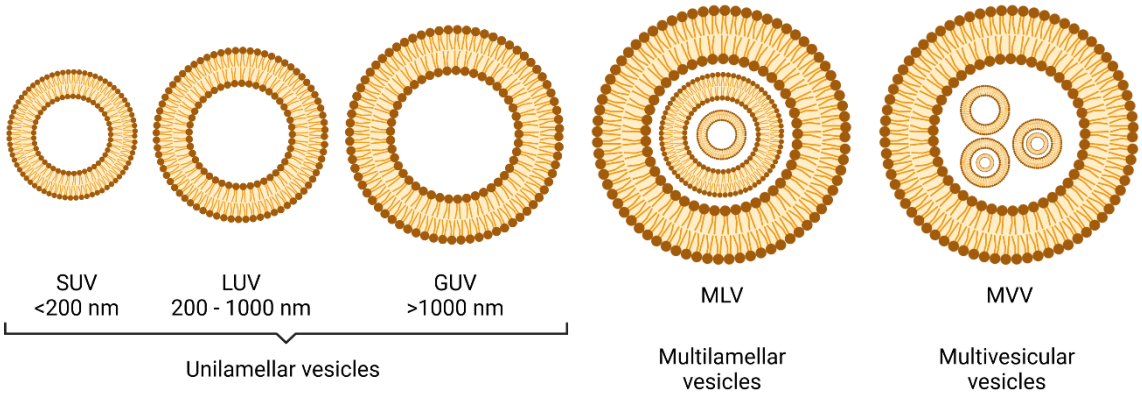

Figure 12. Scheme of the classification of different vesicles according to size and number of bilayers.

Nanovesicles are one of the most versatile supramolecular assemblies used as nano-carriers for therapeutic agents due to their great flexibility in terms of size, composition, surface characteristics, and the ability to trap and deliver active molecules with different

physicochemical properties (Cui et al., 2012; Metselaar & Storm, 2005; Sercombe et al., 2015).

Additionally, their structure allows them to trap hydrophilic compounds (such as therapeutic agents, proteins, or oligonucleotides) inside the lumen or adsorb to the surface, and hydrophobic molecules in the hydrophobic region of the bilayer (Cabrera et al., 2016; Immordino et al., 2006). Furthermore, their membranes can be efficiently functionalized with different targeting units that promote specific and enhanced accumulation of the active (or bioactive) molecule in target cells or diseased organs. Moreover, vesicles can be designed to develop stimulus-sensitive vesicle platforms that are responsive to specific signals, either exogenous (light, heat, magnetic field, etc.) or endogenous (changes in pH or specific enzymes), allowing the delivery of cargoes to specific locations (Cheng et al., 2013).

These characteristics make nanovesicles very attractive candidates for biomedical applications (Barenholz, 2012b; Gregoriadis, 1976, 1995; Islam Shishir et al., 2019; Lian & Ho, 2001). In fact, nanovesicles are one of the most studied NPs due to their versatility and applicability in pharmacological fields, as they are non-toxic, biodegradable, and non-immunogenic (Shen et al., 2019; Soltani et al., 2015). The pharmacological characteristics of nanovesicles strongly depend on their structural features. A high degree of structural homogeneity particle-to-particle, regarding size, morphology, and composition, is crucial for their optimal performance (Bremer-Hoffmann et al., 2018; Tambe et al., 2019).

The stability, rigidity and permeability, functionalization, and response to an external stimulus are regulated by the composition of the nanovesicle membrane and its supramolecular organization. Thus, the behavior of nanovesicles is closely related to their homogeneity in vesicles, both in size and morphology, as well as in composition and supramolecular organization (Elizondo et al., 2011). For example, in the case of nanovesicles used as drug delivery systems, vesicle-to-vesicle homogeneity in terms of size and lamellarity plays a crucial role in providing a precise response to an external stimulus, allowing for the homogeneous release of drugs at the site of action. In fluorescence imaging applications, nanovesicles must be homogeneous in terms of the

loading of their fluorescent dye to ensure that all nanovesicles have the same brightness.

Vesicles can be classified based on the nature of the membrane components. Table 2 summarizes the most well-known types of vesicular systems with their membrane components.

Table 2. Types of lipid-based vesicular systems according to the components of their membrane.

Kind of vesicle	Membrane components
Liposomes	Phospholipids (and cholesterol)
Transferosomes	Phospholipids and surfactants
Ethosomes	Phospholipids and alcohols
Pharmacosomes	Phospholipids and drugs
Virosomes	Phospholipids and viral envelope protein
Ufasomes	Fatty acids and surfactants
Sphigosomes	Cholesterol and sphingolipids
Niosomes	Cholesterol and no ionic surfactants
Quatsomes	Cholesterol and ionic surfactants

1.6.1.1. Liposomes – Properties, Applications, Preparation, and Characterization

Liposomes are the most widely used vesicular systems (Bulbake et al., 2017b; Musacchio & Torchilin, 2011; Torchilin, 2005; Xing et al., 2016). Liposomes were discovered in 1964 by Dr. Alec Bangham and others (Bangham et al., 1965; Bangham & Horne, 1964). Over the past fifty years, liposomal nanotechnology has evolved significantly, and now liposomes are used in various fields beyond the pharmaceutical world, including cosmetics, food, and textiles (Barani & Montazer, 2008; Fathi et al., 2012; Papakostas et al., 2011). Moreover, due to their biocompatibility, biodegradability, and low toxicity, liposomes are well-recognized and applied as pharmaceutical carriers. Relevant pharmacological specifications, such as loading capacity, leakage kinetics, and release of

integrated drug substances, are defined based on the structural properties (e.g., size distribution of vesicles, morphology, supramolecular organization) of these nanocarriers (Amin et al., 2015; Arosio & Casagrande, 2016; Liu et al., 2016; Nagayasu et al., 1999; Shmeeda et al., 2013; Wiklander et al., 2015). In particular, liposomes with sizes around 80 and 100 nm have garnered significant interest in the field of drug delivery for intravenous administrations. These molecular nano-assemblies are large enough to evade renal elimination but small enough to exhibit uptake by the mononuclear phagocytic system of the liver and spleen, prolonging circulation half-life in the body and thereby improving the likelihood of reaching target cells or organs. Moreover, they can accumulate in tumors due to the enhanced permeability and retention effect (EPR) (Greish, 2010; Ngoune et al., 2016).

Some liposomal drugs have met pharmaceutical quality criteria concerning physicochemical properties, reproducibility, stability in storage, and clinical requirements, and have thus been approved by regulatory agencies and are now commercially available (Bulbake et al., 2017b). However, these systems often exhibit some drawbacks, such as poor colloidal and chemical stability during circulation in the bloodstream. This is because pure liposomes are not thermodynamically stable entities as they lack a spontaneous curvature and, therefore, collapse over time into the lamellar equilibrium state of aggregation (Grimaldi et al., 2016). Pure liposomes correspond to kinetically trapped metastable states, formed by an external input of energy over a stable flat lamellar phase.

The kinetic stability of pure liposomes is limited by the insolubility of their structural components, phospholipids, in water (Riehemann et al., 2009; Sercombe et al., 2015). From a thermodynamic standpoint, the equilibrium state is not closed vesicles but a flat lamellar bilayer. Moreover, phospholipids are not chemically stable in the long term and are susceptible to hydrolysis, oxidation, or peroxidation, which is typically mitigated by adding antioxidants and storing at low temperatures. The physical instability of pure liposomes leads to issues related to the permeability of their membrane, causing rapid leakage of their payload. To overcome this problem, cholesterol is often incorporated into liposomes, increasing their rigidity and stability while reducing permeability (Gregoriadis & Davis, 1979; Kirby et al., 1980; Ulrich, 2002).

Generally, liposomes are obtained by forming a lipid film, which is then resuspended in a specific aqueous system, forming multilamellar vesicles (MLVs). From these liposomes, different vesicular structures can be obtained through an extrusion or sonication process. It is through these processes that smaller vesicles formed from a single bilayer, typically ranging from 20 to 400 nm in diameter, can be achieved.

Liposomes can be classified based on their size and lamellarity, like other nanosystems, or based on the preparation method. The following table (Table 3) shows their classification more specifically:

Table 3. Classification of liposomes according to number of bilayers and methods of preparation.

BILAYER NUMBER		PREPARATION METHODS	
Name	**Definition**	**Name**	**Definition**
SUV (Small Unilamellar vesicles)	Small dimensions unilamellar vesicles. Vesicle diameter: 20-80nm.	**REV** (Revers evaporation method)	Formation of 'inverted micelles' that collapse into a viscous state similar to a gel when the organic phase is removed through evaporation.
LUV (Larg unilamellar vesicles)	Large dimensions unilamellar vesicles. Vesicle diameter: 80-100nm.	**SPLV** (Stable plurilamellar vesicles)	Formation of stable multilamellar vesicles with multiple aqueous compartments containing the drug.
GUV (Giant unilamellar vesicles)	Giant dimensions unilamellar vesicles. Vesicle diameter: >1µm.	**FATMLV** (Frozen and Thawed)	It is carried out by submerging the liposome sample under water and changing the temperatures with large gradients.
MLV (Multilamellar large vesicles)	Small dimensions Vesicle diameter: 400 nm a > 1µm.	**VET** (Vesicles prepared by extrusion technique)	It is used to do small monodisperse vesicles.
		DRV (Dehydration-Rehidration method)	It involves hydrating the lipid film in an organic solvent and then removing the organic solvent under vacuum to prepare the liposomes

Despite the morphological differences and physicochemical characteristics of these different types of liposomes, they can be collectively classified as traditional liposomes.

Summarizing the results obtained with liposomes for topical drug administration, it is noteworthy to highlight the study by Du Plessis et al, where up to a five-fold increase in retained triamcinolone acetonide in the epidermis and dermis was observed, with low levels of the drug systemically compared to conventional formulations. Various studies by the same authors show similar results with econazole and progesterone(Du Plessis et al., 2002; Müller et al., 2002).

Subsequent investigations, conducted with corticosteroids, antibiotics, and anti-inflammatory agents, highlighted that conventional liposomes only increase drug deposition in the skin (Bangham, 1995; Mason et al., 2006; Mezei & Gulasekharam, 1980). The lipid composition of the vesicles, the preparation method, and the state of the liposome bilayers are the main factors described to affect liposome deposition (Pierre & Dos Santos Miranda Costa, 2011; Shivakumar & Narsimha, 2010).

After extensive research on their effectiveness as systems for topical drug administration, it has been established that most of these types of liposomes primarily act at the dermal level, as they do not have the ability to penetrate the deeper layers of the skin. However, various experimental results show their effectiveness for transdermal administration, increasing penetration (Fresta & Puglisi, 1997; Mezei, 1985).

1.6.1.2. Mechanisms of Action of Liposomes for Topical Administration

In parallel with the intense research on these vesicular systems, the mechanism of action through which liposomes provide high efficacy in dermal and transdermal drug administration has been investigated. Based on the different permeation mechanisms of liposomes, they can be grouped into four categories:

- Free Drug Mechanism:

According to this process, the drug permeates independently once it is released from the vesicles. In this way, the vesicles are considered solely as a vehicle that can offer controlled drug release (Flaten et al., 2009).

- Permeation Enhancement Mechanism:

The first record describing this mechanism concludes that egg lecithin used for vesicle formation reduces the skin's barrier effect (Ciotti & Weiner, 2002). Subsequently, it is

established that lipids from the SC can solubilize by forming inverse micelles with vesicle phospholipids (Niemiec et al., 1995). Several authors have reported results supporting this mechanism; however, other authors have established results contrary to the previous ones (Ganesan et al., 1984; Kato et al., 2011; Touitou et al., 1994).

- Adsorption and/or Fusion of Vesicles with SC:

This mechanism has emphasized the importance of the interaction of vesicles with the SC. It has been suggested that there is first an adhesion process on the skin's surface and subsequently a possible fusion with the lipid matrix of the SC (Leopold & Lippold, 1995b).

- Appendageal Permeation:

This drug permeation route has been considered generally for topical formulations. In the case of liposomes, specifically Transfersomes®, a decrease in effectiveness under occlusive conditions led to the hypothesis that favoring hydration conditions could cause corneocytes to swell and close the extracellular spaces, which would be the main route for liposomes, and thus appendageal permeation would be the primary mechanism for drug release into the skin. This hypothesis is attempted to be verified by studying the release of insulin topically, using in vivo models such as animals with different densities of hair follicles. Studies indicated no significant differences using the same type of elastic liposomes (El Maghraby et al., 2010). Other authors have demonstrated the effectiveness of this mechanism only when combined with iontophoresis (Zellmer et al., 1995).

There are multiple factors involved in the development of these vesicular systems, as well as in the methodologies used to describe the mechanisms of action. Therefore, it is not possible to describe a general mechanism for these systems. For example, the composition of vesicles would directly influence the mechanism of action. For this reason, ongoing research is essential to provide new insights into establishing the processes occurring during the release stage in the mechanism of action of liposomes.

1.7. CONFOCAL RAMAN SPECTROSCOPY (CRS)

In 1928, Raman and Krishnan first observed the Raman effect, but its widespread use was hindered until the laser was developed. Since the introduction of lasers, progress in Raman spectroscopy has been swift, transforming it from a mere curiosity in laboratories to a valuable analytical tool. The Raman method is non-intrusive, non-invasive, and does not require physical contact or labeling, making it a widely applicable standard method in aqueous environments. The Raman effect involves the interaction of light with a sample's chemical bonds, leading to an energy shift in the backscattered light, creating a distinctive Raman spectrum detectable through spectroscopic methods. This technique enables the identification of chemical and molecular components in a sample, and it can also provide information about factors such as the relative quantities of specific components, stress and strain states, crystallinity, or types of polymorphic structures. Confocal Raman imaging, which combines Raman spectroscopy with a confocal microscope, allows for the visualization of the spatial distribution of compounds and the properties mentioned earlier within a sample (Gomes da Costa et al., 2019).

Raman spectroscopy imaging stands out for its capability to examine biomolecular details within samples. This process involves stimulating the sample with visible or near-infrared laser light, resulting in both elastic Rayleigh scattering and inelastic Stokes Raman scattering. The latter offers insights into the energy levels related to molecular bond vibrations. By breaking down the Raman signal spectrally, it becomes feasible to investigate and distinguish between active ingredients and inherent skin components. Moreover, this analysis can reveal molecular alterations induced by active substances on the skin. Raman spectra serve as unique identifiers, enabling the recognition and potential tracking of molecules within the skin. As a result, it proves to be a valuable tool for delving into cutaneous components and their interactions (Essendoubi et al., 2021).

In Figure 13, we can see a diagram of the more physicochemical functioning that occurs when using Raman radiation on chemical molecules.

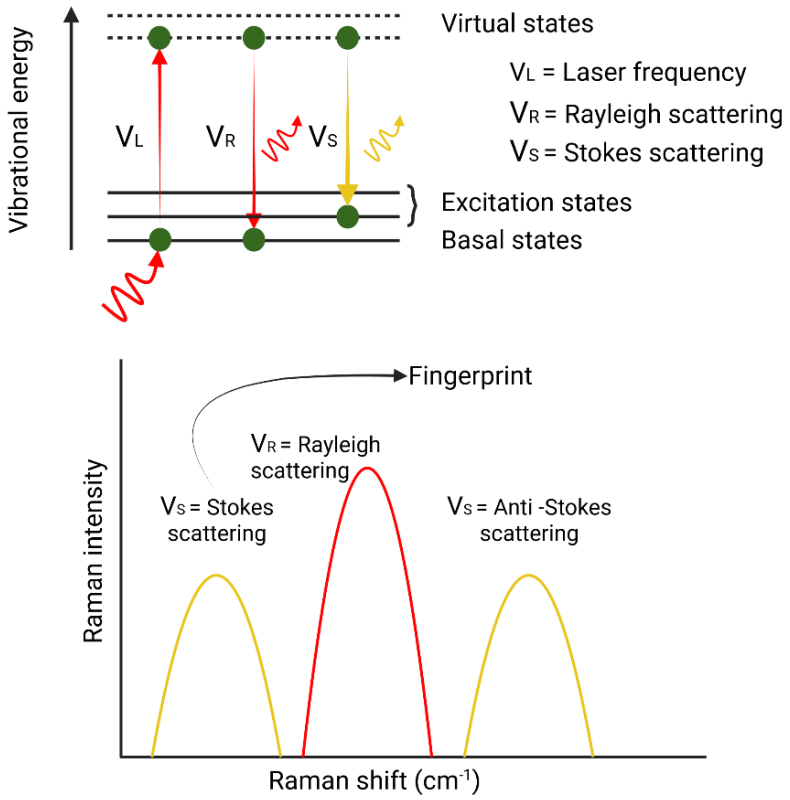

Figure 13. Diagram of the Raman Spectrophotometry Theory. The inelastic Raman scattering or Stokes scattering only occurs once in a million events. For this reason, it is the signal that can provide us with the 'fingerprint.' This signal occurs at wavelengths between 300–1900 cm^{-1}.

CRS has found extensive use in skin research, primarily serving as a qualitative method. As mentioned earlier, it enables the distinction of the studied substance within the skin from other components. A recent development by Caspers et al. introduced a novel application of CRS, extending its utility to quantitative analysis. This advancement allows for the measurement of the amounts of substances penetrating the skin. The quantification of the overall skin absorption is achieved by computing the area under the depth profile curves (AUC) corresponding to the thickness of the SC (Caspers et al., 2019).

1.8. HIGH-PERFORMANCE LIQUID CHROMATOGRAPHY (HPLC)

HPLC is a broad analytical chemistry technique used to separate the components of a chemical mixture. This separation is achieved thanks to the pressure generated by the flow of a mobile phase through a column that incorporates a stationary phase.

The principle of separation in HPLC is based on the distribution of sample compounds between a mobile phase (driven by a pump) and a stationary phase (located in a column). As the sample, together with the mobile phase, passes through the column, compound groups interact differently with the stationary phase, resulting in differential retention based on their chemical properties, thus achieving separation.

Once the different sample compounds exit the column, they continue to be propelled by the mobile phase to the detector. The detector measures the analytes after elution from the column, and a Chromatography Data System (CDS) translates the detected signal. The translated data output from an HPLC analysis is called a chromatogram, where the X-axis represents a measure of time, and the Y-axis measures a specific signal generated by the detector.

Basic principles of HPLC:

- Analyte: Compound(s) of interest for detection in an HPLC analysis.
- Mobile Phase: Moving phase composed of solvents or eluents flowing from injection to detection.
- Stationary Phase: The stationary phase where the physical separation of analytes occurs.
- Flow Rate: The speed at which the mobile phase flows over time.
- Retention Time: The time between sample injection and the peak signal of the analyte in a chromatogram.
- Efficiency: Given as the number of theoretical plates, a key metric to quantify the performance of a separation.
- Resolution: The ability to distinguish between peaks, a primary concern in any separation.
- Selectivity: The ability to separate two analytes.
- Void Volume: All the volume inside a column not occupied by the stationary phase.

- Limit of Detection: The smallest amount of an analyte that can be reliably detected.
- Limit of Quantification: The lower or upper amount of an analyte that can be reliably quantified.

Every HPLC system has four major components: a pump that drives the mobile phase, an autosampler for sample injection, a stationary phase column for separating sample components, and a detector for measuring the separated components. Other elements include connecting capillaries and tubes allowing the continuous flow of the mobile phase and sample throughout the system, and a CDS to control the HPLC instrument, separation, detection, and result evaluation.

Every HPLC analysis includes the following steps:

1. Mobile phase starts flowing: The pump pushes eluents or solvents through the system at the specified flow rate.
2. Sample injection: Once injected into the mobile phase flow, the sample travels with it from the injection point to the column.
3. Separation of components: Physical separation of components occurs in the stationary phase of the column. After elution from the column, separated components of the sample travel to the detector.
4. Detection of analytes: Detection of target analytes based on an electric signal generated by specific properties.
5. Chromatogram generation: Translation of analyte signal detection by the CDS into a chromatogram representing analyte signals against time.

In Figure 14, we can see a schematic of all the parts of the HPLC arranged to give us an idea of the path that each analyzed sample follows.

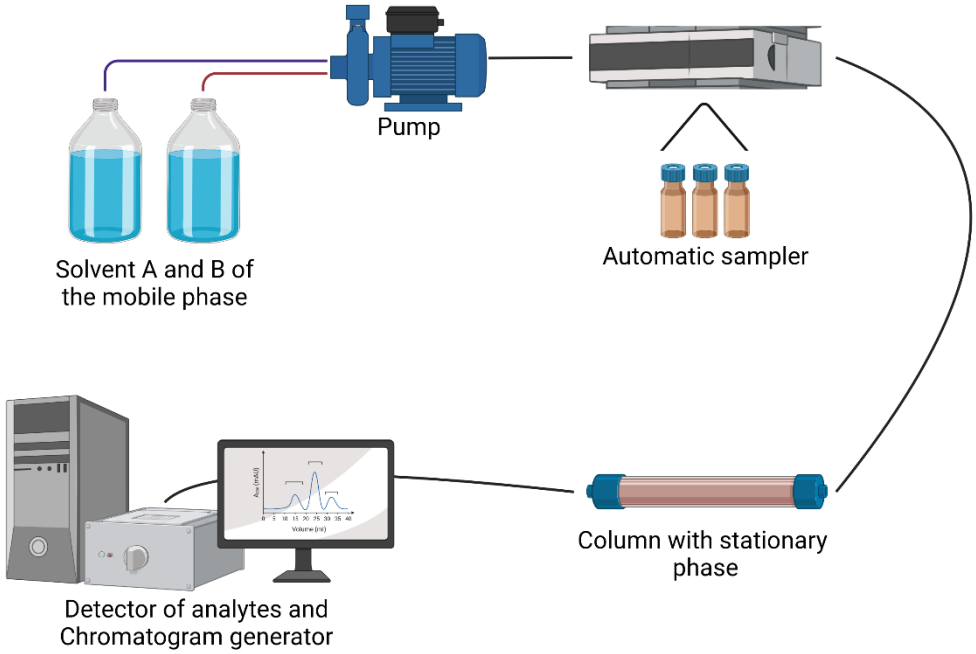

Figure 14. HPLC parts.

Factors influencing the separation of components:

Numerous factors, including the composition of the mobile phase, the chemistry of the stationary phase, and temperature, influence HPLC separation. Successful separation occurs only if analytes have different affinities for the stationary phase, so selecting the appropriate stationary phase for the component under study is crucial. The main factors affecting the separation process are:

- Physicochemical properties of the analyte: size, charge, polarity, and volatility.
- Physicochemical properties of the stationary phase: polarity, charge, and viscosity.
- Physicochemical properties of the mobile phase used: interaction with the analyte and the stationary phase.

HPLC separation methods can be isocratic or gradient. The isocratic method uses a constant eluent composition throughout all analyses. In contrast, the gradient method involves a change in the mobile phase composition during the separation process. These methods often use two solvents, referred to as A and B. The run may start with a certain percentage of A to B, such as 60% water to 40% acetonitrile, for instance, followed by a percentage change during the separation (Thermo Fisher Scientific Inc., n.d.).

Gradient separations typically offer better performance than isocratic modes but are more complex and require advanced pump machinery.

1.8.1. UV Detector

The ultraviolet-visible (UV/Vis) technique (covering a wavelength range from 190 to 800 nm) measures the fraction of radiation that passes through the sample. Its instrumentation requires a source of electromagnetic radiation, a means to select the wavelength at which transmittance is measured, and a detector to measure transmittance. Transmittance is related to absorbance and the concentration of absorbing substances through Beer's law (Martins et al., 2019).

The use of UV/Vis is attributed to its efficiency, low cost, non-destructive and environmentally friendly approach, and operational simplicity, making it suitable for online measurement (Martins et al., 2019).

1.8.2. Fluorímetre Detector

Fluorescence spectroscopy is a non-invasive, non-destructive, and highly sensitive technique that requires minimal sample. For this reason, it is widely used in the study of solid components (Y. Zhang et al., 2023).

The technique is based on the emission of electromagnetic radiation by chemical compounds when a molecule in the lowest vibrational energy level of an excited electronic state returns to a lower energy electronic state, emitting a photon in this process after the absorption of light at a specific wavelength that caused the previous excitation. Fluorescence spectra are thus formed by respective wavelengths for excitation and emission and will depend on the chemical structure of the target compound. Only chemical compounds with rings and rigid chemical structures will emit electromagnetic radiation with a significant intensity, as these structures do not allow the release of absorbed energy through pathways other than light emission (Martins et al., 2019).

Fluorescence instrumentation is similar to UV/Vis spectroscopy, but the analytical results are 1 to 3 orders of magnitude more sensitive than UV/Vis results (Martins et al., 2019). In Figure 15 we can see the difference between both technics.

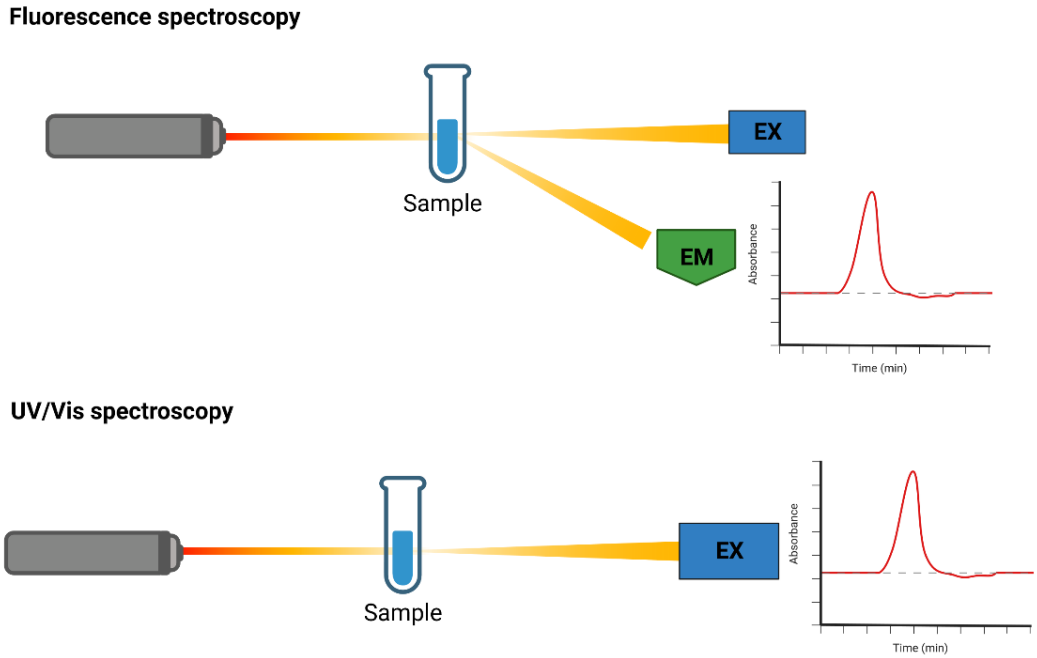

Figure 15. Operating scheme of fluorescence spectroscopy and UV/Vis spectroscopy.

1.9. Justification of Validations

The FDA defines the validation process as the establishment of documented evidence that provides a high degree of assurance that a specific process will consistently produce a product meeting its predetermined specifications and quality characteristics (The FDA Group, 2022).

The validation of a process includes three interrelated steps: Installation Qualification (IQ), Operational Qualification (OQ), and Performance Qualification (PQ). IQ verifies that the equipment and its systems or subsystems have been installed according to installation drawings and/or specifications. Without proper equipment and support system installation, operational and PQs would not provide accurate information that could be used to document consistent and predictable performance. OQ is defined as establishing confidence that the equipment and process subsystems are capable of consistently operating within established limits and tolerances. PQ provides documented evidence that the integrated system or process is capable of consistently producing the intended product safely and of high quality within predefined acceptance criteria. Before conducting process validations, it is essential to have well-defined and documented "sample size" requirements for validation activities (The FDA Group, 2022).

The objective of the analytical procedure must be clearly understood, as this will govern the validation characteristics that need to be assessed. The typical validation characteristics to be considered are Accuracy, Precision, Repeatability, Intermediate Precision, Specificity, Limit of Detection, Limit of Quantification, and Range (ICH Expert Working Group, 2005).

2. OBJECTIVES

The main objective of this research is to develop and biopharmaceutically characterize BNB liposomes for topical application in the treatment of skin and ocular diseases: SS and AD. To achieve these proposed objectives, this work has been divided into several stages leading to the following specific goals:

- Development and validation of a HPLC method with fluorescence and UV/Vis detectors for the detection and quantification of BNB according to criteria such as linearity, accuracy, precision, sensitivity, selectivity, and specificity. Following the recommendations of ICH Q2A and ICH Q2B from the International Conference on Harmonization (ICH).
- Development of different liposomes and optimization of the developed formulations to select the best components and their ratio to produce liposomes and evaluate their impact on morphometry and stability. Thus, selecting the most suitable formulations for further studies.
- Physicochemical characterization of the formulations through the measurement of morphometric characteristics (particle size and polydispersity) by photon correlation spectroscopy, transmission electron microscopy (TEM), and rheological characterization.
- In vitro drug release studies from liposomes using Franz cells in a suitable medium that provides sink conditions (non-saturation) throughout the assay. These studies are conducted at body or skin temperature (37ºC/32ºC) to reproduce the temperature conditions of the body and/or mucous membranes. In vitro release studies provide information on the fraction of the drug released from the formulation and, therefore, will be available for subsequent permeation through the skin/mucous membranes.
- Ex vivo drug permeation studies in human skin and porcine mucous. These studies are conducted with Franz cells and provide information on the drug's permeability through the biological membranes under study. On the other hand, they also provide information on the formulation's ability to modulate drug permeation (in relation to the drug in solution).

- In vitro and in vivo tolerance studies are conducted to assess the compatibility of formulations on skin and mucosa: HET-CAM test, corneal transparency test, modified Draize test, and histological study.

3. MATERIALS AND METHODOLOGY

3.1. MATERIALS

BNB, Ammonium salt formate, 1-palmitoyl-2-oleoyl-glycero-3-phosphocholine (POPC), 1-Palmitoyl-2-oleoyl-sn-glycerol-3-phosphoglycerol (POPG) and the permeation enhancers: Nonane, Lauryl acrylate, Squalene, Atone, Sebacic acid, (R)-(+)-Limnonene, α-Pinene, N-ethylpirrolidine, (+)-3-caren, 1-decanol, Myristic alcohol, Oleic acid, Menthol and Octanoic acid were bought at Sigma-Aldrich (Madrid, Spain). Gattefossé (Barcelona, Spain) supplied Transcutol® P [Diethylene glycol monoethyl ether]. Acetonitrile was purchased at Fisher Chemical (Loughborough, UK). Lipids Lα-phosphatidylcholine (Lα-PC) and 1-palmitoyl-2-oleoyl-phosphatidylethanolamine (POPE) were bought at BOC Sciences (London, UK). Cholesterol (CHOL) (ovine wool > 98%) and ceramides (CER) (bovine spinal cord ≥ 98%) were acquired at Avanti Polar Lipid Inc. (Alabaster, AL, USA). Finally, BeautyBio GloPRO® roller microneedling for histological procedures were bought at Currentbody (Barcelona, Spain), contains 540 titanium needles that are 0.25 mm long, corresponding to 72.3 microneedles/cm^2.

Water Millipore MilliQ purification system (Millipore Corporation, Burlington, USA) was used to obtain ultrapure water for all experiments, and all the other chemical reagents used were of analytical grade.

3.2. BIOLOGICAL MATERIALS

The human abdominal skin, governed by protocol code 93-01162 02/18 approved on 17 January 2020 by the 99 Bioethics Committee of SCIAS Hospital de Barcelona, underwent dermatoming to achieve a thickness of 400 µm (Aesculap GA 630, Aesculap, Tuttligen, Germany).

Corneal and scleral tissues were procured from female pigs (cross Landrace x Large White, 25–30 kg) that had previously participated in surgical university practices, adhering to the guidelines of the Ethics Committee of Animals Experimentation at the University of Barcelona. Immediate enucleation of eyes occurred post-sacrifice, with subsequent excision of corneal and scleral tissues performed in situ. The harvested tissues were transported to the laboratory immersed in an artificial aqueous humour solution for debridement and preparation before permeation experiments.

All the skin samples used to study the liposomes intended for topical use on skin underwent physical alteration using microneedles to simulate an AD skin. This process involved piercing the epidermis to mimic AD skin conditions. Importantly, this technique, performed on live animals, is painless as the needles do not come into contact with nerves or blood vessels.

3.3. METHODS

3.3.1. BNB solution preparation

To create a saturated solution of BNB, an excess of BNB was dissolved in Transcutol®P, and any residual particles were removed through filtration using a 0.45 µm nylon filter. This saturated solution was employed to investigate the intrinsic permeation characteristics of BNB and the effect of physical enhancers (microneedles) in the same study. Additionally, solutions containing BNB at a concentration of 2 mg/mL, with the addition of 5% of various permeation chemical enhancers (as outlined in Table 4), were prepared.

In the permeation study, a 2 mg/mL BNB solution without any enhancers was utilized as the reference to evaluate the enhancement factor provided by the permeation enhancers. The selection of a 2 mg/mL concentration was based on the daily oral dose of BNB available in the market, serving as a reference point. Given the absence of specific topical application data for BNB, this concentration was chosen to initiate an assessment of its permeation capacity and safety, with the aim of achieving a local effect through topical application. This concentration choice allows for the exploration of BNB's permeation behavior and safety considerations in the absence of established topical application guidelines.

Table 4. Permeation enhancers used in the study, along with their molecular formula, molecular mass, and CAS Register number.

Permeation enhancer	Molecular formula	Molecular Mass (g/mol)	CAS Register Number
Nonane	C_9H_{20}	128.26	111-84-2
Lauryl acrylate	$C_{15}O_2H_{28}$	240.38	2156-97-0
Squalene	$C_{30}H_{50}$	410.72	111-02-4
Azone	$C_{18}H_{35}NO$	281.5	59227-89-3
Sebacic acid	$C_{10}O_4H_{18}$	202.25	111-20-6
(R)-(+)-Limonene	$C_{10}H_{16}$	136.23	5989-27-5
α-Pinene	$C_{10}H_{16}$	136.23	80-56-8
N-ethylpirrolidine	C_4H_9N	71.12	123-75-1
(+)-3-caren	$C_{10}H_{16}$	136.23	498-15-7
1-Decanol	$C_{10}OH22$	158.28	112-30-1
Myristyl alcohol	$C_{14}OH_{30}$	214.39	112-72-1
Oleic acid	$C_{18}O_2H_{34}$	282.46	112-80-1
Menthol	$C_{10}OH_{20}$	156.27	89-78-1
Octanoic acid	$C_8O_2H_{16}$	144.21	124-07-2

CAS: Chemical Abstracts Service.

3.3.2. Preparation of the Liposomes

Five different liposome formulations were prepared:

i. Pure POPC liposomes
ii. POPC:CHOL (0.8:0.2, mol/mol) liposomes
iii. POPC:CHOL:CER (0.36:0.24:0.40, mol/mol/mol) liposomes
iv. Pure Lα-PC liposomes
v. POPE:POPG (3:1, mol/mol) liposomes.

All liposome samples were prepared following the methodologies described in previously published works (Vázquez-González et al., 2019). Briefly, for the formulation of each liposome sample, 500 mg of BNB was added to lipid solutions in a round-bottom flask with 10 mM chloroform–methanol (2:1, v/v), achieving the desired molar lipid concentration for each composition. Subsequently, the mixture underwent sonication for 10–15 s to ensure complete dissolution of BNB. After removing the solvent via a rotary evaporator, the resulting thin lipid film was subjected to high vacuum overnight in the absence of light to eliminate any residual traces of organic solvent.

Rehydration of the thin films was carried out using a solution containing 10 mM TRIS·HCl ([tris(hydroxymethyl)aminomethane] 150 mM NaCl) and 5% (v/v) Transcutol® P at pH 7.40 (Ahmed et al., 2015; Botet-Carreras et al., 2021). Energetic vortexing was applied for 5 cycles at a temperature exceeding the lipid mixture's transition temperature, resulting in the formation of large multilamellar vesicles. To homogenize the liposome size, an ultrasound bath with temperature control was employed for 15 minutes. At last, the liposomes underwent purification by passing through a Sephadex® G50 column mounted in a 5 mL syringe and centrifuged at 1000 rpm for 10 s using a Rotanta 460R centrifuge (Andreas Hettich GmbH & Co. KG, DE, Tuttlingen, Germany) to eliminate non-encapsulated BNB.

3.3.3. Liposomes Physicochemical Characterization

The physicochemical characterization encompassed several parameters, including pH, the vesicle size and polydispersity index (PDI), the zeta potential (ZP), the osmolality, and encapsulation efficiency. pH measurements were conducted at room temperature using a pH-meter micro pH 2001 (Crison Instruments SA, Alella, Spain) in triplicate.

Vesicle size, PDI, and ZP were determined using a Zetasizer Nano S (Malvern Instruments, Malvern, UK). All measurements were performed in triplicate, yielding satisfactory deviation values (Moussaoui, Abo-horan, et al., 2021). Surface electrical properties of the liposomes were assessed through electrophoresis measurements

using a Zetasizer 2000 (Malvern Instruments Ltd., UK) after appropriate dilution (0.1% w/v).

Furthermore, for the liposomes intended for ocular use, more in-depth physicochemical studies were conducted to ensure the tolerability of these in the eyes, so the influences of pH and ionic strength were also investigated for the liposomes pure Lα-PC and POPE:POPG (3:1, mol/mol). For this task, dilute liposomal dispersions were prepared at different pH values (3–8), and ZP determinations were made after 24 hours of contact under mechanical stirring (50 rpm) at 25.0 ± 0.5 ºC. pH was checked and readjusted before measurements. ZP values were also recorded for liposomes formulated at pH 6 with various electrolytes (NaCl, $CaCl_2$, and $AlCl_3$) and concentrations ranging from, 2 × 10^{-1}, 10^{-1}, 10^{-2}, 10^{-3}, 10^{-4}, and 10^{-5} M. All measurements, including those on blank and loaded liposomes, were performed nine times.

Osmolality was determined using an Advanced 3320 Micro-Osmometer (Advanced Instruments, LLC, Norwood, MA, USA) (Mallandrich et al., 2021).

Encapsulation efficiency (EE) for the five liposomes was assessed by breaking the liposomes with 80% Transcutol® P and 10% Triton, followed by quantifying the BNB amount using HPLC. The measured BNB amount was compared to the initial amount using Equation (1) (Mallandrich et al., 2021).

$$EE\% = \frac{Q_f}{Q_0} x100 \quad (7)$$

where, EE% represents the effectiveness of encapsulation, Q_f denotes the quantity of BNB in milligrams that is retained within the liposomes, while Q_0 signifies the initial amount of BNB in milligrams utilized for the preparation of the liposome.

3.3.4. Morphological Study of the Liposomes

The analysis of morphology was conducted using a JEM-1010 microscope (JEOL Ltd., Tokyo, Japan) via TEM. A single droplet of each liposome was deposited onto copper grids coated with Formvar®. The liposome sample made contact with the grid for a duration of 1 minute. Following this, a drop of 2% uranyl acetate solution was applied to the grid, succeeded by the addition of methylcellulose for a 10-minute period. Any

excess methylcellulose was removed by gently tapping the filter paper at a diagonal angle. Subsequently, the grid was allowed to air-dry before undergoing image analysis (Andrade-Carrera et al., 2017).

3.3.5. In Vitro Durg Release Study

To evaluate drug release, we employed a dialysis membrane with a molecular cut-off weight of 14,000 Da (Sigma–Aldrich, Madrid, Spain) in Franz-type diffusion cells with a diffusion area of 0.64 cm^2 and a receptor chamber volume of 4.9 mL (Crown Glass Company, Inc., Jersey City, NJ, USA) (Mallandrich et al., 2017; Moussaoui, Fernández-Campos, et al., 2021). Prior to use, the membrane was hydrated in methanol:water (1:1) for 24 hours, washed, and then positioned in the Franz diffusion cells.

Transcutol® P served as the receptor medium and was stirred at 500 r.p.m. to maintain homogeneity and sink conditions. The experiment was conducted at 32°C using a thermostatic water bath. In the donor compartment, 500 µL aliquots of each formulation were added, with five replicates for each liposome. Throughout the 31-hour experiment, 200 µL samples were collected at specific time intervals, and Transcutol® P was refilled after each collection to ensure a constant volume in the cells. The collected samples underwent analysis using a validated HPLC-fluorescence method. The cumulative amounts of BNB released from each liposomal formulation were plotted against time, and different kinetic models were applied for data analysis to describe the drug release profile. The determination coefficient (r^2) was used to evaluate the goodness of fit (Kurakula et al., 2012).

Furthermore, non-modelestic parameters were computed to compare various release profiles, including the MRT of BNB from the formulation, the AUC representing the amount of BNB released and the efficiency (E) indicating the percentage of BNB released from the initial formulation (Pérez-González et al., 2021). Experiment details are provided in Table 5.

Table 5. Experimental conditions for the in vitro release test.

Parameters	Conditions
Receptor fluid	Transcutol® P
Cell volume	4.9 mL
Diffusion area	0.64 cm^2
Membrane	Dialysis membrane
Replicates	5 replicates
Temperature	32 ± 0.5 °C
Stirring	500 r.p.m.
Dose	500 µL of each liposome
Sample volume	200 µL
Sampling times	0 (pre-sample time point), 3.0 h, 7.0 h, 20.3 h, 24.5 h, 28.3 h, and 31.0 h

3.3.6. Ex Vivo Permeation Study

The assessment of BNB's permeation and diffusion through the skin utilized Franz diffusion cells obtained from Crown Glass Company, Inc. (NJ, USA). These cells had a diffusion area of 2.54 cm^2 and a receptor compartment volume of 14 mL. Transcutol® P served as the receptor fluid to maintain skin conditions, and the experiment was conducted at 32 ºC with continuous stirring in the receptor compartment at 500 rpm.

For the study of the intrinsic permeation of the drug, a saturated solution of BNB was applied to human skin dermatomed at 400 µm. Both untreated healthy skin and skin treated with microneedles were included in the investigation. Using a roller with 540 titanium needles (72.3 microneedles/cm^2) with a length of 0.25 mm was used to gently press onto the skin surface. Both types of skin were mounted on Franz cells, and a BNB saturated solution was administered. Samples of 200 µL were collected and replaced with an equal volume of Transcutol® P at predetermined intervals over 24/30 hours. Details regarding the conditions employed in the ex vivo permeation tests are outlined in Table 6.

Furthermore, various solutions of BNB at a concentration of 2 mg/mL, with a chemical permeation enhancer (refer to Table 6), were tested. Aliquots of 600 µL of the BNB solution (either alone or with an enhancer) were applied to the skin. Samples of 200 µL were collected at different time points, with the same volume of fresh receptor fluid replacing each sample immediately after collection to maintain constant cell volume throughout the test. The sampling time points and the experiment duration for both intrinsic permeation and chemical enhancer permeations were determined based on prior method development experiments to ensure a meaningful sampling of the permeation profile. The tests were conducted in triplicate.

Quantification of the samples obtained in both tests was performed using HPLC coupled to a fluorescence detector. Experimental conditions for the ex vivo skin permeation tests are summarized in Table 6.

Table 6. Experimental conditions for different enhancers, physical and chemical, ex vivo skin permeation tests.

Condition	**Description**
Receptor fluid:	Transcutol®P
Cell volume:	14 mL
Diffusion area:	2.54 cm^2
Membrane:	Human skin
Thickness:	400 µm
Replicates:	5 replicates
Temperature:	32 ± 0.5 ºC
Stirring:	500 r.p.m.
Dose:	600 µL
Sample volume:	200 µL

To investigate the ex vivo permeation of liposomes intended for topical application in a potential treatment for AD (POPC, POPC:CHOL, and POPC:CHOL:CER), we adopted similar conditions used for the direct permeation of BNB in a transcutol solution. The permeation studies were conducted using Franz diffusion cells with a surface area of 0.64 cm^2 and a receptor chamber of 4.9 mL. Altered abdominal human skin to simulate AD was positioned between the donor and receptor compartments (Mallandrich et al., 2017; Moussaoui, Fernández-Campos, et al., 2021). Transcutol® P served as the receptor medium, maintained at 32 ºC and constantly stirred. 500 µL of each liposome was applied to the donor compartment. Samples of 200 µL were collected over 25 hours, and Transcutol® P was added after each sampling time. Analysis of the samples was performed using the validated HPLC-fluorescence method.

Ex vivo corneal and scleral permeation studies were conducted using Franz diffusion cells, we used the same diffusion cells as the previous study, a surface area of 0.64 cm^2 and a receptor chamber of 4.9 mL. Tissues were positioned between the donor and receptor compartments (Mallandrich et al., 2017; Moussaoui, Fernández-Campos, et al., 2021). We applied 500 µL of liposome, either Lα-PC or POPE:POPG, in the donor compartment, with five replicates for each tissue. Receptor compartment was Transcutol® P kept at 37 ºC, and stirred continuously. A volume of 200 µL was withdrawn from the receptor compartment at fixed intervals and replaced by an equivalent volume of Transcutol® P. Quantification of the samples was conducted using HPLC with a fluorescence detector.

The experimental conditions for both permeation studies, one involving altered human skin (AHS) with liposomes intended for AD treatment and the other in ocular tissues, are delineated in Table 7 and in Figure 16 we can see the diagram followed by all the tissues on the ex vivo and extraction studies.

Table 7. Experimental conditions for the ex vivo permeation test in skin and ocular tissues with the different liposomes.

Parameter	Conditions
Receptor fluid	Transcutol® P
Cell volume	4.9 mL
Diffusion area	0.64 cm^2
Membrane	Altered Human Skin Cornea and Sclera
Replicates	5 replicates
Temperature	37 ± 0.5 °C for Sclera and Cornea 32 ± 0.5 °C for skin
Stirring	500 r.p.m.
Dose	500 µL of liposomes (Lα-PC or POPE:POPG) on sclera and cornea 500 µL of liposomes (POPC, POPC:CHOL, and POPC:CHOL:CER) on skin
Sample volume	200 µL
Sampling times on sclera and cornea	0 (pre-sample time point), 2.1 h, 4.2 h, and 6.0 h
Sampling times on skin	0 (pre-sample time point), 7.0 h, 14.5 h, 19.7 h, 22.5 h and 25.0 h

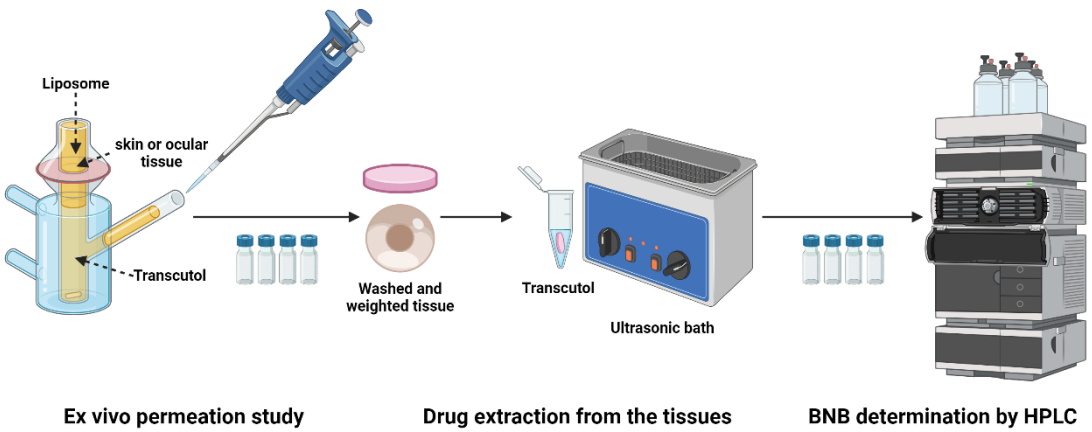

Figure 16. Ex vivo permeation and extraction studies diagram.

3.3.7. Retention Study

After completing the permeation study, all tissues were removed from the diffusion cells and washed with distilled water to eliminate any remaining liposomes or BNB solution on the tissue surface. To extract BNB retained in the tissues (Moussaoui, Abo-horan, et al., 2021), the permeation area was excised, weighed, and immersed in 1 mL of Transcutol® P, followed by sonication for 10 minutes using an ultrasonic water bath. Subsequently, the supernatant was filtered and quantified using HPLC with a UV/Vis detector. The extraction process from various tissues is illustrated in Figure 16. The amount retained in the tissues [Qret (µg/g skin/cm^2)] was calculated using Equation (2), and the results are expressed normalized by the weight of the tissue as well as by the diffusion area (0.64 cm^2 or 2.54 cm^2) and multiplied by the recovery of the drug:

$$Qret = \frac{Q_{ext}}{W \times A} \times \frac{100}{R}, \quad (8)$$

In the provided equation, Qext represents the amount of drug extracted from the tissue, measured in µg. W denotes the weight of the tissue in grams, and A represents the diffusion area in cm^2. Lastly, R signifies the proportion of BNB that is recovered in each tissue also known as recovery constant (Mallandrich et al., 2017).

3.3.8. Biopharmaceutical parameter data analysis

Three parameters were calculated for each type of permeation: flux (Jss, µg/h), permeability coefficient (Kp, cm/h), and the theoretical predicted plasma concentration in human steady state applied to a 10 cm^2 surface (Css, ng/mL).

The permeation profile was generated by plotting the cumulative permeated amounts of BNB against time. Flux was determined by analyzing the linear portion of the permeation profile using regression analysis (GraphPad Software Inc. version 5.0, San Diego, CA, USA) (Sanz et al., 2017). The resulting slope, corresponding to the flux, is described in Equation 2:

$$Jss = \frac{Q_t}{A * t}, \quad (9)$$

Where, Jss represents the flux (μg/h·cm^2) at the steady state; at the steady state, Qt denotes the amount of drug in the receptor fluid that diffused through the skin (μg), A signifies the cell diffusion area (cm^2); and t is the time during which the receptor medium has been accepting the drug (h).

The permeability coefficient was determined by the ratio of flux to the initial concentration, as described in Equation 3:

$$Kp = \frac{Jss}{C_0}, \tag{10}$$

Where, Kp represents the permeability coefficient expressed in cm/h, where Jss denotes the flux, and C_0 corresponds to the initial concentration of the applied drug expressed in μg/mL.

The predicted plasma concentration at the steady state in humans was determined based on Equation 4:

$$Css = \frac{J_{ss} * A}{[Cl_p]}, \tag{11}$$

Css (μg/mL) represents the predicted concentration of BNB in the plasma, considering a hypothetical application surface of 10 cm^2 (A), and the plasma clearance in humans (Clp) (Gómez-Segura, Parra, Calpena-Campmany, et al., 2020) obtained from literature sources (9.42 L/h) (CHMP, n.d.).

The MTT signifies the duration in which BNB traverses the skin. The MTT of BNB was calculated for both skin treated with enhancers and non-treated skin, the equation used is described in the Equation 3 from the introduction. As well as all the elements needed for calculations are defined in the equations 4 and 5 from the same segment: the partition coefficient (P_1) and the diffusion coefficient (P_2) and the Tl.

Lastly, the enhancement factor (EF) was calculated as the ratio of the permeability coefficient (Kp) of the enhancer to that of the non-treated skin, as per Equation 8 (Shaikh et al., 2009):

$$EF = \frac{K_p enhancer}{K_p(non-treated)}, \tag{12}$$

3.3.9. In Vitro Tolerance Study

The potential risk of ocular irritation induced by BNB liposomes was assessed through the HET-CAM test. This test measures the capacity to induce toxicity on the CAM of a 10-day embryonated hen's egg, sourced from the G.A.L.L.S.A. farm in Tarragona, Spain. The effects observed include the onset of hemorrhage (bleeding), coagulation (blood vessel disintegration), and vessel lysis coagulation (protein denaturation intra- and extra-vascular) (Mallandrich et al., 2021). Each of these elements were evaluated individually, and their cumulative impact was used to determine a score (IS). This score was subsequently utilized to classify the irritancy level of the test substance (Spielmann, 1995b). The equation used to calculate the IS value is described in the introduction in the equation 6.

For the HET-CAM test, 300 µL of liposomes was applied to the CAM, and the membrane was observed for 5 minutes to assess the severity of each reaction, following the INVITTOX protocol. A solution of NaOH 0.1 N served as the positive control, while a 0.9% NaCl solution was used as the negative control (Interagency Coordinating Committee on the Validation of Alternative Methods (ICCVAM), 2010).

Furthermore, we assessed alterations in corneal transparency following the application of liposomes to the cornea. The method involved exposing the cornea to a specified beam of light and detecting the transmitted light without absorption or scattering (Meek & Knupp, 2015). Transmittance was examined in the wavelength range of 150 to 760 nm for corneas that had been immersed in Liposome Lα-PC, Liposome POPE:POPG, PBS pH 7.4 (negative control), and ethanol (positive control) for a duration of 10 minutes (García-Otero et al., 2021).

3.3.10. Corneal and Scleral Histological Study

For the histological examination of the cornea and sclera, tissue samples from both were exposed to dilutions of Liposome Lα-PC, Liposome POPE:POPG, or distilled water (negative control) for a duration of 6 hours. Subsequently, the samples were processed for hematoxylin and eosin staining, following the methodology outlined by Gómez Segura et al. (Gómez-Segura, Parra, Calpena, et al., 2020). In a summary, corneal and scleral tissues were fixed in 4% buffered paraformaldehyde for 24 hours.

After dehydration, these tissues were embedded in paraffin, cut into 6 µm sections, stained, and mounted on DPX (Sigma Aldrich). The samples were observed under a microscope (Olympus BX41 and camera Olympus XC50) in a blind-coded fashion.

3.3.11. In Vivo Skin Tolerance Study and Histological Analysis

Liposomes designed for topical application, specifically POPC liposome, POPC:CHOL liposome, and POPC:CHOL:CER liposome, underwent evaluation using a modified Draize skin test to investigate their impact on induced erythema and edema. This test involved simulating atopic skin flare-up conditions with xylol. Non-anesthetized New Zealand healthy rabbits from Harlan (Barcelona, Spain) were employed, adhering to standard care conditions with ad libitum access to food and water.

The objective was to identify potential signs of damage on altered skin, gauged by the levels of erythema and edema (Gupta, 2016; Lee et al., 2017). The studies were conducted in accordance with the Mexican Official Norm for Animal Care and Handling (NOM-062-ZOO-1999).

To induce altered rabbit skin (ARS) to simulate a normal skin from an AD patient, microneedles were utilized to compromise the skin barrier function on the rabbits' backs, one day after baseline measurements and shaving. Animals were categorized into different groups: the negative control group, which only underwent microneedles; the positive control group, which, in addition to microneedles, received xylol to induce skin irritation; and three other groups that received microneedles, xylol, and one of the liposomes.

Subsequently, 0.5 mL of xylol was applied to all rabbits except the negative control. The positive control received microneedles plus xylol. Responses were recorded at 15 minutes, 45 minutes, and 3 hours 30 minutes. Simultaneously, transepidermal water loss (TEWL) and skin hydration were measured at these time points. A visual scoring system assessed inflammation, classifying from 1 to 4 based on the extent of erythema and edema (S. Singh & Singh, 2004): 0 denotes no erythema and no edema, 1 denotes a little sign of erythema or edema, 2 denotes explicit erythema or slight edema, 3 denotes a moderate to severe erythema or edema and 4 refers to serious

erythema (beet redness) through to the first signs of depth injuries or severe edema (Mehanna et al., 2020).

Xylol served as an irritant to induce allergic contact dermatitis (ACD), characterized by manifestations such as skin redness, swelling, warmth, itching, dryness, and flaking. Other articles, like those of Patricia L Nadworny et al. (Nadworny et al., 2010) or Liu Tang et al. (Tang et al., 2021), used dinitrochlorobenzene, or Paul L. Stanley et al. (Stanley et al., 1991), who used 12-O-tetradecanoylphorbol-13-acetate (TPA).

TEWL, measured by Tewameter (TEWL-Dermalab, Agaram Industries, India), indicates the amount of water that can diffuse through the skin SC per unit of time, with higher values suggesting damage to the skin barrier (Netzlaff et al., 2006). The appropriate structure of intracellular lipids in the SC is one of the key factors in retaining transdermal water (Alexander et al., 2018; Verdier-Sévrain & Bonté, 2007). The skin hydration was measured by a Corneometer (EnviroDerm, Ireland), quantifying the water content within the corneum.

Following the 3-hour monitoring of the mentioned parameters, the animal specimens subjected to treatment underwent a histological evaluation to analyze the impact of the administered liposomes. To ensure this assessment, the animals were humanely euthanized using xylazine (Rompun® 20 mg/mL, Bayer Hispania, Sant Joan Despí, Spain) and ketamine (Imalgene® 100 mg/mL, Boehringer Ingelheim Animal Health España, Sant Cugat del Vallès, Spain). The euthanasia mixture was injected through the right ear vein at a dosage of 4 mg/kg, as detailed in Parra-Coca et al. (Parra-Coca et al., 2021).

Following the confirmation of clinical death, the skin from the dorsal area was promptly excised, rinsed with PBS pH 7.4, and left overnight at room temperature in 4% buffered formaldehyde. Subsequently, the skin samples were embedded in paraffin wax. Transverse sections of 5 µm thickness were prepared, stained with hematoxylin and eosin, and subjected to examination using a light microscope (Olympus BX41 and camera Olympus XC50) on blinded-coded samples to assess the histological structure (Garrós et al., 2022).

3.3.12. Confocal Raman profiling

The Raman analysis was conducted utilizing a Model 3510 SCA Skin Analyzer, equipped with RiverICon version 3.0.130327 software from RiverD International B.V., Rotterdam, The Netherlands. The instrument was configured with two near-infrared (NIR) lasers emitting monochromatic light at 785 nm and 690 nm, respectively. Spectra were captured in two regions: the fingerprint region (FP) spanning 400–1800 cm^{-1} and the high wavenumber region (HWN) ranging from 2500 to 4000 cm^{-1}.

Prior to the experiment, the instrument underwent calibration using an external National Institute of Standards and Technology (NIST) glass calibration standard, in addition to the instrument's internal Raman calibration standards, which included a neon lamp and a polymethylmethacrylate Raman sample. Calibration success was determined by meeting the predefined criteria within the software and achieving a signal-to-noise ratio exceeding 30.

To generate the Raman profile of BNB, ten frames were sequentially captured with a 30-second exposure time, and the average of these frames was computed. Two different solutions were prepared using solvents: a 2% BNB solution in Transcutol and a 5% BNB solution in DMSO. DMSO and Transcutol blanks were also prepared to eliminate reference signals from the solvents, facilitating the isolation and analysis of the signal specific to the drug.

While the majority of Raman spectroscopy typically employs a single wavelength like 785 nm and focuses on the FP region from 450 to 1750 cm^{-1}, encompassing Raman signatures of various skin components, including natural moisturizing factor (NMF), ceramide, uranic acid, etc., it is noteworthy that the HWN region (2800–3800 cm^{-1}) with prominent Raman peaks of water and methyl groups is also crucial in assessing tissue hydration(R. Zhang et al., 2021).

3.3.13. BNB Determination by HPLC

The quantification of BNB in samples obtained from both in vitro release studies and ex vivo permeation studies (in skin and ocular tissue) was carried out using an HPLC system equipped with a fluorescence detector. However, the analysis of samples derived from the study of the drug amount retained in the tissue was conducted using an HPLC system with a UV detector.

The HPLC system with a fluorescence detector (HPLC-F) comprises a Chromatograph Waters Alliance 2695 and a Fluorescence Jasco FP-1520 detector set at an excitation wavelength (EX) of 310 nm and an emission wavelength (EM) of 390 nm. The chromatographic conditions for the determination of BNB are presented in Table 8.

Table 8. Chromatographic conditions for the determination of BNB with a Fluorescence detector.

Parameters	**Conditions**
Chromatographic column	Symmetry C18 (4.6 × 75 mm, 3.5 µm)
Mobile phase	Ammonium Formate 10 mM pH 7:ACN (75:25 *v*/*v*)
Flux	1 mL/min
Injection volume	10 µL
Wavelength	Ex 310 nm and Em 390 nm
Standard concentrations range	0.031 to 1 µg/mL

The HPLC system with a UV detector (HPLC-UV) consists of a Waters 1525 pump and a 2487 UV-VIS detector (Waters, Milford, USA) operating at a wavelength of 310 nm. Table 9 outlines the chromatographic conditions employed for the analysis of BNB.

Table 9. Chromatographic conditions for the determination of BNB with a UV detector.

Parameters	Conditions
Chromatographic column	Symmetry C18 (4.6 × 75 mm, 3.5 µm)
Mobile phase	Ammonium Formate 10 mM pH 7:ACN (75:25 *v*/*v*)
Flux	1 mL/min
Injection volume	10 µL
Wavelength	EX 310 nm
Standard concentrations range	2.5 - 40 µg/mL

3.3.14. Validation of the Analytical Methods

Due to the broad concentration range observed in the samples collected from the ex vivo permeation study and drug extraction from the different tissues, two distinct HPLC methods were validated and used as we explained in the previous section *3.3.13* for the quantification of BNB: HPLC-UV for samples with concentrations falling within the range of 2.5 - 40 µg/mL, and HPLC-Fluorescence for samples within the concentration range of 0.063 to 1 µg/mL.

All the components and characteristics of both methods have just been explained; we will now proceed to describe the validations of both HPLC procedures.

Calibration curves for both analytical methods were established by diluting BNB in Transcutol®P, starting from a stock solution of 60 µg/mL of BNB in Transcutol®P. The concentrations of the working standard solutions are provided below:

- HPLC-F curve: 0.063, 0.125, 0.25, 0.5 and 1 µg/mL;
- HPLC-UV curve: 2.5, 5, 10, 20 and 40 µg/mL.

Empower 3 software (Waters, Milford, USA) was used to process the data. The validation of the methods was performed as described in the ICH Q2A and ICH Q2B

Guidelines (ICH Expert Working Group, 2005), in terms of, precision, accuracy, linearity, sensitivity and specificity.

Linearity:

Five calibration curves at 5 concentration levels were prepared to evaluate the linearity of both methods. The correlation coefficient (r^2) of the calibration curves was calculated by linear regression analysis, and the response factor for each calibration curve was evaluated, by one-way analysis of variance (ANOVA).

Accuracy and Precision:

The inter-day precision of both methods was determined with five calibration curves prepared on different days by two different researchers and the relative standard deviation (%RSD) indicated the precision at each concentration level.

The accuracy was assessed by calculating the percentage of relative error (%RE) of the estimated concentration to the nominal one, at each concentration level (Equation 9):

$$\%RE = \frac{(C_0 - C_n)}{C_n * 100}, \quad (13)$$

where, C_0 is the observed concentration and Cn is the nominal concentration.

Sensitivity and specificity:

The limits of detection (LOD) and quantification (LOQ) led to stablish the sensibility of the methods. The LOD and LOQ were calculated starting from the relationship between the standard deviation of the response and the slope of the calibration curve. Equation 10 and Equation 11 describe the estimation of LOD and LOQ, respectively:

$$LOD = \frac{3.3 * s}{p}, \quad (14)$$

$$LOQ = \frac{10 * s}{p}, \quad (15)$$

where, s is the standard deviation of the response, and p is the slope of the calibration curve.

The specificity was evaluated as the absence of any peaks interfering at the retention time of BNB in the chromatographic conditions.

3.3.15. Statistical Analysis

Prism®, v. 5.00 software (GraphPad Software Inc., San Diego, CA, USA) was used for all statistical studies. The T-test was performed on the permeation with non-treated and treated skin with microneedles and ANOVA analysis was conducted on the permeation data regarding the chemical enhancers with statistical significance of $p<0.05$.

4. RESULTS

In this section, we delve into the results of the thesis, presenting a comprehensive analysis of the findings obtained through various experiments and studies. The outcomes discussed here provide valuable insights into the use of topical BNB.

I present all the findings at the same order I have written the different methodologies.

4.1. LIPOSOMES PHYSICOCHEMICAL CHARACTERIZATION

4.1.1. Liposomes Intended for SS Treatment: Lα-PC and POPE:POPG

The liposomes underwent measurements for pH, osmolality, and encapsulation efficiency, with the corresponding outcomes detailed in Table 10. Both liposomal formulations exhibited a pH within the physiological range, an osmolality value suitable for ophthalmic application, and an encapsulation efficiency below 20%.

Table 10. Results for pH, osmolality, and encapsulation efficiency (EE) of the liposomes. The values are expressed as the mean ± SD (n = 3).

Liposome	**pH**	**Osmolality (mOsm/Kg)**	**EE (%)**
Lα-PC	7.4 ± 0.1	306 ± 2	12 ± 0.9
POPE:POPG	7.4 ± 0.1	305 ± 5	11 ± 1.1

The liposomes share comparable sizes and bear a negative charge, with POPE:POPG displaying a notably higher ZP. The specific values are detailed in Table 11.

Table 11. Liposome composition alongside their respective hydrodynamic diameter, PDI, and ZP The outcomes are presented as the mean ± SD (n = 3).

Composition	**Formulation**	**Hydrodynamic Diameter (nm)**	**PDI**	**Zeta Potential (mV)**
Lα-PC	blank	73.0 ± 3.0	0.040	−22.5 ± 1.1
	+BNB	61.7 ± 0.5	0.081	−20.7 ± 0.5
POPE:POPG	blank	60.5 ± 0.6	0.124	−32.0 ± 3.0
	+BNB	51.7 ± 0.8	0.202	−37.0 ± 5.0

The investigation into surface electrical properties demonstrated a pH-dependent behavior in the liposomes. ZP values indicated a consistently negative surface charge across the entire pH range for all formulations, with no discernible distinctions between blank and loaded liposomes. Figure 17 illustrates the ZP variation of the liposomes relative to pH.

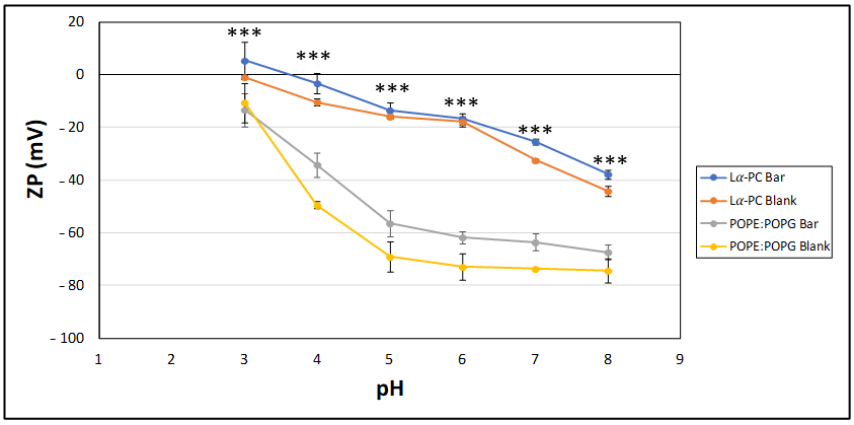

Figure 17. ZP of liposomes as a function of pH. Each point represents the Mean ± SD (n = 9). *** Statistical differences between Lα-PC liposomes and POPE:POPG liposomes ($p < 0.0001$) on a t-test analysis comparing Lα-PC vs. POPE:POPG loaded with BNB. Significance level set at $p < 0.05$.

The ZP results concerning the influence of ionic strength are depicted in Figure 18. Generally, there is an observable trend of decreasing absolute values as the concentration of electrolytes increases.

In the pH investigation, no significant differences between blank and loaded liposomes were detected. Specifically, in the presence of monovalent and divalent cations, ZP exhibited negative values at low electrolyte concentrations, with absolute values decreasing as the electrolyte concentration rose. With NaCl, the negativity persisted around 0 and slightly became positive at concentrations of 10^{-2} M, 10^{-1} M, and 2×10^{-1} M, respectively. For Ca^{2+} ions, ZP values turned positive or approached 0 from concentrations of 10^{-4} M or 10^{-2} M, depending on the liposome type. Finally, ZP values remained positive across the entire range of concentrations tested for Al^{+3}.

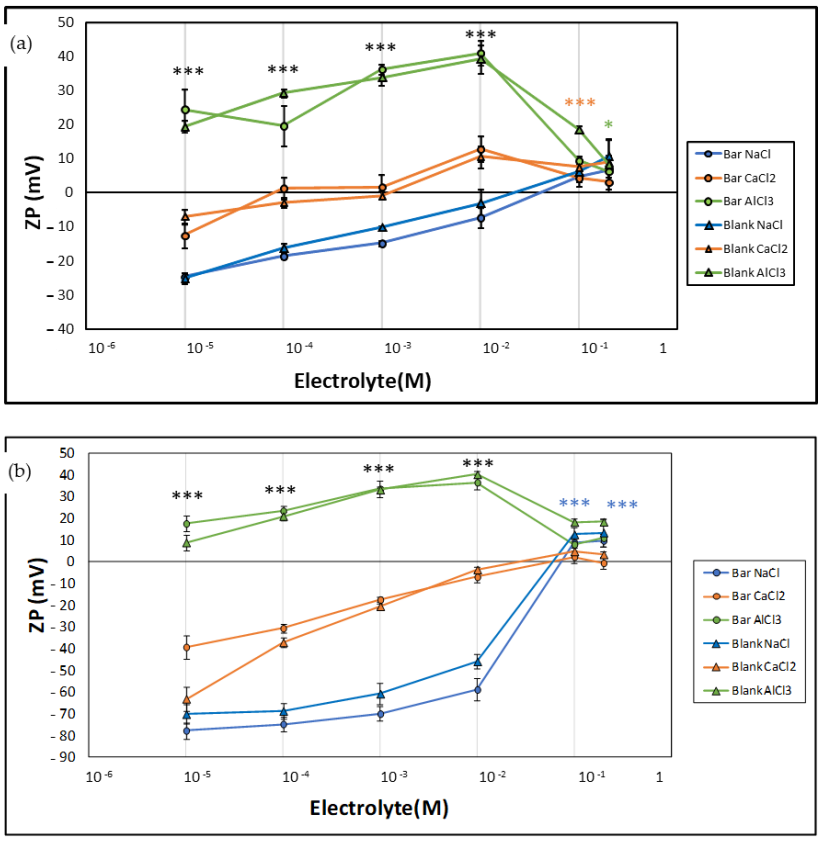

Figure 18. ZP of liposomes as a function of the concentration of NaCl, $CaCl_2$, and $AlCl_3$ at pH 7.4. (a) Lα-PC liposomes and (b) POPE:POPG liposomes. Each point represents the mean ± SD (n = 9). An ANOVA was conducted and then followed by Tukey analysis, considering three groups of electrolyte types at each concentration for both liposomes Lα-PC and POPE:POPG loading BNB. *** Statistical differences $p < 0.0001$ between all the electrolytes; *** Statistical differences $p < 0.0001$ between NaCl vs. $AlCl_3$ for Lα-PC; * Statistical differences $p < 0.05$ between NaCl and $CaCl_2$ vs. $AlCl_3$ for Lα-PC; *** Statistical differences $p < 0.0001$ between NaCl and $AlCl_3$ vs. $CaCl_2$.

4.1.2. Liposomes Intended for AD Treatment: POPC, POPC:CHOL and POPC:CHOL:CER

The three liposomes mentioned at the title section (POPC, POPC:CHOL and POPC:CHOL:CER) were characterized for pH, particle size and size distribution, EE and surface charge. The evaluations were conducted on freshly prepared liposomes and after storage at 4 °C for 1 month.

The pH value of all liposomes was consistent at 7.4 ± 0.1, aligning with the requirements for effective atopic skin treatments. Additionally, the EE was

comparable across formulations, with EE (%) values of 6.21 ± 0.55% for POPC, 5.57 ± 0.50% for POPC:CHOL, and 6.21 ± 0.63% for POPC:CHOL:CER.

Table 12 provides details on the vesicle size, PDI, and ZP for each liposome. While all liposomes exhibited similar characteristics, POPC:CHOL:CER liposomes displayed a higher ZP. The table also includes information on the physical stability of the liposomes over a one-month period.

Table 12. Liposomes composition: hydrodynamic diameter, PDI and ZP; and physical stability for 1 month. The results are presented as mean ± SD (n = 3).

Composition	Hydrodynamic Diameter (nm)		PDI		Zeta Potential (mV)	
	1 Day	1 Month	1 Day	1 Month	1 Day	1 Month
POPC	86.0 ± 1.4	86.9 ± 1.1	0.120	0.119	−14.2 ± 0.3	−13.9 ± 0.8
POPC:CHOL (8:2, mol/mol)	53.5 ± 0.9	55.4 ± 1.3	0.174	0.172	−13.2 ± 1.3	−13.5 ± 0.9
POPC:CHOL:CER (3.6:2.4:4.0 mol/mol/mol)	64.1 ± 0.3	65.0 ± 0.7	0.120	0.117	−18.3 ± 1.9	−18.1 ± 1.3

A one-way ANOVA test was carried out and then followed by Tukey's multiple comparison test. All three liposome sizes are statistically different from each other ($p < 0.0001$). Similarly, the ZP of POPC:CHOL:CER is different from the other two liposomes ($p < 0.05$). Liposome POPC and POPC:CHOL do not have a significantly different ZP compared to each other.

As we can see in the Table 12, one month after their preparation, these values were recalculated, and no significant changes were observed, with the maximum variation being limited to 4%.

4.2. MORPHOLOGICAL STUDY OF THE LIPOSOMES

TEM images of all the investigated liposomes are illustrated in Figure 19. The liposomes obtained exhibited a spherical shape, and no aggregates were observed.

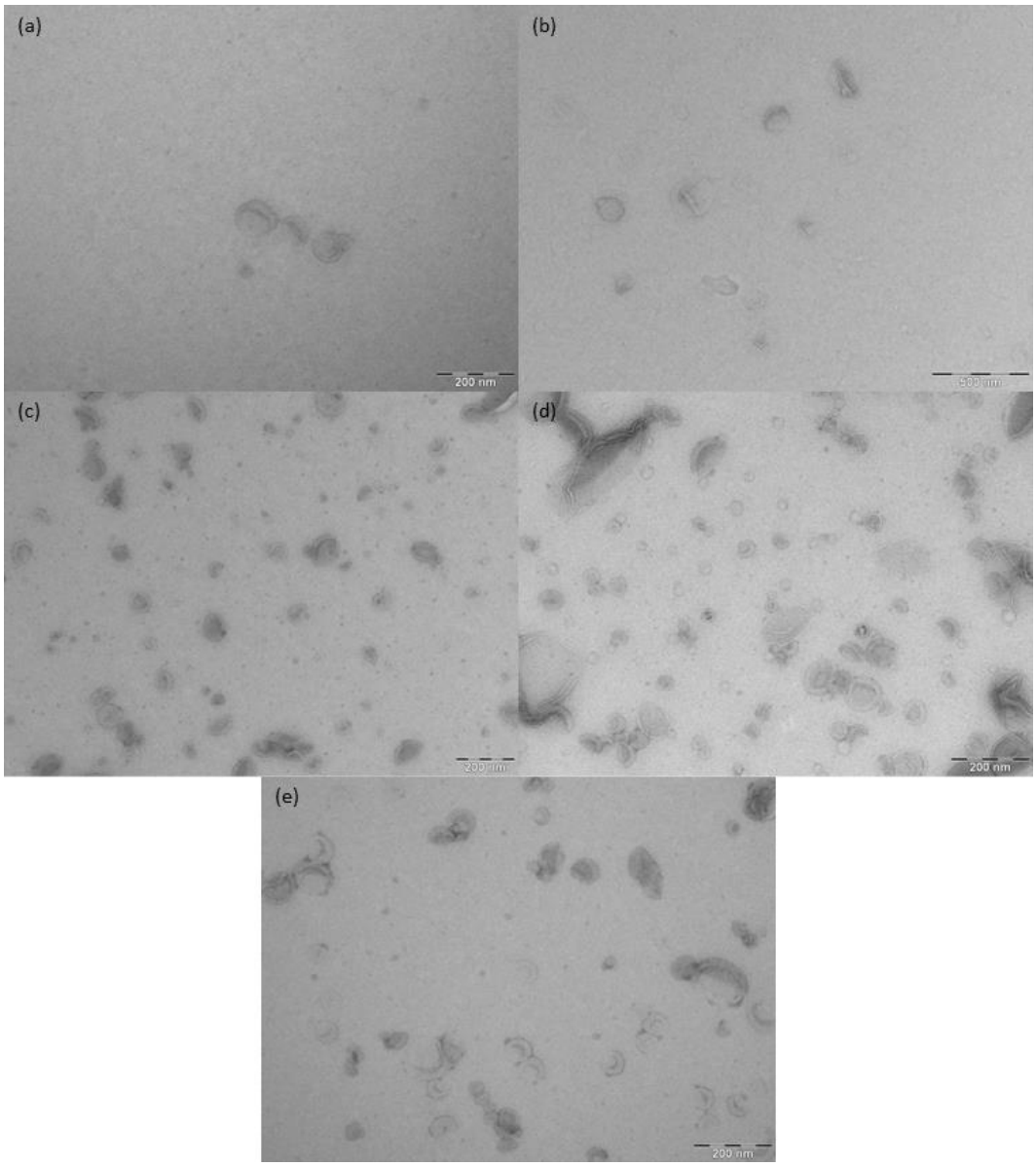

Figure 19. TEM images of the liposomes. (a) Liposome Lα-PC; (b) POPE:POPG. (c) Liposome POPC; (d) Liposome POPC:CHOL; (e) Liposome POPC:CHOL:CER. The scale bar stands for 200 nm less in image B, which represents 500nm.

4.3. IN VITRO DRUG RELEASE STUDY

The release data from all liposomal studies were subjected to various kinetic models. None of the liposomes' release profiles aligned with a nonlinear regression model. Among the five liposomes studied, four exhibited a drug release kinetic profile fitting the One Site Binding (hyperbolic) equation, while the POPC liposome displayed a distinct profile, aligning with the Polynomial: Second Order equation.

When comparing liposomes designed for ophthalmological application, both followed a hyperbolic system. Specifically, liposome Lα-PC demonstrated a faster drug release compared to liposome POPE:POPG. Moreover, liposome Lα-PC achieved complete drug release, while liposome POPE:POPG released only 64%, with the remainder retained.

Regarding liposomes designed for skin application, it was observed that liposome POPC:CHOL:CER exhibited a faster drug release than the other two liposomes. By the 8th hour, the release of BNB had reached a plateau, indicating that the maximum amount of drug release had been achieved. However, the total amount of drug released was lower than that observed with the other liposomes. In contrast, liposomes POPC and POPC:CHOL showed sustained release profiles for up to 53 hours, achieving a 2-fold drug release compared to liposome POPC:CHOL:CER, as illustrated in Figure 20.

Figure 20 depicts the release profiles of BNB with four liposomes' data fitted to the one-site binding model (Y = Bmax∗X/KD + X) and one liposomes' data fitted to Polynominal: Second Order ($y = A + Bx + Cx^2$).

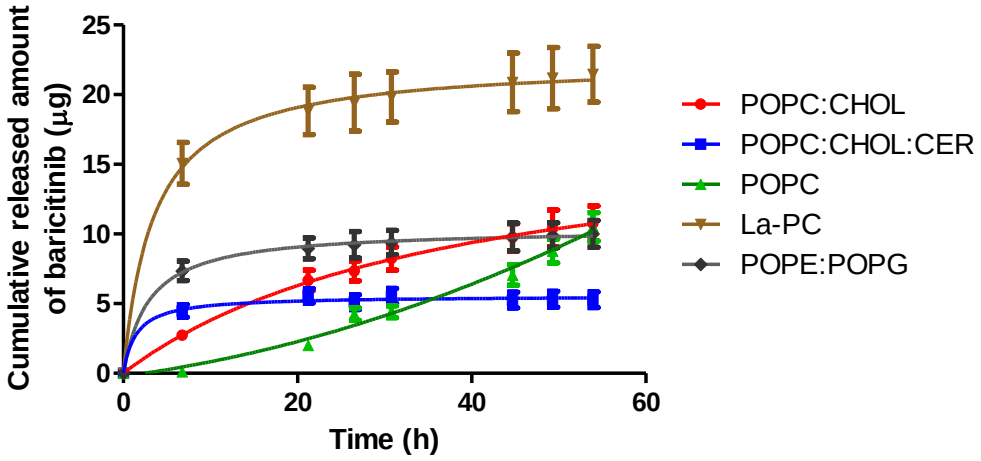

Figure 20. Release profiles of BNB from the liposomes intended to use in AD treatment: POPC, POPC:CHOL and POPC:CHOL:CER; and release profiles of BNB from the liposomes intended to use in SS treatment: Lα- PC and POPE:POPG. The graph stands for BNB cumulative released (µg) vs. time (h). Results are expressed by mean ± SD (n = 5).

As we have investigated the drug release from the 5 liposomes in the same way, so to better appreciate the differences in the release profiles among them, we have depicted them in a single graph. Subsequently, in view of we want to apply the liposomes for different purposes, we have presented their kinetic modeling characteristics in separate tables. First, we have liposomes intended for ophthalmological use (Table 13) which provides the fitted values for the model's parameters Bmax and KD. A T-test comparing Lα-PC and POPE:POPG revealed significant differences for Bmax. And in the following table, we have liposomes designed for direct applications on the skin (Table 14) which present the equations for each of the three liposomes.

Table 13. Best fit values in the kinetic modeling for the liposomal formulations and the statistical analysis by a T-Test between Lα-PC and POPE:POPG. Significance level set at $p < 0.05$.

Parameters	**Lα-PC**	**POPE:POPG**
Bmax (μg)	21.42	6.836
KD (h)	2.735	2.398
SE Bmax	0.424	0.052
SE KD	0.290	0.105
95% CI Bmax	20.33 to 22.51	6.701 to 6.971
95% CI KD	1.989 to 3.480	2.128 to 2.668
R^2	0.9992	0.9999
p-value Bmax	<0.0001	
p-value KD	0.3047	

Bmax = maximum amount released (μg); KD = time required to reach 50% of the drug release (h); SE = standard error; CI = confidence interval.

The context of our investigation into the treatment of AD, it is noteworthy that the liposomes designed for this study present divergent drug release profiles, as we previously mentioned. Particularly, the formulation containing POPC exhibits a

unique release profile, deviating from the equations characterizing the other two formulations, namely POPC:CHOL and POPC:CHOL:CER. The intricate dynamics of drug release are visually represented in Figure 20, elucidating the distinct kinetic behaviors of these liposomal formulations. Table 14 provides detailed information on the best-fit values obtained through kinetic release modeling for each liposome formulation.

Table 14. Best-fit values for liposome formulations in kinetic release modeling.

Liposome	**Equation**	**Best-Fit Values According to the Equation**				
		A	**B**	**C**	**B_{max} (µg)**	**K_d (h)**
POPC	Polynominal: Second Order $y = A + Bx + Cx^2$	0.21	0.08	0.002	-	-
POPC:CHOL	One site binding (hyperbola) $y = B_{max}x/(K_d + x)$	-	-	-	18.37	38.34
POPC:CHOL:CER	One site binding (hyperbola) $y = B_{max}x/(K_d + x)$	-	-	-	5.55	1.45

A, B and C = parabola coefficients. Hyperbola parameters Bmax = maximum amount of BNB that can be released; and Kd = drug release constant.

For the comparison of distinct drug release profiles among the three liposome formulations, non-modelistic parameters such as AUC, release efficiency and MRT were calculated. As shown in Figure 21, the non-modelistic parameters, along with the corresponding statistical tests, affirm the presence of significant differences among the three liposomes. Specifically, liposome POPC:CHOL exhibits the highest AUC values and the greatest release efficiency percentage. However, in contrast, it registers the lowest MRT value, indicating a comparatively faster drug release profile compared to the other liposomal formulations.

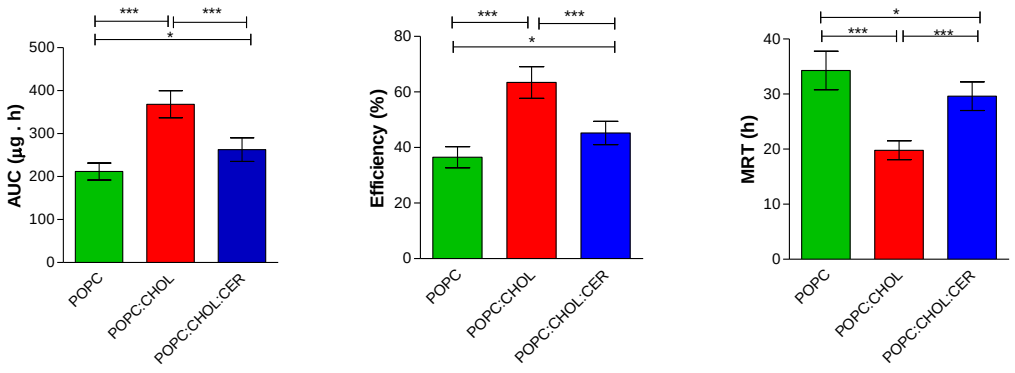

Figure 21. Non-modelistic parameters of: (a) Area Under the Curve (AUC: µg/h); (b) Efficiency (E: %); (c) Mean Release Time (MRT: h). A one-way ANOVA test was carried out, followed by Tukey's multiple comparison test (* $p < 0.05$, *** $p < 0.0001$). The results are presented as the mean ± SD (n = 5).

4.4. EX VIVO PERMEATION STUDIES

In the results of the ex vivo permeation studies, I first present those conducted with BNB solutions, including the intrinsic solution used on skin treated with physical promoters, such as microneedles, and the 2 mg/mL BNB solutions employed with various chemical promoters. Next, I present the results obtained from ex vivo permeation in the cornea and sclera using the Lα-PC liposome and the POPE:POPG liposome. Finally, we have the results of ex vivo permeation in the skin using the POPC liposome, the POPC:CHOL liposome, and the POPC:CHOL:CER liposome.

4.4.1. Intrinsic permeation of BNB in human skin (non-treated and treated skin with microneedles)

First, the intrinsic permeation study was performed using a saturated solution of BNB in Transcutol®P on intact healthy skin and skin treated with microneedles as a physical promoter. We present the results of the following study in Table 15, which shows us permeation parameters such as the MTT in the skin and the enhancer factor (EF), and Figure 22, where we can observe the drug permeation profile in both types of skin, its flux (Jss, µg/h·cm^2), the permeability coefficient of BNB to permeate each of the skins (Kp, cm/h), and finally, the predicted plasma concentration at the steady-state in human skin (Css, µg/mL).

Table 15. Biopharmaceutical parameters of BNB solutions with and without physical penetration enhancer.

Parameter	Normal skin	Treated with microneedles
MTT (days)	93.8	31.2
EF	-	3.0

MTT = mean transit time in the skin; EF= enhancement factor.

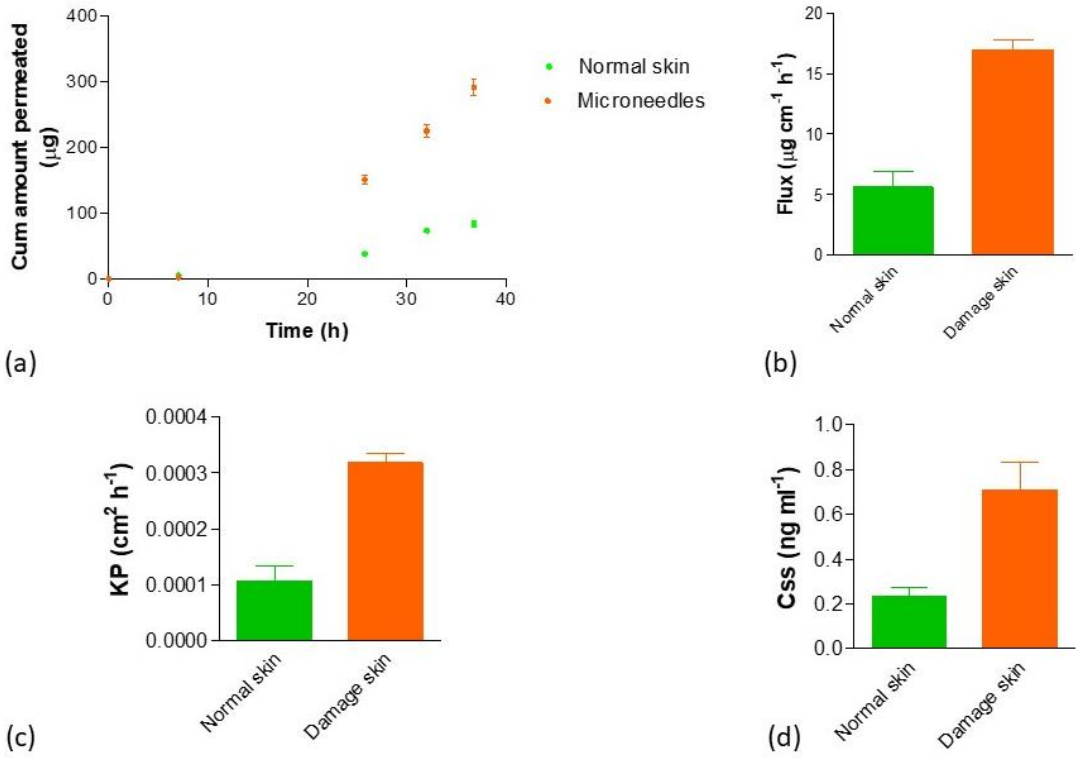

Figure 22. BNB permeation profile in normal and skin treated with microneedles: (a) BNB cumulative amount permeated (µg) vs time (h); (b) BNB solutions flux (Jss; µg/h·cm^2); (c) The permeability coefficient of BNB (Kp; cm/h); (d) Predicted plasma concentration of BNB at the steady state in the plasma considering a hypothetical surface of application of 10 cm^2 (Css) (ng/mL). Results are expressed by mean ± SD (n = 5). T-test analysis of variance with a statistically significant difference: ** = $p < 0.01$; *** = $p < 0.0001$.

In all cases, the value of the studied parameters was higher in the skin treated with microneedles compared to normal skin, with the amount permeated in the skin where we used the physical enhancer being 2.5 times higher than the amount permeated in normal skin.

4.4.2. Evaluation of Chemical enhancers on BNB's permeation through human skin

The impact of the chemical enhancers was assessed by a permeation study using a 2mg/mL solution of BNB in Transcutol®P with different chemical enhancers on intact healthy skin The permeation profile of BNB with the tested enhancers and without enhancer is presented in Figure 23, the Jss (µg/h·cm^2) is depicted in Figure 24 and Table 16 shows the rest of the permeation parameters: Kp (cm/h), Css (µg/mL), the MTT (days) and the EF for each penetration enhancer. A solution at the same concentration of BNB was used as a control (Non E). See Table 16 for the equivalence of the enhancers code and their identity.

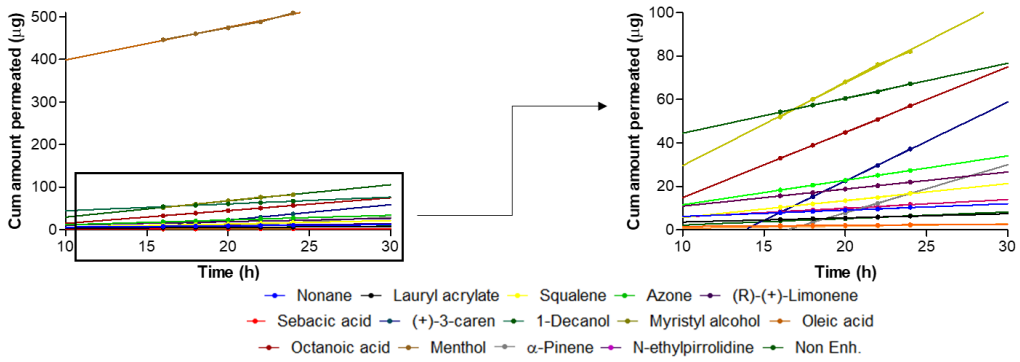

(a) **(b)**

Figure 23. BNB permeation profile: BNB cumulative amount permeated (µg) vs time (h): (a) Mean cumulative amount BNB permeated; (b) mean cumulative amount BNB permeated without M enhancer.

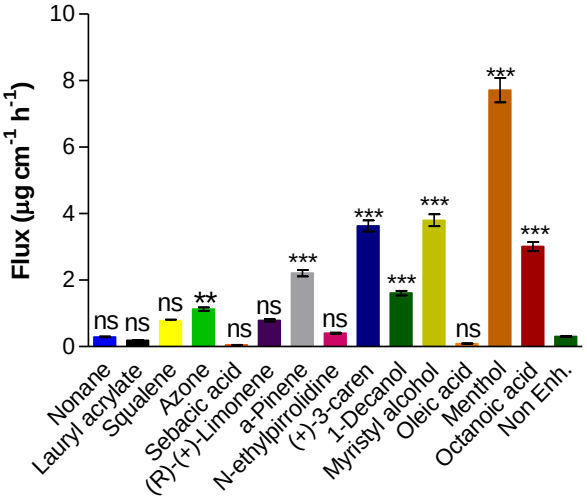

Figure 24. Flux of BNB obtained from the permeation of solutions with different enhancers and comparison to the plain solution without chemical enhancer. Results are expressed by mean ± SD (n = 5). ANOVA with Turkey's Multiple Comparison Test. Statistically significant difference between solutions vs no enhancer: ** = $p < 0.01$; *** = $p < 0.0001$.

Table 16. Biopharmaceutical parameters of BNB solutions with and without a penetration enhancer. Parameters presented are Kp, predicted plasma concentration of BNB at the steady state in humans (Css), MTT in the skin and the EF.

Permeation enhancer	Kp (x 10^{-4} cm/h)	Css (ng/mL)	MTT (days)	EF
Nonane	0.57±0.05	0.12±0.01	NA	0.97
Lauryl acrylate	0.37±0.03	0.08±0.01	NA	0.63
Squalene	1.54±0.16	0.33±0.02	64.1	2.59
Azone	2.22±0.23	0.47±0.05	NA	3.73
Sebacic acid	0.10±0.01	0.02±0.00	NA	0.17
(R)-(+)-Limonene	1.55±0.15	0.33±0.03	NA	2.61
α-Pinene	4.35±0.42	0.92±0.09	22.7	7.32
N-ethylpirrolidine	0.79±0.08	0.17±0.02	NA	1.33.
(+)-3-caren	7.14±0.74	1.51±0.16	13.8	12.02
1-Decanol	3.17±0.32	0.67±0.07	NA	5.33
Myristyl alcohol	7.49±0.78	1.59±0.17	13.2	12.60
Oleic acid	0.18±0.01	0.04±0.00	535.2	0.31
Menthol	15.18±1.60	3.22±0.34	NA	25.55
Octanoic acid	5.92±0.60	1.26±0.13	16.6	9.97
Non-Enhancer	0.59±0.06	0.13±0.01	165.7	-

Results are expressed by mean ± SD (n = 5).

Menthol by far achieves superior permeation compared to the other studied situations, followed by Myristyl alcohol and (+)-3-carene. Specifically, compared to permeation without using any chemical enhancer, they manage to multiply the permeation of BNB in the skin by 25, 12, and 12, respectively.

4.4.3. Ex Vivo Sclera and Cornea Permeation Study

The evaluation of both liposomes on the cornea exhibited robust correlation with r^2 reaching 0.99, indicating a strong association. In the sclera, the r^2 values were even higher, surpassing 0.97. Subsequent to this analysis, a comprehensive set of permeation parameters was calculated, encompassing the permeation profile, flux (Jss, µg/h), permeability coefficient (Kp, cm/h), cumulative permeated amount at 24 h (Cum BNB 6 h, µg), and theoretical plasma concentration in humans at the steady state (Css, ng/mL) for BNB. The distinctive behavior of both liposomes on the sclera is visually depicted in Figure 25, while Figure 26 illustrates their respective impact on the cornea.

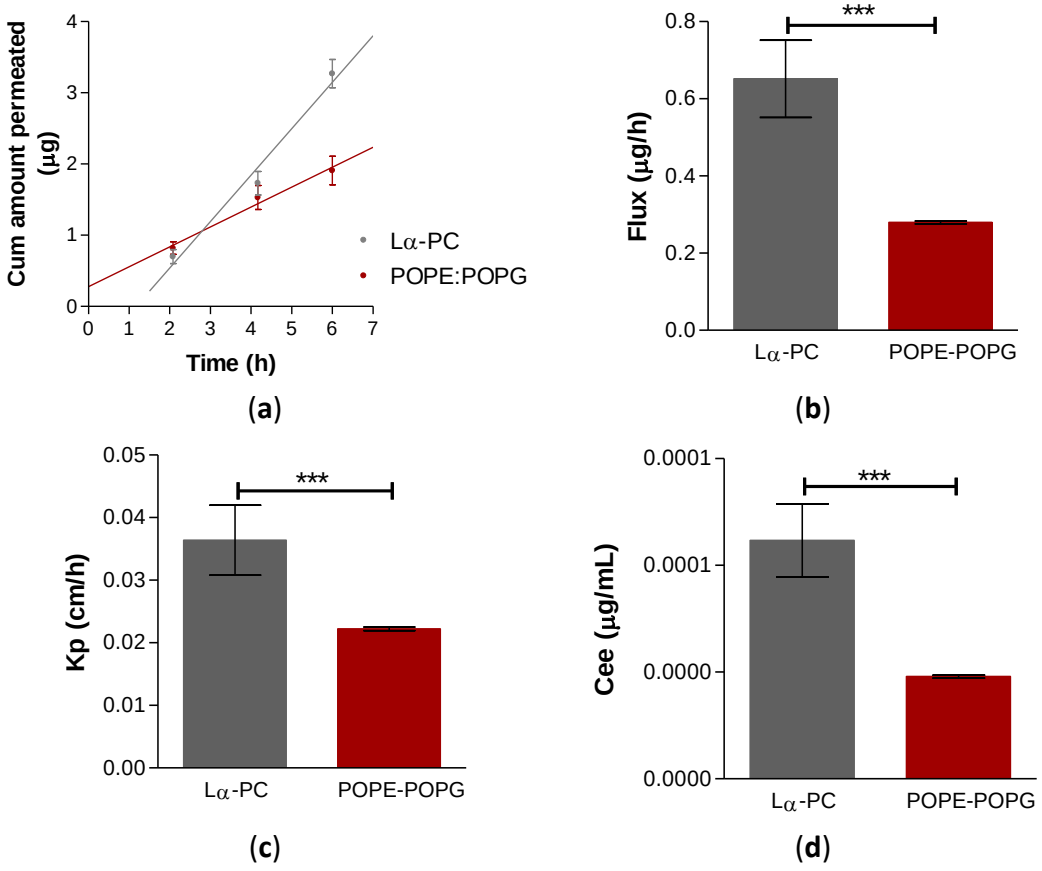

Figure 25. Ex vivo scleral permeation. (a) BNB permeation profile: BNB cumulative amount permeated (µg) vs. time (h); (b) BNB flux for each liposome; (c) BNB amount retained in the scleral tissue; (d) theoretical plasma concentration at the steady-state in humans. Results are expressed by mean ± SD (n=5). T-test analysis with statistically significant difference: *** = $p < 0.0001$.

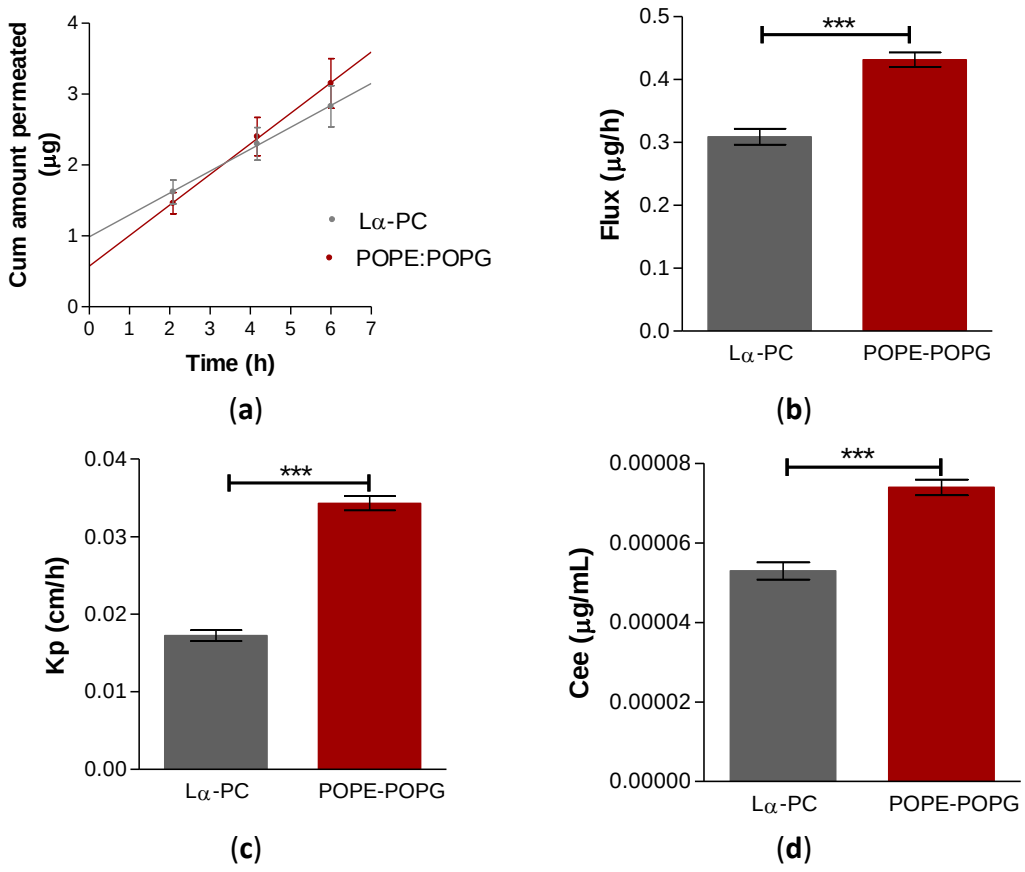

Figure 26. Ex vivo transcorneal permeation. (a) BNB permeation profile: BNB cumulative amount permeated (µg) vs. time (h); (b) BNB flux for each liposome; (c) BNB retained amount in the cornea; (d) theoretical plasma concentration at the steady state in humans. Results are expressed by mean ± SD (n=5). t-Test analysis, statistically significant difference: *** = $p < 0.0001$.

4.4.4. Ex Vivo Skin Permeation Study

In view of the heightened permeability characteristic of AD skin relative to healthy skin, microneedles were utilized to augment skin permeability, resulting in a more permeable skin known AHS as we mentioned in the methodology section.

The permeation profile, showcasing the cumulative amount permeated through AHS over a 25-hour duration, is illustrated in Figure 27. Notably, liposome POPC:CHOL exhibited the highest permeation, closely trailed by liposome POPC:CHOL:CER, while liposome POPC displayed the lowest permeation among the three liposomes tested. The calculated permeation parameters, including flux (Jss, µg/h), permeability coefficient (Kp, cm/h), and theoretical predicted plasma concentration in human steady state (Css, ng/mL), are detailed in Table 17.

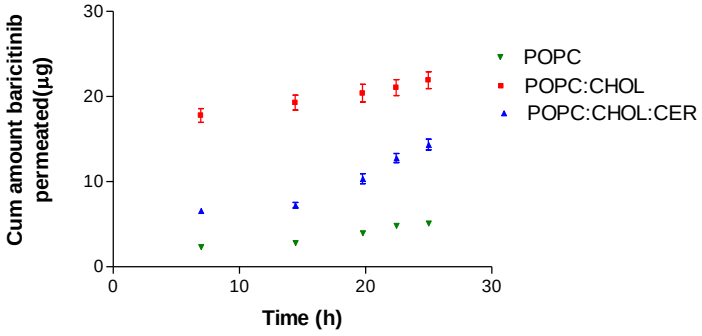

Figure 27. BNB permeation profile: cumulative amount of BNB permeated (µg) vs. time (h). The results are presented as mean ± SD (n = 5).

Table 17. Permeation parameters of three liposomes: cumulative amount of BNB permeated at 25 h (AP25h, µg), flux (Jss, µg/h), permeability coefficient (Kp, cm/h) and predicted steady-state plasma concentration in human steady state on a 10 cm2 surface application (Css, ng/mL).

	AP_{25h} (µg)	*Jss* (µg/h)	*Kp* (10^{-4} cm/h)	*Css* (ng/mL)
POPC	5.13 ± 0.52	0.22 ± 0.03	1.14 ± 0.16	0.36 ± 0.05
POPC:CHOL	21.93 ± 2.20	0.29 ± 0.03	1.52 ± 0.16	0.48 ± 0.05
POPC:CHOL:CER	14.36 ± 1.40	0.77 ± 0.07	4.01 ± 0.37	1.28 ± 0.12

ANOVA test analysis of variance, followed by Tukey's multiple comparison test, were performed, and all were statistically different from each other ($p < 0.001$). Results are expressed by mean ± SD (n = 5).

4.5. AMOUNT OF DRUG RETAINED

The results of the studies on the amount of drug retained in the tissue, whether skin, cornea, or sclera, are presented in the same order as the ex vivo permeation results. I first present the amount of drug retained using physical promoters, followed by the amount of drug retained using chemical promoters, and concluding with the results of the different liposomes. I start with those studied using ocular tissue and finish with those studied using skin.

4.5.1. Intrinsic Permeation of BNB in Human Skin (Non-Treated vs. Treated Skin with Microneedles)

The BNB retained in the skin after conducting the permeation study, both in non-treated skin and treated skin, is shown in Figure 28 and Table 18, skin treated with microneedles retained about 2.5-fold BNB more than non-treated skin.

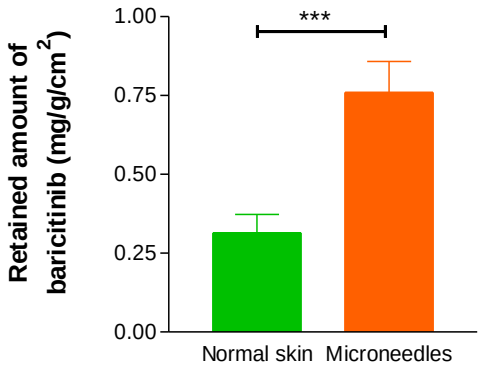

Figure 28. BNB amount retained in skin. Results are expressed as mean ± SD (n = 5). t-test analysis of variance. Statistically significant difference: *** = $p < 0.0001$.

Table 18. The amount of BNB retained in the skin is expressed as mg/g/cm^2 and the percentage of the amount spread at the beginning.

	Qret (mg/g/cm^2)	% BNB retained (%/g skin)
Non-treated skin	0.31±0.06	6.66±0.99
Treated skin with MN	0.76±0.09	16.08±1.90

Results are expressed by mean ± SD (n = 5). MN: microneedles.

4.5.2. Evaluation of the Effect of Chemical Enhancers on BNB's Permeation Through Skin

The BNB retained in the skin after conducting the permeation study with different chemical enhancers is shown in Figure 29. The enhancer which led to a higher retention of BNB in the skin was B (Lauryl acrylate). Table 19 shows the amount and percentage retained in the skin for each enhancer tested, as well as the drug amount retained in the skin with no enhancer.

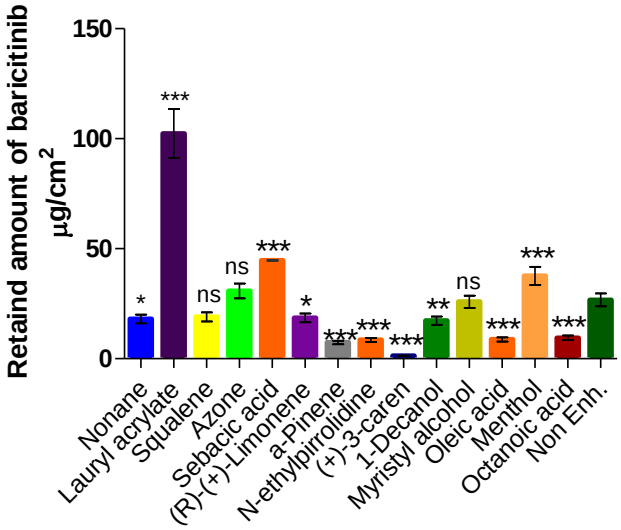

Figure 29. BNB amount retained in the skin treated with different permeation enhancers. Results are expressed as mean ± SD (n = 5). ANOVA with Turkey's Multiple Comparison Test. Statistically significant difference between solutions vs No enhancer: * = $p < 0.05$; ** = $p < 0.01$; *** = $p < 0.0001$.

Table 19. BNB amount retained in skin expressed as µg/cm2 and %/g of BNB retained from the initial amount of seeding.

Code	Permeation enhancer	Qret (µg/cm²)	% BNB retained (%/g skin)
A	Nonane	1.04 ± 0.21	0.08 ± 0.01
B	Lauryl acrylate	5.91 ± 0.53	0.49 ± 0.04
C	Squalene	1.10 ± 0.13	0.09 ± 0.01
D	Azone	1.78 ± 0.12	0.14 ± 0.01
E	Sebacic acid	2.59 ± 0.22	0.21 ± 0.01
F	(R)-(+)-Limonene	1.07 ± 0.12	0.09 ± 0.01
G	α-Pinene	0.43 ± 0.02	0.03 ± 0.00
H	N-ethylpirrolidine	0.49 ± 0.35	0.04 ± 0.02
I	(+)-3-caren	0.08 ± 0.00	0.00 ± 0.00
J	1-Decanol	1.00 ± 0.09	0.08 ± 0.00
K	Myristyl alcohol	1.50 ± 0.12	0.12 ± 0.01
L	Oleic acid	0.51 ± 0.04	0.04 ± 0.00
M	Menthol	2.18 ± 0.19	0.18 ± 0.01
N	Octanoic acid	0.55 ± 0.06	0.05 ± 0.00
Non-E	-	1.55 ± 0.17	0.13 ± 0.01

Results are expressed as mean ± SD (n = 5)

4.5.3. Retained BNB in the Cornea and Sclera

Figure 30 portrays the quantity of BNB retained in the sclera and cornea, revealing notable disparities between the liposomes in the sclera. Specifically, POPE:POPG retained BNB at a rate two times higher than Lα-PC. Conversely, no statistical variances were detected in the amount of BNB retained in the cornea, with both liposomes demonstrating comparable levels of retention.

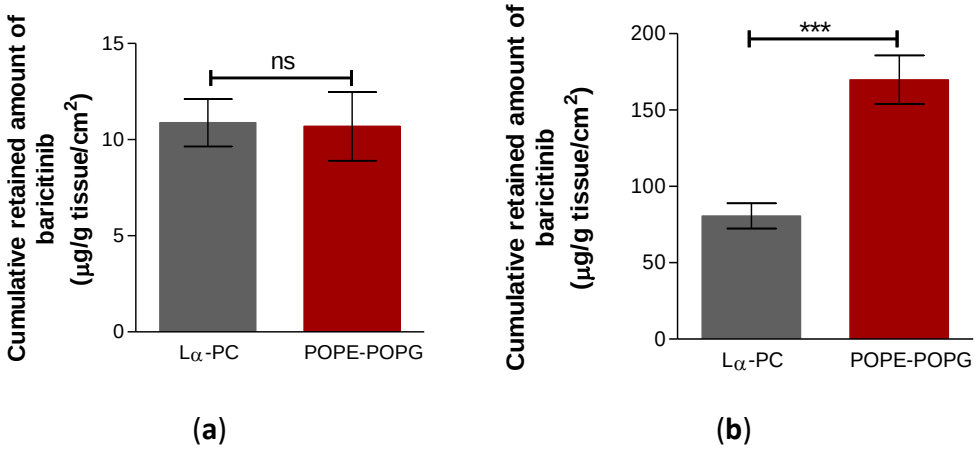

Figure 30. BNB amount retained in the tissues: (a) cornea (b) sclera. Results are expressed as mean ± SD (n = 5). T-Test analysis with a statistically significant difference: *** = $p < 0.0001$; ns = non-significant.

4.5.4. Retained BNB in the Skin

Figure 31 visually displays the quantity of BNB retained in the tissues, accompanied by the pertinent statistical outcomes. Remarkably, liposome POPC demonstrated noteworthy statistical differences when compared to both liposome POPC:CHOL and liposome POPC:CHOL:CER. Interestingly, no significant distinctions were observed between liposome POPC:CHOL and liposome POPC:CHOL:CER regarding BNB retention in the tissues.

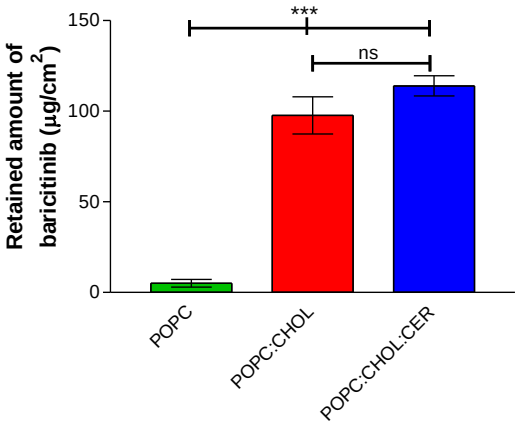

Figure 31. Retained amount (µg/cm^2) of BNB at 25 h in the AHS. Results are expressed as mean ± SD (n = 5). ANOVA test analysis of variance, followed by Tukey's multiple comparison test, were performed. Statistically significant difference: *** = $p < 0.0001$; ns = no statistically significant difference.

4.6. TOLERANCE STUDY AND HISTOLOGICAL ANALYSIS

4.6.1. HET-CAM

The potential irritant effect of the liposome formulations on both eyes and skin was assessed using the HET-CAM method, involving the application of the liposomes on the CAM of 10-day embryonated eggs. Intriguingly, no signs of hemorrhaging, coagulation, or vessel lysis were observed within 5 minutes after the application of the formulations, as illustrated in Figure 32. In stark contrast, the positive control displayed immediate hemorrhaging, and after 5 minutes, both hemorrhaging and coagulation were evident, highlighting the effectiveness of the HET-CAM method in discerning potential irritant effects.

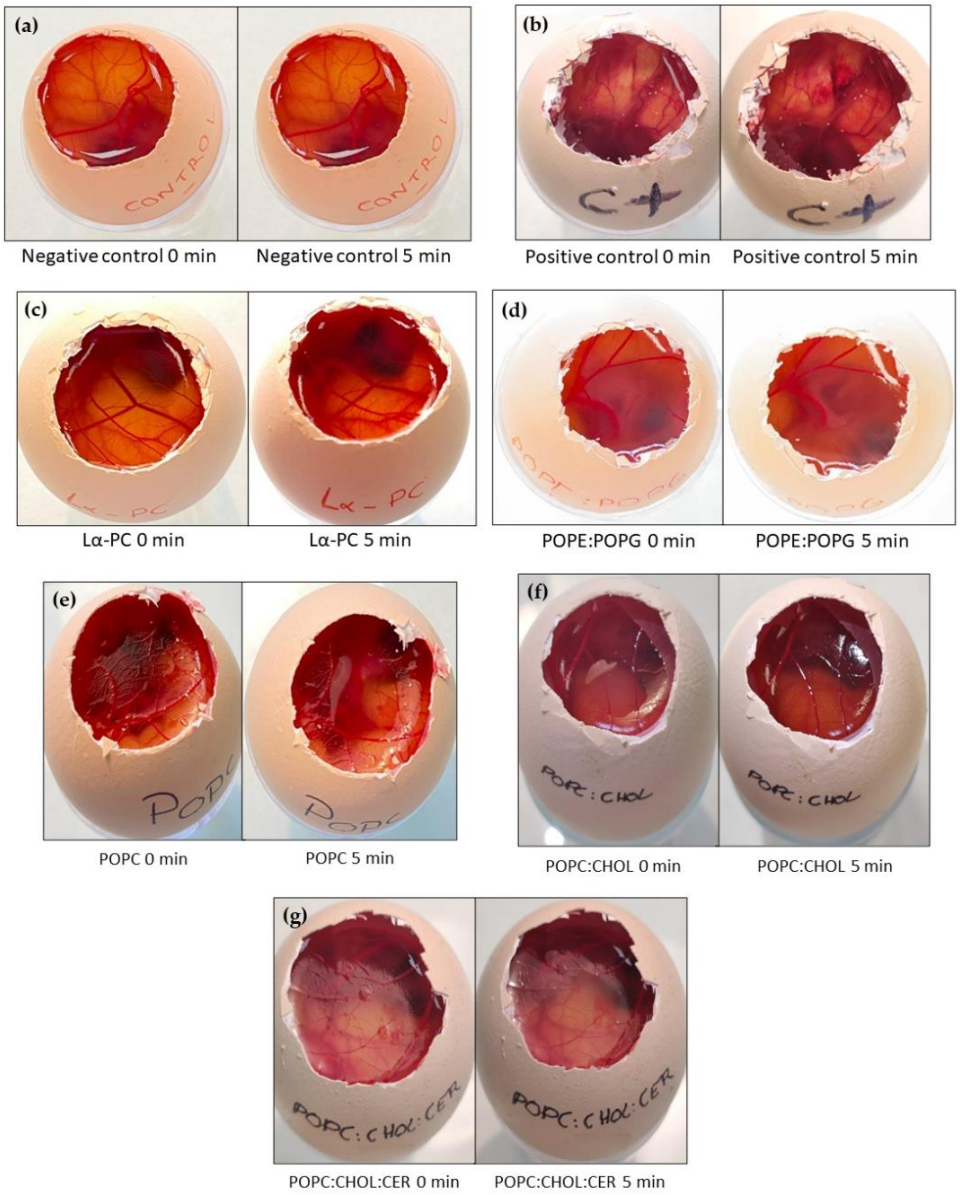

Figure 32. Evaluation of the irritant effect of the formulations by HET-CAM. (a) negative control (saline solution), (b) positive control (sodium hydroxide solution 0.1N, (c) Lα-PC liposome, (d) POPE:POPG liposome, (e) POPC liposome, (f) POPC:CHOL liposome and (g) POPC:CHOL:CER liposome

The IS obtained after the HET-CAM test are meticulously documented in Table 20. Impressively, the IS values for all liposomes remained consistently below 0.9, signifying an absence of any discernible irritating potential. This outcome underscores the favorable safety profile of the liposomes as assessed through the HET-CAM technique.

Table 20. IS of the liposomes tested by the HET-CAM technique.

Formulation	**IS**	**Classification**
Positive control (0.1 N NaOH)	16.10 ± 0.08	Irritating
Negative control	0.07 ± 0.00	Non-irritating
Lα-PC	0.07 ± 0.00	Non-irritating
POPE:POPC	0.07 ± 0.00	Non-irritating
POPC	0.07 ± 0.00	Non-irritating
POPC:CHOL	0.07 ± 0.00	Non-irritating
POPC:CHOL:CER	0.07 ± 0.00	Non-irritating

IS ≤ 0.9, non-irritating/slightly irritating; 0.9 < IS ≤ 4.9, moderately irritating; 4.9 < IS ≤ 8.9, irritating; and 8.9 < IS ≤ 21, severely irritating (Mallandrich et al., 2021).

AD can extend to facial skin, manifesting symptoms like dryness, redness, sensitivity, and itching. Given the need for soothing the liposomes destined for AD on facial skin, the potential tolerance of the liposomal formulations was evaluated for periocular application. This assessment provides valuable insights into the compatibility and safety of the liposomal formulations when applied around the eyes, acknowledging the specific challenges posed by AD symptoms on facial skin.

4.6.2. Cornea Transparency

The assessment of corneal transparency played a pivotal role in evaluating the potential irritant effect of the liposomes. Notably, corneas treated with ethanol, serving as the positive control, displayed a distinct reduction in transmittance within the 300–650 nm wavelength range, indicating a substantial decrease in corneal transparency by up to 20% compared to the negative control. Conversely, the transmittance profiles of both liposomes closely mirrored that of the negative control, suggesting that the liposomes did not adversely affect the transparency of the cornea. This observation is crucial in affirming the safety profile of the liposomes concerning potential irritant effects on the cornea, as illustrated in Figure 33.

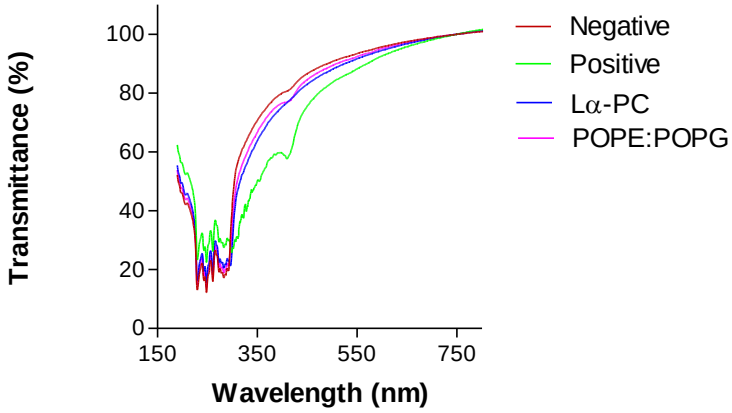

Figure 33. Transmittance from 190 to 850 nm wavelength of the corneas treated with PBS (negative control), ethanol (positive control), Lα-PC (L-α-phosphatidylcholine), and POPE:POPG liposomes after 10 min of incubation.

4.7. IN VIVO TOLERANCE STUDY

The tolerance of the liposomal formulations on altered skin, subjected to microneedle punches, was assessed in New Zealand rabbits. As depicted in Figure 34, the progression of ARS monitored for 3 h 30 min after applying xylol to induce erythema and edema, simulating flare-ups associated with AD. Intriguingly, all three liposomes demonstrated a delay in the onset of edema and erythema induced by xylol. Notably, the use of POPC liposomes was particularly notable for reducing the damage caused by xylol. The negative control of ARS, untreated with any substance or formulation, served as a baseline reference. This experiment provides sheds light

on the potential protective effects of the liposomal formulations against irritants on altered skin.

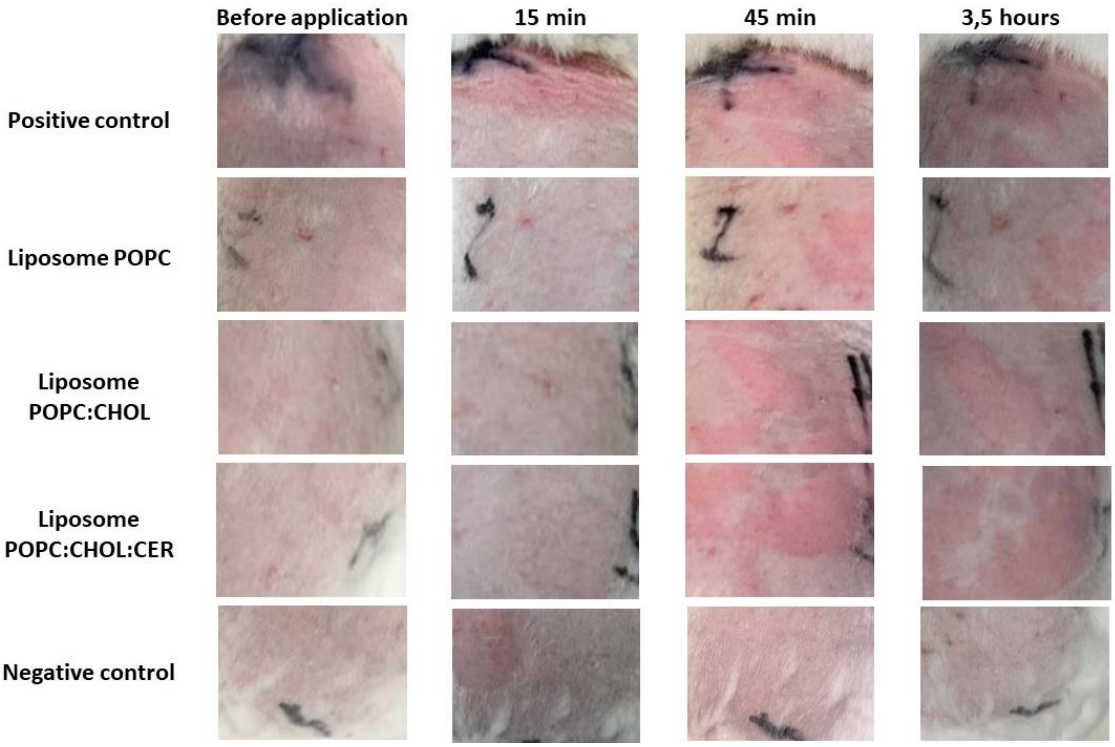

Figure 34. Pictures of 5 groups of rabbits used for the modified Draize test: before the application of xylol and liposomes, at 15 min, 45 min and 3 and a half hours after the respective applications.

The erythema and edema presented on the rabbits' backs are classified by the view scoring system (see Table 21).

Table 21. A modified Draize score was employed to evaluate erythema and edema resulting from xylol exposure, both with and without subsequent application of the liposomes (mean ± SD, n = 5).

Chemicals	Before Induced Er and Ed		15 min		45 min		3 h	
	Er	Ed	Er	Ed	Er	Ed	Er	Ed
Negative control	0.00 ± 0.00	0.00 ± 0.00	0.00 ± 0.00	0.00 ± 0.00	0.00 ± 0.00	0.00 ± 0.00	0.00 ± 0.00	0.00 ± 0.00
Liposome POPC	0.00 ± 0.00	0.00 ± 0.00	0.00 ± 0.00	0.00 ± 0.00	0.00 ± 0.00	0.00 ± 0.00	0.00 ± 0.00	0.00 ± 0.00
Liposome POPC:CHOL	0.00 ± 0.00	0.00 ± 0.00	0.00 ± 0.00	0.00 ± 0.00	1.00 ± 0.53	0.00 ± 0.00	0.65 ± 0.40	0.00 ± 0.00
Liposome POPC:CHOL:CER	0.00 ± 0.00	0.00 ± 0.00	0.00 ± 0.00	0.00 ± 0.00	1.45 ± 0.42	0.00 ± 0.00	0.37 ± 0.03	0.00 ± 0.00
Positive control (xylol)	0.00 ± 0.00	0.00 ± 0.00	3.54 ± 0.20	1.62 ± 0.41	3.50 ± 0.40	1.84 ± 0.13	2.40 ± 0.30	0.50 ± 0.02

Er = erythema; Ed = Edema.

The pictures of Figure 34 are supported by the graphs shown in Figure 35, which show the evolution of the transepidermal water loss (TEWL), and the evolution of the skin hydration, of rabbits with altered skin.

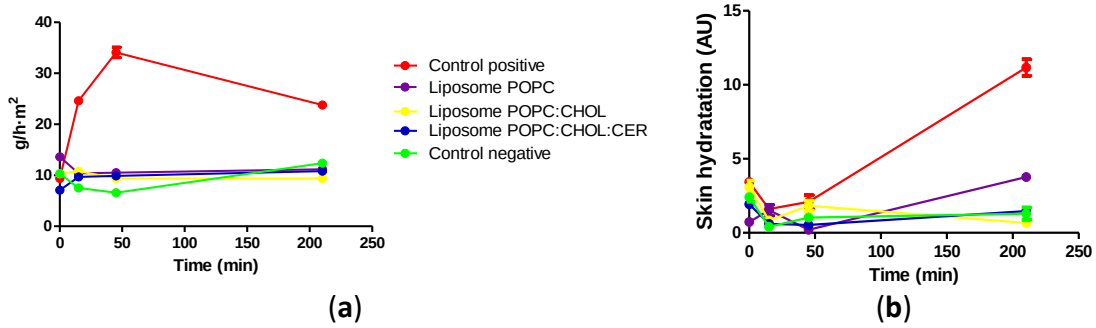

Figure 35. Results of TEWL and skin hydration during 210 min before and after formulations application on rabbits with induced dermatitis by xylol, except for the negative control. (a) TEWL; (b) Skin hydronation (AU). Results are expressed as mean ± SD (n = 5).

4.8. CORNEAL AND SCLERAL HISTOLOGICAL STUDY

No structural changes were observed in the sclera and cornea in the histological analysis using hematoxylin and eosin staining under control conditions (Figure 36). The application of two diluted liposome treatments did not induce any modifications in either the cornea or the sclera.

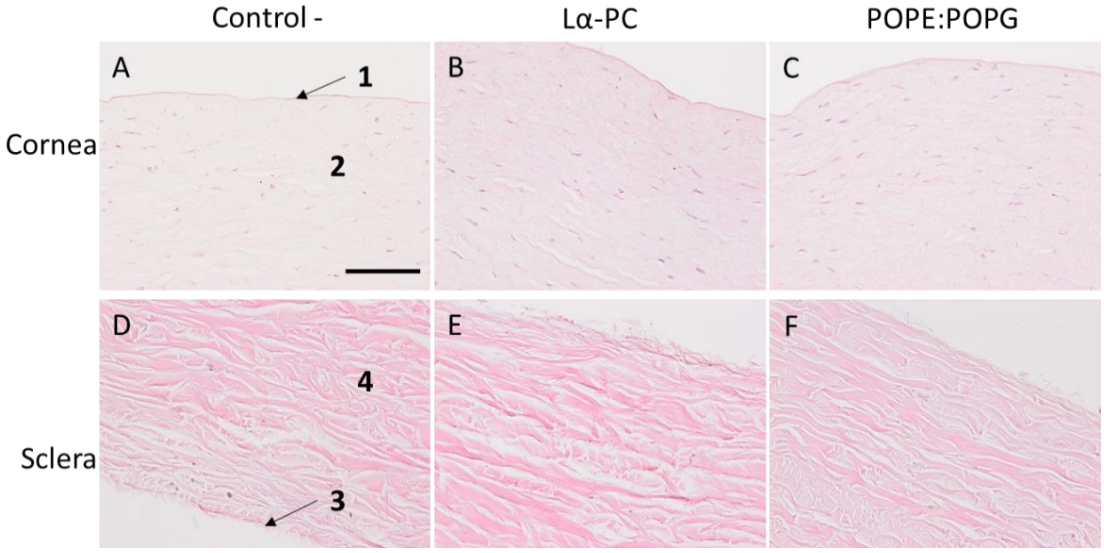

Figure 36. Sclera and cornea sections stained with hematoxylin and eosin. The upper row shows the cornea (A–C) and the sclera is shown below (D–F) in different conditions: control conditions (A,D); Lα-PC (B,E) and POPE:POPG (C,F); (1) corneal epithelium (non-keratinized stratified squamous epithelium); (2) substantia propria; (3) episcleral; and (4) stroma. Magnification = 200x, scale bar = 100µm.

4.9. SKIN HISTOLOGICAL STUDY

After the completion of the modified Draize test, a histological study was performed to assess potential structural changes in the modified skin resulting from the application of the formulations. The histology results for various liposomes, along with positive and negative controls, are depicted in Figure 37. The skin treated with the POPC:CHOL:CER liposome exhibited SC loss (Figure 37e), suggesting a disruptive effect. In contrast, skins treated with either POPC or POPC:CHOL liposomes did not show any discernible alterations.

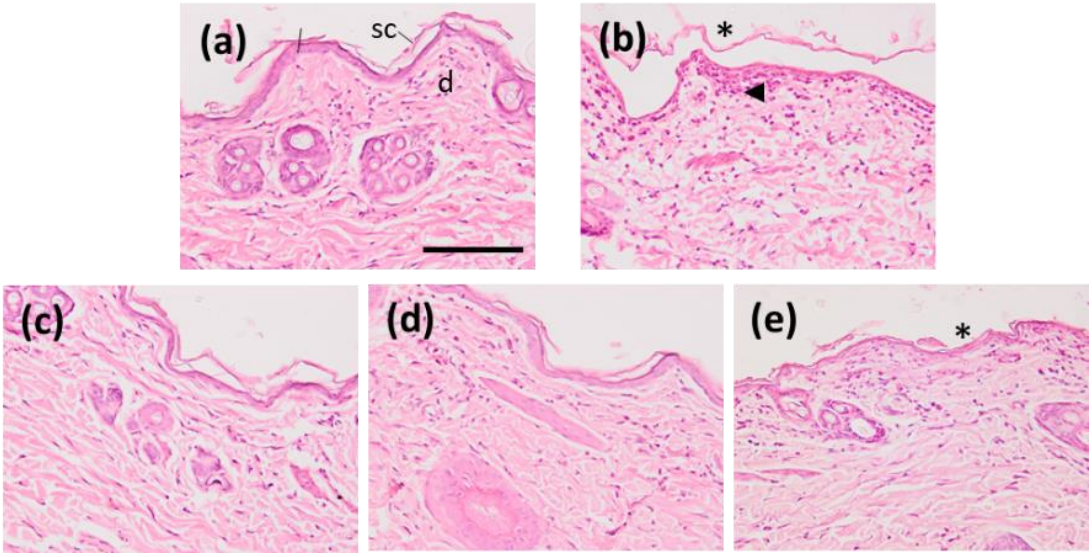

Figure 37. Skin sections colored with eosin and hematoxylin. (a) Control negative skin; (b) positive control; (c) treated with POPC; (d) treated with POPC:CHOL; and (e) treated with POPC:CHOL:CER. sc = stratum corneum, d = dermis, * shows loss of SC, Δ arrowhead indicates leukocyte infiltrate. Magnification = 200×, scale bar = 100 µm

4.10. CONFOCAL RAMAN PROFILING

The profile of the confocal spectrum of BNB is depicted in the following figure. We present the spectrum in the HWN range (2500-4000 cm^{-1}) and the FP region (400-1800 cm^{-1}).

Analyzing the spectra obtained from the Transcutol solution and the DMSO solution in Figure 38, we present the signal obtained with DMSO, as we observe that it exhibits higher quality and definition.

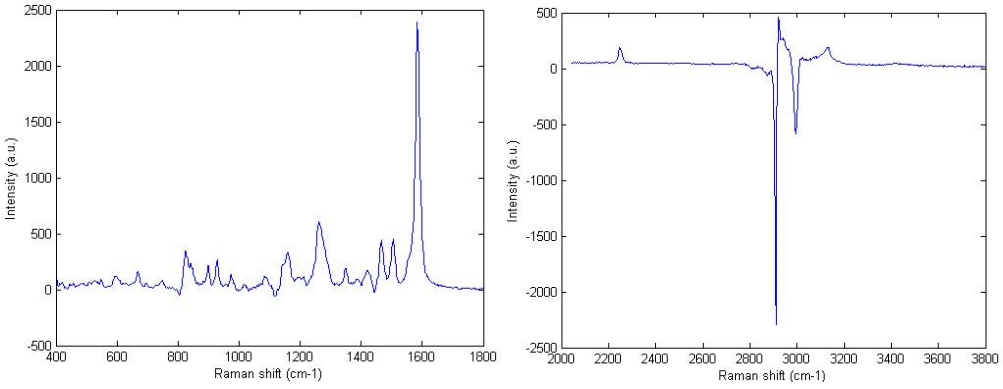

Figure 38. BNB spectrum based on the isolated signal attributed to BNB from the spectra of BNB solution on DMSO. Left: FP region and right: HWN region.

As we can see in Figure 38, BNB shows enhancement of vibrational modes around 1600 cm^{-1}, which can be indicative of the purine structure present in BNB. The band near 1200 cm^{-1} corresponds to the sulfone group. Finally, in the HWN, we observe a peak around 2810–2960 cm^{-1} that is associated with the C-CH_3 bonds.

4.11. VALIDATION OF ANALYTICAL METHODS

Two validated methods were established for quantifying BNB in the collected samples. Due to the low concentration in ex vivo permeation test samples, an HPLC-fluorescence method was developed and validated. For higher concentration, samples obtained from skin extraction after permeation tests, an HPLC-UV method was utilized and validated. The results of both method validations are detailed in the subsequent sections.

4.11.1. HPLC-UV method

The parameters studied included linearity, accuracy, precision, specificity, and sensitivity. Figure 39 shows the calibration curves obtained; the r2 values of each calibration curve were >0.999. The ANOVA showed no statistically significant differences between the response factor obtained ($p > 0.05$) demonstrating that the method is linear within the concentration range of 2.5 - 40 µg/mL.

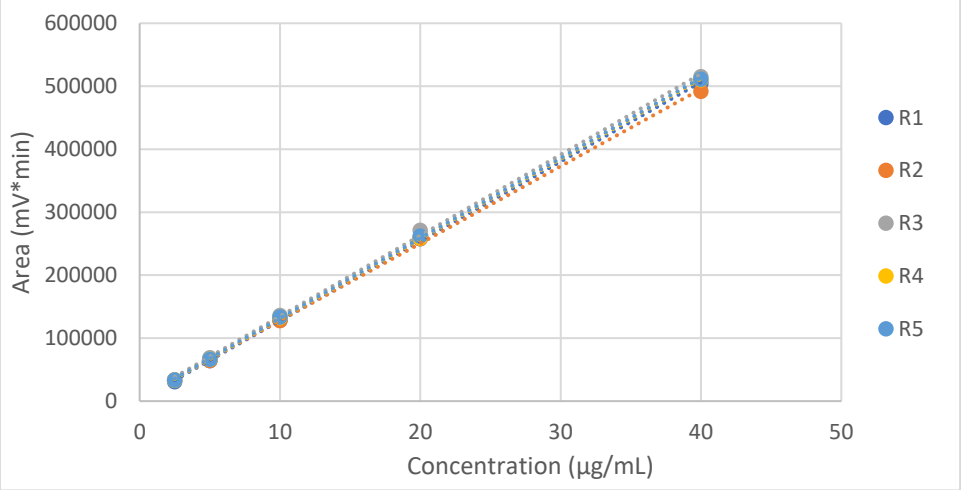

Figure 39. Linearity of the HPLC-UV method for the quantification of BNB within the con-centration range of 2.5 - 40 µg/mL. The linearity was assessed by linear regression of the response (area) versus concentration from the standard working solutions by quintuplicated.

The accuracy and precision of the method were calculated as the percentage of the RE and the RSD, respectively. The data are shown in Table 22. The results of the %RE and %RSD are below 10% indicating that the method has enough precision and accuracy within the range 2.5 – 40 µg/mL, this criterium is based on the ICH Q2 and Q14 guidelines (Committee for Medicinal Products for Human Use, 2022; ICH Expert Working Group, 2005).

Table 22. Accuracy (%RE) and inter-day precision (%RSD) for BNB standard solutions. Esti-mated concentration results are expressed by mean ± SD (n = 5).

Concentration of the standard solution (µg/mL)	**Estimated Concentration (µg/mL)**	**%RE** (%)	**%RSD** (%)
2.50	2.28 ± 0.06	8.50	2.90
5.00	4.90 ±0.06	1.81	1.28
10.00	10.09 ± 0.06	-0.96	0.69
20.00	20.41 ± 0.22	-2.06	1.11
40.00	39.79 ± 0.09	0.51	0.24

The specificity of the analytical method was demonstrated because there was no interference of any other compound at the retention time of BNB (Figure 40). The retention time of BNB was 3.16 min.

The LOQ provided the sensitivity of the method. Both, the LOD and the LOQ, were calculated from the standard deviation of the response and the slope of the calibration curve of 2.5 - 40 µg/mL. According to equations 8 and 9, the LOD for BNB was established at 0.70 ± 0.29 µg/mL and the LOQ was established at 2.11 ± 0.31 µg/mL. These results indicate that the method is sensitive enough for the quantification of BNB in the samples from the drug extraction procedure.

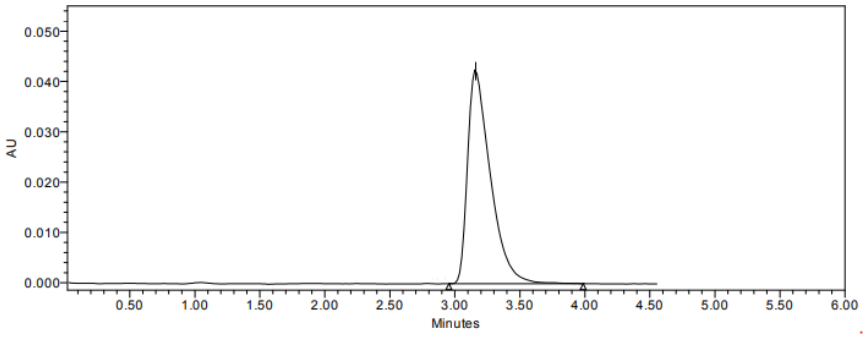

Figure 40. Chromatogram of BNB standard 40 µg/mL.

4.11.2. HPLC-Fluorescence Method

As in the HPLC-UV method, the parameters studied were linearity, accuracy, precision, specificity, and sensitivity. The r^2 values of each calibration curve were >0.999 as Figure 41 shows. The ANOVA showed no statistically significant differences between the response areas obtained (p = 0.05) demonstrating that the method is linear within the concentration range of 0.063 – 1.000 µg/mL.

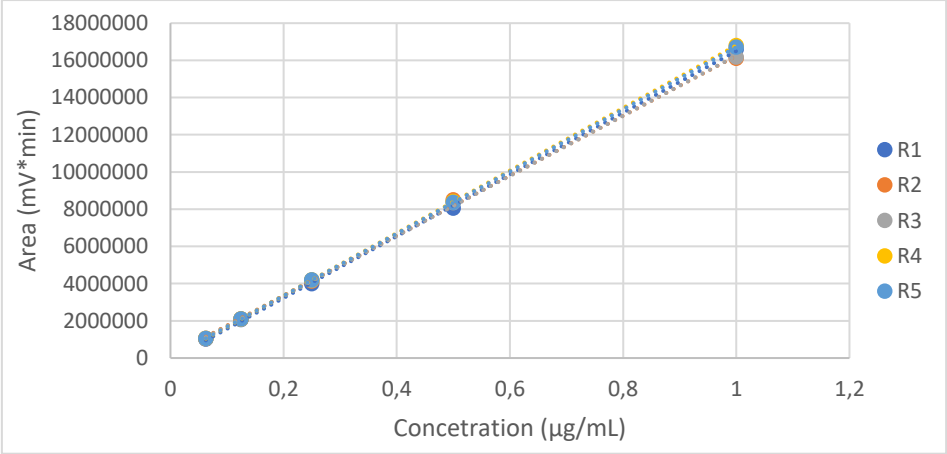

Figure 41. Linearity of the HPLC-F method for the quantification of BNB within the concentration range of 0.063 – 1.000 µg/mL. The linearity was assessed by linear regression of the response (area) versus concentration from the standard working solutions by quintuplicated.

The accuracy and precision of the method were obtained within the concentration range of 0.063 – 1.000 µg/mL. The results are shown in Table 23 expressed as percentages of the %RE and %RSD, respectively. These results show suitable precision

and accuracy for the intended analysis (Committee for Medicinal Products for Human Use, 2022; ICH Expert Working Group, 2005).

Table 23. Accuracy and inter-day precision for BNB standard solutions. Estimated concentration results are expressed by mean ± SD (n = 5).

Concentration of the standard solution (µg/mL)	**Estimated Concentration (µg/mL)**	**%RE** (%)	**%RSD** (%)
0.063	0.06 ± 0.00	-1.31	4.08
0.125	0.12 ± 0.00	0.11	1.65
0.250	0.25 ± 0.00	-0.22	1.16
0.500	0.50 ± 0.01	0.82	2.22
1.000	1.00 ± 0.01	-0.23	0.63

The analytical method was considered specific because it demonstrated that there is no interference of any other compound at the retention time of BNB (Figure 42). The retention time of BNB was 3.16 min.

Figure 42. Chromatogram of BNB standard 0.25 µg/mL.

The LOD and LOQ were calculated within the concentration range 0.063 - 1 µg/mL, the LOD for BNB was established at 0.0116 ± 0.009 µg/mL and the LOQ was established at 0.040 ± 0.006 µg/mL. These results indicate that the method is sensitive enough for the determination of BNB in samples from the receptor fluid collected in the ex vivo permeation assays.

5. DISCUSSION

In the present work, the study of BNB liposomes has been conducted as a new formula for the topical treatment of autoimmune diseases, specifically AD, and SS. The goal is to provide the possibility of developing an alternative or adjunct treatment with easy application and fewer adverse effects. Consequently, achieving greater patient adherence to the prescribed treatment. To accomplish this, an initial study of BNB in solution was conducted to understand its permeation and retention capabilities on the skin. This involved comparing a simple solution of BNB in Glycol monoethyl ether (DEGEE), commercially known as Transcutol®, with the same solution in the presence of different chemical enhancers or using direct physical enhancers. After studying the drug's behavior, various liposomes were formulated, and 5 were selected to continue with the thesis—three for skin application and two for ophthalmic application.

In all studies, the same receptor medium was used in permeation tests, transcutol®. We chose this solvent because of its high solubility and its good safety profile that does not compromise the skin's structure (Osborne & Musakhanian, 2018).

For the first time, we were able to observe the BNB spectrum using CRS technique. The FP region is crucial for identifying and characterizing molecular structures, it contains unique vibrational modes associated with specific chemical bonds, allowing for the identification of functional groups and overall molecular structure. In drug analysis, the FP is often essential for confirming the identity of a particular drug compound. The HWNs associated with functional groups involving hydrogen atoms. It is important for studying hydrogen bonding, which can provide information about the molecular interactions and the solid-state structure of the sample. We initially employed the CRS technique to explore the depth of BNB penetration into the skin. The signal strength proved insufficient for studying the low concentrations typical of our permeation and retention studies. The primary requirement for conducting measurements using CRS is that the molecule under examination must exhibit spectral characteristics of adequate intensity, allowing the signals to be distinguished from those originating from the skin components. This limitation was not due to the inefficiency of the CRS technique but rather to the specific solution we aimed to use for our study which was not sufficient at the low concentrations we found the drug

to overcome the various usual noises present in the measurement and surpass the signal from the pigskin. Consequently, we continued our analyses using the HPLC.

So to analyze the samples generated in the study, we have developed and validated two new methods. One of them is an HPLC-UV/Vis method with isocratic elution, offering the advantages of being faster and simpler than those already published in the literature for analyzing BNB (Gandhi & Kapoor, 2019; Hoang et al., 2021). For those samples with a lower drug concentration (fluid from the permeation assays), a second HPLC method coupled with a fluorescence detector, which is more sensitive, was developed. To the best of our knowledge, there are no publications addressing any fluorescence analytical technique for this drug.

As mentioned earlier in this work, we have investigated the use of different enhancers, both chemical and physical strategies, to enhance the viability of BNB on the skin. As a physical enhancer, solid metal microneedles were used to assess the intrinsic permeation of BNB into human skin. As expected, the skin treated with microneedles showed greater penetration of BNB, creating an annular pathway that increases permeability. Therefore, this is a strategy to consider in the topical delivery of BNB, as microneedles are minimally invasive and painless due to their small size, as indicated by their name. Not only was permeation improved with microneedles, but the drug was also retained more on the treated skin. This allows for a depot effect that can enhance treatment effectiveness by depositing a greater quantity of the drug at the target organ.

In a healthy adult, the maximum concentration (Cmax) achieved with multiple doses of 2 mg every 24 hours is 6.96 µg/mL, and the minimum concentration is 3.57 µg/mL. Taking these data into account, we can consider that the saturated concentration of BNB does not reach the minimum concentration necessary for a systemic therapeutic effect (Shi et al., 2014).

Regarding chemical enhancers of permeation, menthol exhibited the most significant effect on the penetration of BNB through human skin, increasing permeation approximately 25-fold compared to permeation without any enhancer (H. Wang & Meng, 2017). Myristyl alcohol, carene, and octanoic acid followed the effect of

menthol in decreasing order. Menthol belongs to the class of terpenes. These compounds have demonstrated an ability to increase the penetration of lipophilic drugs by altering the structure of lipids in the SC, interacting with intracellular proteins, or enhancing the partition coefficient of the drug's co-solvent (Maibach & Wane Smith, 2005). Myristyl alcohol is a saturated fatty alcohol with 14 carbon atoms (C14). There are several studies on the impact of the carbon chain length of fatty acids on the improvement of permeation. A chain length around C12 has shown an optimal balance between skin affinity and partition coefficient. A shorter chain may not be sufficiently lipophilic for the skin (for example, octanoic acid), while longer chains may have a high affinity for the lipids in the SC (Maibach & Wane Smith, 2005). However, when evaluating the amount retained on the skin, it is noteworthy that lauryl acrylate showed the maximum effect despite having a low flux value. This enhancer offers promising prospects for improved treatment because it limits the amount of permeated drug while keeping the drug on the skin, thereby avoiding a systemic effect (Shi et al., 2014).

In summary, microneedles improved the penetration and retention of the drug through the skin in a range of 2 to 3 times. Terpenes and fatty acids had a more significant impact on the penetration of BNB, with menthol increasing the permeation of BNB 25 times compared to a simple solution, and esters can multiply the retention of BNB on the skin up to 3 times. Therefore, percutaneous delivery of BNB is a promising alternative to the oral route.

Once we understand the permeation and retention capabilities of BNB with the different enhancers, we decide that, for the characteristics we are seeking in our product in the thesis, the same nanosystem formulation would suffice to provide the needed assistance for both permeation and retention in the skin and ocular tissues. BNB has been used orally, and there is currently no available literature on nanostructured systems loaded with BNB for topical administration.

BNB has been tested (only) once on the skin, and there is very little information on the formulation of this drug in nano-systems. Author Bhaskarmurthy et al. investigated the potential of BNB in reducing inflammation-induced edema in the ear by TPA in mice, and it was administered from a solution of BNB in acetone:DMSO

(Hiraganahalli Bhaskarmurthy & Evan Prince, 2021). Our study, therefore, encourages further research by building on the potential of BNB for use also on ocular mucosa.

Of the 5 liposomes formulated with different lipids, two were selected for the treatment of SS, and three for the treatment of AD.

The two liposomes for SS were formulated using three different types of lipids combined, resulting in the following two liposomes: Lα-P and POPE:POPG. These liposomes were selected to combine the immunomodulatory effect and the lipid effect to supplement the layer of the lacrimal lipid film. It is known that lipid composition alterations, besides the downregulation of specific proteins or changes in the rheological behavior of tears, are common in dry eye disease. The goal of lipid-based formulations is to mimic the lipid layer of the lacrimal film by combining the two components, aqueous and lipid (Garrigue et al., 2017). The author Hofauer et al. had also attempted to apply liposomes to the buccal, nasal, and ocular mucosa in patients with SS to alleviate symptoms such as xerostomia, dry keratoconjunctivitis, and dry rhinitis, and they achieved positive results. Therefore, it could be fruitful to load the liposomes with a specific immunomodulator so that the two components synergize, thus achieving a more advanced treatment (Hofauer et al., 2013).

The two liposomes have exhibited suitable characteristics for ophthalmic application: their small size will not damage the cornea upon application, and their pH is close to that of tears (7.4 – 7.5), so no irritation is expected. Additionally, their osmolarity also falls within stipulated criteria. The liposomes should resist aggregation due to van der Waals forces, as the ZP value is highly negative (Samimi et al., 2019; Watters et al., 2012). The electrical surface of the study focuses on two aspects: first, the dependence on lipid composition, and second, the influence of pH and ionic strength on the ZP.

One of the major limitations of liposomal systems is the aggregation of vesicles, leading to the destabilization of the system (Clares et al., 2009). In the same line, the study of the electrical properties of the surface provides the expected relevant information; the lipid composition of liposomes has a direct influence on the ZP due to the different net charges of the lipids used: POPE:POPG liposomes have much

more negativity than the Lα-P liposome. Another aspect is that the surface charge could also determine the interaction of liposomes with the ocular membrane due to the high negative charge of mucins.

Absolute values of the ZP show a marked increase when the pH is elevated. Changes in pH can also affect the degree of ionization of lipids. Specifically, the phosphate groups of the polar heads of phosphatidylcholine and phosphoglycerol are neutralized with acidic pH by hydrogen ions dispersed in the medium. In contrast, as the pH value increases and hydroxyl groups in the medium increase, a greater number of phosphate groups on the surface are dissociated, leading to an increase in the electrical charge of the surface of these particles (Clares et al., 2013). The pH of tears is approximately 7.45, ranging from 7.14 to 7.82, depending on daily and seasonal influences, and it can even rise to 7.89 in patients with dry eye syndrome, such as SS (Van Haeringen, 1981). Nano-systems with a ZP between +30 mV and -30 mV are considered to have low stability (Raval et al., 2019). Under these conditions, our formulations would have values outside the range of +30 mV/-30 mV, which would likely provide adequate stability (Clares et al., 2014).

Aqueous media are most used as a vehicle in ocular drop preparations, examples being sterile water for injections, isotonic sterile saline solution, balanced salt solution (BSS®), and a balanced salt solution with a composition similar to the intraocular medium. Both the composition of these vehicles and the conditions of physiological buffering introduce electrolytes with different valences that could influence the surface electrical characteristics of liposomes. The main electrolytes are Na^+, K^+, Cl^-, and HCO^-, with lower levels of Mg^{2+} and Ca^{2+}. Thus, the results of electrokinetic analysis of liposomes as a function of the ionic strength of the medium could serve to predict their dispersion stability (tendency to aggregate) and their mucoadhesive capacity.

The eye can tolerate tonicity within the equivalent range of 0.6-2% NaCl. However, to achieve isotonic solutions with tears and ensure they are comfortable for the eyes, a quantity equivalent to 0.9% NaCl 0.15 M is generally used. According to our results, as the concentration of salts increases, counterions accumulate closer to the

particle's surface, compressing the double layer and weakening repulsive forces, thus reducing the ZP (Hunter, 2001).

Regarding the effect of $AlCl_3$, ZP values were positive across the entire range, likely due to the adsorption of this ion to the surface of liposomes. Finally, a high concentration of electrolytes equivalent to an isotonic solution can produce an increase in charge, showing slightly positive values. This phenomenon can lead to the formation of large aggregates and rapid sedimentation, resulting in a flocculated system that is easily redispersible (Arias et al., 2008). Additionally, due to their positive charge, liposomes could interact better with the ocular film, prolonging the drug's residence time on the cornea and thereby extending the therapeutic interval (Astarita et al., 2021; Mishra et al., 2011).

A rapid release of BNB is observed in the first 4-6 hours, followed by a slower release for both liposomes after these initial 6 hours. A released amount of BNB is obtained from the Lα-PC liposome, approximately three times higher than that of the POP:POPG liposome. This suggests that the lipid used in the preparation of liposomes has a significant impact on the extent of drug release. The release profiles of both liposomes fit the "one-site binding" mathematical model or a single binding site corresponding to a hyperbolic curve. The parameters of this model are Bmax, which corresponds to the maximum amount of drug that can be released, and KD, referring to the time needed to achieve 50% drug release. Statistically significant differences were observed in Bmax. However, no statistically significant differences were found in KD, indicating that both liposomes achieve 50% drug release in a similar time frame (approximately within the first 2 and a half hours).

The author Ansari et al. developed polymeric NPs loaded with BNB with the aim of improving BNB's bioavailability to reduce the dosage and minimize adverse effects (Ansari & Alshahrani, 2019). The authors prepared NPs with poly-lactic-co-glycolic acid and conducted a thorough characterization, obtaining an optimized formulation that exhibited sustained release for 24 hours, aligning with the Higuchi model.

Despite the fact that the Lα-PC liposome shows higher release in in vitro models, this has not been a limiting factor for POPE:POPG in terms of penetration and permeation

through the cornea, where the amount retained in the tissue was similar for both liposomes. In the case of permeation, it was the POPE:POPG liposome that showed higher permeation. Conversely, Lα-PC was superior to POPE:POPG in permeation and penetration in the sclera. This is likely due to the difference in composition between the sclera and cornea, with the latter primarily composed of type I collagen and proteoglycans, while the sclera is mainly composed of connective tissue (Nishida et al., 2022). The amount of retained BNB in the corneal and scleral tissue would act as a reservoir and likely act as a local anti-inflammatory and immunomodulator, avoiding systemic side effects since the predicted concentration in steady-state plasma (Css) is lower than the concentration achieved with oral administrations (Shi et al., 2014).

Focusing now on the liposomes developed to serve as adjuvant treatment in AD: POPC liposome, POPC:CHOL liposome, and POPC:CHOL:CER liposome, we can discuss the following results. Starting with the physicochemical characteristics, such as pH, vesicle size, and ZP, influence the skin (González-Rodríguez & Rabasco, 2011). The POPC liposome has the largest vesicles, followed by the POPC:CHOL liposome, and the one with the smallest vesicles is the POPC:CHOL:CER liposome. All of them have a PDI below 0.2, which indicates uniformity in particle size. Their small size and low PDI mean that the formulations tend to pass more easily through sterilizing filters, making them more suitable for application on damaged skin that can easily become infected. In contrast, the ZP helps predict particle stability; a high ZP indicates a stable formulation. Therefore, the POPC:CHOL:CER liposome is the most stable among the three tested liposomes (Paranjpe & Müller-Goymann, 2014). The differences between the lipids used in each formulated liposome can lead to different release profiles described by various kinetic models (Schroeder et al., 2009). In our study, the two liposomes containing CHOL exhibit the same kinetic model, suggesting that the presence of CHOL in the liposome has a strong impact on the drug release characteristics. The fastest release of BNB over a short period was presented by the POPC:CHOL:CER liposome but not by the POPC:CHOL liposome. Although the POPC and POPC:CHOL liposomes exhibited a similar amount of released BNB at 54 hours, the POPC:CHOL liposome showed higher AUC levels than the POPC:CHOL:CER,

indicating superior performance for POPC:CHOL. The mathematical release model is an excellent tool for assessing differences between formulations (Campos et al., 2012; Domínguez-Villegas et al., 2014; D'Souza, 2014). Furthermore, non-modelistic parameters are useful for comparing formulations with different kinetic models. In this study, non-modelistic parameters show a relationship between the amount of released BNB from each formulation along with release efficiency, with the POPC:CHOL liposome formulation showing higher values. BNB is a molecule with low solubility in water under physiological conditions, as observed from its structure. It does not exhibit charged structures at pH 7.40, suggesting that it could be found within the depths of the lipid bilayer. Additionally, it presents several groups capable of stabilizing the molecule in hydrophobic regions through hydrogen bonds. These facts indicate that BNB incorporates into the lipid membrane of the liposome, remaining there and not being released to permeate through the skin. To overcome this issue, liposomes containing BNB were supplemented with 5% Transcutol. The structure of Transcutol allows it to be incorporated parallel to the hydrocarbon chains with its OH group close to the main group of phospholipids, distorting the phospholipid bilayer. Then, when liposomes containing BNB interact with the skin surface, BNB can be easily released from the liposome, and Transcutol molecules can increase the water solubility of BNB, facilitating its distribution to the skin surface. Various authors have demonstrated that if the lipids are like those found in the SC, more drugs will penetrate the skin (González-Rodríguez & Rabasco, 2011).

It is worth mentioning that human skin contains cholesterol and ceramides, and imbalances in their levels cause alterations in the skin's barrier function. Thus, restoring ceramide and cholesterol levels in the skin harmonizes this function (Pappas, 2009). Authors Sinico and Fadda explain that permeation and release could be higher when liposomes are formed with lipids already present in the skin (Sinico & Fadda, 2009). This would explain the greater permeation of POPC:CHOL and POPC:CHOL:CER liposomes compared to POPC liposomes. POPC:CHOL:CER liposomes tripled the values of flux, permeability coefficient, and theoretical steady-state plasma concentration in humans compared to the other liposomes studied. Therefore, ceramide could be acting as a permeation enhancer. Ceramides have been

considered the main factor in controlling the skin barrier function, and the enhancing effect of ceramide analogs has been demonstrated in various studies (Chen et al., 2014). Since the predicted steady-state plasma concentration does not reach therapeutic levels, BNB will only exert a local effect on the skin (Committee for Medicinal Products for Human Use (CHMP), 2020).

The retention of BNB in the skin was not statistically different between POPC:CHOL and POPC:CHOL:CER; therefore, both liposomes would be a good option to achieve a local effect of BNB since both liposomes achieve values 100 times higher than POPC liposomes (Figure 31). Liposomes with cholesterol and ceramide – which are lipids found in the skin – are capable of diffusing through the skin, thus creating a reservoir effect for BNB. The concentrations achieved inside the skin are higher than those obtained in the blood with oral therapy for AD treatments, considering the density of human skin as 1 g/ml (Rins et al., 1991; Shi et al., 2014).

The HET-CAM test did not show any irritation effects caused by any of the three liposomes. Regarding the modified Draize test, a good score was observed for erythema and edema (Table 21). The POPC liposome effectively counteracted the impact of xylene on the skin, and neither erythema nor edema was observed during the 3 hours of the tolerance study. Xylene caused both reactions, erythema and edema, which were observed from the first assessment (after 15 minutes) until the end of the tolerance study, which was after 3 hours.

The POPC:CHOL and POPC:CHOL:CER liposomes also effectively counteracted the edema caused by xylene. However, after 45 minutes of application, a slight erythema appeared in the areas where the POPC:CHOL and POPC:CHOL:CER liposomes were tested. Nevertheless, this effect was more than 2 and 3 times lower than the erythema caused by xylene. TEWL values were consistent for all liposomes, with values similar to the negative control (within the range of 8-15 g/h·m2, indicating a healthy value for rabbits), while the positive control showed a significant increase. The results are in line with those obtained in control rabbits, as observed by authors Babu M. Medi and Angela Anigbogu (A. Anigbogu et al., 2000; Medi & Singh, 2006). The skin hydration values remained constant and followed the trend of the negative control, while the positive control showed a consistent increase during the tolerance

study. Finally, the histological study demonstrated that the POPC and POPC:CHOL liposomes prevented any damage to tissue structures. Based on these promising results, further biochemical studies need to be conducted to test the effectiveness of these liposomal formulations in animal models of the disease, including mutant animals, before proceeding to clinical trials.

6. CONCLUSIONS

Throughout the research, significant advances have been made in understanding the study of BNB liposomes as a new formulation for the topical treatment of autoimmune diseases, contributing to existing knowledge through the studies conducted to achieve the aforementioned objectives.

These results have important practical implications in the field of biotechnology, as well as theoretical contributions to understanding the behaviour of BNB. The main goal of this thesis has been to develop and biopharmaceutically characterize (in vitro and ex vivo) BNB liposomes for topical application in the treatment of topical diseases: SS and AD. For this purpose, we have reached the following conclusions:

- Two high-resolution liquid chromatography methods with fluorescence and UV/Vis detection have been developed and validated for the detection and quantification of BNB according to the criteria of linearity, accuracy, precision, sensitivity, selectivity, and specificity. These methods have allowed us to obtain many of the conclusions mentioned below.
- Among the developed liposomes, five have been selected and have shown promising results, either for topical application as an adjunct treatment for AD or as an adjunct treatment for SS.
- The physicochemical characteristics of the formulations have consistently shown conditions compatible with the intended applications.
- Release studies have demonstrated sufficient drug release from the formulations under conditions like those found on the skin and/or mucous membranes.
- Permeation studies on human skin and porcine mucous have confirmed that the permeation occurring in both skin and mucous membranes would not be sufficient to produce a systemic effect. However, they have shown retention in the tissue sufficient for a local effect.
- In all cases, the formulations have been compatible for application on both skin and mucous membranes.

BIBLIOGRAFIA

Adler-Neal, A. L., Cline, A., Frantz, T., Strowd, L., Feldman, S. R., & Taylor, S. (2019). Complementary and Integrative Therapies for Childhood Atopic Dermatitis. *Children*, *6*(11), 121. https://doi.org/10.3390/children6110121

Ahmed, O. A. A., Kurakula, M., Banjar, Z. M., Afouna, M. I., & Zidan, A. S. (2015). Quality by Design Coupled with Near Infrared in Formulation of Transdermal Glimepiride Liposomal Films. *Journal of Pharmaceutical Sciences*, *104*(6), 2062–2075. https://doi.org/10.1002/jps.24448

Albanese, A., Tang, P. S., & Chan, W. C. W. (2012). The Effect of Nanoparticle Size, Shape, and Surface Chemistry on Biological Systems. *Annu. Rev. Biomed. Eng. 2012*, *14*, 1–16. https://doi.org/10.1146/annurev-bioeng-071811-150124

Alexander, H., Brown, S., Danby, S., & Flohr, C. (2018). Research Techniques Made Simple: Transepidermal Water Loss Measurement as a Research Tool. *Journal of Investigative Dermatology*, *138*(11), 2295-2300.e1. https://doi.org/10.1016/j.jid.2018.09.001

Al-Khamis, K. I., Davis, S. S., & Hadgraft, J. (1986). Microviscosity and drug release from topical gel formulations. *Pharmaceutical Research*, *3*(4), 214–217. https://doi.org/10.1023/A:1016386613239

Allan, G. (1995). Azone®. In E. W. Smith & H. I. Maibach (Eds.), *Percutaneous Penetration Enhancers*. CRC Press.

Alshetaili, A. S. (2019). Solubility and Solution Thermodynamics of Baricitinib in Six Different Pharmaceutically Used Solvents at Different Temperatures. *Zeitschrift Für Physikalische Chemie*, *233*(8), 1129–1144. https://doi.org/10.1515/zpch-2018-1323

Amin, M., Mansourian, M., Koning, G. A., Badiee, A., Jaafari, M. R., & Ten Hagen, T. L. M. (2015). Development of a novel cyclic RGD peptide for multiple targeting approaches of liposomes to tumor region. *Journal of Controlled Release : Official Journal of the Controlled Release Society*, *220*(Pt A), 308–315. https://doi.org/10.1016/J.JCONREL.2015.10.039

Andrade-Carrera, B., Clares, B., Noé, V., Mallandrich, M., Calpena, A., García, M., & Garduño-Ramírez, M. (2017). Cytotoxic Evaluation of (2S)-5,7-Dihydroxy-6-prenylflavanone Derivatives Loaded PLGA Nanoparticles against MiaPaCa-2 Cells. *Molecules*, *22*(9), 1553. https://doi.org/10.3390/molecules22091553

Andrés-Guerrero, V., & Herrero-Vanrell, R. (2008). *Absorción de fármacos por vía tópica. Papel de la conjuntiva* (12th ed., Vol. 83). Archivos de la Sociedad Española de Oftalmología.

Anigbogu, A. N. C., Williams, A. C., Barry, B. W., & Edwards, H. G. M. (1995). Fourier transform raman spectroscopy of interactions between the penetration enhancer dimethyl sulfoxide and human stratum corneum. *International Journal of Pharmaceutics*, *125*(2), 265–282. https://doi.org/10.1016/0378-5173(95)00141-5

Anigbogu, A., Patil, S., Singh, P., Liu, P., Dinh, S., & Maibach, H. (2000). An in vivo investigation of the rabbit skin responses to transdermal iontophoresis. *International Journal of Pharmaceutics*, *200*(2), 195–206. https://doi.org/10.1016/S0378-5173(00)00371-9

Ansari, M. J., & Alshahrani, S. M. (2019). Nano-encapsulation and characterization of baricitinib using poly-lactic-glycolic acid co-polymer. *Saudi Pharmaceutical Journal*, *27*(4), 491–501. https://doi.org/10.1016/j.jsps.2019.01.012

Anwer, Md. K., Ali, E. A., Iqbal, M., Ahmed, M. M., Aldawsari, M. F., Saqr, A. al, Ansari, M. N., & Aboudzadeh, M. A. (2021). Development of Sustained Release Baricitinib Loaded Lipid-Polymer Hybrid Nanoparticles with Improved Oral Bioavailability. *Molecules*, *27*(1), 168. https://doi.org/10.3390/molecules27010168

Arias, J. L., López-Viota, M., Clares, B., & Ruiz, M. A. (2008). Stability of fenbendazole suspensions for veterinary use: Correlation between zeta potential and sedimentation. *European Journal of Pharmaceutical Sciences*, *34*(4–5), 257–262. https://doi.org/10.1016/J.EJPS.2008.04.008

Arosio, D., & Casagrande, C. (2016). Advancement in integrin facilitated drug delivery. *Advanced Drug Delivery Reviews*, *97*, 111–143. https://doi.org/10.1016/J.ADDR.2015.12.001

Ashton, P., Walters, K. A., Brain, K. R., & Hadgraft, J. (1992). Surfactant effects in percutaneous absorption II. Effects on protein and lipid structure of the stratum corneum. *International Journal of Pharmaceutics*, *87*(1–3), 265–269. https://doi.org/10.1016/0378-5173(92)90252-W

Astarita, C., Palchetti, S., Massaro-Giordano, M., Domenico, M. Di, Petrillo, F., Boffo, S., Caracciolo, G., Giordano, A., Júnior, C., & Heard, C. M. (2021). *Artificial Protein Coronas Enable Controlled Interaction with Corneal Epithelial Cells: New Opportunities for Ocular Drug Delivery*. https://doi.org/10.3390/pharmaceutics13060867

Aungst, B. J., Blake, J. A., Rogers, N. J., & Hussain, M. A. (1990). Transdermal oxymorphone formulation development and methods for evaluating flux and lag times for two skin permeation-enhancing vehicles. *Journal of Pharmaceutical Sciences*, *79*(12), 1072–1076. https://doi.org/10.1002/JPS.2600791207

Bangham, A. D. (1995). Surrogate cells or trojan horses. The discovery of liposomes. *BioEssays*, *17*(12), 1081–1088. https://doi.org/10.1002/bies.950171213

Bangham, A. D., & Horne, R. W. (1964). Negative staining of phospholipids and their structural modification by surface-active agents as observed in the electron microscope. *Journal of Molecular Biology*, *8*(5), 660-IN10. https://doi.org/10.1016/S0022-2836(64)80115-7

Bangham, A. D., Standish, M. M., & Watkins, J. C. (1965). Diffusion of univalent ions across the lamellae of swollen phospholipids. *Journal of Molecular Biology*, *13*(1), 238-IN27. https://doi.org/10.1016/S0022-2836(65)80093-6

Barani, H., & Montazer, M. (2008). A review on applications of liposomes in textile processing. *Journal of Liposome Research*, *18*(3), 249–262. https://doi.org/10.1080/08982100802354665

Barenholz, Y. (2012a). Doxil®--the first FDA-approved nano-drug: lessons learned. *Journal of Controlled Release : Official Journal of the Controlled Release Society*, *160*(2), 117–134. https://doi.org/10.1016/J.JCONREL.2012.03.020

Barenholz, Y. (2012b). Doxil®--the first FDA-approved nano-drug: lessons learned. *Journal of Controlled Release : Official Journal of the Controlled Release Society*, *160*(2), 117–134. https://doi.org/10.1016/J.JCONREL.2012.03.020

Barry, B. W. (1983a). Methods for studing percutaneous absorption. In B. W. Barry (Ed.), *Dermatological formulations: percutaneous absorption* (pp. 234–295). Marcel Dekker.

Barry, B. W. (1983b). Properties that influence percuataneous absorption. In *Dermatological formulations : percutaneous absorption* (pp. 160–172). Marcel Dekker.

Barry, B. W. (1987). Mode of action of penetration enhancers in human skin. *Journal of Controlled Release*, *6*(1), 85–97. https://doi.org/10.1016/0168-3659(87)90066-6

Barry, B. W. (1988). Action of skin penetration enhancers-the Lipid Protein Partitioning theory. *International Journal of Cosmetic Science*, *10*(6), 281–293. https://doi.org/10.1111/J.1467-2494.1988.TB00028.X

Barry, B. W. (1991). Lipid-Protein-Partitioning theory of skin penetration enhancement. *Journal of Controlled Release*, *15*(3), 237–248. https://doi.org/10.1016/0168-3659(91)90115-T

Basketter, D. A., York, M., McFadden, J. P., & Robinson, M. K. (2004). Determination of skin irritation potential in the human 4-h patch test. *Contact Dermatitis*, *51*(1), 1–4. https://doi.org/10.1111/j.0105-1873.2004.00385.x

Beastall, J. C., Hadgraft, J., & Washington, C. (1988). Mechanism of action of Azone as a percutaneous penetration enhancer: Lipid bilayer fluidity and transition temperature effects. *International Journal of Pharmaceutics*, *43*(3), 207–213. https://doi.org/10.1016/0378-5173(88)90275-X

Bechman, K., Subesinghe, S., Norton, S., Atzeni, F., Galli, M., Cope, A. P., Winthrop, K. L., & Galloway, J. B. (2019). A systematic review and meta-analysis of infection risk with small molecule JAK inhibitors in rheumatoid arthritis. *Rheumatology*, *58*(10), 1755–1766. https://doi.org/10.1093/rheumatology/kez087

Berner, B., Juang, R.-H., & Mazzenga, G. C. (1989). Ethanol and Water Sorption into Stratum Corneum and Model Systems. *Journal of Pharmaceutical Sciences*, *78*(6), 472–476. https://doi.org/10.1002/jps.2600780611

Bhatia, K. S., & Singh, J. (2008). Percutaneous Absorption of LHRH Through Porcine Skin: Effect of N-Methyl 2-Pyrrolidone and Isopropyl Myristate. *Http://Dx.Doi.Org/10.3109/03639049709150501*, *23*(11), 1111–1114. https://doi.org/10.3109/03639049709150501

Bjordal, O., Norheim, K. B., Rødahl, E., Jonsson, R., & Omdal, R. (2020). Primary Sjögren's syndrome and the eye. *Survey of Ophthalmology*, *65*(2), 119–132. https://doi.org/10.1016/j.survophthal.2019.10.004

Bonina, F. P., Montenegro, L., Micali, G., West, D. P., Palicharla, P., & Koch, R. L. (1993). In vitro percutaneous absorption evaluation of phenobarbital through hairless mouse, adult and premature human skin. *International Journal of Pharmaceutics*, *98*(1–3), 93–99. https://doi.org/10.1016/0378-5173(93)90045-H

Bonnel, D., Legouffe, R., Eriksson, A. H., Mortensen, R. W., Pamelard, F., Stauber, J., & Nielsen, K. T. (2018). MALDI imaging facilitates new topical drug development process by determining quantitative skin distribution profiles. *Analytical and Bioanalytical Chemistry*, *410*(11), 2815–2828. https://doi.org/10.1007/s00216-018-0964-3

Botet-Carreras, A., Montero, M. T., Sot, J., Domènech, Ò., & Borrell, J. H. (2021). Engineering and development of model lipid membranes mimicking the HeLa cell membrane. *Colloids and Surfaces A: Physicochemical and Engineering Aspects*, *630*, 127663. https://doi.org/10.1016/j.colsurfa.2021.127663

Bouwstra, J. A., de Vries, M. A., Gooris, G. S., Bras, W., Brussee, J., & Ponec, M. (1991). Thermodynamic and structural aspects of the skin barrier. *Journal of Controlled Release*, *15*(3), 209–219. https://doi.org/10.1016/0168-3659(91)90112-Q

Bremer-Hoffmann, S., Halamoda-Kenzaoui, B., & Borgos, S. E. (2018). Identification of regulatory needs for nanomedicines. *Journal of Interdisciplinary Nanomedicine*, *3*(1), 4–15. https://doi.org/10.1002/JIN2.34

Brown, M. B., Martin, G. P., Jones, S. A., & Akomeah, F. K. (2006). Dermal and Transdermal Drug Delivery Systems: Current and Future Prospects. *Drug Delivery*, *13*(3), 175–187. https://doi.org/10.1080/10717540500455975

Bulbake, U., Doppalapudi, S., Kommineni, N., & Khan, W. (2017a). Liposomal Formulations in Clinical Use: An Updated Review. *Pharmaceutics*, *9*(2). https://doi.org/10.3390/PHARMACEUTICS9020012

Bulbake, U., Doppalapudi, S., Kommineni, N., & Khan, W. (2017b). Liposomal Formulations in Clinical Use: An Updated Review. *Pharmaceutics*, *9*(2). https://doi.org/10.3390/PHARMACEUTICS9020012

Cabrera, I., Abasolo, I., Corchero, J. L., Elizondo, E., Gil, P. R., Moreno, E., Faraudo, J., Sala, S., Bueno, D., González-Mira, E., Rivas, M., Melgarejo, M., Pulido, D., Albericio, F., Royo, M., Villaverde, A., García-Parajo, M. F., Schwartz, S., Ventosa, N., & Veciana, J. (2016). α-Galactosidase-A Loaded-Nanoliposomes with Enhanced Enzymatic Activity and Intracellular Penetration. *Advanced Healthcare Materials*, *5*(7), 829–840. https://doi.org/10.1002/ADHM.201500746

Campos, F. F., Calpena Campmany, A. C., Delgado, G. R., Serrano, O. L., & Naveros, B. C. (2012). Development and Characterization of a Novel Nystatin-Loaded Nanoemulsion for the Buccal Treatment of Candidosis: Ultrastructural Effects and Release Studies. *Journal of Pharmaceutical Sciences*, *101*(10), 3739–3752. https://doi.org/10.1002/JPS.23249

Cardona Villa, R., & Serrano Reyes, C. (2010). *Alergia: abordaje clínico, diagnóstico y tratamiento*. Médica Panamericana.

Carelli, V., Di Colo, G., Nannipieri, E., & Serafini, M. F. (1992). Enhancement effects in the permeation of Alprazolam through hairless mouse skin. *International Journal of Pharmaceutics*, *88*(1–3), 89–97. https://doi.org/10.1016/0378-5173(92)90306-M

Caspers, P. J., Nico, C., Bakker Schut, T. C., de Sterke, J., Pudney, P. D. A., Curto, P. R., Illand, A., & Puppels, G. J. (2019). Method to quantify the in vivo skin penetration of topically

applied materials based on confocal Raman spectroscopy. *Translational Biophotonics*, *1*(1–2). https://doi.org/10.1002/tbio.201900004

Cassel, E. J. (1982). The Nature of Suffering and the Goals of Medicine. *New England Journal of Medicine*, *306*(11), 639–645. https://doi.org/10.1056/NEJM198203183061104

Cevc, G., Blume, G., Schätzlein, A., Gebauer, D., & Paul, A. (1996). The skin: a pathway for systemic treatment with patches and lipid-based agent carriers. *Advanced Drug Delivery Reviews*, *18*(3), 349–378. https://doi.org/10.1016/0169-409X(95)00091-K

Chen, Y., Quan, P., Liu, X., Wang, M., & Fang, L. (2014). Novel chemical permeation enhancers for transdermal drug delivery. *Asian Journal of Pharmaceutical Sciences*, *9*(2), 51–64. https://doi.org/10.1016/J.AJPS.2014.01.001

Cheng, R., Meng, F., Deng, C., Klok, H. A., & Zhong, Z. (2013). Dual and multi-stimuli responsive polymeric nanoparticles for programmed site-specific drug delivery. *Biomaterials*, *34*(14), 3647–3657. https://doi.org/10.1016/J.BIOMATERIALS.2013.01.084

CHMP. (n.d.). *Anexo I - Ficha Técnica o Resumen de las características del producto*. Retrieved February 22, 2022, from https://www.ema.europa.eu/en/documents/product-information/olumiant-epar-product-information_es.pdf

Chovatiya, R., & Paller, A. S. (2021). JAK inhibitors in the treatment of atopic dermatitis. *Journal of Allergy and Clinical Immunology*, *148*(4), 927–940. https://doi.org/10.1016/j.jaci.2021.08.009

Ciotti, S. N., & Weiner, N. (2002). Follicular lipsomal delivery systems. *Journal of Liposome Research*, *12*(1–2), 143–148. https://doi.org/10.1081/LPR-120004787

Clares, B., Biedma-Ortiz, R. A., Sáez-Fernández, E., Prados, J. C., Melguizo, C., Cabeza, L., Ortiz, R., & Arias, J. L. (2013). Nano-engineering of 5-fluorouracil-loaded magnetoliposomes for combined hyperthermia and chemotherapy against colon cancer. *European Journal of Pharmaceutics and Biopharmaceutics*, *85*(3), 329–338. https://doi.org/10.1016/j.ejpb.2013.01.028

Clares, B., Calpena, A. C., Parra, A., Abrego, G., Alvarado, H., Fangueiro, J. F., & Souto, E. B. (2014). Nanoemulsions (NEs), liposomes (LPs) and solid lipid nanoparticles (SLNs) for retinyl palmitate: effect on skin permeation. *International Journal of Pharmaceutics*, *473*(1–2), 591–598. https://doi.org/10.1016/j.ijpharm.2014.08.001

Clares, B., Gallardo, V., Medina, M., & Ruiz, M. (2009). Multilamellar liposomes of triamcinolone acetonide: preparation, stability, and characterization. *Journal of Liposome Research*, *19*(3), 197–206. https://doi.org/10.1080/08982100902736571

Committee for Medicinal Products for Human Use. (2022). *ICH guideline Q14 on analytical procedure development*. www.ema.europa.eu/contact

Committee for Medicinal Products for Human Use (CHMP). (2020). *Olumiant - Assesment report*. https:// www.ema.europa.eu/en/medicines/human/EPAR/ olumiant

Cui, Z. K., Bouisse, A., Cottenye, N., & Lafleur, M. (2012). Formation of pH-sensitive cationic liposomes from a binary mixture of monoalkylated primary amine and cholesterol.

Langmuir : The ACS Journal of Surfaces and Colloids, *28*(38), 13668–13674. https://doi.org/10.1021/LA302278Q

de Brouwer, A. J., Flanagan, J. R., & Spering, M. (2021). Functional Use of Eye Movements for an Acting System. *Trends in Cognitive Sciences*, *25*(3), 252–263. https://doi.org/10.1016/j.tics.2020.12.006

de Paiva, C. S., & Rocha, E. M. (2015). Sjögren syndrome: what and where are we looking for? *Current Opinion in Ophthalmology*, *26*(6), 517–525. https://doi.org/10.1097/ICU.0000000000000208

Díez-Sales, O., Watkinson, A. C., Herráez-Domínguez, M., Javaloyes, C., & Hadgraft, J. (1996). A mechanistic investigation of the in vitro human skin permeation enhancing effect of Azone®. *International Journal of Pharmaceutics*, *129*(1–2), 33–40. https://doi.org/10.1016/0378-5173(95)04237-7

Domínguez-Villegas, V., Clares-Naveros, B., García-López, M. L., Calpena-Campmany, A. C., Bustos-Zagal, P., & Garduño-Ramírez, M. L. (2014). Development and characterization of two nano-structured systems for topical application of flavanones isolated from Eysenhardtia platycarpa. *Colloids and Surfaces B: Biointerfaces*, *116*, 183–192. https://doi.org/10.1016/j.colsurfb.2013.12.009

Draize, J. H., Woodard, G., & Calvery, H. O. (1944). Methods for the Study of Irritation and Toxicity of Substances Applied Topically to the Skin and Mucous Membranes. *Journal of Pharmacology and Experimental Therapeutics November*, *82*(3), 377–390.

D'Souza, S. (2014). A Review of In Vitro Drug Release Test Methods for Nano-Sized Dosage Forms. *Advances in Pharmaceutics*, *2014*, 1–12. https://doi.org/10.1155/2014/304757

Du Plessis, J., Pugh, W. J., Judefeind, A., & Hadgraft, J. (2002). Physico-chemical determinants of dermal drug delivery: Effects of the number and substitution pattern of polar groups. *European Journal of Pharmaceutical Sciences*, *16*(3), 107–112. https://doi.org/10.1016/S0928-0987(02)00085-4

Eichenfield, L. F., Tom, W. L., Chamlin, S. L., Feldman, S. R., Hanifin, J. M., Simpson, E. L., Berger, T. G., Bergman, J. N., Cohen, D. E., Cooper, K. D., Cordoro, K. M., Davis, D. M., Krol, A., Margolis, D. J., Paller, A. S., Schwarzenberger, K., Silverman, R. A., Williams, H. C., Elmets, C. A., … Sidbury, R. (2014). Guidelines of care for the management of atopic dermatitis. *Journal of the American Academy of Dermatology*, *70*(2), 338–351. https://doi.org/10.1016/j.jaad.2013.10.010

El Maghraby, G. M. M., Williams, A. C., & Barry, B. W. (2010). Skin Delivery of Oestradiol from Deformable and Traditiona Liposomes: Mechanistic Studies. *Journal of Pharmacy and Pharmacology*, *51*(10), 1123–1134. https://doi.org/10.1211/0022357991776813

Elizondo, E., Moreno, E., Cabrera, I., Córdoba, A., Sala, S., Veciana, J., & Ventosa, N. (2011). Liposomes and other vesicular systems: structural characteristics, methods of preparation, and use in nanomedicine. *Progress in Molecular Biology and Translational Science*, *104*, 1–52. https://doi.org/10.1016/B978-0-12-416020-0.00001-2

Elmas, A., Akyüz, G., Bergal, A., Andaç, M., & Andaç, Ö. (2020). Mathematical Modelling of Drug Release. *Research on Engineering Structures and Materials*. https://doi.org/10.17515/resm2020.178na0122

Elmowafy, M. (2021). Skin penetration/permeation success determinants of nanocarriers: Pursuit of a perfect formulation. *Colloids and Surfaces B: Biointerfaces*, *203*, 111748. https://doi.org/10.1016/j.colsurfb.2021.111748

Escobar-Chavez, J. J., Merino-Sanjuán, V., López-Cervantes, M., Urban-Morlan, Z., Piñón-Segundo, E., Quintanar-Guerrero, D., & Ganem-Quintanar, A. (2008). The Tape-Stripping Technique as a Method for Drug Quantification in Skin. *Journal of Pharmacy & Pharmaceutical Sciences*, *11*(1), 104. https://doi.org/10.18433/J3201Z

Essendoubi, M., Alsamad, F., Noël, P., Meunier, M., Scandolera, A., Sandré, J., Manfait, M., Gobinet, C., Reynaud, R., & Piot, O. (2021). Combining Raman imaging and MCR-ALS analysis for monitoring retinol permeation in human skin. *Skin Research and Technology*, *27*(6), 1100–1109. https://doi.org/10.1111/srt.13069

European Medicines Agency. (n.d.). *Draft guideline on quality and equivalence of topical products*. www.ema.europa.eu/contact

Fathi, M., Mozafari, M. R., & Mohebbi, M. (2012). Nanoencapsulation of food ingredients using lipid based delivery systems. *Trends in Food Science & Technology*, *23*(1), 13–27. https://doi.org/10.1016/J.TIFS.2011.08.003

Feldmann, R. J. (1965). Penetration of 14C Hydrocortisone Through Normal Skin. *Archives of Dermatology*, *91*(6), 661–666. https://doi.org/10.1001/archderm.1965.01600120093023

Flaten, G. E., Awoyemi, O., Luthman, K., Brandl, M., & Massing, U. (2009). The Phospholipid Vesicle-Based Drug Permeability Assay: 5. Development toward an Automated Procedure for High-Throughput Permeability Screening. *Journal of Laboratory Automation*, *14*(1), 12–21. https://doi.org/10.1016/j.jala.2008.04.002

Fleischer, A. B., Parrish, C. A., Glenn, R., & Feldman, S. R. (2001). Condylomata Acuminata (Genital Warts). *Sexually Transmitted Diseases*, *28*(11), 643–647. https://doi.org/10.1097/00007435-200111000-00006

Flühmann, B., Ntai, I., Borchard, G., Simoens, S., & Mühlebach, S. (2019). Nanomedicines: The magic bullets reaching their target? *European Journal of Pharmaceutical Sciences : Official Journal of the European Federation for Pharmaceutical Sciences*, *128*, 73–80. https://doi.org/10.1016/J.EJPS.2018.11.019

Food and Drug Administration. (1997). *Office of Training and Communications Division of Communications Management The Drug Information Branch* (Vol. 20857). Tel. http://www.fda.gov/cder/guidance.htm

Franzen, L., Selzer, D., Fluhr, J. W., Schaefer, U. F., & Windbergs, M. (2013). Towards drug quantification in human skin with confocal Raman microscopy. *European Journal of Pharmaceutics and Biopharmaceutics*, *84*(2), 437–444. https://doi.org/10.1016/j.ejpb.2012.11.017

Fresta, M., & Puglisi, G. (1997). Corticosteroid dermal delivery with skin-lipid liposomes. *Journal of Controlled Release*, *44*(2–3), 141–151. https://doi.org/10.1016/S0168-3659(96)01519-2

Fuhrman, L. C., Michniak, B. B., Behl, C. R., & Malick, A. W. (1997). Effect of novel penetration enhancers on the transdermal delivery of hydrocortisone: an in vitro species comparison. *Journal of Controlled Release*, *45*(2), 199–206. https://doi.org/10.1016/S0168-3659(96)01573-8

Ganapathy, S., Vedam, V., Rajeev, V., & Arunachalam, R. (2017). Autoimmune Disorders – Immunopathogenesis and Potential Therapies. *Journal of Young Pharmacists*, *9*(1), 14–22. https://doi.org/10.5530/jyp.2017.9.4

Gandhi, S. V., & Kapoor, B. G. (2019). Development and Validation of UV Spectroscopic Method for Estimation of Baricitinib. *Journal of Drug Delivery and Therapeutics*, *9*(4-s), 488–491. https://doi.org/10.22270/jddt.v9i4-s.3230

Ganesan, M. G., Weiner, N. D., Flynn, G. L., & Ho, N. F. H. (1984). Influence of liposomal drug entrapment on percutaneous absorption. *International Journal of Pharmaceutics*, *20*(1–2), 139–154. https://doi.org/10.1016/0378-5173(84)90225-4

García-Otero, X., Díaz-Tomé, V., Varela-Fernández, R., Martín-Pastor, M., González-Barcia, M., Blanco-Méndez, J., Mondelo-García, C., Bermudez, M. A., Gonzalez, F., Aguiar, P., Fernández-Ferreiro, A., & Otero-Espinar, F. J. (2021). Development and Characterization of a Tacrolimus/Hydroxypropyl-β-Cyclodextrin Eye Drop. *Pharmaceutics*, *13*(2), 149. https://doi.org/10.3390/pharmaceutics13020149

Garrigue, J. S., Amrane, M., Faure, M. O., Holopainen, J. M., & Tong, L. (2017). Relevance of Lipid-Based Products in the Management of Dry Eye Disease. *Journal of Ocular Pharmacology and Therapeutics*, *33*(9), 647–661. https://doi.org/10.1089/JOP.2017.0052

Garrós, N., Mallandrich, M., Beirampour, N., Mohammadi, R., Domènech, Ò., Rodríguez-Lagunas, M. J., Clares, B., & Colom, H. (2022). Baricitinib Liposomes as a New Approach for the Treatment of Sjögren's Syndrome. *Pharmaceutics*, *14*(9), 1895. https://doi.org/10.3390/pharmaceutics14091895

Gasull, X. (2003). Entender la función de la red trabecular mejorará el tratamiento del glaucoma. *Archivos de La Sociedad Española de Oftalmología*, *78*(7), 347–348. https://scielo.isciii.es/scielo.php?script=sci_arttext&pid=S0365-66912003000700002&lng=es&nrm=iso&tlng=es

Gomes da Costa, S., Richter, A., Schmidt, U., Breuninger, S., & Hollricher, O. (2019). Confocal Raman microscopy in life sciences. *Morphologie*, *103*(341), 11–16. https://doi.org/10.1016/j.morpho.2018.12.003

Gómez-Segura, L., Parra, A., Calpena, A. C., Gimeno, Á., & Boix-Montañes, A. (2020). Carprofen permeation test through porcine ex vivo mucous membranes and ophthalmic tissues for tolerability assessments: Validation and histological study. *Veterinary Sciences*, *7*(4), 1–17. https://doi.org/10.3390/vetsci7040152

Gómez-Segura, L., Parra, A., Calpena-Campmany, A. C., Gimeno, Á., de Aranda, I. G., & Boix-Montañes, A. (2020). Ex Vivo Permeation of Carprofen Vehiculated by PLGA Nanoparticles through Porcine Mucous Membranes and Ophthalmic Tissues. *Nanomaterials 2020, Vol. 10, Page 355*, *10*(2), 355. https://doi.org/10.3390/NANO10020355

González-Rodríguez, M., & Rabasco, A. (2011). Charged liposomes as carriers to enhance the permeation through the skin. *Expert Opinion on Drug Delivery*, *8*(7), 857–871. https://doi.org/10.1517/17425247.2011.574610

Goodman, M., & Barry, B. W. (1989). Action of penetration enhancers on human stratum corneum as assessed by differential scanning calorimetry. In R. Bronaugh & H. Maibach (Eds.), *Percutaneous absorption Mechanisms-Methodology-Drug Delivery* (pp. 567–593). Marcel Dekker.

Goodman, M., & Barry, B. W. (2011). Action of Skin Permeation Enhancers Azone, Oleic Acid and Decylmethyl Sulphoxide: Permeation and Dsc Studies. *Journal of Pharmacy and Pharmacology*, *38*(Supplement_12), 71P-71P. https://doi.org/10.1111/J.2042-7158.1986.TB14300.X

Grammer, L., & Greenberger, P. (2011). *Patterson enfermedades alérgicas* (7th ed.). Aula Médica.

Gregoriadis, G. (1976). The carrier potential of liposomes in biology and medicine (first of two parts). *The New England Journal of Medicine*, *295*(13), 704–710. https://doi.org/10.1056/NEJM197609232951305

Gregoriadis, G. (1995). Engineering liposomes for drug delivery: progress and problems. *Trends in Biotechnology*, *13*(12), 527–537. https://doi.org/10.1016/S0167-7799(00)89017-4

Gregoriadis, G., & Davis, C. (1979). Stability of liposomes invivo and invitro is promoted by their cholesterol content and the presence of blood cells. *Biochemical and Biophysical Research Communications*, *89*(4), 1287–1293. https://doi.org/10.1016/0006-291X(79)92148-X

Greish, K. (2010). Enhanced permeability and retention (EPR) effect for anticancer nanomedicine drug targeting. In S. R. Grobmyer & B. M. Moudgil (Eds.), *Methods in molecular biology (Clifton, N.J.)* (Vol. 624). Humana Press. https://doi.org/10.1007/978-1-60761-609-2_3

Grimaldi, N., Andrade, F., Segovia, N., Ferrer-Tasies, L., Sala, S., Veciana, J., & Ventosa, N. (2016). Lipid-based nanovesicles for nanomedicine. *Chemical Society Reviews*, *45*(23), 6520–6545. https://doi.org/10.1039/C6CS00409A

Gu, Z., Biswas, A., Zhao, M., & Tang, Y. (2011). Tailoring nanocarriers for intracellular protein delivery. *Chemical Society Reviews*, *40*(7), 3638–3655. https://doi.org/10.1039/C0CS00227E

Guida, V. (2010). Thermodynamics and kinetics of vesicles formation processes. *Advances in Colloid and Interface Science*, *161*(1–2), 77–88. https://doi.org/10.1016/J.CIS.2009.11.004

Gujjar, M., & Banga, A. (2014). Iontophoretic and Microneedle Mediated Transdermal Delivery of Glycopyrrolate. *Pharmaceutics*, *6*(4), 663–671. https://doi.org/10.3390/pharmaceutics6040663

Gupta, P. K. (2016). Toxicological testing: In vivo systems. *Fundamentals of Toxicology*, 131–150. https://doi.org/10.1016/B978-0-12-805426-0.00012-3

Guy, R. H., Hadgraft, J., & Bucks, D. A. W. (1987). Transdermal drug delivery and cutaneous metabolism. *Xenobiotica*, *17*(3), 325–343. https://doi.org/10.3109/00498258709043943

Hiraganahalli Bhaskarmurthy, D., & Evan Prince, S. (2021). Effect of Baricitinib on TPA-induced psoriasis like skin inflammation. *Life Sciences*, *279*, 119655. https://doi.org/10.1016/j.lfs.2021.119655

Hoang, T. N., Pino, M., Boddapati, A. K., Viox, E. G., Starke, C. E., Upadhyay, A. A., Gumber, S., Nekorchuk, M., Busman-Sahay, K., Strongin, Z., Harper, J. L., Tharp, G. K., Pellegrini, K. L., Kirejczyk, S., Zandi, K., Tao, S., Horton, T. R., Beagle, E. N., Mahar, E. A., … Paiardini, M. (2021). Baricitinib treatment resolves lower-airway macrophage inflammation and neutrophil recruitment in SARS-CoV-2-infected rhesus macaques. *Cell*, *184*(2), 460-475.e21. https://doi.org/10.1016/j.cell.2020.11.007

Hofauer, B., Bas, M., Manour, N., & Knopf, A. (2013). Effekt liposomaler Lokaltherapie auf die Sicca-Symptomatik des primären Sjögren-Syndroms. *HNO*, *61*(11), 921–927. https://doi.org/10.1007/s00106-013-2736-x

Hopf, N. B., Champmartin, C., Schenk, L., Berthet, A., Chedik, L., Du Plessis, J. L., Franken, A., Frasch, F., Gaskin, S., Johanson, G., Julander, A., Kasting, G., Kilo, S., Larese Filon, F., Marquet, F., Midander, K., Reale, E., & Bunge, A. L. (2020). Reflections on the OECD guidelines for in vitro skin absorption studies. *Regulatory Toxicology and Pharmacology*, *117*, 104752. https://doi.org/10.1016/j.yrtph.2020.104752

Hunter, R. J. (2001). *Foundations of Colloid Science* (2nd ed.). Oxford University Press.

ICH Expert Working Group. (2005). *ICH Harmonised Tripartite Guideline - Validation of analytical procedures: text and methodology Q2(R1)*.

Idson, B. (1975). *Percutaneous absorption.* (Vol. 64). https://doi.org/10.1002/jps.2600640604

Immordino, M. L., Dosio, F., & Cattel, L. (2006). Stealth liposomes: review of the basic science, rationale, and clinical applications, existing and potential. *International Journal of Nanomedicine*, *1*(3), 297. /pmc/articles/PMC2426795/

Interagency Coordinating Committee on the Validation of Alternative Methods (ICCVAM). (2010). *Test Method Protocol: Hen's Egg Test-Chorioallantoic Membrane (HET-CAM) Test Method*. http://iccvam.niehs.nih.gov/methods/ocutox/MildMod-TMER.htm

Islam Shishir, M. R., Karim, N., Gowd, V., Zheng, X., & Chen, W. (2019). Liposomal delivery of natural product: A promising approach in health research. *Trends in Food Science & Technology*, *85*, 177–200. https://doi.org/10.1016/j.tifs.2019.01.013

Jacobi, U., Tassopoulos, T., Surber, C., & Lademann, J. (2006). Cutaneous distribution and localization of dyes affected by vehicles all with different lipophilicity. *Archives of Dermatological Research*, *297*(7), 303–310. https://doi.org/10.1007/S00403-005-0621-5

Janib, S. M., Moses, A. S., & MacKay, J. A. (2010). Imaging and drug delivery using theranostic nanoparticles. *Advanced Drug Delivery Reviews*, *62*(11), 1052–1063. https://doi.org/10.1016/J.ADDR.2010.08.004

Jiang, R., Benson, H. A. E., Cross, S. E., & Roberts, M. S. (1998). In Vitro Human Epidermal and Polyethylene Membrane Penetration and Retention of the Sunscreen Benzophenone-3 from a Range of Solvents. *Pharmaceutical Research*, *15*(12), 1863–1868. https://doi.org/10.1023/A:1011958006973

K, K., N, K., S, A., & M, S. (1999). Effect of fatty acids on the permeation of melatonin across rat and pig skin in-vitro and on the transepidermal water loss in rats in-vivo. *The Journal of Pharmacy and Pharmacology*, *51*(7), 783–790. https://doi.org/10.1211/0022357991773140

Kai, T., Nakazono, M., Kurosaki, Y., Nakayama, T., & Kimura, T. (1993). Keratinized epithelial transport of beta-blocking agents. III. Evaluation of enhancing effect on percutaneous absorption using model lipid liposomes. *Biological & Pharmaceutical Bulletin*, *16*(8), 801–805. https://doi.org/10.1248/BPB.16.801

Kato, A., Ishibashi, Y., & Miyake, Y. (2011). Effect of egg yolk lecithin on transdermal delivery of bunazosin hydrochloride. *Journal of Pharmacy and Pharmacology*, *39*(5), 399–400. https://doi.org/10.1111/j.2042-7158.1987.tb03407.x

Kewal K., J. (Ed.). (2008). *Drug Delivery Systems* (Vol. 437). Human Press.

Khodabandehloo, H., Zahednasab, H., & Hafez, A. A. (2016). Nanocarriers Usage for Drug Delivery in Cancer Therapy. *Iranian Journal of Cancer Prevention*, *9*(2), 3966. https://doi.org/10.17795/IJCP-3966

Kim, B., Park, J. H., & Sailor, M. J. (2019). Rekindling RNAi Therapy: Materials Design Requirements for In Vivo siRNA Delivery. *Advanced Materials (Deerfield Beach, Fla.)*, *31*(49), e1903637. https://doi.org/10.1002/ADMA.201903637

Kim, C. K., Kim, J. J., Chi, S. C., & Shim, C. K. (1993). Effect of fatty acids and urea on the penetration of ketoprofen through rat skin. *International Journal of Pharmaceutics*, *99*(2–3), 109–118. https://doi.org/10.1016/0378-5173(93)90352-G

Kim, M.-K., Lee, C.-H., & Kim, D.-D. (2010). Skin Permeation of Testosterone and its Ester Derivatives in Rats. *Journal of Pharmacy and Pharmacology*, *52*(4), 369–375. https://doi.org/10.1211/0022357001774101

Kim, Y. H., Ghanem, A. H., Mahmoud, H., & Higuchi, W. I. (1992). Short chain alkanols as transport enhancers for lipophilic and polar/ionic permeants in hairless mouse skin: Mechanism(s) of action. *International Journal of Pharmaceutics*, *80*(1–3), 17–31. https://doi.org/10.1016/0378-5173(92)90258-4

Kirby, C., Clarke, J., & Gregoriadis, G. (1980). Effect of the cholesterol content of small unilamellar liposomes on their stability *in vivo* and *in vitro*. *Biochemical Journal*, *186*(2), 591–598. https://doi.org/10.1042/bj1860591

Kogan, A., & Garti, N. (2006). Microemulsions as transdermal drug delivery vehicles. *Advances in Colloid and Interface Science*, *123–126*(SPEC. ISS.), 369–385. https://doi.org/10.1016/J.CIS.2006.05.014

Koyama, Y., Bando, H., Yamashita, F., Takakura, Y., Sezaki, H., & Hashida, M. (1994). Comparative Analysis of Percutaneous Absorption Enhancement by d-Limonene and Oleic Acid Based on a Skin Diffusion Model. *Pharmaceutical Research: An Official*

Journal of the American Association of Pharmaceutical Scientists, *11*(3), 377–383. https://doi.org/10.1023/A:1018904802566/METRICS

Kramer, E. (2022, July 13). *Five Things You Can Expect When You Start Wearing Scleral Lenses*. Weston Contact Lens Istitute. https://www.westoncontactlens.com/five-things-you-can-expect-when-you-start-wearing-scleral-lenses/

Kunta, J. R., Goskonda, V. R., Brotherton, H. O., Khan, M. A., & Reddy, I. K. (1997). Effect of menthol and related terpenes on the percutaneous absorption of propranolol across excised hairless mouse skin. *Journal of Pharmaceutical Science*, *86*(12), 1369–1373.

Kurakula, M., Srinivas, C., Kasturi, N., & Diwan, P. V. (2012). Formulation and Evaluation of Prednisolone Proliposomal Gel for Effective Topical Pharmacotherapy. *International Journal of Pharmaceutical Sciences and Drug Research*, *4*(1), 35–43. https://www.researchgate.net/publication/289098891_Formulation_and_Evaluation_of_Prednisolone_Proliposomal_Gel_for_Effective_Topical_Pharmacotherapy

Lai, F., Caddeo, C., Manca, M. L., Manconi, M., Sinico, C., & Fadda, A. M. (2020). What's new in the field of phospholipid vesicular nanocarriers for skin drug delivery. *International Journal of Pharmaceutics*, *583*, 119398. https://doi.org/10.1016/j.ijpharm.2020.119398

Lee, M., Hwang, J.-H., & Lim, K.-M. (2017). Alternatives to *In Vivo* Draize Rabbit Eye and Skin Irritation Tests with a Focus on 3D Reconstructed Human Cornea-Like Epithelium and Epidermis Models. *Toxicological Research*, *33*(3), 191–203. https://doi.org/10.5487/TR.2017.33.3.191

Leopold, C. S., & Lippold, B. C. (1995a). Enhancing Effects of Lipophilic Vehicles on Skin Penetration of Methyl Nicotinate in Vivo. *Journal of Pharmaceutical Sciences*, *84*(2), 195–198. https://doi.org/10.1002/jps.2600840214

Leopold, C. S., & Lippold, B. C. (1995b). Enhancing Effects of Lipophilic Vehicles on Skin Penetration of Methyl Nicotinate in Vivo. *Journal of Pharmaceutical Sciences*, *84*(2), 195–198. https://doi.org/10.1002/jps.2600840214

Lian, T., & Ho, R. J. Y. (2001). Trends and developments in liposome drug delivery systems. *Journal of Pharmaceutical Sciences*, *90*(6), 667–680. https://doi.org/10.1002/JPS.1023

Lipowsky, Reinhard, & Sackmann, E. (Eds.). (1995). *Structure and Dynamics of Membranes: From cells to membranes* (1st ed.). Elsevier Science.

Lippold, B. C. (1992). How to optimize drug penetration through the skin. *Pharmaceutica Acta Helvetiae*, *67*(11), 294–300.

Liu, M. C., Liu, L., Wang, X. R., Shuai, W. P., Hu, Y., Han, M., & Gao, J. Q. (2016). Folate receptor-targeted liposomes loaded with a diacid metabolite of norcantharidin enhance antitumor potency for H22 hepatocellular carcinoma both in vitro and in vivo. *International Journal of Nanomedicine*, *11*, 1395. https://doi.org/10.2147/IJN.S96862

López-Pintor, R. M., Fernández Castro, M., & Hernández, G. (2015). Afectación oral en el paciente con síndrome de Sjögren primario. Manejo multidisciplinar entre odontólogos y reumatólogos. *Reumatología Clínica*, *11*(6), 387–394. https://doi.org/10.1016/j.reuma.2015.03.010

Lorenzo, P., Moreno, A., Lizasoain, I., Leza, J. C., Moro, M. A., & Portoles, A. (2008). *Velázquez: farmacología básica y clínica* (18th ed., Vol. 23). Medica Panamericana.

Lu, G. W., & Gao, P. (2010). Emulsions and Microemulsions for Topical and Transdermal Drug Delivery. In *Handbook of Non-Invasive Drug Delivery Systems* (1st ed., pp. 59–94). Elsevier. https://doi.org/10.1016/B978-0-8155-2025-2.10003-4

Maibach, H. I., & Wane Smith, E. (Eds.). (2005). *Percutanepus penetration enhancers* (2nd ed.). Taylor & Francis group.

Malam, Y., Loizidou, M., & Seifalian, A. M. (2009). Liposomes and nanoparticles: nanosized vehicles for drug delivery in cancer. *Trends in Pharmacological Sciences*, *30*(11), 592–599. https://doi.org/10.1016/J.TIPS.2009.08.004

Mallandrich, M., Calpena, A. C., Clares, B., Parra, A., García, M. L., Soriano, J. L., & Fernández-Campos, F. (2021). Nano-engineering of ketorolac tromethamine platforms for ocular treatment of inflammatory disorders. *Nanomedicine*, *16*(5), 401–414. https://doi.org/10.2217/nnm-2020-0403

Mallandrich, M., Fernández-Campos, F., Clares, B., Halbaut, L., Alonso, C., Coderch, L., Garduño-Ramírez, M. L., Andrade, B., del Pozo, A., Lane, M. E., & Calpena, A. C. (2017). Developing Transdermal Applications of Ketorolac Tromethamine Entrapped in Stimuli Sensitive Block Copolymer Hydrogels. *Pharmaceutical Research*, *34*(8), 1728–1740. https://doi.org/10.1007/s11095-017-2181-8

Markham, A. (2017). Baricitinib: First Global Approval. *Drugs*, *77*(6), 697–704. https://doi.org/10.1007/s40265-017-0723-3

Martín, M. B., & Bueno, S. T. (1994). *Visión normal en Deficiencia visual: aspectos psicoevolutivos y educativos*. Editorial Aljibe.

Martins, F. C. O. L., Sentanin, M. A., & De Souza, D. (2019). Analytical methods in food additives determination: Compounds with functional applications. *Food Chemistry*, *272*, 732–750. https://doi.org/10.1016/j.foodchem.2018.08.060

Mason, T. G., Wilking, J. N., Meleson, K., Chang, C. B., & Graves, S. M. (2006). Nanoemulsions: formation, structure, and physical properties. *Journal of Physics: Condensed Matter*, *18*(41), R635–R666. https://doi.org/10.1088/0953-8984/18/41/R01

Medi, B. M., & Singh, J. (2006). Skin targeted DNA vaccine delivery using electroporation in rabbits: II. Safety. *International Journal of Pharmaceutics*, *308*(1–2), 61–68. https://doi.org/10.1016/J.IJPHARM.2005.10.035

Meek, K. M., & Knupp, C. (2015). Corneal structure and transparency. In *Progress in Retinal and Eye Research* (Vol. 49, pp. 1–16). Elsevier Ltd. https://doi.org/10.1016/j.preteyeres.2015.07.001

Megrab, N. A., Williams, A. C., & Barry, B. W. (1995). Oestradiol permeation across human skin, silastic and snake skin membranes: The effects of ethanol/water co-solvent systems. *International Journal of Pharmaceutics*, *116*(1), 101–112. https://doi.org/10.1016/0378-5173(94)00321-U

Mehanna, M. M., Abla, K. K., & Elmaradny, H. A. (2020). Tailored Limonene-Based Nanosized Microemulsion: Formulation, Physicochemical Characterization and In Vivo Skin

Irritation Assessment. *Advanced Pharmaceutical Bulletin*, *11*(2), 274–285. https://doi.org/10.34172/APB.2021.040

Metselaar, J. M., & Storm, G. (2005). Liposomes in the treatment of inflammatory disorders. *Expert Opinion on Drug Delivery*, *2*(3), 465–476. https://doi.org/10.1517/17425247.2.3.465

Mezei, M. (1985). *Liposomes as a skin drug delivery system* (Breimer. DD & P. Speiser, Eds.). Topics in Pharmaceutical Sciences.

Mezei, M., & Gulasekharam, V. (1980). Liposomes - a selective drug delivery system for the topical route of administration I. Lotion dosage form. *Life Sciences*, *26*(18), 1473–1477. https://doi.org/10.1016/0024-3205(80)90268-4

Mishra, G. P., Bagui, M., Tamboli, V., & Mitra, A. K. (2011). Recent Applications of Liposomes in Ophthalmic Drug Delivery. *Journal of Drug Delivery*, *2011*, 1–14. https://doi.org/10.1155/2011/863734

Montagna, W., & Parakkal, P. F. (1974). *The Structure and Function of Skin* (3rd ed.). Academic Press.

Morimoto, Y., Sugibayashi, K., & Natsume, H. (1994). The transdermal drug delivery system and transcutaneous absorption. *Acta Dermato-Venereologica. Supplementum*, *185*, 15–17.

Moussaoui, S. El, Abo-horan, I., Halbaut, L., Alonso, C., Coderch, L., Garduño-ramírez, M. L., Clares, B., Soriano, J. L., Calpena, A. C., Fernández-campos, F., & Mallandrich, M. (2021). Polymeric nanoparticles and chitosan gel loading ketorolac tromethamine to alleviate pain associated with condyloma acuminata during the pre- and post-ablation. *Pharmaceutics*, *13*(11). https://doi.org/10.3390/pharmaceutics13111784

Moussaoui, S. El, Fernández-Campos, F., Alonso, C., Limón, D., Halbaut, L., Garduño-Ramirez, M. L., Calpena, A. C., & Mallandrich, M. (2021). Topical mucoadhesive alginate-based hydrogel loading ketorolac for pain management after pharmacotherapy, ablation, or surgical removal in condyloma acuminata. *Gels*, *7*(1), 1–20. https://doi.org/10.3390/gels7010008

Müller, R. H., Radtke, M., & Wissing, S. A. (2002). Solid lipid nanoparticles (SLN) and nanostructured lipid carriers (NLC) in cosmetic and dermatological preparations. *Advanced Drug Delivery Reviews*, *54*, S131–S155. https://doi.org/10.1016/S0169-409X(02)00118-7

Musacchio, T., & Torchilin, V. P. (2011). Recent developments in lipid-based pharmaceutical nanocarriers. *Frontiers in Bioscience (Landmark Edition)*, *16*(4), 1388–1412. https://doi.org/10.2741/3795

Muth, C. C. (2017). Eye Emergencies. *JAMA*, *318*(7), 676. https://doi.org/10.1001/jama.2017.9899

Nadworny, P. L., Wang, J., Tredget, E. E., & Burrell, R. E. (2010). Anti-inflammatory activity of nanocrystalline silver-derived solutions in porcine contact dermatitis. *Journal of Inflammation*, *7*(1), 13. https://doi.org/10.1186/1476-9255-7-13

Nafisi, S., & Maibach, H. I. (2018). Skin penetration of nanoparticles. In *Emerging Nanotechnologies in Immunology* (pp. 47–88). Elsevier. https://doi.org/10.1016/B978-0-323-40016-9.00003-8

Nagayasu, A., Uchiyama, K., & Kiwada, H. (1999). The size of liposomes: a factor which affects their targeting efficiency to tumors and therapeutic activity of liposomal antitumor drugs. *Advanced Drug Delivery Reviews*, *40*(1–2), 75–87. https://doi.org/10.1016/S0169-409X(99)00041-1

Nair, J., & Singh, T. (2017). Sjogren's syndrome: Review of the aetiology, Pathophysiology a Potential therapeutic interventions. *Journal of Clinical and Experimental Dentistry*, 0–0. https://doi.org/10.4317/jced.53605

Netzlaff, F., Kostka, K. H., Lehr, C. M., & Schaefer, U. F. (2006). TEWL measurements as a routine method for evaluating the integrity of epidermis sheets in static Franz type diffusion cells in vitro. Limitations shown by transport data testing. *European Journal of Pharmaceutics and Biopharmaceutics*, *63*(1), 44–50. https://doi.org/10.1016/J.EJPB.2005.10.009

Ngoune, R., Peters, A., von Elverfeldt, D., Winkler, K., & Pütz, G. (2016). Accumulating nanoparticles by EPR: A route of no return. *Journal of Controlled Release*, *238*, 58–70. https://doi.org/10.1016/J.JCONREL.2016.07.028

Nguyen, D., & Maharaj, R. (2020, August 17). *Sjogren's Syndrome and Dry Eye*. MyDryEye.Ca. https://mydryeye.ca/sjogrens-syndrome-and-dry-eye/#:~:text=Punctal%20Plugs,-The%20next%20treatment&text=These%20plugs%20are%20inserted%20by,is%20inflammation%20in%20the%20tears.

Niemiec, S. M., Ramachandran, C., & Weiner, N. (1995). Influence of Nonionic Liposomal Composition on Topical Delivery of Peptide Drugs into Pilosebaceous Units: An in Vivo Study Using the Hamster Ear Model. *Pharmaceutical Research: An Official Journal of the American Association of Pharmaceutical Scientists*, *12*(8), 1184–1188. https://doi.org/10.1023/A:1016268027854/METRICS

Nishida, T., Saika, S., & Morishige, N. (2022). *Cornea and Sclera: anatomy and Physiology in Cornea: Fundamentals, Diagnosis and Management.* (M. J. Mannis & E. J. Holland, Eds.; 5th ed.). Elsvier.

Ogiso, T., Iwaki, M., & Paku, T. (1995). Effect of various enhancers on transdermal penetration of indomethacin and urea, and relationship between penetration parameters and enhancement factors. *Journal of Pharmaceutical Sciences*, *84*(4), 482–488. https://doi.org/10.1002/JPS.2600840418

Oranje, A. P. (2011). *Practical Issues on Interpretation of Scoring Atopic Dermatitis: SCORAD Index, Objective SCORAD, Patient-Oriented SCORAD and Three-Item Severity Score* (pp. 149–155). https://doi.org/10.1159/000323308

Osborne, D. W., & Musakhanian, J. (2018). Skin Penetration and Permeation Properties of Transcutol®—Neat or Diluted Mixtures. In *AAPS PharmSciTech* (Vol. 19, Issue 8, pp. 3512–3533). Springer New York LLC. https://doi.org/10.1208/s12249-018-1196-8

Oyster, C. W. (1999). *The human eye: structure and function*. Sinauer Associates, Inc.

Paola, T. P. (2012). Visión panorámica del sistema inmune. *Revista Médica Clínica Las Condes*, *23*(4), 446–457. https://doi.org/10.1016/S0716-8640(12)70335-8

Papakostas, D., Rancan, F., Sterry, W., Blume-Peytavi, U., & Vogt, A. (2011). Nanoparticles in dermatology. *Archives of Dermatological Research*, *303*(8), 533–550. https://doi.org/10.1007/S00403-011-1163-7

Pappas, A. (2009). Epidermal surface lipids. *Dermato-Endocrinology*, *1*(2), 72–76. https://doi.org/10.4161/derm.1.2.7811

Paranjpe, M., & Müller-Goymann, C. C. (2014). Nanoparticle-Mediated Pulmonary Drug Delivery: A Review. *International Journal of Molecular Sciences 2014, Vol. 15, Pages 5852-5873*, *15*(4), 5852–5873. https://doi.org/10.3390/IJMS15045852

Parra-Coca, A., Boix-Montañés, A., Calpena-Campmany, A. C., & Colom, H. (2021). In vivo pharmacokinetic evaluation of carprofen delivery from intra-articular nanoparticles in rabbits: A population modelling approach. *Research in Veterinary Science*, *137*, 235–242. https://doi.org/10.1016/J.RVSC.2021.05.012

Patzelt, A., & Lademann, J. (2020). Recent advances in follicular drug delivery of nanoparticles. *Expert Opinion on Drug Delivery*, *17*(1), 49–60. https://doi.org/10.1080/17425247.2020.1700226

Pérez-González, N., Bozal-De Febrer, N., Calpena-Campmany, A. C., Nardi-Ricart, A., Rodríguez-Lagunas, M. J., Morales-Molina, J. A., Soriano-Ruiz, J. L., Fernández-Campos, F., Clares-Naveros, B., & Dinu, V. (2021). *New Formulations Loading Caspofungin for Topical Therapy of Vulvovaginal Candidiasis*. *7*, 259. https://doi.org/10.3390/gels7040259

Pierre, M. B. R., & Dos Santos Miranda Costa, I. (2011). Liposomal systems as drug delivery vehicles for dermal and transdermal applications. *Archives of Dermatological Research 2011 303:9*, *303*(9), 607–621. https://doi.org/10.1007/S00403-011-1166-4

Potts, R. O., Golden, G. M., Francoeur, M. L., Mak, V. H. W., & Guy, R. H. (1991). Mechanism and enhancement of solute transport across the stratum corneum. *Journal of Controlled Release*, *15*(3), 249–260. https://doi.org/10.1016/0168-3659(91)90116-U

Prausnitz, M. R., & Noonan, J. S. (1998). Permeability of cornea, sclera, and conjunctiva: A literature analysis for drug delivery to the eye. *Journal of Pharmaceutical Sciences*, *87*(12), 1479–1488. https://doi.org/10.1021/js9802594

Puri, A., Loomis, K., Smith, B., Lee, J. H., Yavlovich, A., Heldman, E., & Blumenthal, R. (2009). Lipid-Based Nanoparticles as Pharmaceutical Drug Carriers: From Concepts to Clinic. *Critical Reviews™ in Therapeutic Drug Carrier Systems*, *26*(6), 523–580. https://doi.org/10.1615/CRITREVTHERDRUGCARRIERSYST.V26.I6.10

Qin, X., Yu, C., Wei, J., Li, L., Zhang, C., Wu, Q., Liu, J., Yao, S. Q., & Huang, W. (2019). Rational Design of Nanocarriers for Intracellular Protein Delivery. *Advanced Materials (Deerfield Beach, Fla.)*, *31*(46). https://doi.org/10.1002/ADMA.201902791

Raval, N., Maheshwari, R., Kalyane, D., Youngren-Ortiz, S. R., Chougule, M. B., & Tekade, R. K. (2019). Importance of Physicochemical Characterization of Nanoparticles in

Pharmaceutical Product Development. *Basic Fundamentals of Drug Delivery*, 369–400. https://doi.org/10.1016/B978-0-12-817909-3.00010-8

Riehemann, K., Schneider, S. W., Luger, T. A., Godin, B., Ferrari, M., & Fuchs, H. (2009). Nanomedicine – challenge and perspectives. *Angewandte Chemie (International Ed. in English)*, *48*(5), 872. https://doi.org/10.1002/ANIE.200802585

Rins, M., Diez, I., Calpena, A. C., & Obach, R. (1991). Skin density in the hairless rat. Evidence of regional differences. *European Journal of Drug Metabolism and Pharmacokinetics*, *Spec No 3*, 456–457. https://europepmc.org/article/med/1820922

Samimi, S., Maghsoudnia, N., Eftekhari, R. B., & Dorkoosh, F. (2019). Lipid-Based Nanoparticles for Drug Delivery Systems. In *Characterization and Biology of Nanomaterials for Drug Delivery* (pp. 47–76). Elsevier. https://doi.org/10.1016/B978-0-12-814031-4.00003-9

Sanz, R., Calpena, A. C., Mallandrich, M., Gimeno, Á., Halbaut, L., & Clares, B. (2017). Development of a buccal doxepin platform for pain in oral mucositis derived from head and neck cancer treatment. *European Journal of Pharmaceutics and Biopharmaceutics*, *117*, 203–211. https://doi.org/10.1016/J.EJPB.2017.04.019

Sato, K., Sugibayashi, K., & Morimoto, Y. (1988). Effect and mode of action of aliphatic esters on the in vitro skin permeation of nicorandil. *International Journal of Pharmaceutics*, *43*(1–2), 31–40. https://doi.org/10.1016/0378-5173(88)90055-5

Sawant, R. R., & Torchilin, V. P. (2010). Liposomes as 'smart' pharmaceutical nanocarriers. *Soft Matter*, *6*(17), 4026–4044. https://doi.org/10.1039/B923535N

Scheuplein, R. J., & Blank, I. H. (1971). *Permeability of the skin.* (Vol. 51). https://doi.org/10.1152/physrev.1971.51.4.702

Schoenwald, R. D., & Stewart, P. (1980). Effect of Particle Size on Ophthalmic Bioavailability of Dexamethasone Suspensions in Rabbits. *Journal of Pharmaceutical Sciences*, *69*(4), 391–394. https://doi.org/10.1002/jps.2600690407

Schoenwald, R. D., & Ward, R. L. (1978). Relationship between Steroid Permeability across Excised Rabbit Cornea and Octanol–Water Partition Coefficients. *Journal of Pharmaceutical Sciences*, *67*(6), 786–788. https://doi.org/10.1002/jps.2600670614

Schroeder, A., Kost, J., & Barenholz, Y. (2009). Ultrasound, liposomes, and drug delivery: principles for using ultrasound to control the release of drugs from liposomes. *Chemistry and Physics of Lipids*, *162*(1–2), 1–16. https://doi.org/10.1016/J.CHEMPHYSLIP.2009.08.003

Sercombe, L., Veerati, T., Moheimani, F., Wu, S. Y., Sood, A. K., & Hua, S. (2015). Advances and Challenges of Liposome Assisted Drug Delivery. *Frontiers in Pharmacology*, *6*(DEC). https://doi.org/10.3389/FPHAR.2015.00286

Shaikh, I., Jadhav, S., Jadhav, K., Kadam, V., & Pisal, S. (2009). Aceclofenac Organogels: In Vitro and In Vivo Characterization. *Current Drug Delivery*, *6*(1), 1–7. https://doi.org/10.2174/156720109787048320

Shen, J., Wang, Y., Fan, P., Jiang, L., Zhuang, W., Han, Y., & Zhang, H. (2019). Self-assembled vesicles formed by C18 unsaturated fatty acids and sodium dodecyl sulfate as a drug

delivery system. *Colloids and Surfaces A: Physicochemical and Engineering Aspects*, *568*, 66–74. https://doi.org/10.1016/J.COLSURFA.2019.01.070

Shi, J. G., Chen, X., Lee, F., Emm, T., Scherle, P. A., Lo, Y., Punwani, N., Williams, W. V., & Yeleswaram, S. (2014). The pharmacokinetics, pharmacodynamics, and safety of baricitinib, an oral JAK 1/2 inhibitor, in healthy volunteers. *Journal of Clinical Pharmacology*, *54*(12), 1354–1361. https://doi.org/10.1002/jcph.354

Shivakumar, H., & Narsimha, S. (2010). Topical and Transdermal Drug delivery. In V. Hulkarni (Ed.), *Handbook of non-invasive drug delivery system and personal care products* (pp. 1–36). Elsevier.

Shmeeda, H., Amitay, Y., Tzemach, D., Gorin, J., & Gabizon, A. (2013). Liposome encapsulation of zoledronic acid results in major changes in tissue distribution and increase in toxicity. *Journal of Controlled Release*, *167*(3), 265–275. https://doi.org/10.1016/J.JCONREL.2013.02.003

Siepmann, J. (2001). Modeling of drug release from delivery systems based on hydroxypropyl methylcellulose (HPMC). *Advanced Drug Delivery Reviews*, *48*(2–3), 139–157. https://doi.org/10.1016/S0169-409X(01)00112-0

Silva-Abreu, M., Carolina Espinoza, L., Halbaut, L., Espina, M., Luisa García, M., & Cristina Calpena, A. (2018). *Comparative Study of Ex Vivo Transmucosal Permeation of Pioglitazone Nanoparticles for the Treatment of Alzheimer's Disease*. https://doi.org/10.3390/polym10030316

Singh, S. K., Durrani, M. J., Reddy, I. K., & Khan, M. A. (1996). Effect of permeation enhancers on the release of ketoprofen through transdermal drug delivery systems. *Die Pharmazie*, *51*(10), 741–744.

Singh, S., & Singh, J. (2004). Dermal toxicity and microscopic alterations by JP-8 jet fuel components in vivo in rabbit. *Environmental Toxicology and Pharmacology*, *16*(3), 153–161. https://doi.org/10.1016/J.ETAP.2003.12.001

Sinico, C., & Fadda, A. M. (2009). Vesicular carriers for dermal drug delivery. *Expert Opinion on Drug Delivery*, *6*(8), 813–825. https://doi.org/10.1517/17425240903071029

Soltani, F., Parhiz, H., Mokhtarzadeh, A., & Ramezani, M. (2015). Synthetic and Biological Vesicular Nano-Carriers Designed for Gene Delivery. *Current Pharmaceutical Design*, *21*(42), 6214–6235. https://doi.org/10.2174/1381612821666151027153410

Southwell, D., & Barry, B. W. (1983). Penetration Enhancers for Human Skin: Mode of Action of 2-Pyrrolidone and Dimethylformamide on Partition and Diffusion of Model Compounds Water, n-Alcohols, and Caffeine. *Journal of Investigative Dermatology*, *80*(6), 507–514. https://doi.org/10.1111/1523-1747.ep12535090

Souto, E. B., Cano, A., Martins-Gomes, C., Coutinho, T. E., Zielińska, A., & Silva, A. M. (2022). Microemulsions and Nanoemulsions in Skin Drug Delivery. *Bioengineering*, *9*(4), 158. https://doi.org/10.3390/bioengineering9040158

Spielmann, H. (1995a). HET-CAM Test. In *In Vitro Toxicity Testing Protocols* (pp. 199–204). Humana Press. https://doi.org/10.1385/0-89603-282-5:199

Spielmann, H. (1995b). HET-CAM test. *Methods in Molecular Biology (Clifton, N.J.)*, *43*, 199–204. https://doi.org/10.1385/0-89603-282-5:199

Sroka-Tomaszewska, J., & Trzeciak, M. (2021a). Molecular Mechanisms of Atopic Dermatitis Pathogenesis. *International Journal of Molecular Sciences*, *22*(8), 4130. https://doi.org/10.3390/ijms22084130

Sroka-Tomaszewska, J., & Trzeciak, M. (2021b). Molecular Mechanisms of Atopic Dermatitis Pathogenesis. *International Journal of Molecular Sciences*, *22*(8), 4130. https://doi.org/10.3390/ijms22084130

Stanley, P. L., Steiner, S., Havens, M., & Tramposch, K. M. (1991). Mouse Skin Inflammation Induced by Multiple Topical Applications of 12-O-Tetradecanoylphorbol-13-Acetate. *Skin Pharmacology and Physiology*, *4*(4), 262–271. https://doi.org/10.1159/000210960

Stefanski, A.-L., Tomiak, C., Pleyer, U., Dietrich, T., Burmester, G. R., & Dörner, T. (2017). The Diagnosis and Treatment of Sjögren's Syndrome. *Deutsches Ärzteblatt International*. https://doi.org/10.3238/arztebl.2017.0354

Supe, S., & Takudage, P. (2021). Methods for evaluating penetration of drug into the skin: A review. *Skin Research and Technology*, *27*(3), 299–308. https://doi.org/10.1111/srt.12968

Takanashi, Y., Higashiyama, K., Komiya, H., Takayama, K., & Nagai, T. (1999). Thiomenthol derivatives as novel percutaneous absorption enhancers. *Drug Development and Industrial Pharmacy*, *25*(1), 89–94. https://doi.org/10.1081/DDC-100102146

Takeuchi, Y., Yasukawa, H., Yamaoka, Y., Taguchi, K., Fukushima, S., Shimonaka, Y., Nishinaga, H., & Morimoto, Y. (1995). Behavior of propylene glycol (PG) in dermis after treatment of rat intact skin surface with fatty acids, fatty amines or azone dissolved in PG. *Biological & Pharmaceutical Bulletin*, *18*(2), 304–309. https://doi.org/10.1248/BPB.18.304

Takeuchi, Y., Yasukawa, H., Yamaoka, Y., Takahashi, N., Tamura, C., Morimoto, Y., Fukushima, S., & Vasavada, R. C. (1993). Effects of oleic acid/propylene glycol on rat abdominal stratum corneum: lipid extraction and appearance of propylene glycol in the dermis measured by Fourier transform infrared/attenuated total reflectance (FT-IR/ATR) spectroscopy. *Chemical & Pharmaceutical Bulletin*, *41*(8), 1434–1437. https://doi.org/10.1248/CPB.41.1434

Tambe, V., Maheshwari, R., Chourasiya, Y., Choudhury, H., Gorain, B., & Tekade, R. K. (2019). Clinical Aspects and Regulatory Requirements for Nanomedicines. *Basic Fundamentals of Drug Delivery*, 733–752. https://doi.org/10.1016/B978-0-12-817909-3.00018-2

Tang, L., Cao, X., Li, X., & Ding, H. (2021). Topical application with conjugated linoleic acid ameliorates 2, 4-dinitrofluorobenzene-induced atopic dermatitis-like lesions in BALB/c mice. *Experimental Dermatology*, *30*(2), 237–248. https://doi.org/10.1111/exd.14242

Tanner, T., & Marks, R. (2008). Delivering drugs by the transdermal route: review and comment. *Skin Research and Technology : Official Journal of International Society for Bioengineering and the Skin (ISBS) [and] International Society for Digital Imaging of Skin (ISDIS) [and] International Society for Skin Imaging (ISSI)*, *14*(3), 249–260. https://doi.org/10.1111/J.1600-0846.2008.00316.X

Taylor, L. J., Lee, R. S., Long, M., Rawlings, A. V., Tubek, J., Whitehead, L., & Moss, G. P. (2002). Effect of occlusion on the percutaneous penetration of linoleic acid and glycerol. *International Journal of Pharmaceutics*, *249*(1–2), 157–164. https://doi.org/10.1016/S0378-5173(02)00489-1

Tenzer, S., Docter, D., Rosfa, S., Wlodarski, A., Kuharev, J., Rekik, A., Knauer, S. K., Bantz, C., Nawroth, T., Bier, C., Sirirattanapan, J., Mann, W., Treuel, L., Zellner, R., Maskos, M., Schild, H., & Stauber, R. H. (2011). Nanoparticle size is a critical physicochemical determinant of the human blood plasma corona: A comprehensive quantitative proteomic analysis. *ACS Nano*, *5*(9), 7155–7167. https://doi.org/10.1021/NN201950E/SUPPL_FILE/NN201950E_SI_003.XLS

The FDA Group. (2022, August 2). *A Basic Guide to Process Validation in the Pharmaceutical Industry*. https://www.thefdagroup.com/blog/process-validation-pharmaceutical-industry#:~:text=What%20is%20Process%20Validation%3F,of%20consistently%20delivering%20quality%20product%E2%80%9D.

Thermo Fisher Scientific Inc. (n.d.). *HPLC Basics*. Retrieved July 11, 2023, from https://www.thermofisher.com/uk/en/home/industrial/chromatography/chromatography-learning-center/liquid-chromatography-information/hplc-basics.html#:~:text=High%2Dperformance%20liquid%20chromatography%20(HPLC,packed%20with%20a%20stationary%20phase.

Thomas, B. J., & Finnin, B. C. (2004). The transdermal revolution. *Drug Discovery Today*, *9*(16), 697–703. https://doi.org/10.1016/S1359-6446(04)03180-0

Torchilin, V. P. (2005). Recent advances with liposomes as pharmaceutical carriers. *Nature Reviews. Drug Discovery*, *4*(2), 145–160. https://doi.org/10.1038/NRD1632

Touitou, E., Levi-Schaffer, F., Dayan, N., Alhaique, F., & Riccieri, F. (1994). Modulation of caffeine skin delivery by carrier design: liposomes versus permeation enhancers. *International Journal of Pharmaceutics*, *103*(2), 131–136. https://doi.org/10.1016/0378-5173(94)90093-0

Touitou, E., Meidan, V. M., & Horwitz, E. (1998). Methods for quantitative determination of drug localized in the skin. *Journal of Controlled Release*, *56*(1–3), 7–21. https://doi.org/10.1016/S0168-3659(98)00060-1

Tsai, T. F., & Maibach, H. I. (1999). How irritant is water? An overview. *Contact Dermatitis*, *41*(6), 311–314. https://doi.org/10.1111/J.1600-0536.1999.TB06990.X

Turi, J. S., Danielson, D., & Woltersom, J. W. (1979). Effects of polyoxypropylene 15 stearyl ether and propylene glycol on percutaneous penetration rate of diflorasone diacetate. *Journal of Pharmaceutical Sciences*, *68*(3), 275–280. https://doi.org/10.1002/JPS.2600680306

Ulrich, A. S. (2002). Biophysical aspects of using liposomes as delivery vehicles. *Bioscience Reports*, *22*(2), 129–150. https://doi.org/10.1023/A:1020178304031

Valenta, C., Wanka, M., & Heidlas, J. (2000). Evaluation of novel soya-lecithin formulations for dermal use containing ketoprofen as a model drug. *Journal of Controlled Release : Official Journal of the Controlled Release Society*, *63*(1–2), 165–173. https://doi.org/10.1016/S0168-3659(99)00199-6

Van Haeringen, N. J. (1981). Clinical biochemistry of tears. *Survey of Ophthalmology*, *26*(2), 84–96. https://doi.org/10.1016/0039-6257(81)90145-4

Vázquez-González, M. L., Botet-Carreras, A., Domènech, Ò., Teresa Montero, M., & Borrell, J. H. (2019). Planar lipid bilayers formed from thermodynamically-optimized liposomes as new featured carriers for drug delivery systems through human skin. *International Journal of Pharmaceutics*, *563*, 1–8. https://doi.org/10.1016/j.ijpharm.2019.03.052

Verdier-Sévrain, S., & Bonté, F. (2007). Skin hydration: a review on its molecular mechanisms. *Journal of Cosmetic Dermatology*, *6*(2), 75–82. https://doi.org/10.1111/j.1473-2165.2007.00300.x

Voulgarelis, M., & Tzioufas, A. G. (2010). Pathogenetic mechanisms in the initiation and perpetuation of Sjögren's syndrome. *Nature Reviews Rheumatology*, *6*(9), 529–537. https://doi.org/10.1038/nrrheum.2010.118

Walker, M., & Hadgraft, J. (1991). Oleic acid — a membrane "fluidiser" or fluid within the membrane? *International Journal of Pharmaceutics*, *71*(1–2), R1–R4. https://doi.org/10.1016/0378-5173(91)90078-3

Wang, H., & Meng, F. (2017). The permeability enhancing mechanism of menthol on skin lipids: a molecular dynamics simulation study. *Journal of Molecular Modeling*, *23*(10), 279. https://doi.org/10.1007/s00894-017-3457-y

Wang, S., Zuo, A., & Guo, J. (2021). Types and evaluation of in vitro penetration models for buccal mucosal delivery. *Journal of Drug Delivery Science and Technology*, *61*, 102122. https://doi.org/10.1016/j.jddst.2020.102122

Watters, R. J., Kester, M., Tran, M. A., Loughran, T. P., & Liu, X. (2012). *Development and Use of Ceramide Nanoliposomes in Cancer* (pp. 89–108). https://doi.org/10.1016/B978-0-12-391860-4.00005-7

Wertz, P. W. (1996). The nature of the epidermal barrier: biochemical aspects. *Advanced Drug Delivery Reviews*, *18*(3), 283–294. https://doi.org/10.1016/0169-409X(95)00077-K

Wester, R., & Maibach, H. (1999). Regional Variation in Percutaneous Absorption. In R. Bronaugh & H. Maibach (Eds.), *Percutaneous Absorption Drugs, Cosmetics, Mechanisms, Methods* (4th ed., p. 219). Marcel Dekker Inc.

Whitesides, G. M., & Grzybowski, B. (2002). Self-assembly at all scales. *Science (New York, N.Y.)*, *295*(5564), 2418–2421. https://doi.org/10.1126/SCIENCE.1070821

Wicki, A., Witzigmann, D., Balasubramanian, V., & Huwyler, J. (2015). Nanomedicine in cancer therapy: challenges, opportunities, and clinical applications. *Journal of Controlled Release : Official Journal of the Controlled Release Society*, *200*, 138–157. https://doi.org/10.1016/J.JCONREL.2014.12.030

Wiklander, O. P. B., Nordin, J. Z., O'Loughlin, A., Gustafsson, Y., Corso, G., Mäger, I., Vader, P., Lee, Y., Sork, H., Seow, Y., Heldring, N., Alvarez-Erviti, L., Edvard Smith, C. I., Le Blanc, K., Macchiarini, P., Jungebluth, P., Wood, M. J. A., & El Andaloussi, S. (2015). Extracellular vesicle in vivo biodistribution is determined by cell source, route of

administration and targeting. *Journal of Extracellular Vesicles*, *4*(2015), 1–13. https://doi.org/10.3402/JEV.V4.26316

Williams, A. C., & Barry, B. W. (1991). The enhancement index concept applied to terpene penetration enhancers for human skin and model lipophilic (oestradiol) and hydrophilic (5-fluorouracil) drugs. *International Journal of Pharmaceutics*, *74*(2–3), 157–168. https://doi.org/10.1016/0378-5173(91)90232-D

Wishart, D. S., Feunang, Y. D., Guo, A. C., Lo, E. J., & Marcu, A. (2023, January 3). *Baricitinib*. Drug Bank. https://go.drugbank.com/drugs/DB11817

Wollenberg, A., Barbarot, S., Bieber, T., Christen-Zaech, S., Deleuran, M., Fink-Wagner, A., Gieler, U., Girolomoni, G., Lau, S., Muraro, A., Czarnecka-Operacz, M., Sch€, T., Schmid-Grendelmeier, P., & Simon, D. (2018). *Consensus-based European guidelines for treatment of atopic eczema (atopic dermatitis) in adults and children: part I European Federation of Allergy and Airways Diseases Patients' Associations (EFA), Global Allergy and Asthma Patient Platform*. *16*, 657–682. https://doi.org/10.1111/jdv.14891

Xing, H., Hwang, K., & Lu, Y. (2016). Recent Developments of Liposomes as Nanocarriers for Theranostic Applications. *Theranostics*, *6*(9), 1336–1352. https://doi.org/10.7150/THNO.15464

Yamada, M., & Uda, Y. (1987). Enhancement of Percutaneous Absorption of Molsidomine. *Chemical and Pharmaceutical Bulletin*, *35*(8), 3390–3398. https://doi.org/10.1248/CPB.35.3390

Yamashita, F., Koyama, Y., Kitano, megumi, Takakura, Y., & Hashida, M. (1995). Analysis of in vivo skin penetration enhancement by oleic acid based on a two-layer diffusion model with polar and nonpolar routes in the stratum corneum. *International Journal of Pharmaceutics*, *117*(2), 173–179. https://doi.org/10.1016/0378-5173(94)00327-2

Yum, S., Lee, E., Taskovich, L., & Theeuwes, F. (1994). Permeation enhancement with ethanol: mechanism of action through skin. In D. S. Hsieh (Ed.), *Drug Permeation Enhancement* (Vol. 62, pp. 143–170). Marcel Dekker Inc.

Zellmer, S., Pfeil, W., & Lasch, J. (1995). Interaction of phosphatidylcholine liposomes with the human stratum corneum. *Biochimica et Biophysica Acta (BBA) - Biomembranes*, *1237*(2), 176–182. https://doi.org/10.1016/0005-2736(95)00100-H

Zhang, R., Bi, R., Ho Jun Hui, C., Rajarahm, P., Dinish, U. S., & Olivo, M. (2021). A Portable Ultrawideband Confocal Raman Spectroscopy System with a Handheld Probe for Skin Studies. *ACS Sensors*, *6*(8), 2960–2966. https://doi.org/10.1021/acssensors.1c00761

Zhang, Y., Guo, S., & Wei, C. (2023). Fluorescence Spectroscopy: Part I Principles. *Encyclopedia of Soils in the Environment*, 544–551. https://doi.org/10.1016/B978-0-12-822974-3.00081-1

Zimmer, A., & Kreuter, J. (1995). Microspheres and nanoparticles used in ocular delivery systems. *Advanced Drug Delivery Reviews*, *16*(1), 61–73. https://doi.org/10.1016/0169-409X(95)00017-2

Zou, Y., & Maibach, H. I. (2018). Dermal–epidermal separation methods: research implications. *Archives of Dermatological Research*, *310*(1), 1–9. https://doi.org/10.1007/s00403-017-1774-8

Zsikó, Csányi, Kovács, Budai-Szűcs, Gácsi, & Berkó. (2019). Methods to Evaluate Skin Penetration In Vitro. *Scientia Pharmaceutica*, *87*(3), 19. https://doi.org/10.3390/scipharm87030019

ANNEXES

Baricitinib Liposomes as a New Approach for the Treatment of Sjögren's Syndrome

Núria Garrós, Mireia Mallandrich, Negar Beirampour, Roya Mohammadi, Òscar Domènech, Maria José Rodríguez-Lagunas, Beatriz Clares i Helena Colom.

Pharmaceutics 2022, 14, 1895.

https://doi.org/10.3390/pharmaceutics14091895

Quartil Q1; factor d'impacte 5.4 l'any 2022.

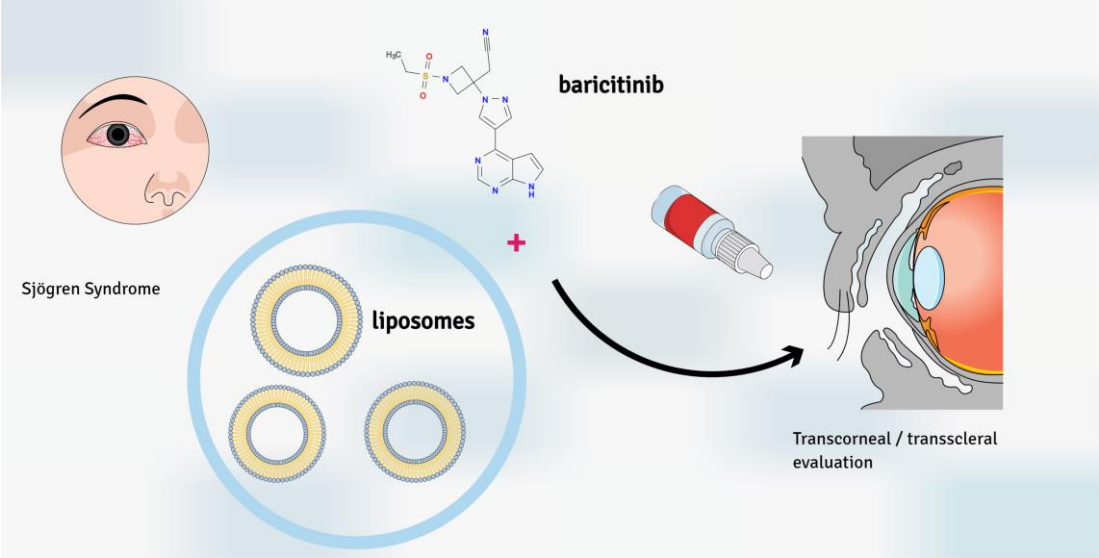

pharmaceutics

MDPI

Article

Baricitinib liposomes as a new approach for the treatment of Sjögren's Syndrome

Núria Garrós[1], Mireia Mallandrich[1,4]*, Negar Beirampour[1], Roya Mohammadi[1,4], Oscar Domènech[1,4], Maria J. Rodríguez-Lagunas[2], Beatriz Clares[3,4] and Helena Colom[1]

[1] Department of Pharmacy, Pharmaceutical Technology and Physical Chemistry, Faculty of Pharmacy and Food Sciences, University of Barcelona, 08028 Barcelona, Spain; ngarroar50@alumnes.ub.edu (N.G.), mireia.mallandrich@ub.edu (M.M.); nbeirabe7@alumnes.ub.edu (N.B.); rmohammo31@alumnes.ub.edu (R.M.); odomenech@ub.edu (O.D.); helena.colom@ub.edu (H.C.)
[2] Department of Physiology, Faculty of Pharmacy and Food Sciences, University of Barcelona, Av. Joan XXIII, 08028 Barcelona, Spain; mjrodriguez@ub.edu (M.J.R-L.)
[3] Department of Pharmacy and Pharmaceutical Technology, Faculty of Pharmacy, University of Granada, 18071 Granada, Spain; beatrizclares@ugr.es
[4] Institute of Nanoscience and nanotechnology, University of Barcelona. 645 Diagonal Avenue, 08028 Barcelona, Spain.
* Correspondence: mireia.mallandrich@ub.edu

Abstract: Sjögren's syndrome is a chronic systemic autoimmune disease affecting from 0.2 to 3% of the general population. The current treatment for Sjögren's syndrome is aimed at controlling symptoms such as dry eyes and xerostomia. Systemic therapy with glucocorticoids or immunosuppressants is also used. Baricitinib is an immunosuppressant drug, specifically a Janus kinases 1 and 2 selective inhibitor. We propose ocular liposomal formulations loaded with baricitinib for the management of Sjögren's syndrome. The novelty of the work relies on the fact that, for the first time, baricitinib is intended to be used for topical delivery. Two liposomal formulations were prepared with different lipids: (i) L-α-phosphatidylcholine (Lα-PC) and (ii) a combination of lipids 1-palmitoyl-2-oleoyl-phosphatidylethanolamine: s1-Palmitoyl-2-oleoyl-sn-glycerol-3-phosphoglycerol (3:1, mol/mol) (POPE:POPG), and they were physicochemically characterized. The in vitro drug release and the ex vivo permeation through corneal and scleral tissues were also assessed. Finally, the tolerance of the formulations on the ocular tissues was evaluated by the HET-CAM technique, as well as through the histological analysis of the cornea and sclera and the cornea transparency. Both liposomes resulted in small, spherical shapes, with suitable physicochemical properties for the ocular administration. Lα-PC led to higher flux, permeation, and retention in the sclera, whereas POPE:POPG led to higher flux and permeation in the cornea. The formulations showed no irritant effects on the chorioallantoic membrane. Additionally, the liposomes did not affect the cornea transparency when they were applied, and the histological analysis did not reveal any structural alteration.

Keywords: Sjögren's Syndrome; liposomes; baricitinib; JAK inhibitor; ocular delivery; transcorneal permeation; transscleral permeation; ocular tolerance.

Citation: Garrós, N.; Mallandrich, M.; Beirampour, N; Mohammadi, R; Domènec, Ò.; Rodríguez-Lagunas, M.J.; Clares, B.; Colom, H. Baricitnib Liposomes as a New Approach for the Treatment of Sjögren's Syndrome. *Pharmaceutics 2022, 14, 1895.* https://doi.org/10.3390/pharmaceutics14091895

Academic Editor: Natasa Skalko-Basnet, Amparo Sánchez Navarro and María José de Jesús Valle

Received: 8 July 2022
Accepted: 4 September 2022
Published: 7 September 2022

1. Introduction

Immunologic diseases are caused by an imbalance between the immune system function to protect the body from bacteria and viruses and tissue damage because of the immune response [1]. Some kinds of autoimmune diseases are immunologic diseases, which are the result of identifying the patient's own organs, tissues, and cells as foreign and activating an immune response against them. Individually, these diseases are rare, but as a group, they are the most common diseases in industrialized countries [2], and they affect between 5 and 10% of the European and North American population [3].

Sjögren's syndrome (SS) is a chronic systemic autoimmune disease that can be suffered as a unique disease (primary SS) or can be a consequence of another autoimmune disease (secondary SS) [4]. Primary SS is a highly prevalent, chronic, autoimmune exocrinopathy today, affecting from 0.2 to 3% of the general population. It is caused by the loss of central tolerance, which generates epithelitis and acinar atrophy due to predominantly inflammatory cell types which infiltrate into the exocrine glands and certain extraglandular tissues [5]. It is characterized by keratoconjunctivitis sicca (dry eyes) and xerostomia (dry mouth) [4,6].

The European Study Group on Classification Criteria developed and validated a criteria classification for primary SS between 1989 and 1996. It was made observing 180 people, of which 76 were affected by primary SS and 104 were not. It is organized in a classification tree performance and has a sensitivity of 96.1% and a specificity of 94.2% [7].

Different anti-inflammatory and immunomodulatory drugs are used in the treatment of ocular inflammatory and immunological diseases. Two examples are diclofenac, used as an anti-inflammatory agent, and cyclosporine, used an as anti-inflammatory and immunomodulatory drug [8]. Baricitinib is an immunosuppressant drug that acts inhibiting selectively Janus kinases 1 and 2, among others, and reduces disease signs and symptoms by decreasing inflammation, cellular activation, and proliferation of key immune cells. Baricitinib has already been used for the treatment of atopic dermatitis through oral administration with good outcomes: oral baricitinib improved signs and resolved symptoms better than topic cyclosporin [9]. Another advantage is that baricitinib has anti-inflammatory properties due to its therapeutic path. Now, baricitinib is orally administrated for the treatment of moderate-to-severe atopic dermatitis and rheumatoid arthritis, and it is also being studied for its oral administration for systemic erythematosusmatous, psoriasis, and primary SS [10,11]. The pilot study of baricitinib oral administration conducted in China using active SS patients seemed to show efficacy and safety [12]. The actual treatment for primary SS is divided into topical treatment for the mouth and eyes to control the symptoms and avoid complications, and systemic treatment for parotid enlargement and extraglandular signs. Topical treatments are preventive: fluor is used to avoid periodontal diseases and chlorhexidine for electrostimulation; and for the eyes, artificial tears are used. Anti-inflammatory drugs and local ciclosporin, pilocarpine, or cevimeline secretagogue are used in both cases to stimulate saliva or lacrimal flow. Systemic treatments consist of glucocorticoids and different immunosuppressants [13].

Liposomes are spherically shaped nano-sized to micro-sized vesicles composed of biodegradable natural or synthetic phospholipids. They are formed spontaneously in an aqueous medium so that inside the vesicles different agents can be encapsulated; the hydrophobic agents between the lipids and the hydrophilic ones in the aqueous core [14]. Liposomes can have very different properties because of their composition, surface charge, size, phospholipid bilayer membrane, and method of preparation [15–17]. One way for liposomes to be classified is by their size and number of bilayers: multilamellar liposome vesicles (MLV) and unilamellar vesicles (UV). The latter group has three more stages, as shown in Figure 1.

The liposomes' composition is biocompatible, biodegradable, and non-toxic, and the flexibility of their formulation allows for different sizes of liposomes that make it possible to use them as eye drops [8]. These characteristics also help at the time of preparing an ophthalmic formulation, during which, some points need to be studied to avoid compatibility problems: the pH has to be in a range close to the physiologic pH, the osmolarity has to be isotonic with the tears and to prevent infections, and sterility is also necessary [18]. The high capacity of entrapment relies on its ability to encapsulate a wide range of drugs, and having this advantage overcomes the common problem of drugs that are water-insoluble or poorly soluble in this kind of formulation [19]. As for liposome size and charge for eye application, it has been shown that the interaction of liposomes with cornea follow this order: MLV+ > SUV+ > MLV− > SUV− > MLV [8].

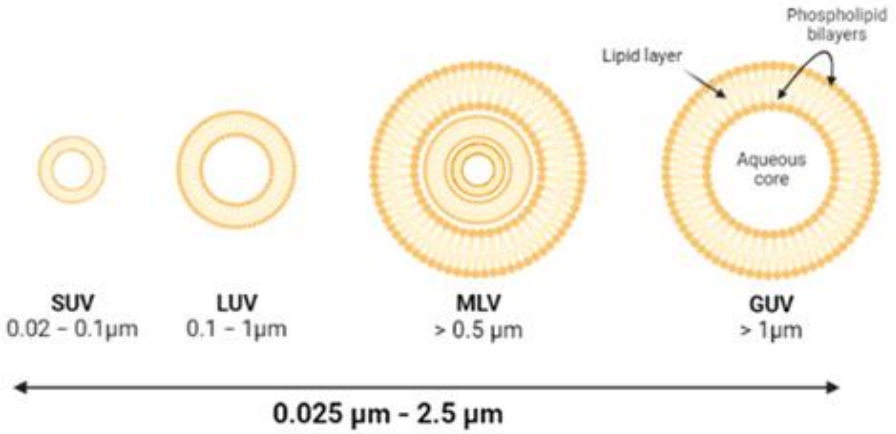

Figure 1. Classification of the liposomes based on their size and number of lipid layers. SUV, small unilamellar vesicle; LUV, large unilamellar vesicle; MLV, multilamellar liposome vesicle; GUV, giant unilamellar vesicle.

To our knowledge, no studies involving baricitinib administered by the ophthalmic route have been conducted. Stevenson and co-workers determined the efficacy of another Janus kinase inhibitor; 0.003% tofacitinib was applied ocularly in mice which had induced corneal thermocautery, resulting in a decrease in the interleukins [20]. In another study, Hofauer and colleagues investigated the efficacy of liposomal agents for the symptoms of xerostomia, keratoconjunctivitis sicca, and rhinitis sicca in a clinical trial involving patients with Sjögren's syndrome. The authors concluded that liposomes were an effective local approach since they significantly reduced the symptoms of xerostomia, keratoconjunctivitis sicca, and rhinitis sicca after 2 months of treatment [21]. Taking into account the satisfactory results obtained by Stevenson et al. with tofacitinib and those obtained by Hofauer with liposomal agents, we aimed to formulate liposomes loading baricitinib for ophthalmic administration as an alternative or co-adjuvant treatment for Sjögren's syndrome [9]. Therefore, our intention with these formulations is to simplify the eye topical treatment to one step. We characterized two liposomes with two different lipids and we assessed the baricitinib release from the formulations as well as the capacity of baricitinib to penetrate the corneal and scleral tissues through ex vivo permeation tests. We also investigated the tolerability of the developed formulations on the eye by alternative in vitro methods, such as the HET-CAM technique and the evaluation of the cornea transparency. Finally, we conducted histological studies on the tissues after the permeation test.

2. Materials and Methods

2.1. Materials

Baricitinib and an Ammonium salt formate were bought at Sigma-Aldrich (Madrid, Spain). Gattefossé (Barcelona, Spain) supplied Transcutol® P [Diethylene glycol monoethyl ether]. Acetonitrile was purchased at Fisher Chemical (Loughborough, UK). Lipids L-α-phosphatidylcholine (Lα-PC) and 1-palmitoyl-2-oleoyl-phosphatidylethanolamine (POPE) were bought at BOC Sciences (London, UK) and 1-Palmitoyl-2-oleoyl-sn-glycerol-3-phosphoglycerol (POPG) was obtained at Sigma-Aldrich (Madrid, Spain).

2.2. Biological Materials

Cornea and sclera were obtained from residual individuals of female pigs (cross Landrace x Large White, 25–30 kg), previously used in surgical university practices and according to the Ethics Committee of Animals Experimentation at the University of

Barcelona. The eyes were immediately enucleated after the animals were sacrificed, and corneas and scleral tissues were excised in situ and transported to the laboratory immersed in artificial aqueous humor solution to be debrided and plain-prepared for the permeation experiments.

2.3. Methods

2.3.1. Preparation of the Liposomes

A total of 500 mg of baricitinib was placed in a round-bottom flask and 10 mM chloroform-methanol (2:1, v/v) lipid solutions -Lα-PC or POPE:POPG (3:1, mol/mol) were added to the flask to obtain the required lipid molar concentration for each composition [22]. To ensure the baricitinib was fully dissolved, the solution was sonicated for 10–15 s. The round-bottom flask was then mounted on a rotary evaporator and the solvent was evaporated protected from the light. Dry lipids with baricitinib were left under a high vacuum in a desiccator protected from light overnight. Thin films were rehydrated with 10 mM TRIS·HCl, 150 mM NaCl pH 7.40 [23,24] supplemented with a 5% (v/v) of Transcutol® P. Large multilamellar vesicles were obtained after 5 cycles of vigorous vortexing of the solution over and below the transition temperature of the lipid mixture. To homogenize the liposome size, the liposome solution was placed in an ultrasound bath with 100% sonication amplitude (the controlling temperature did not exceed the 37 ◦C) for 15 min. Finally, non-encapsulated baricitinib was eliminated by filtering the liposomal solution through a Sephadex® G50 column mounted in a 5 mL syringe and centrifuged at 1000× g rpm in a Rotanta 460R centrifuge (Andreas Hettich GmbH & Co. KG, Tuttlingen, Germany).

2.3.2. Liposomes Physicochemical Characterization

The physicochemical characterization included the measurement of pH, the vesicle size and polydispersity index, the zeta potential, the osmolality, and the efficiency of encapsulation.

pH was measured at room temperature with pH-metre micro pH 2001 (Crison Instruments SA, Alella, Spain) by triplicate.

Liposome size, polydispersity index (PDI), and zeta potential (ZP) were measured with a Zetasizer Nano S (Malvern Instruments, Malvern, UK); all measurements were made in triplicate and showed satisfactory deviation values [25]. The surface electrical properties of the liposomes were measured after suitable dilution (0.1% *w*/*v*) by electrophoresis measures using a Zetasizer 2000 (Malvern Instruments Ltd., UK). Furthermore, the influences of pH and ionic strength were also investigated. For this task, dilute liposomal dispersions were prepared at different pHs (3–8) and ZP determinations were done after they had been in contact for 24 h under mechanical stirring (50 rpm) and at 25.0 ± 0.5 °C. Before carrying out the measurement, the pH was checked and readjusted. Similarly, the ZP values were also recorded for liposomes formulated at pH 6 with different electrolytes. Hence, the effect of the particular electrolyte (NaCl, $CaCl_2$, and $AlCl_3$) and concentrations ranging from, 2×10^{-1}, 10^{-1}, 10^{-2}, 10^{-3}, 10^{-4}, and 10^{-5} M, were assayed. All measurements were also performed on blank liposomes and loaded liposomes nine times.

Osmolality was measured using an Advanced 3320 Micro-Osmometer (Advanced Instruments, LLC, Norwood, MA, USA) [26].

The efficiency of encapsulation (EE) was measured by breaking the liposomes with 80% of Transcutol® P and a 10% of 10% Triton and quantifying the amount of baricitinib by HPLC. The amount of baricitinib was compared to the initial amount (Equation (1)) [26].

$$\boldsymbol{EE\%} = \frac{\boldsymbol{Q_f}}{\boldsymbol{Q_o}} \times \mathbf{100}, \quad (1)$$

where, *EE%* is the efficiency of encapsulation, *Qf* is the amount of baricitinib in mg retained inside liposomes, and *Qo* is the amount of baricitinib in mg used initially to elaborate liposomes.

2.3.3. Morphological Study of the Liposomes

The morphological study was carried out by TEM with a JEM-1010 microscope (JEOL Ltd., Tokyo, Japan). One drop of each liposome was put on copper grids covered with a layer of Formvar®. The sample was in contact with the grid for 1 min. Next, one drop of 2% uranyl acetate solution was placed on the grid, and subsequently, a drop of methylcellulose was placed on the grid for 10 min; the excess methylcellulose was wiped with filter paper, tapping the filter diagonally. Finally, the grid was allowed to dry before image analysis [27].

2.3.4. In Vitro Drug Release Study

In vitro release studies were carried out using Franz-type diffusion cells [28,29] with a diffusion area of 0.64 cm^2 and a receptor chamber of 4.9 mL. We used a dialysis membrane with a molecular cut-off weight of 14,000 Da (Sigma-Aldrich, Madrid, Spain). The membrane was hydrated for 24 h in methanol:water (1:1) and rinsed before being mounted in the Franz diffusion cell (Crown Glass Company, Inc., Jersey City, NJ, USA).

Transcutol® P was the receptor medium which provided the sink conditions throughout the study. Aliquots of 500 μL of two different liposomes were added to the donor compartment. A volume of 200 μL was taken and replaced with Transcutol® P at established times over 31 h. The experiment conditions are set out in Table 1. The samples obtained were analyzed by a validated HPLC-fluorescence method. The concentrations of baricitinib in the liposomes were determined as described in the efficiency encapsulation section. The data were fitted to different kinetic models and the best fit was selected based on the determination coefficient r^2 [30].

Table 1. Experimental conditions for the in vitro release test.

Parameters	Conditions
Receptor fluid	Transcutol® P
Cell volume	4.9 mL
Diffusion area	0.64 cm^2
Membrane	Dialysis membrane
Replicates	5 replicates
Temperature	32 ± 0.5 °C
Stirring	500 r.p.m.
Dose	500 μL of liposomes (Lα-PC 13.99 μg/mL and POPE:POPG 9.83 μg/mL)
Sample volume	200 μL
Sampling times	0 (pre-sample time point), 3.0 h, 7.0 h, 20.3 h, 24.5 h, 28.3 h, and 31.0 h

Lα-PC = L-α-phosphatidylcholine; POPE:POPG = 1-palmitoyl-2-oleoyl-phosphatidylethanolamine: 1-Palmitoyl-2-oleoyl-sn-glycerol-3-phosphoglycerol (3:1, mol/mol).

2.3.5. Ex Vivo Permeation Study

Ex vivo corneal and scleral permeation was conducted with Franz diffusion cells. The tissues were fixed between the donor and the receptor compartments [29,28]; the area exposed to permeations was 0.64 cm^2. We applied 500 μL of liposome, either Lα-PC or POPE:POPG, in the donor compartment, with five replicates for each tissue. receptor compartment was Transcutol® P kept at 37 ◦C for the scleral tissue and at 32 ªC for the cornea, and stirred continuously. A volume of 200 μL was withdrawn from the receptor compartment at fixed times and replaced by an equivalent volume of Transcutol® P. Experimental conditions for the ex vivo permeation test are shown in Table 2. The samples were quantified by HPLC with a fluorescence detector.

Once the permeation study was complete, all tissues were removed from the diffusion cells and rinsed with distilled water to eliminate the liposomes remaining on the tissue surface. To extract baricitinib retained in the tissues [25], the permeation area was cut out, weighed, and immersed in 1 mL of Transcutol® P and sonicated for 10 min using an ultrasonic water bath. The supernatant was filtered and quantified by HPLC. Figure 2 depicts the procedure for drug extraction from the corneal and scleral tissues. The amount retained in the tissues (Qret) was calculated according to Equation (2), and the results are expressed normalized by the weight of the tissue as well as by the diffusion area (0.64 cm^2) and multiplied by the recovery of the drug:

$$Qret = \frac{Q_{ext}}{W \times A} \times \frac{100}{R}, \quad (2)$$

where, Qext is the amount of drug extracted expressed in μg, W is the weight of the tissue ((g), A is the diffusion area (cm^2), and R is the recovery of baricitinib in each tissue [29].

Table 2. Experimental conditions for the ex vivo permeation test.

Parameter	Conditions
Receptor fluid	Transcutol® P
Cell volume	4.9 mL
Diffusion area	0.64 cm^2
Membrane	Cornea and Sclera
Replicates	5 replicates
Temperature	37 ± 0.5 °C or 32 ± 0.5 °C
Stirring	500 r.p.m.
Dose	500 μL of liposomes (Lα-PC or POPE:POPG)
Sample volume	200 μL
Sampling times	0 (pre-sample time point), 2.1 h, 4.2 h, and 6.0 h

Lα-PC = L-α-phosphatidylcholine; POPE:POPG = 1-palmitoyl-2-oleoyl-phosphatidylethanolamine: 1-Palmitoyl-2-oleoyl-sn-glycerol-3-phosphoglycerol (3:1, mol/mol).

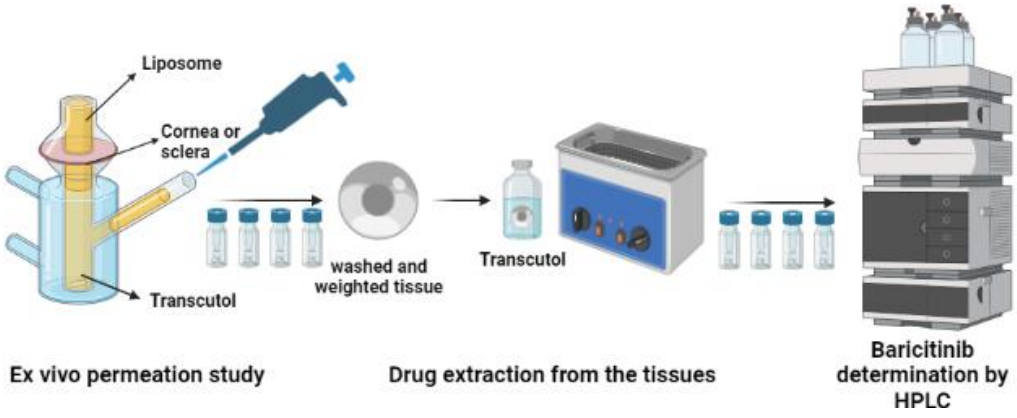

Figure 2. Ex vivo permeation studies diagram.

2.3.6. Baricitinib Determination by HPLC

The amount of baricitinib in each sample was quantified by HPLC with a fluorescence detector. The HPLC is composed of a Chromatograph Waters Alliance 2695 and a Fluorescence Jasco FP-1520 detector at an Ex wavelength of 310 nm and an Em wavelength of 390 nm. Table 3 shows the chromatographic conditions for analyzing baricitinib.

Table 3. Chromatographic conditions for the determination of baricitinib.

Parameters	Conditions
Chromatographic column	Symmetry C18 (4.6 × 75 mm, 3.5 μm)
Mobile phase	Ammonium Formate 10 mM pH 7:ACN (75:25 *v*/*v*)
Flux	1 mL/min
Injection volume	10 μL
Wavelength	Ex 310 nm and Em 390 nm
Standard concentrations range	0.031 to 1 μg/mL

2.3.7. In Vitro Tolerance Study

The potential risk of ocular irritation caused by baricitinib liposomes was studied by the HET-CAM test, which measured the ability to induce toxicity on the chorioallantoic membrane (CAM) of a 10-day embryonated hen's egg (from the G.A.L.L.S.A. farm, Tarragona, Spain). The effects are recorded in seconds during 5 min by the onset of hemorrhage (bleeding), coagulation (blood vessel disintegration), and vessel lysis coagulation (protein denaturation intra- and extra-vascular) [26]. These elements were considered individually and then combined to derive a score (*IS*), which was used to classify the irritancy level of the test substance [31].

$$IS = \frac{301-sec\,H}{300} \cdot 5 + \frac{301-sec\,L}{300} \cdot 7 + \frac{301-sec\,C}{300} \cdot 9, \quad (3)$$

where, *H* is the hemorrhage, *L* is vessel lysis, *C* is coagulation, and *sec* is the time in seconds when signs started.

We applied 300 μL of liposomes to CAM and we observed the membrane for 5 min to determine the degree of severity of each reaction according to the INVITTOX protocol [32]. We used NaOH 0.1 N as the positive control, and a solution of 0.9% NaCl as the negative control [32].

Additionally, we evaluated changes in the corneal transparency after applying the liposomes to the cornea. The technique consists of exposing the cornea under a defined beam of light and detecting the light transmitted without absorption or scattering [33]. We examined the transmittance from 150 to 760 nm on corneas after these had been immersed in Liposome Lα-PC, Liposome POPE:POPG, PBS pH 7.4 (negative control), and ethanol (positive control) for 10 min [34].

2.3.8. Corneal and Scleral Histological Study

For the histological study of cornea and sclera, samples of both tissues were exposed to the dilution of Liposome Lα-PC, the dilution of Liposome POPE:POPG, or to distilled water (negative control) for 6 h, and then processed for hematoxylin and eosin staining [35]. In a brief summary, corneas and scleral tissues were fixed in 4% buffered paraformaldehyde for 24 h and then, after dehydration, these tissues were embedded in paraffin and cut at 6 μm, stained, and mounted on DPX (Sigma Aldrich). Samples were observed under the microscope (Olympus BX41 and camera Olympus XC50) on a blind coded sample.

3. Results

3.1. Liposomes Physicochemical Characterization

The pH, osmolality, and encapsulation efficiency of the liposomes were measured and the results are presented in Table 4. Both liposomes showed physiological pH, a suitable osmolality value for the ophthalmic application, and encapsulation efficiency below 20%.

Table 4. pH, osmolality, and encapsulation efficiency (EE) of the liposomes. Results are expressed by mean ± SD (n = 3).

Liposome	pH	Osmolality (mOsm/Kg)	EE (%)
Lα-PC	7.4 ± 0.1	306 ± 2	12 ± 0.9
POPE:POPG	7.4 ± 0.1	305 ± 5	11 ± 1.1

Lα-PC = L-α-phosphatidylcholine; POPE:POPG = 1-palmitoyl-2-oleoyl-phosphatidylethanolamine: 1-Palmitoyl-2-oleoyl-sn-glycerol-3-phosphoglycerol (3:1, mol/mol).

Both liposomes have similar sizes and are negatively charged. Specifically, POPE:POPG exhibits a higher ZP. Values are shown in Table 5.

Table 5. Liposome composition with their respective hydrodynamic diameter, polydispersity index (PDI), and zeta potential (ZP). Results are expressed by mean ± SD (n = 3).

Composition	Formulation	Hydrodynamic Diameter (nm)	PDI	Zeta Potential (mV)
Lα-PC	blank	73.0 ± 3.0	0.040	−22.5 ± 1.1
	+baricitinib	61.7 ± 0.5	0.081	−20.7 ± 0.5
POPE:POPG	blank	60.5 ± 0.6	0.124	−32.0 ± 3.0
	+baricitinib	51.7 ± 0.8	0.202	−37.0 ± 5.0

Lα-PC = L-α-phosphatidylcholine; POPE:POPG = 1-palmitoyl-2-oleoyl-phosphatidylethanolamine: 1-Palmitoyl-2-oleoyl-sn-glycerol-3-phosphoglycerol (3:1, mol/mol).

The surface electrical study revealed that liposomes showed dependence on the pH. The ZP values revealed the negative surface charge of the liposomes in the entire pH range for all formulations, and no differences between blank liposomes and loaded liposomes were observed. Figure 3 shows the zeta potential of the liposomes as a function of pH.

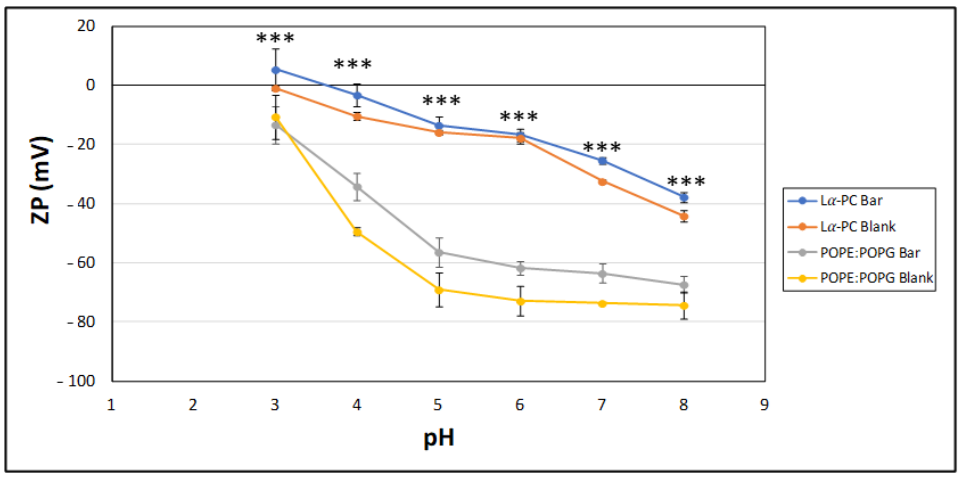

Figure 3. ZP of liposomes as a function of pH. Each point represents the Mean ± SD (n = 9). *** Statistical differences between Lα-PC liposomes and POPE:POPG liposomes ($p < 0.0001$) on a *t*-test analysis comparing Lα-PC vs. POPE:POPG loaded with baricitinib. Significance level set at $p < 0.05$

Lα-PC = L-α-phosphatidylcholine; POPE:POPG = 1-palmitoyl-2-oleoyl-phosphatidylethanolamine: 1-Palmitoyl-2-oleoyl-sn-glycerol-3-phosphoglycerol (3:1, mol/mol).

The results of ZP as a function of ionic strength are shown in Figure 4. In general, it is observed that the absolute value tended to decrease as the concentration of either electrolyte increased.

Regarding the pH study, no differences between blank liposomes and loaded liposomes were recorded. Specifically, for monovalent and divalent cations, the ZP at low electrolyte concentrations showed negative values and decreasing absolute values as the

electrolyte concentration increased. In the case of NaCl, this negativity was maintained throughout the range in the vicinity of 0, and was slightly positive when the salt reached a concentration of 10^{-2} M, 10^{-1} M, and 2×10^{-1} M, respectively. In the presence of Ca^{2+} ions, ZP values became positive or close to 0 from 10^{-4} M or 10^{-2} M, depending on the type of liposome. Finally, ZP values were positive throughout the range of concentrations tested for Al^{3+}.

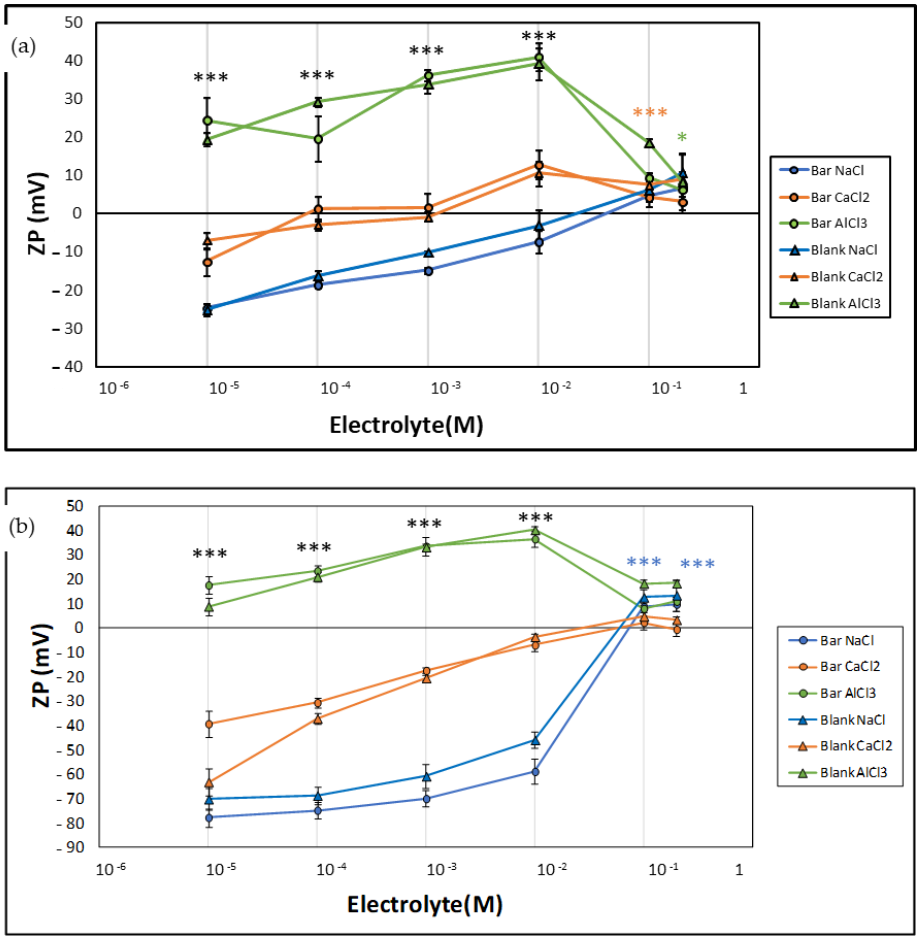

Figure 4. P of liposomes as a function of the concentration of NaCl, $CaCl_2$, and $AlCl_3$ at pH 7.4. (**a**) Lα-PC liposomes and (**b**) POPE:POPG liposomes. Each point represents the mean ± SD (n = 9). An ANOVA was conducted and then followed by Tukey analysis, considering three groups of electrolyte types at each concentration for both liposomes Lα-PC and POPE:POPG loading baricitinib. *** Statistical differences $p < 0.0001$ between all the electrolytes; *** Statistical differences $p < 0.0001$ between NaCl vs. $AlCl_3$ for Lα-PC; * Statistical differences $p < 0.05$ between NaCl and $CaCl_2$ vs. $AlCl_3$ for Lα-PC; *** Statistical differences $p < 0.0001$ between NaCl and $AlCl_3$ vs. $CaCl_2$. Lα-PC = L-α-phosphatidylcholine; POPE:POPG = 1-palmitoyl-2-oleoyl-phosphatidylethanolamine: 1-Palmitoyl-2-oleoyl-sn-glycerol-3-phosphoglycerol (3:1, mol/mol).

3.2. Morphological Study of the Liposomes

TEM images of both liposomes are shown in Figure 5. The liposomes obtained resulted in a spherical shape and no aggregates were observed.

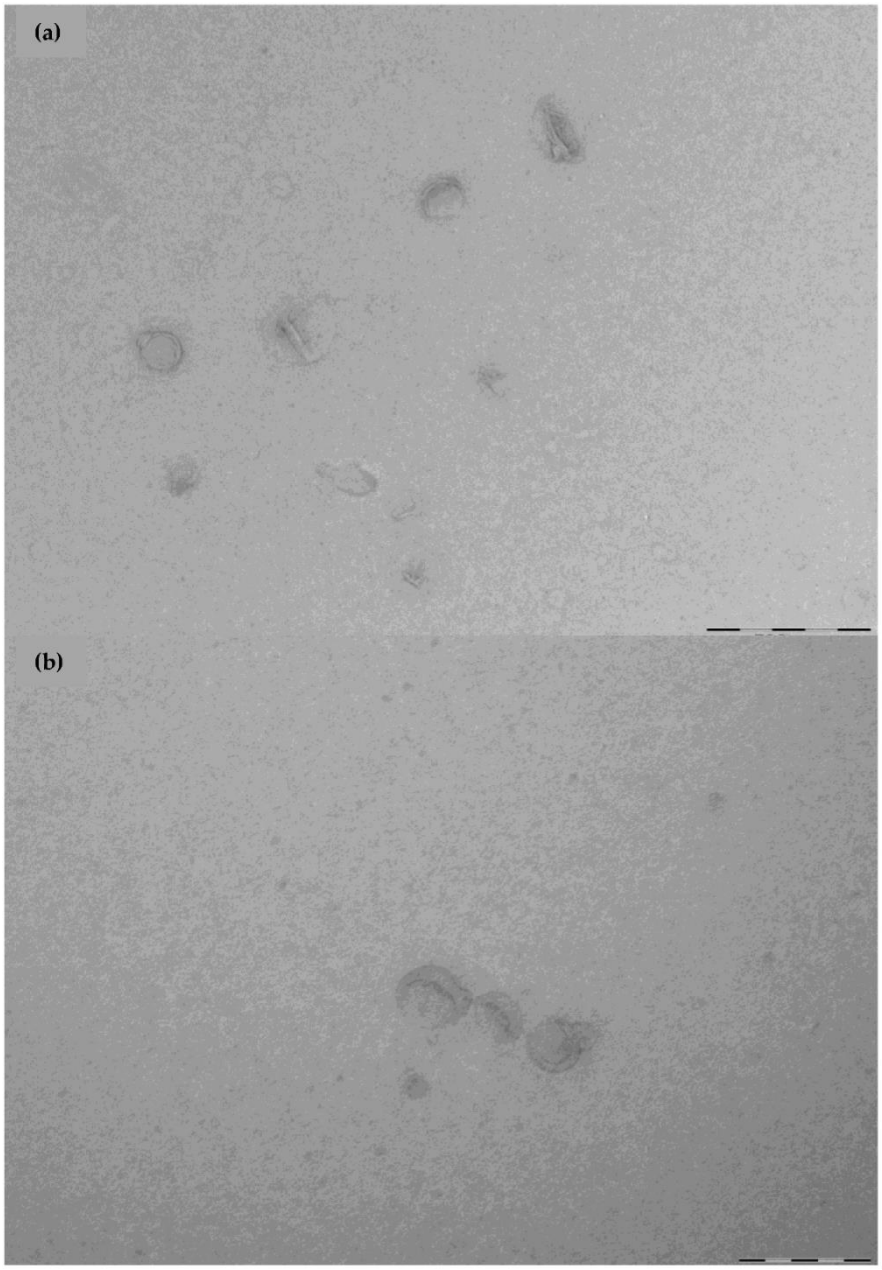

Figure 5. TEM images of the liposomes. (**a**) Liposome Lα-PC (L-α-phosphatidylcholine), and (**b**) POPE:POPG (1-palmitoyl-2-oleoyl-phosphatidylethanolamine: 1-Palmitoyl-2-oleoyl-sn-glycerol-3-phosphoglycerol (3:1, mol/mol). The scale bar stands for 200 nm.

3.3. In Vitro Drug Release Study

The release profile of both liposomes fits a nonlinear regression. They follow a hyperbola system where the liposome Lα-PC can release the drug faster than liposome POPE:POPG, and in addition, the liposome Lα-PC can release all of the drug, whereas liposome POPE:POPG can release just 64%. The rest remains trapped. Figure 6 shows the release profiles of baricitinib. Both liposomes' data are fitted to the one-site binding model (Y = Bmax∗X/KD + X). Table 6 shows the fitted values for the model's parameters Bmax and KD. The statistical analysis by a *T*-test comparing Lα-PC and POPE:POPG showed significant differences for Bmax.

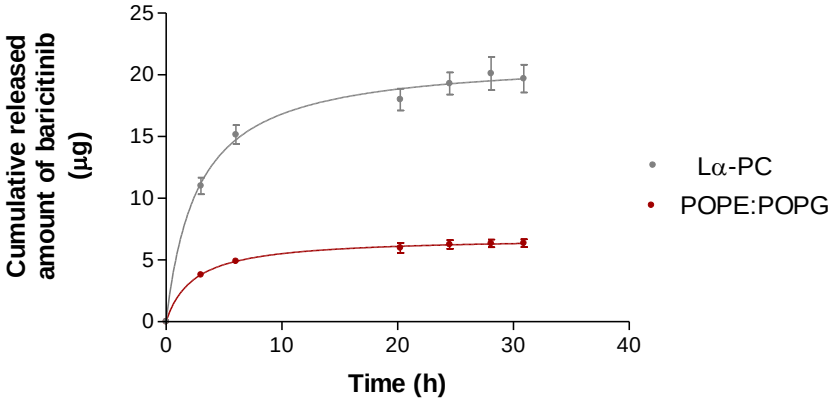

Figure 6. Release profiles of baricitinib from the liposomes POPE:POPG (1-palmitoyl-2-oleoyl-phosphatidylethanolamine: 1-Palmitoyl-2-oleoyl-sn-glycerol-3-phosphoglycerol (3:1, mol/mol), and Lα-PC (L-α-phosphatidylcholine): baricitinib cumulative released (µg) vs. time (h). Results are expressed by mean ± SD (n = 5).

Table 6. Best fit values in the kinetic modeling for the liposomal formulations and the statistical analysis by a *T*-Test between Lα-PC and POPE:POPG. Significance level set at $p < 0.05$.

Parameters	**Lα-PC**	**POPE:POPG**
Bmax (µg)	21.42	6.836
KD (h)	2.735	2.398
SE Bmax	0.424	0.052
SE KD	0.290	0.105
95% CI Bmax	20.33 to 22.51	6.701 to 6.971
95% CI KD	1.989 to 3.480	2.128 to 2.668
R^2	0.9992	0.9999
p-value Bmax	<0.0001	
p-value KD	0.3047	

Lα-PC = L-α-phosphatidylcholine; POPE:POPG = 1-palmitoyl-2-oleoyl-phosphatidylethanolamine: 1-Palmitoyl-2-oleoyl-sn-glycerol-3-phosphoglycerol (3:1, mol/mol). Bmax = maximum amount released (µg) ; KD = time required to reach 50% of the drug release (h); SE = standard error; CI = confidence interval.

3.4. Ex Vivo Permeation Study

Both liposomes on the cornea have r^2 values of 0.99, whereas for the sclera, r^2 were greater than 0.97. The permeation parameters were calculated, including permeation profile, flux (Jss, µg/h), permeability coefficient (Kp, cm/h), the cumulative permeated amount at 24 h (Cum baricitinib 6 h, µg), and theoretical plasma concentration in humans at the steady-state (Css, ng/mL), of baricitinib. Figure 7 shows the behavior of both liposomes on the sclera and Figure 8 shows the behavior of both liposomes on the cornea.

The baricitinib retained in the sclera and cornea is shown in Figure 9, both liposomes have significant differences in the sclera, but no statistical differences were found in the amount of baricitinib retained in the cornea. POPE:POPG retained baricitinib in the scleral tissue two-fold compared to Lα-PC, whereas baricitinib was retained equally by both liposomes in corneal tissue.

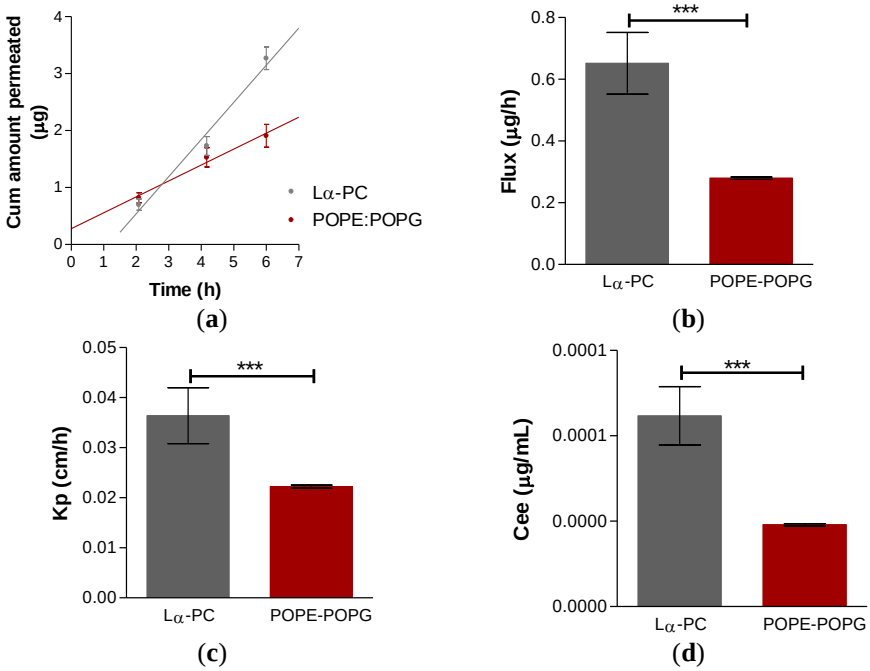

Figure 7. Ex vivo transscleral permeation. (**a**) Baricitinib permeation profile: baricitinib cumulative amount permeated (µg) vs. time (h); (**b**) baricitinib flux for each liposome; (**c**) baricitinib amount retained in the scleral tissue; (**d**) theoretical plasma concentration at the steady-state in humans. Results are expressed by mean ± SD (n=5). L*α*-PC = L-*α*-phosphatidylcholine; POPE:POPG = 1-palmitoyl-2-oleoyl-phosphatidylethanolamine:1-Palmitoyl-2-oleoyl-sn-glycerol-3-phosphoglycerol (3:1, mol/mol). *t*-test analysis with statistically significant difference: *** = $p < 0.0001$.

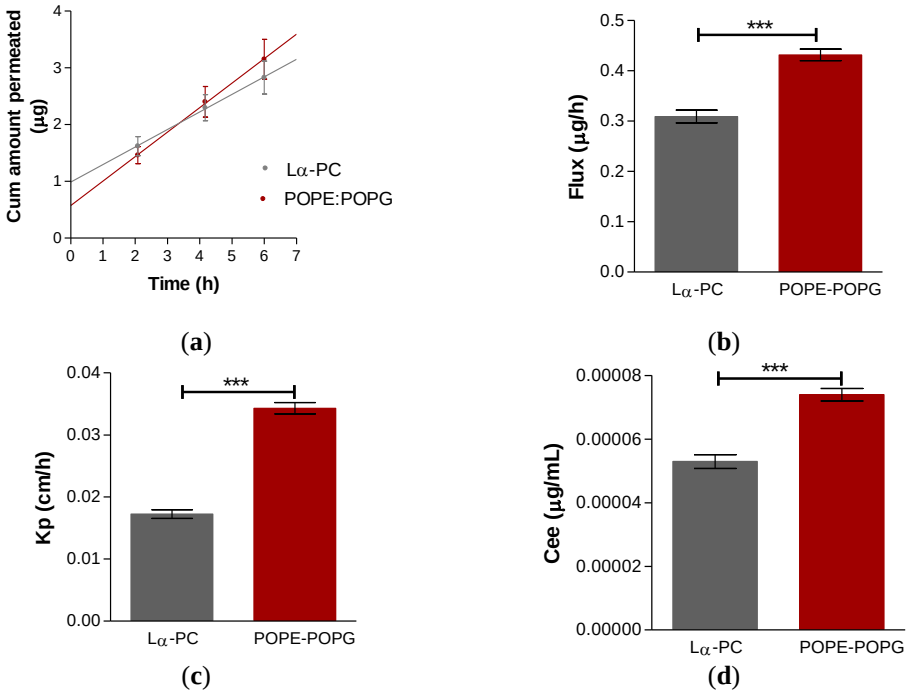

Figure 8. Ex vivo transcorneal permeation. (**a**) Baricitinib permeation profile: baricitinib cumulative amount permeated (µg) vs. time (h); (**b**) baricitinib flux for each liposome; (**c**) baricitinib retained amount in the cornea; (**d**) theoretical plasma concentration at the steady-state in humans. Results are expressed by mean ± SD (n=5). L*α*-PC = L-*α*-phosphatidylcholine; POPE:POPG = 1-palmitoyl-2-oleoyl-phosphatidylethanolamine: 1-Palmitoyl-2-oleoyl-sn-glycerol-3-phosphoglycerol (3:1, mol/mol). *t*-Test analysis, statistically significant difference: *** = $p < 0.0001$.

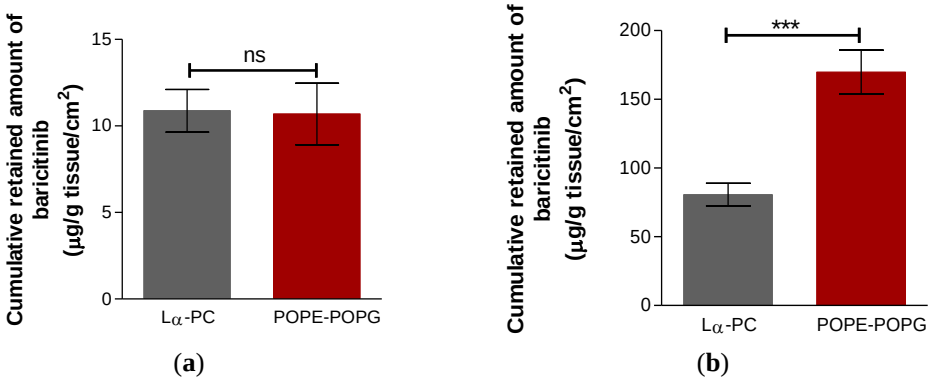

Figure 9. Baricitinib amount retained in the tissues: (**a**) cornea (**b**) sclera. Results are expressed as mean ± SD (n = 5). Lα-PC = L-α-phosphatidylcholine; POPE:POPG = 1-palmitoyl-2-oleoyl-phosphatidylethanolamine: 1-Palmitoyl-2-oleoyl-sn-glycerol-3-phosphoglycerol (3:1, mol/mol). *T*-Test analysis with a statistically significant difference: *** = $p < 0.0001$; ns = non-significant.

3.5. In Vitro Tolerance Study

3.5.1. HET-CAM

The potential irritant effect of the formulations on the eyes was evaluated by the HET-CAM method, which consisted of applying the liposomes on the chorioallantoic membrane of 10-day embryonated eggs. No hemorrhaging, coagulation, or vessel lysis were observed 5 min after the application of the formulations (Figure 10). In contrast, hemorrhaging was observed in the positive control from the very beginning of applying the control, and after 5 min both hemorrhaging and coagulation were observed.

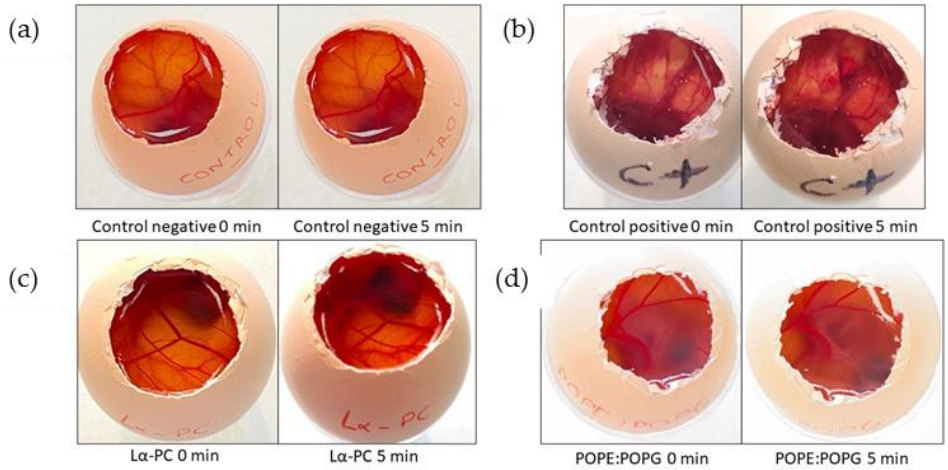

Figure 10. Evaluation of the irritant effect of the formulations by HET-CAM. (**a**) negative control (saline solution), (**b**) positive control (sodium hydroxide solution 0.1N, (**c**) Lα-PC liposome (L-α-phosphatidylcholine), and (**d**) POPE:POPG liposome (1-palmitoyl-2-oleoyl-phosphatidylethanolamine: 1-Palmitoyl-2-oleoyl-sn-glycerol-3-phosphoglycerol (3:1, mol/mol).

The values of the IS obtained after the HET-CAM test are reported in Table 7. IS values obtained for both liposomes were below 0.9, indicating that the liposomes did not show any irritating potential.

Table 7. Irritation score (IS) of the liposomes tested by the HET-CAM technique.

Formulation	Irritation Score (IS)	Classification
Lα-PC	0.03	Non-irritating
POPE:POPC	0.02	Non-irritating

IS ≤ 0.9, non-irritating/slightly irritating; 0.9 < IS ≤ 4.9, moderately irritating; 4.9 < IS ≤ 8.9, irritating; and 8.9 < IS ≤ 21, severely irritating [26]. Lα-PC = L-α-phosphatidylcholine; POPE:POPG = 1-palmitoyl-2-oleoyl-phosphatidylethanolamine:1-Palmitoyl-2-oleoyl-sn-glycerol-3-phosphoglycerol (3:1, mol/mol).

3.5.2. Cornea Transparency

The transparency of the cornea was observed to assess any potential irritant effect of the liposomes on the cornea. Corneas treated with ethanol (positive control) show a decrease in the transmittance of up to 20% within the wavelengths 300–650 nm compared with the negative control, indicating a reduction of the transparency of the cornea. In contrast, the transmittance profile of both liposomes overlaps the negative control indicating that they do not affect the cornea transparency (Figure 11).

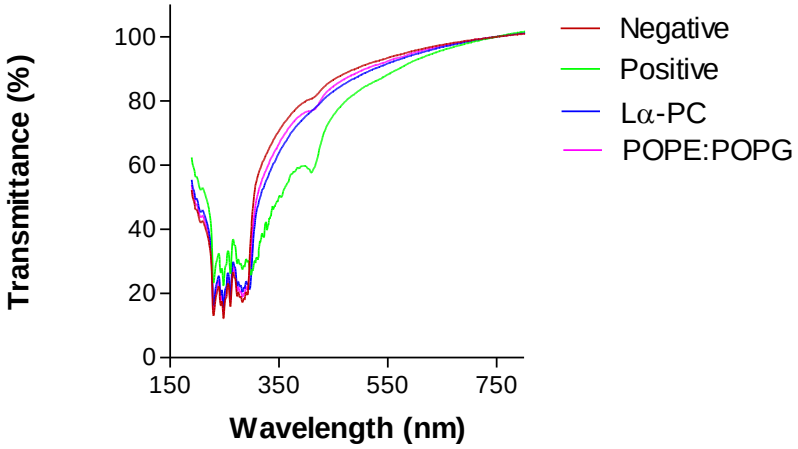

Figure 11. Transmittance from 190 to 850 nm wavelength of the corneas treated with PBS (negative control), ethanol (positive control), Lα-PC (L-α-phosphatidylcholine), and POPE:POPG liposomes (Lα-PC = L-α-phosphatidylcholine; POPE:POPG = 1-palmitoyl-2-oleoyl-phosphatidylethanolamine: 1-Palmitoyl-2-oleoyl-sn-glycerol-3-phosphoglycerol (3:1, mol/mol) after 10 min of incubation.

3.6. Corneal and Scleral Histological Study

Sclera and cornea did not show architectural alterations in the hematoxylin and eosin staining histological analysis in the control condition (Figure 12). The treatment with the two diluted liposomes did not alter either the cornea or the sclera.

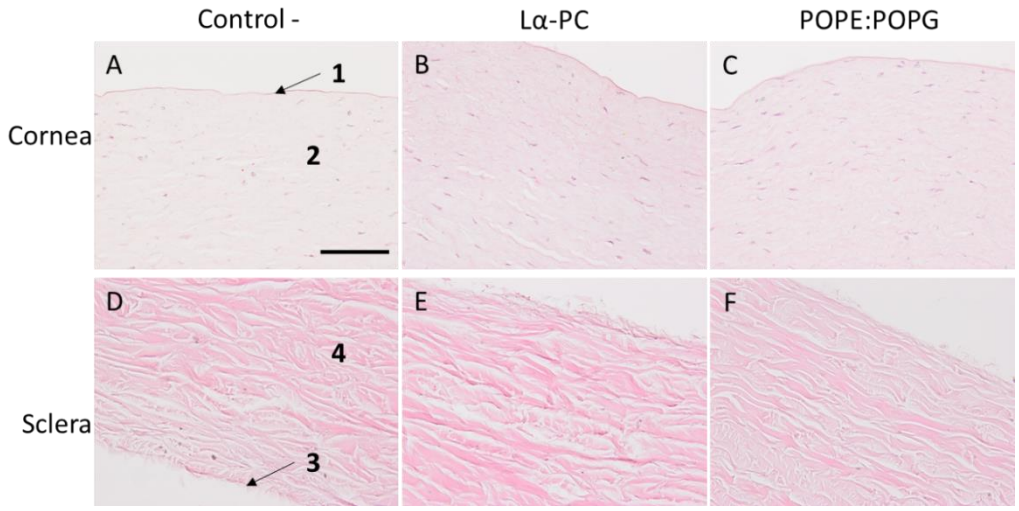

Figure 12. Sclera and cornea sections stained with hematoxylin and eosin. The upper row shows the cornea (**A**–**C**) and the sclera is shown below (**D**–**F**) in different conditions: control conditions (**A**,**D**); Lα-PC (**B**,**E**) and POPE:POPG (**C**,**F**); (1) corneal epithelium (non-keratinized stratified squamous epithelium); (2) substantia propria; (3) episclera; and (4) stroma. Magnification = 200x, scale bar = 100μm.

4. Discussion

Two liposomes loading baricitinib were developed using two different lipids (Lα-P and POPE:POPG) with the aim of combining the effect of an immunomodulator and the effect of the lipids to supplement the tear film lipid layer. It is known that alterations in lipid composition, besides down-regulation in specific proteins or changes in the rheological behavior of the tears, are common in dry eye disease. Lipid-based formulations aim to mimic the tear film lipid layer by combining both components, the aqueous one and the lipid one [36]. As Hofauer and co-workers in a previous work had applied liposomal agents on buccal, nasal, and ocular mucosa in patients with Sjögrens' syndrome to alleviate symptoms such as xerostomia, keratoconjunctivis sicca, and rhinitis sicca [21], and they had achieved positive results, it could be fruitful to load up liposomes with a specific immunomodulator, as it may result in synergistic effects, achieving an advance in the treatment.

Baricitinib has been used orally and no literature is available reporting nanostructured systems loading baricitinib for the topical route. It has been tested (only) once on the skin and there is very little information on formulating baricitinib in nano-systems. Bhaskarmurthy et al. [37] investigated the potential of baricitinib in reducing the inflammation in ear oedema TPA-induced inflammation in mice; we can underscore that they used a solution of baricitinib in acetone:DMSO, and they were testing on the skin, not on the mucosa or eye. Our study, therefore, encourages further research, building on the potential of baricitinib and its use in ocular mucosa. Both liposomes exhibit suitable characteristics for the ophthalmic application: their smallness in size will not damage the cornea upon application, and their pH is close to the tears' value (7.4–7.5), so no irritation is expected; additionally, the osmolality was also within the criterium. The liposomes should resist aggregation due to Waals attraction forces because the zeta potential value is highly negative [38,39]. The surface electrical study focuses on two aspects. First, the dependence of the lipid composition, and secondly, the influence of the pH and ionic strength on ZP.

One of the major constraints of liposomal systems is the vesicle aggregation, with the concomitant destabilization of the system [40]. Moreover, the surface electrical charge of liposomes does play a fundamental role in the affinity on the corneal surface [41]. Along

the same lines, the study of the surface electrical properties provides the expected relevant information; the lipid composition of liposomes has a direct influence on ZP, due to the different net charges of the lipids used: POPE:POPG liposomes showed much more negativity than Lα-PC liposomes. Another question is that the surface charge might also determine the interaction of liposomes with the ocular membrane due to the high negative charge of its mucins.

Absolute values of ZP showed a marked increase when the pH was increased (Figure 3). Changes in pH can affect the degree of lipid ionization. Specifically, the phosphate groups of the polar head of PC and PG are neutralized at acidic pH by the hydrogen ions of the dispersion medium. In contrast, as the pH value increased, that is, as the concentration of hydroxyl groups in the medium increased, a greater number of surface phosphate groups were dissociated. This determined the increase in the surface electric charge of these particles [42]. Nanosystems with ZP between +30 mV and −30 mV are considered to possess low stability [43]. The pH of tears is approximately 7.45 and ranges from 7.14 to 7.82, depending on diurnal and seasonal influences, or even 7.89 in dry eye patients with Sjögren's disease [44]. Under these conditions, our liposomal formulations would have values outside the range +30 mV/−30 mV, which, predictably, will provide suitable stability [45].

The most frequently used aqueous vehicles in the preparation of eye drops are water for injection, isotonic sterile saline (SF), balanced salt solution (BSS®), and balanced salt solutions whose composition is similar to that of the internal ocular medium. Both the composition of these vehicles and physiologically buffer conditions mean that there are electrolytes of different valences that could influence the surface electrical characteristics of the liposomes. The electrolytes are mainly Na^+, K^+, Cl^-, and HCO^-, with lower levels of Mg^{2+} and Ca^{2+}. In this way, the results of the electrokinetic analysis of the liposomes as a function of the ionic strength of the medium could be used to predict their stability in dispersion (aggregation tendency) and their mucoadhesive capacity.

The eye can tolerate tonicities within the equivalent range of 0.6–2% NaCl. However, to achieve isotonic solutions with tears, and to ensure that they are comfortable for the eye, an amount equivalent to 0.9% NaCl 0.15 M is generally used.

According to our results, shown in Figure 4, as the concentration of the salts increases the counterions accumulate closer to the particle surface, which compresses the double layer and weakens repulsive forces by reducing ZP [46].

Regarding the effect of $AlCl_3$, ZP values were positive across the whole range, probably due to the adsorption of this ion into the surface of the liposomes. Finally, a high concentration of electrolytes equivalent to an isotonic solution might produce charge reversal or a large drop, showing slightly positive values. This fact will cause large size aggregates and rapid settling, which could give rise to a flocculated system that is easy to redisperse [47]. Additionally, thanks to their positive charge, they could interact better with the ocular film and prolong the residence time of the drug in the cornea, and they have increased the therapeutic interval [41,48].

A rapid release of baricitinib is observed within the first 4–6 h and it is followed by a slower drug release for both liposomes after these first six hours. Higher released amounts of baricitinib were obtained from the liposomes Lα-PC, about three-fold higher than the POPE:POPG liposomes, and this suggests that the lipid used in preparing the liposomes has a great impact on the extent of drug released. The release profile of both liposomes fitted to a one-site binding model corresponding to a hyperbola curve. The parameters of this model are Bmax, which corresponds to the maximum amount that can be released, and KD, which is the time needed to reach 50% of the drug released. Statistically significant differences were observed for Bmax. However, no statistical differences were found for KD, meaning that both liposomes release 50% of the drug within a similar time period (more or less in the first two and a half hours). Ansari et al. [49] developed polymeric nanoparticles loading baricitinib with the aim of improving baricitinib's bioavailability in order to reduce the dose, and in turn, reducing the side effects. The

authors prepared nanoparticles with poly-lactic-co-glycolic acid, and they conducted a deep characterization, obtaining an optimized formulation that exhibited sustained release over 24 h, which fitted the Higuchi model.

Despite the fact that liposome Lα- PC showed a higher in vitro drug release, this was not limiting for POPE:POPG in the penetration and permeation through the cornea, where the amount retained in the tissue was similar for both liposomes. It was POPE:POPG that showed higher permeation. In contrast, Lα- PC was superior to POPE:POPG in the permeation and penetration of baricitinib into and through the sclera. This is probably due to the difference in the composition of sclera and cornea, whereas the latter is mainly composed of type I collagen and proteoglycans, the sclera is primarily composed of connective tissue [50]. The amount of baricitinib retained in the corneal and scleral tissue would act as a reservoir and might enable a local anti-inflammatory and immunomodulatory effect without systemic side effects since the predicted plasma concentration at the steady-state (Css) is far below the concentration achieved in an oral administration [51].

5. Conclusions

The HET-CAM technique is an ideal model for testing ocular irritation since the chorioallantoic membrane is a highly vascularized structure and it is sensitive to chemicals such as the conjunctiva [52]. Both liposomes are supposed to be well-tolerated since no irritant potential was detected by the HET-CAM technique nor was any change observed in the histological analysis after the application of the liposomes on the corneal and scleral tissues. Additionally, no changes in the transparency of the cornea were observed either, meaning that the liposomes do not cause damage to the tissue exposed to them [34]. In light of these promising results, further studies should be carried out and looked at so as to better assess the efficacy of the liposomes in vivo. For instance, a dry eye in mice models would allow for the evaluation of the efficacy of the liposomes similarly to the work of Stevenson et al. [19,20], in which the researchers tested tofacitinib, a JAK inhibitor, applied topically in dry eye-induced mice, and they monitored cytokines expression obtaining excellent outcomes in reducing the ocular inflammation. Since the products intended for ophthalmic use should be sterilized, in this sense, future studies should also consider extruding the liposomes through a 0.22 μm pore size, as well as, investigating the effect of the number of lipid layers composing the liposome on the drug release. Another important point for future studies is the shelf-life of the formulations, and stability studies should also be performed.

Two liposomal formulations have been developed for ocular delivery intended for alleviating dry eyes related to Sjögren's syndrome. The liposomes were prepared using two different lipids, Lα-PC and POPE:POPG, both loading baricitinib, a Janus kinase inhibitor. Lα-PC led to higher flux, permeation, and retention in the sclera, whereas POPE:POPG led to higher flux and permeation in the cornea. The formulations showed no irritant effects on the chorioallantoic membrane. Additionally, the liposomes did not affect the cornea transparency when applied and the histological analysis did not reveal any structural alteration. The two liposomes have shown promising results for ocular application, and further studies, such as in vivo tests, should be conducted to evaluate their efficacy, and hence, confirm their suitability in the management of dry eyes in Sjögren's syndrome.

Author Contributions: Conceptualization, Ò.D. and M.M.; methodology, Ò.D., M.M., and H.C.; validation, M.M. and H.C.; formal analysis, N.G.; investigation, N.G., R.M., and N.B.; resources, Ò.D., B.C., M.J.R.-L., M.M., and H.C.; data curation, M.M.; writing—original draft preparation, N.G.; writing—review and editing, M.M.; visualization, M.M.; supervision, M.M. and H.C.; project administration, M.M. and H.C.; funding acquisition, M.M. and H.C. All authors have read and agreed to the published version of the manuscript.

Funding: This research received no external funding.

Institutional Review Board Statement: The study was conducted in accordance with the Declaration of Helsinki, and approved by the Ethics Committee of the University of Barcelona (protocol code 10619 approved on 10 January 2019).

Informed Consent Statement: Not applicable.

Data Availability Statement: The data presented in this study are available on request from the corresponding author.

Acknowledgments: The authors would like to thank Ángel Moreno for his technical support in the surface electrical study, Ana Calpena for supporting this work, and Harry Paul for revising the English language.

Conflicts of Interest: The authors declare no conflicts of interest.

References

1. Williams, M.A.; Fujinami, R.S. Immunopathology☆. *Ref. Modul. Biomed. Sci.* **2014**, *2008*, 78–83. https://doi.org/10.1016/B978-0-12-801238-3.02605-2.
2. Rose, N.R. Autoimmune Diseases. In *International Encyclopedia of Public Health*; Elsevier: Amsterdam, The Netherlands, 2008; pp. 267–271.
3. Ahmed, S.S.; Lambert, P.H. Autoimmune Diseases: The Role for Vaccines. In *The Autoimmune Diseases*, 5th ed.; Academic Press: Cambridge, MA, USA, 2014; pp. 275–282. https://doi.org/10.1016/B978-0-12-384929-8.00020-4.
4. Shahane, A.; Patel, R. The Epidemiology of Sjögren's Syndrome. *Clin. Epidemiol.* **2014**, *6*, 247. https://doi.org/10.2147/CLEP.S47399.
5. Aránzazu Ceballos, A.D.; Escobar Restrepo, J.; Ramírez Pulgarín, S. Síndrome de Sjögren, Más Que Un Ojo Seco. In *Archivos De Medicina (Manizales)*; Universidad de Manizales: Caldas, Colombia, 2015; Volume 15, pp. 343–351.
6. Anaya, J.-M.; Camilo Sarmiento-Monroy, J.; García-Carrasco, M. *Síndrome De Sjögren*, 2nd ed.; Anaya, J.-M., Camilo, S.-M.J.C., García-Carrasco, M., Eds.; Editorial Universidad del Rosario: Bogotá, Colombia, 2017.
7. Vitali, C.; Bombardieri, S.; Jonsson, R.; Moutsopoulos, H.; Alexander, E.; Carsons, S.; Daniels, T.; Fox, P.C.; Kassan, S.; Pillemer, S.; et al. Classification Criteria for Sjogren's Syndrome: A Revised Version of the European Criteria Proposed by the American-European Consensus Group. *Ann. Rheum. Dis.* **2002**, *61*, 554–558. https://doi.org/10.1136/ard.61.6.554.
8. Agarwal, R.; Iezhitsa, I.; Agarwal, P.; Alimah Abdul Nasir, N.; Razali, N.; Alyautdin, R.; Mohd Ismail, N. Liposomes in Topical Ophthalmic Drug Delivery: An Update. *Drug Deliv.* **2016**, *23*, 1075–1091. https://doi.org/10.3109/10717544.2014.943336.
9. Bieber, T.; Reich, K.; Paul, C.; Tsunemi, Y.; Augustin, M.; Lacour, J.-P.; Ghislain, P.-D.; Dutronc, Y.; Liao, R.; Yang, F.E.; et al. Efficacy and Safety of Baricitinib in Combination with Topical Corticosteroids in Patients with Moderate-to-Severe Atopic Dermatitis With Inadequate Response, Intolerance, or Contraindication to Cyclosporine: Results from a Randomized, Placebo-Controlled, Phase III Clinical Trial (BREEZE-AD4) Running Head: Baricitinib and Topical Corticosteroids for Atopic Dermatitis. *Br. J. Dermatol.* **2022**, *187*, 338–352. https://doi.org/10.1111/bjd.21630.
10. Markham, A. Baricitinib: First Global Approval. *Drugs* **2017**, *77*, 697–704. https://doi.org/10.1007/s40265-017-0723-3.
11. Committee for Medicinal Products for Human Use (CHMP). *Olumiant-Assesment Report*; European Medicine Agency: London, UK, 2020.
12. Bai, W.; Yang, F.; Xu, H.; Hospital, C.; Wei, W.; Zhang, L.; Zhao, Y.; Shi, X.; Zhang, Y. *A Multi-Center, Prospective, Open-Label, Randomized Study to Explore Ecacy and Safety of Baricitinib in Active Primary Sjogren's Syndrome Patients*; Research Square: Durham, North Carolina, USA, 2022. https://doi.org/10.21203/rs.3.rs-1406859/v1.
13. Saraux, A.; Pers, J.O.; Devauchelle-Pensec, V. Treatment of Primary Sjögren Syndrome. *Nat. Rev. Rheumatol.* **2016**, *12*, 456–471. https://doi.org/10.1038/NRRHEUM.2016.100.
14. Rai, M.; Ingle, A.P.; Bansod, S.; Kon, K. Tackling the Problem of Tuberculosis by Nanotechnology: Disease Diagnosis and Drug Delivery. In *Nanotechnology in Diagnosis, Treatment and Prophylaxis of Infectious Diseases*; Academic Press: Cambridge, MA, USA, 2015; pp. 133–149. https://doi.org/10.1016/B978-0-12-801317-5.00009-8Deb, P.K.; Al-Attraqchi, O.; Chandrasekaran, B.; Paradkar, A.; Tekade, R.K. Protein/Peptide Drug Delivery Systems: Practical Considerations in Pharmaceutical Product Development. In *Basic Fundamentals of Drug Delivery*; Academic Press: Cambridge, MA, USA, 2019; pp. 651–684. https://doi.org/10.1016/B978-0-12-817909-3.00016-9.
15. Nagalingam, A. Drug Delivery Aspects of Herbal Medicines. In *Japanese Kampo Medicines for the Treatment of Common Diseases: Focus on Inflammation*; Academic Press: Cambridge, MA, USA, 2017; pp. 143–164. https://doi.org/10.1016/B978-0-12-809398-6.00015-9.
16. Akbarzadeh, A.; Rezaei-Sadabady, R.; Davaran, S.; Woo Joo, S.; Zarghami, N.; Hanifehpour, Y.; Samiei, M.; Kouhi, M.; Nejati-Koshki, K. Liposome: Classification, Preparation, and Applications. *Nanoscale Res. Lett.* **2013**, *8*, 102. https://doi.org/10.1186/1556-276X-8-102.
17. Amarji, B.; Abed, S.N.; Bairagi, U.; Deb, P.K.; Al-Attraqchi, O.; Choudhury, A.A.; Tekade, R.K. Four Stages of Pharmaceutical Product Development: Preformulation, Prototype Development and Scale-Up, Biological Aspects, and Commercialization. In

Dosage Form Design Considerations; Academic Press: Cambridge, MA, USA, 2018; Volume I, pp. 637–668. https://doi.org/10.1016/B978-0-12-814423-7.00018-6.
18. Yamaguchi, M.; Yasueda, S.; Isowaki, A.; Yamamoto, M.; Kimura, M.; Inada, K.; Ohtori, A. Formulation of an Ophthalmic Lipid Emulsion Containing an Anti-Inflammatory Steroidal Drug, Difluprednate. *Int. J. Pharm.* **2005**, *301*, 121–128. https://doi.org/10.1016/j.ijpharm.2005.05.036.
19. Stevenson, W.; Sadrai, Z.; Hua, J.; Kodati, S.; Huang, J.-F.; Chauhan, S.K.; Dana, R. Effects of Topical Janus Kinase Inhibition on Ocular Surface Inflammation and Immunity. *Cornea* **2014**, *33*, 177–183. https://doi.org/10.1097/ICO.0000000000000019.
20. Hofauer, B.; Bas, M.; Manour, N.; Knopf, A. Effekt Liposomaler Lokaltherapie Auf Die Sicca-Symptomatik Des Primären Sjögren-Syndroms. *HNO* **2013**, *61*, 921–927. https://doi.org/10.1007/s00106-013-2736-x.
21. Picas, L.; Suárez-Germà, C.; Teresa Montero, M.; Hernández-Borrell, J. Force Spectroscopy Study of Langmuir−Blodgett Asymmetric Bilayers of Phosphatidylethanolamine and Phosphatidylglycerol. *J. Phys. Chem. B* **2010**, *114*, 3543–3549. https://doi.org/10.1021/jp910882e.
22. Botet-Carreras, A.; Montero, M.T.; Sot, J.; Domènech, Ò.; Borrell, J.H. Engineering and Development of Model Lipid Membranes Mimicking the HeLa Cell Membrane. *Colloids Surf. A Physicochem. Eng. Asp.* **2021**, *630*, 127663. https://doi.org/10.1016/j.colsurfa.2021.127663.
23. Ahmed, O.A.A.; Kurakula, M.; Banjar, Z.M.; Afouna, M.I.; Zidan, A.S. Quality by Design Coupled with Near Infrared in Formulation of Transdermal Glimepiride Liposomal Films. *J. Pharm. Sci.* **2015**, *104*, 2062–2075. https://doi.org/10.1002/jps.24448.
24. El Moussaoui, S.; Abo-Horan, I.; Halbaut, L.; Alonso, C.; Coderch, L.; Garduño-Ramírez, M.L.; Clares, B.; Soriano, J.L.; Calpena, A.C.; Fernández-Campos, F.; et al. Polymeric Nanoparticles and Chitosan Gel Loading Ketorolac Tromethamine to Alleviate Pain Associated with Condyloma Acuminata during the Pre- and Post-Ablation. *Pharmaceutics* **2021**, *13*, 1784. https://doi.org/10.3390/pharmaceutics13111784.
25. Mallandrich, M.; Calpena, A.C.; Clares, B.; Parra, A.; García, M.L.; Soriano, J.L.; Fernández-Campos, F. Nano-Engineering of Ketorolac Tromethamine Platforms for Ocular Treatment of Inflammatory Disorders. *Nanomedicine* **2021**, *16*, 401–414. https://doi.org/10.2217/nnm-2020-0403.
26. Andrade-Carrera, B.; Clares, B.; Noé, V.; Mallandrich, M.; Calpena, A.; García, M.; Garduño-Ramírez, M. Cytotoxic Evaluation of (2S)-5,7-Dihydroxy-6-Prenylflavanone Derivatives Loaded PLGA Nanoparticles against MiaPaCa-2 Cells. *Molecules* **2017**, *22*, 1553. https://doi.org/10.3390/molecules22091553.
27. El Moussaoui, S.; Fernández-Campos, F.; Alonso, C.; Limón, D.; Halbaut, L.; Garduño-Ramirez, M.L.; Calpena, A.C.; Mallandrich, M. Topical Mucoadhesive Alginate-Based Hydrogel Loading Ketorolac for Pain Management after Pharmacotherapy, Ablation, or Surgical Removal in Condyloma Acuminata. *Gels* **2021**, *7*, 8. https://doi.org/10.3390/gels7010008.
28. Mallandrich, M.; Fernández-Campos, F.; Clares, B.; Halbaut, L.; Alonso, C.; Coderch, L.; Garduño-Ramírez, M.L.; Andrade, B.; del Pozo, A.; Lane, M.E.; et al. Developing Transdermal Applications of Ketorolac Tromethamine Entrapped in Stimuli Sensitive Block Copolymer Hydrogels. *Pharm. Res.* **2017**, *34*, 1728–1740. https://doi.org/10.1007/s11095-017-2181-8.
29. Kurakula, M.; Srinivas, C.; Kasturi, N.; Diwan, P. v Formulation and Evaluation of Prednisolone Proliposomal Gel for Effective Topical Pharmacotherapy. *Int. J. Pharm. Sci. Drug Res.* **2012**, *4*, 35–43.
30. Spielmann, H. HET-CAM Test. *Methods Mol. Biol* **1995**, *43*, 199–204. https://doi.org/10.1385/0-89603-282-5:199.
31. Interagency Coordinating Committee on the Validation of Alternative Methods (ICCVAM). *Test Method Protocol: Hen's Egg Test-Chorioallantoic Membrane (HET-CAM) Test Method*; Interagency Coordinating Committee on the Validation of Alternative Methods (ICCVAM), Research Triangle Park, NC, USA : 2010.
32. Meek, K.M.; Knupp, C. Corneal Structure and Transparency. *Prog. Retin. Eye Res.* **2015**, *49*, 1–16.
33. García-Otero, X.; Díaz-Tomé, V.; Varela-Fernández, R.; Martín-Pastor, M.; González-Barcia, M.; Blanco-Méndez, J.; Mondelo-García, C.; Bermudez, M.A.; Gonzalez, F.; Aguiar, P.; et al. Development and Characterization of a Tacrolimus/Hydroxypropyl-β-Cyclodextrin Eye Drop. *Pharmaceutics* **2021**, *13*, 149. https://doi.org/10.3390/pharmaceutics13020149.
34. Gómez-Segura, L.; Parra, A.; Calpena, A.C.; Gimeno, Á.; Boix-Montañes, A. Carprofen Permeation Test through Porcine Ex Vivo Mucous Membranes and Ophthalmic Tissues for Tolerability Assessments: Validation and Histological Study. *Vet. Sci.* **2020**, *7*, 152. https://doi.org/10.3390/vetsci7040152.
35. Garrigue, J.S.; Amrane, M.; Faure, M.O.; Holopainen, J.M.; Tong, L. Relevance of Lipid-Based Products in the Management of Dry Eye Disease. *J. Ocul. Pharmacol. Ther.* **2017**, *33*, 647–661. https://doi.org/10.1089/JOP.2017.0052.
36. Hiraganahalli Bhaskarmurthy, D.; Evan Prince, S. Effect of Baricitinib on TPA-Induced Psoriasis like Skin Inflammation. *Life Sci.* **2021**, *279*, 119655. https://doi.org/10.1016/j.lfs.2021.119655.
37. Watters, R.J.; Kester, M.; Tran, M.A.; Loughran, T.P.; Liu, X. Development and Use of Ceramide Nanoliposomes in Cancer. *Methods Enzymol.* **2012**, *508*, 89–108.
38. Samimi, S.; Maghsoudnia, N.; Eftekhari, R.B.; Dorkoosh, F. Lipid-Based Nanoparticles for Drug Delivery Systems. In *Characterization and Biology of Nanomaterials for Drug Delivery*; Elsevier: Amsterdam, The Netherlands, 2019; pp. 47–76.
39. Clares, B.; Gallardo, V.; Medina, M.; Ruiz, M. Multilamellar Liposomes of Triamcinolone Acetonide: Preparation, Stability, and Characterization. *J. Liposome Res.* **2009**, *19*, 197–206. https://doi.org/10.1080/08982100902736571.
40. Mishra, G.P.; Bagui, M.; Tamboli, V.; Mitra, A.K. Recent Applications of Liposomes in Ophthalmic Drug Delivery. *J. Drug Deliv.* **2011**, *2011*, 1–14. https://doi.org/10.1155/2011/863734.

41. Clares, B.; Biedma-Ortiz, R.A.; Sáez-Fernández, E.; Prados, J.C.; Melguizo, C.; Cabeza, L.; Ortiz, R.; Arias, J.L. Nano-Engineering of 5-Fluorouracil-Loaded Magnetoliposomes for Combined Hyperthermia and Chemotherapy against Colon Cancer. *Eur. J. Pharm. Biopharm.* **2013**, *85*, 329–338. https://doi.org/10.1016/j.ejpb.2013.01.028.
42. Raval, N.; Maheshwari, R.; Kalyane, D.; Youngren-Ortiz, S.R.; Chougule, M.B.; Tekade, R.K. Importance of Physicochemical Characterization of Nanoparticles in Pharmaceutical Product Development. In *Basic Fundamentals of Drug Delivery*; Elsevier: Amsterdam, The Netherlands, 2019; pp. 369–400. https://doi.org/10.1016/B978-0-12-817909-3.00010-8.
43. van Haeringen, N.J. Clinical Biochemistry of Tears. *Surv. Ophthalmol.* **1981**, *26*, 84–96. https://doi.org/10.1016/0039-6257(81)90145-4.
44. Clares, B.; Calpena, A.C.; Parra, A.; Abrego, G.; Alvarado, H.; Fangueiro, J.F.; Souto, E.B. Nanoemulsions (NEs), Liposomes (LPs) and Solid Lipid Nanoparticles (SLNs) for Retinyl Palmitate: Effect on Skin Permeation. *Int. J. Pharm.* **2014**, *473*, 591–598. https://doi.org/10.1016/J.IJPHARM.2014.08.001.
45. Hunter, R.J. *Foundations of Colloid Science*, 2nd ed.; Oxford University Press: New York, NY, USA, 2001.
46. Arias, J.L.; López-Viota, M.; Clares, B.; Ruiz, M.A. Stability of Fenbendazole Suspensions for Veterinary Use: Correlation between Zeta Potential and Sedimentation. *Eur. J. Pharm. Sci.* **2008**, *34*, 257–262. https://doi.org/10.1016/J.EJPS.2008.04.008.
47. Astarita, C.; Palchetti, S.; Massaro-Giordano, M.; Domenico, M.d.; Petrillo, F.; Boffo, S.; Caracciolo, G.; Giordano, A.; Júnior, C.; Heard, C.M. Artificial Protein Coronas Enable Controlled Interaction with Corneal Epithelial Cells: New Opportunities for Ocular Drug Delivery. *Pharmaceutics* **2021**, *13*, 867. https://doi.org/10.3390/pharmaceutics13060867.
48. Ansari, M.J.; Alshahrani, S.M. Nano-Encapsulation and Characterization of Baricitinib Using Poly-Lactic-Glycolic Acid Co-Polymer. *Saudi Pharm.* **2019**, *27*, 491–501. https://doi.org/10.1016/j.jsps.2019.01.012.
49. Nishida, T.; Saika, S.; Morishige, N. *Cornea and Sclera: Anatomy and Physiology in Cornea: Fundamentals, Diagnosis and Management*, 5th ed.; Mannis, M.J., Holland, E.J., Eds.; Elsevier: Amsterdam, The Netherlands, 2022.
50. Shi, J.G.; Chen, X.; Lee, F.; Emm, T.; Scherle, P.A.; Lo, Y.; Punwani, N.; Williams, W.v.; Yeleswaram, S. The Pharmacokinetics, Pharmacodynamics, and Safety of Baricitinib, an Oral JAK 1/2 Inhibitor, in Healthy Volunteers. *J. Clin. Pharmacol.* **2014**, *54*, 1354–1361. https://doi.org/10.1002/jcph.354.
51. Silva-Abreu, M.; Calpena, A.C.; Espina, M.; Silva, A.M.; Gimeno, A.; Egea, M.A.; García, M.L. Optimization, Biopharmaceutical Profile and Therapeutic Efficacy of Pioglitazone-Loaded PLGA-PEG Nanospheres as a Novel Strategy for Ocular Inflammatory Disorders. *Pharm. Res.* **2018**, *35*, 11. https://doi.org/10.1007/s11095-017-2319-8.

Baricitinib Lipid-Based Nanosystems as a Topical Alternative for Atopic Dermatitis Treatment

Núria Garrós, Paola Bustos, Òscar Domènech, María José Rodríguez-Lagunas, Negar Bei-rampour, Roya Mohammadi, Mireia Mallandrich, Ana C. Calpena i Helena Colom.

Pharmaceuticals 2023, 16, 894.

https://doi.org/10.3390/ph16060894

Quartil Q2; factor d'impacte 4.6 l'any 2022.

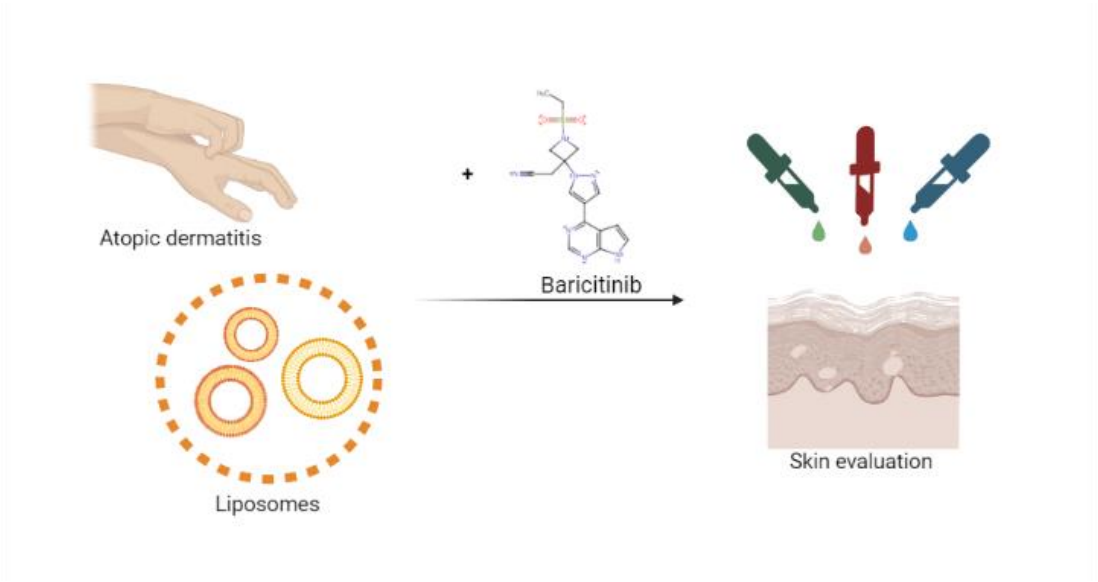

pharmaceuticals

MDPI

Article

Baricitinib Lipid-Based Nanosystems as a Topical Alternative for Atopic Dermatitis Treatment

Núria Garrós[1,2], Paola Bustos-Salgados[1], Òscar Domènech[1,2], María José Rodríguez-Lagunas[3], Negar Beirampour[1], Roya Mohammadi-Meyabadi[1,2], Mireia Mallandrich[1,2,*], Ana C. Calpena[1,2] and Helena Colom[1]

[1] Departament de Farmàcia i Tecnologia Farmacèutica, i Fisicoquímica, Facultat de Farmàcia i Ciències de l'Alimentació, Universitat de Barcelona (UB), 08028 Barcelona, Spain
[2] Institut de Nanociència i Nanotecnologia, Universitat de Barcelona (UB), 645 Diagonal Avenue, 08028 Barcelona, Spain
[3] Departament de Bioquímica i Fisiologia, Facultat de Farmàcia i Ciències de l'Alimentació, Universitat de Barcelona (UB), Av. Joan XXIII,08028 Barcelona, Spain; mjrodriguez@ub.edu
* Correspondence: mireia.mallandrich@ub.edu

Abstract: Atopic dermatitis (AD) is a chronic autoimmune inflammatory skin disorder which causes a significant clinical problem due to its prevalence. The ongoing treatment for AD is aimed at improving the patient's quality of life. Additionally, glucocorticoids or immunosuppressants are being used in systemic therapy. Baricitinib (BNB) is a reversible Janus-associated kinase (JAK)-inhibitor; JAK is an important kinase involved in different immune responses. We aimed at developing and evaluating new topical liposomal formulations loaded with BNB for the treatment of flare ups. Three liposomal formulations were elaborated using POPC (1-palmitoyl-2-oleoyl-glycero-3-phosphocholine), CHOL (Cholesterol) and CER (Ceramide) in different proportions: (i) POPC, (ii) POPC:CHOL (8:2, mol/mol) and (iii) POPC:CHOL:CER (3.6:2.4:4.0 mol/mol/mol). They were physiochemically characterized over time. In addition, an in vitro release study, ex vivo permeation and retention studies in altered human skin (AHS) were also performed. Histological analysis was used to study the tolerance of the formulations on the skin. Lastly, the HET-CAM test was also performed to evaluate the irritancy capacity of the formulations, and the modified Draize test was performed to evaluate the erythema and edema capacity of the formulations on the altered skin. All liposomes showed good physicochemical properties and were stable for at least one month. POPC:CHOL:CER had the highest flux and permeation, and the retention in the skin was equal to that of POPC:CHOL. The formulations exhibited no harmful or irritating effects, and the histological examination revealed no changes in structure. The three liposomes have shown promising results for the aim of the study.

Keywords: liposomes; baricitinib; JAK-inhibitor; transepidermal delivery; skin permeation

Citation: Garrós, N.; Bustos-Salgados, P.; Domènech, Ò.; Rodríguez-Lagunas, M.J.; Beirampour, N.; Mohammadi-Meyabadi, R.; Mallandrich, M.; Calpena, A.C.; Colom, H. Baricitinib Lipid-Based Nanosystems as a Topical Alternative for Atopic Dermatitis Treatment. Pharmaceuticals 2023, 16, 894. https://doi.org/10.3390/ph16060894

Academic Editor(s): Ana Catarina Silva, João Nuno Moreira and José Manuel Sousa Lobo

Received: 3 April 2023
Revised: 15 June 2023
Accepted: 15 June 2023
Published: 18 June 2023

1. Introduction

Lipid-based nanosystems (LBN) are formed through a lipid phase and surfactants [1]. They have demonstrated that they improve the delivery of various active principles to specific skin layers, with stated localization in the upper layers of the skin [2]. There are different kinds of LBN: liposomes, ethosomes, transferosomes, solid lipid nanoparticles, nanostructured lipid carriers, cubosomes, and monoolein aqueous dispersions [3].

The study of liposomes for drug delivery or targeting on specific sites of the body has been going on since 1970. Liposomes possess structural flexibility in terms of their size, composition, surface charge, bilayer fluidity, and their capacity to incorporate virtually any drug irrespective of its solubility, or to display cell-specific ligands on their

surface. Consequently, liposomes can be customized in numerous ways so as to create formulations that are ideal for clinical use [4].

The structural similarity between the lipids composing the nano systems and those composing the skin represents one of the main advantages of LBN, allowing the interaction between the nanosystem matrix and the stratum corneum [3]. CHOL, CER and free fatty acids are present in the stratum corneum, the superficial layer of the skin. All of them are involved in different cellular processes at some level, such as transport functions and immune activity [5,6]. Different subclasses of CER exist in the skin, all interacting with the lipids [6]. Patients with AD have a different composition of lipids in their skin, and, in particular, this arises from them having a lower proportion of CER and increased proportions of unsaturated free fatty acids. These differences with normal skin lead to a different organization of the lipids in the skin and thus a different skin structure [7,8,9]. AD affects populations of all ages, particularly children. It is a worldwide chronic autoimmune inflammatory skin disorder highly prevalent in developed countries and it has been increasing over the most recent decades. This disease implies a deterioration of quality of life, worn down by the symptoms and secondary infections [10]. The treatment of the disease will depend on the degree to which these manifestations are present in the patients. It is also very important to be aware of the individual trigger factors so as to avoid them and reduce flare-ups (Figure 1) [11]. The European Academy of Dermatology and Venereology classifies the different treatments, grading them into six signs: erythema, exudation, excoriation, dryness, cracking and lichenification [12]. Additional therapeutic options should be considered in every treatment phase if established therapy is insufficient or in cases of major infections.

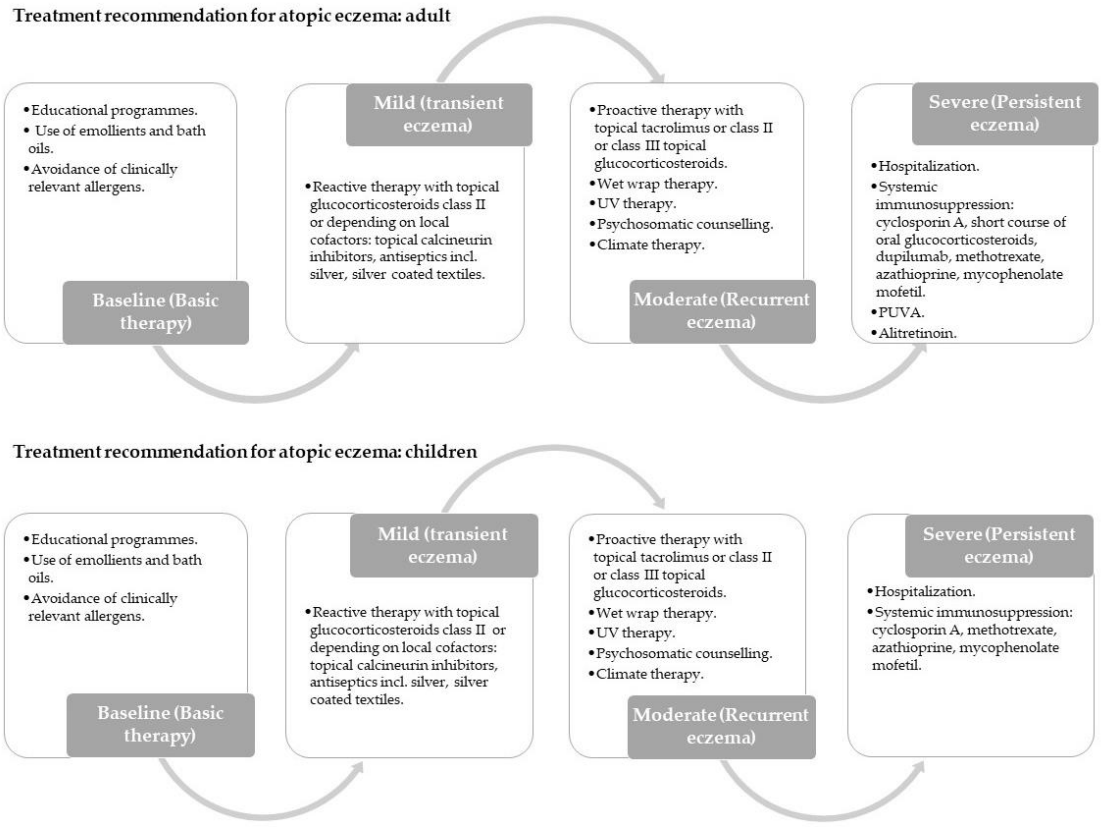

Figure 1. Treatment recommendations for adults and children with atopic eczema according to European guidelines. PUVA = Psoralen and ultraviolet light therapy.

Baricitinib (BNB) is a reversible Janus-associated kinase (JAK)-inhibitor. JAK is important because it stimulates the signal transducers and activators of transcription

(STAT) that cause different immune responses. These include monocyte activation, antibody secretion, erythropoiesis and acute phase reactant production [13]. Furthermore, BNB has recently been introduced orally in cases of moderate-to-severe AD, showing good results in reducing clinical symptoms and improving the quality of life. The most frequent oral doses used are 2 and 4 mg, resulting in a therapeutic plasma concentration of 0.055 μg/mL [14]. However, it has some side effects such as infectious diseases, cardiovascular events and deep venous thrombosis [15]. Topical drug administration is an alternative to avoid systemic effects. To our knowledge, there are no published studies of BNB for the topical route of administration. The main aim of this work was to develop liposomes loaded with BNB for topical administration using natural lipids as a possible topical alternative to the oral route currently available for patients with AD. To achieve this, the following specific objectives were set: (i) to study the physicochemical characteristics of each liposome differentiated by the formulations of three natural lipids: POPC (1-palmitoyl-2-oleoyl-glycero-3-phosphocholine), CHOL (Cholesterol) and CER (Ceramide) in different proportions; (ii) to investigate their drug release profile, as well as the permeation of BNB through physically altered human skin (AHS), the skin being a model of a compromised permeability barrier, which is a particular feature in AD; and (iii) to study the drug retention capacity on AHS, and the tolerability of the formulations by a modified Draize rabbit test and hen's egg chorioallantoic membrane test (HET-CAM test). It is worth mentioning that POPC is a natural lipid found in different microorganisms but not in human skin [16], while CHOL and CER are found in the stratum corneum, as previously mentioned.

2. Results

2.1. Liposomes Physicochemical Characterization

Three liposome formulations were prepared: POPC liposomes, POPC:CHOL liposomes and POPC:CHOL:CER liposomes. The formulations were characterized for pH, particle size and size distribution, encapsulation efficiency and surface charge. This was carried out when the formulations were freshly prepared and when they had been stored at 4 °C.

The pH value for all the liposomes prepared was the same (7.4 ± 0.1), which is adequate for atopic skin treatments [17]. Likewise, the liposomal formulations exhibited comparable efficiency of encapsulation (EE): EE (%) of 6.21 ± 0.55% for POPC; 5.57 ± 0.50% for POPC:CHOL; and 6.21 ± 0.63% for POPC:CHOL:CER.

The results of vesicle size, polydispersity index (PDI) and Zeta potential (ZP) for each liposome are presented in Table 1. All liposomes share similar characteristics, except for liposome POPC:CHOL:CER, which has a higher ZP.

Table 1. Liposomes composition: hydrodynamic diameter, PDI and ZP; and physical stability for 1 month. The results are presented as mean ± SD (n = 3).

Composition	Hydrodynamic Diameter (nm)		PDI		Zeta Potential (mV)	
	1 Day	1 Month	1 Day	1 Month	1 Day	1 Month
POPC	86.0 ± 1.4	86.9 ± 1.1	0.120	0.119	−14.2 ± 0.3	−13.9 ± 0.8
POPC:CHOL (8:2, mol/mol)	53.5 ± 0.9	55.4 ± 1.3	0.174	0.172	−13.2 ± 1.3	−13.5 ± 0.9
POPC:CHOL:CER (3.6:2.4:4.0 mol/mol/mol)	64.1 ± 0.3	65.0 ± 0.7	0.120	0.117	−18.3 ± 1.9	−18.1 ± 1.3

A one-way ANOVA test was carried out and then followed by Tukey's multiple comparison test. All three liposome sizes are statistically different from each other ($p < 0.0001$). Similarly, the ZP of POPC:CHOL:CER is different from the other two liposomes ($p < 0.05$). Liposome POPC and POPC:CHOL do not have a significantly different ZP compared to each other.

These values were also calculated one month after their elaboration and no-significant change was observed, the maximum being 4%.

2.2. In Vitro Drug Release Study

The drug release from the liposomes was evaluated by Franz diffusion cells using a dialysis membrane at the cutaneous temperature, 32 °C, yielding the cumulative amount of BNB released as a function of time. The data were then fitted to different kinetic models. The BNB release profiles from the three liposomes varied; Table 2 indicates the corresponding equations. The liposomes POPC:CHOL:CER and POPC:CHOL fitted a hyperbola model, while liposome POPC was in accordance with a polynomial (second order) model. The modeling of the release profile is shown in Figure 2.

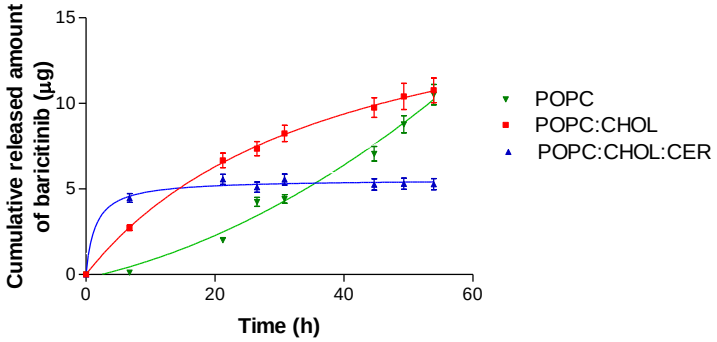

Figure 2. The BNB release profiles from liposomes POPC, POPC:CHOL and POPC:CHOL:CER. BNB cumulative released amount (µg) vs. time (h). The results are presented as mean ± SD (n = 5).

Table 2. Liposome formulations' best-fit values in the kinetic release modeling.

Liposome	Equation	Best-Fit Values According to the Equation				
		A	B	C	B_{max} (µg)	K_d (h)
POPC	Polynominal: Second Order $y = A + Bx + Cx^2$	0.21	0.08	0.002	-	-
POPC:CHOL	One site binding (hyperbola) $y = B_{max}x/(K_d + x)$	-	-	-	18.37	38.34
POPC:CHOL:CER	One site binding (hyperbola) $y = B_{max}x/(K_d + x)$	-	-	-	5.55	1.45

A, B and C = parabola coefficients. Hyperbola parameters Bmax = maximum amount of BNB that can be released; and Kd = drug release constant.

The liposome POPC:CHOL:CER releases the drug faster than the other two liposomes; after 8 h, the release of BNB had already reached a plateau, indicating that the maximum amount of the drug that could be released had been reached. Nevertheless, the total amount of drug released is lower than with the other liposomes. In contrast, the liposomes, POPC and POPC:CHOL, have a sustained release of up to 53 h. At this time, those liposomes exhibited a 2-fold drug release compared to liposome POPC:CHOL:CER, as demonstrated in Figure 2.

To compare different drug release profiles, non-modelistic parameters such as area under the curve (AUC), release efficiency and mean release time (MRT) were calculated. Figure 3 shows the non-modelistic parameters as well as the statistical parameters test, which confirmed there were differences between the three liposomes. Liposome POPC:CHOL displayed the highest values of AUC and the greatest efficiency percentage, but, in contrast, it has the lowest MRT value.

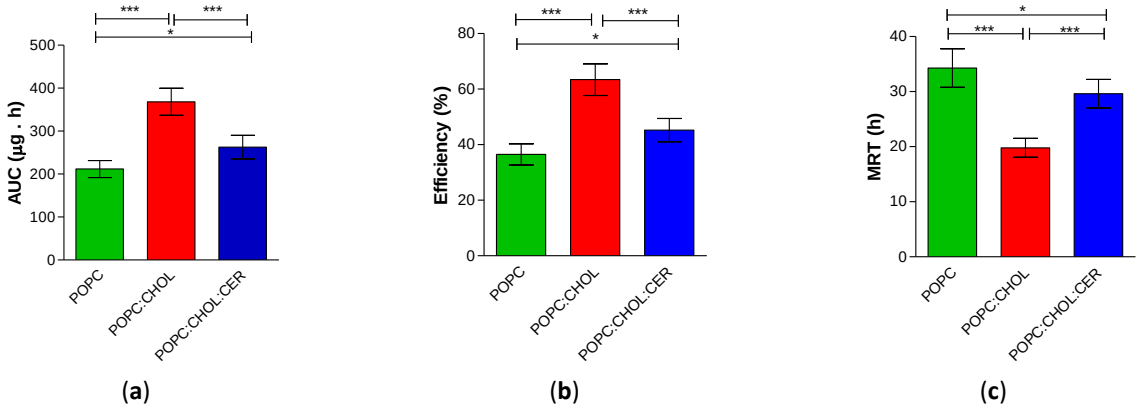

Figure 3. Non-modelistic parameters of: (a) area under the curve (AUC: µg/h); (b) efficiency (E:%); (c) mean release time (MRT: h). A one-way ANOVA test was carried out, followed by Tukey's multiple comparison test (* $p < 0.05$, *** $p < 0.0001$). The results are presented as the mean ± SD (n = 5).

2.3. Ex Vivo Permeation Study

As with the in vitro drug release study, the amount of BNB that was capable of permeating through the human skin was evaluated by Franz cells. Since dermatitis atopic skins present increased permeability relative to healthy skin, the skin was subjected to microneedles to obtain a more permeable skin (hereinafter AHS) and was then mounted on the Franz cells.

The permeation profile, as the cumulative amount permeated through AHS over 25 h, is outlined in Figure 4. It shows that the liposome POPC:CHOL exhibited the highest permeation, with liposome POPC:CHOL:CER following behind, and liposome POPC showing the lowest permeation of the three liposomes tested. The permeation parameters calculated are presented in Table 3.

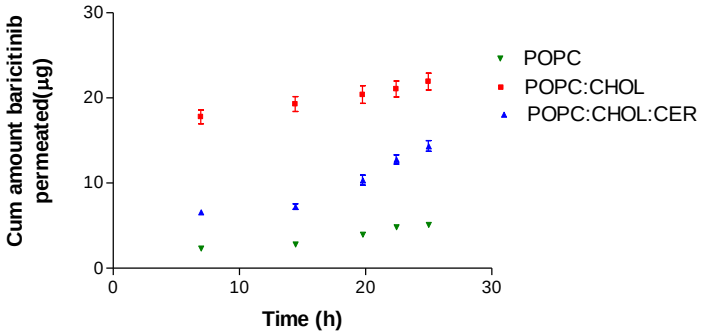

Figure 4. BNB permeation profile: cumulative amount of BNB permeated (µg) vs. time (h). The results are presented as mean ± SD (*n* = 5).

Table 3. Permeation parameters of three liposomes: cumulative amount of BNB permeated at 25 h (AP25h, µg), flux (Jss, µg/h), permeability coefficient (Kp, cm/h) and predicted steady-state plasma concentration in human steady state on a 10 cm2 surface application (Css, ng/mL).

	AP_{25h} (µg)	*Jss* (µg/h)	*Kp* (10^{-4} cm/h)	*Css* (ng/mL)
POPC	5.13 ± 0.52	0.22 ± 0.03	1.14 ± 0.16	0.36 ± 0.05
POPC:CHOL	21.93 ± 2.20	0.29 ± 0.03	1.52 ± 0.16	0.48 ± 0.05
POPC:CHOL:CER	14.36 ± 1.40	0.77 ± 0.07	4.01 ± 0.37	1.28 ± 0.12

ANOVA test analysis of variance, followed by Tukey's multiple comparison test, were performed, and all were statistically different from each other ($p < 0.001$). Results are expressed by mean ± SD (n = 5).

Figure 5 illustrates the quantity of BNB retained in the tissues and the corresponding statistical outcomes. Liposome POPC demonstrated significant statistical differences

when compared to liposome POPC:CHOL and liposome POPC:CHOL:CER. However, no significant differences were observed between liposome POPC:CHOL and liposome POPC:CHOL:CER.

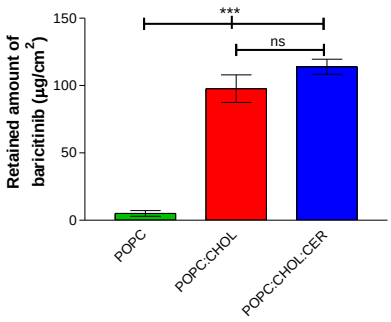

Figure 5. Retained amount (µg/cm²) of BNB at 25 h in the AHS. Results are expressed as mean ± SD (n = 5). ANOVA test analysis of variance, followed by Tukey's multiple comparison test, were performed. Statistically significant difference: *** = $p < 0.0001$; ns = no statistically significant difference.

2.4. Tolerance Study and Histological Analysis

2.4.1. In Vivo Tolerance Study

The tolerability of the liposomal formulations on altered skin (previously subjected to microneedle punches) was evaluated on New Zealand rabbits. Figure 6 shows the progression of altered rabbit's skin (ARS) monitored for 3 h 30 min after applying xylol so as to induce erythema and edema. This was intended to stimulate AD flare-ups. All three liposomes appear to delay the onset of edema and erythema caused by xylol. The use of POPC liposomes was found to reduce the damage caused by xylol. The negative control of ARS was not treated with any substance or formulation.

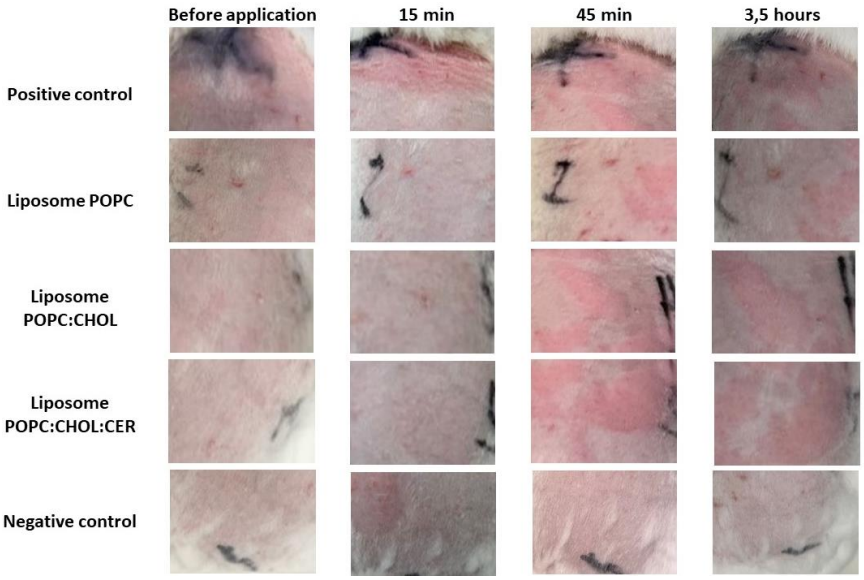

Figure 6. Pictures of 5 groups of rabbits used for the modified Draize test: before the application of xylol and liposomes, at 15 min, 45 min and 3 and a half hours after the respective applications.

The erythema and edema presented on the rabbits' backs are classified by the view scoring system (see Table 4).

Table 4. A modified Draize score was employed to evaluate erythema and edema resulting from xylol exposure, both with and without subsequent application of the liposomes (mean ± SD, *n* = 5).

Chemicals	Before Induced Er and Ed		15 min		45 min		3 h	
	Erythema	**Edema**	**Erythema**	**Edema**	**Erythema**	**Edema**	**Erythema**	**Edema**
Negative control	0.00 ± 0.00	0.00 ± 0.00	0.00 ± 0.00	0.00 ± 0.00	0.00 ± 0.00	0.00 ± 0.00	0.00 ± 0.00	0.00 ± 0.00
Liposome POPC	0.00 ± 0.00	0.00 ± 0.00	0.00 ± 0.00	0.00 ± 0.00	0.00 ± 0.00	0.00 ± 0.00	0.00 ± 0.00	0.00 ± 0.00
Liposome POPC:CHOL	0.00 ± 0.00	0.00 ± 0.00	0.00 ± 0.00	0.00 ± 0.00	1.00 ± 0.53	0.00 ± 0.00	0.65 ± 0.40	0.00 ± 0.00
Liposome POPC:CHOL:CER	0.00 ± 0.00	0.00 ± 0.00	0.00 ± 0.00	0.00 ± 0.00	1.45 ± 0.42	0.00 ± 0.00	0.37 ± 0.03	0.00 ± 0.00
Positive control (xylol)	0.00 ± 0.00	0.00 ± 0.00	3.54 ± 0.20	1.62 ± 0.41	3.50 ± 0.40	1.84 ± 0.13	2.40 ± 0.30	0.50 ± 0.02

Er = erythema; Ed = Edema.

The pictures of Figure 6 are supported by the graphs shown in Figure 7, which show the evolution of the transepidermal water loss (TEWL), and the evolution of the skin hydration, of rabbits with altered skin.

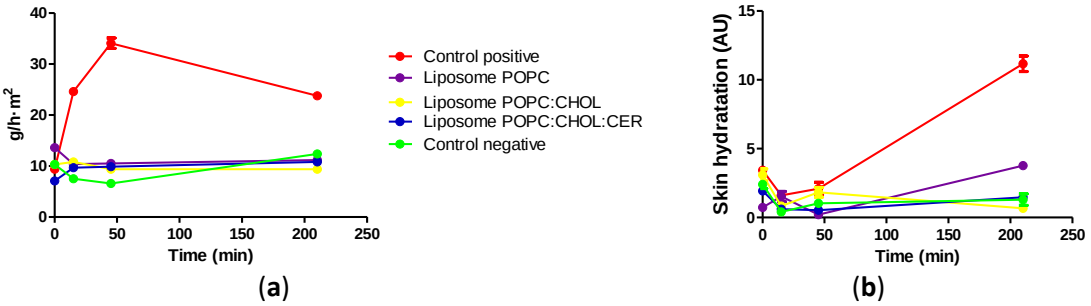

Figure 7. Results of TEWL and skin hydration during 210 min before and after formulations application on rabbits with induced dermatitis by xylol, except for the negative control. (a) TEWL; (b) Skin hydronation (AU). Results are expressed as mean ± SD (n = 5).

2.4.2. Histological Analysis

Once the modified Draize test had been finished, a histological study was conducted to evaluate whether any structural change had occurred to the altered skin due to the application of the formulations. The histology results of the different liposomes, as well as the positive and negative controls, are set out in Figure 8. The skin treated with liposome POPC:CHOL:CER presented stratum corneum loss (Figure 8e) indicating some disruptive effect. This is in contrast to the skins treated with either liposomes POPC or POPC:CHOL, which do not demonstrate any alteration to the skin.

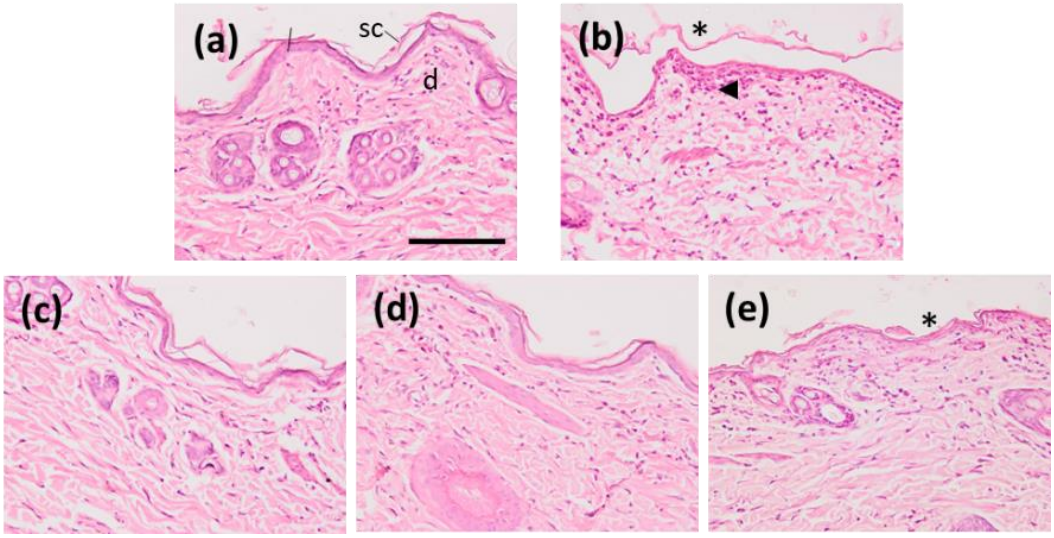

Figure 8. Skin sections colored with eosin and hematoxylin. (a) Control negative skin; (b) positive control; (c) treated with POPC; (d) treated with POPC:CHOL; and (e) treated with POPC:CHOL:CER. sc = stratum corneum, d = dermis, * shows loss of stratum corneum, Δ arrowhead indicates leukocyte infiltrate. Magnification = 200×, scale bar = 100 μm.

2.4.3. In Vitro Tolerance of the Liposomal Formulations for Periocular Application

AD can also be present on facial skin, with symptoms such as dryness, redness, sensitivity and itching, and facial skin might need the application of soothing formulations. This is why the potential tolerance of the liposomal formulations on the eye, after a periocular application on the eye, was assessed by the in vitro technique HET-CAM of fertilized chicken eggs. Table 5 shows the irritation score (IS) estimated for the liposomal formulations. The three liposomes resulted in non-irritant formulations exhibiting IS values similar to the negative control, whereas the positive control resulted in higher IS values corresponding to a severely irritant substance.

Table 5. Irritation score calculated for the liposomal formulations (mean ± SD of n = 3). The scores obtained for the positive and negative controls are also reported.

	Formulation				
	Negative control	Positive control (0.1 N NaOH)	POPC	POPC:CHOL	POPC:CHOL:CER
Irritation score (IS)	0.07 ± 0.00	16.10 ± 0.08	0.07 ± 0.00	0.07 ± 0.00	0.07 ± 0.00

IS ≤ 0.9, non-irritating/slightly irritating; 0.9 < IS ≤ 4.9, moderately irritating; 4.9 < IS ≤ 8.9, irritating; and 8.9 < IS ≤ 21, severely irritating [18].

Figure 9 shows the results from the HET-CAM test. They revealed no irritant effect of any kind; no hemorrhage, coagulation or lysis vessel were observed 5 min after 300 μL of the respective formulations had been applied. This is opposite to the positive control, in which lysis vessel and coagulation appeared (Figure 9b).

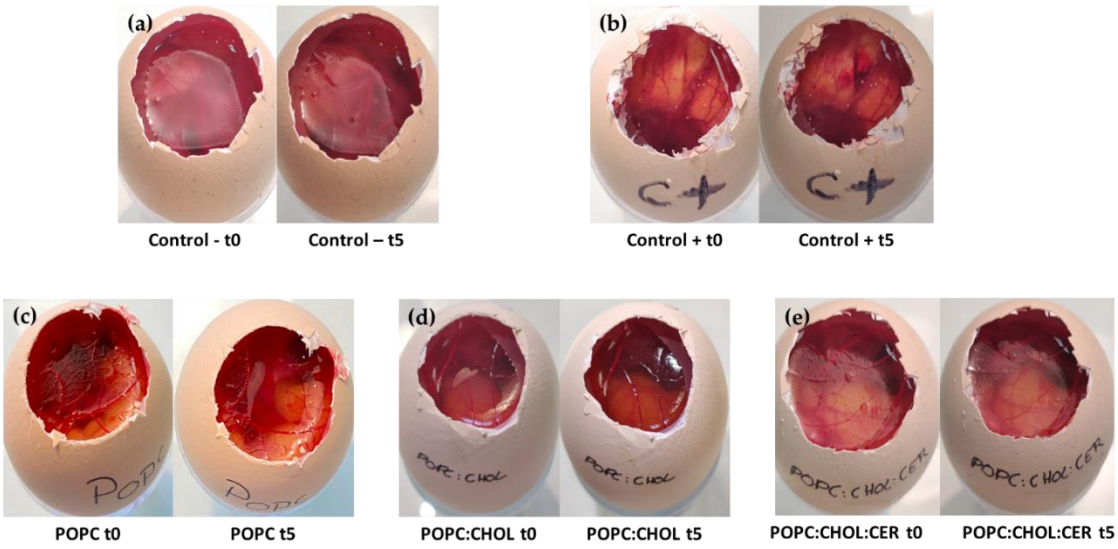

Figure 9. The irritant effect of the formulations was evaluated using the HET-CAM method, with (**a**) a negative control using saline solution, and (**b**) a positive control using 0.1 N sodium hydroxide solution. The other three images show the evolution of the liposomal formulations: (**c**) POPC liposome, (**d**) POPC:CHOL liposome and (**e**) POPC:CHOL:CER liposome.

3. Discussion

All physicochemical characteristics, such as pH, vesicle size and ZP, influence the liposome interaction with the skin [19]. Liposome POPC was the largest vesicle, followed by POPC:CHOL, and the smallest was POPC:CHOL:CER. All of them had a PDI below 0.2, which is indicative of the uniformity of the particle size, and their small size and the low PDI mean the formulations tend to pass more easily through the sterilizing filters, which, in turn, renders them suitable for skins that are grazed or scratched and could become infected. Instead, the ZP helps to predict the stability of particles. A high ZP indicates a stable formulation, so the liposome POPC:CHOL:CER is the most stable of the tested liposomes [20]. Differences in the lipid used for each liposome elaboration may lead to different release profiles described by different kinetic models [21]. In our work, the two liposomes containing CHOL displayed the same kinetic model suggesting that the presence of CHOL in the liposome strongly impacts on their drug release characteristics. The fastest BNB release over a short period of time was presented only by liposome POPC:CHOL:CER but not by liposome POPC:CHOL (Figure 2). Although liposomes POPC and POPC:CHOL exhibited similar BNB released at 54 h, POPC:CHOL showed a higher AUC than POPC:CHOL:CER, indicating a superior performance by POPC:CHOL. The mathematical modelling in the release studies is an excellent tool to evaluate differences between formulations [22,23,24]. Furthermore, the non-modelistic parameters are useful to compare formulations which exhibit different kinetic models. In this work, the non-modelistic parameters showed a relation between the amount of BNB that is released from the formulation and the release efficiency, with the cumulative permeated amount throughout the 25 h period being the liposome POPC:CHOL, the formulation with the highest values. Baricitnib is a molecule with poor water solubility under physiological conditions, as observed from its structure. It does not present charged structures at pH 7.40, suggesting that it could be found deep within the lipid bilayer. Moreover, it presents several groups capable of stabilizing the molecule in hydrophobic regions through hydrogen bonds. These facts point to baricitinib incorporating into the liposome lipid membrane, remaining there and not being released to permeate through the skin. To overcome this problem, liposomes containing baricitinib were supplemented with 5% Transcutol. The structure of Transcutol allows it to be incorporated in parallel to

hydrocarbon chains with its OH group near the headgroup of the phospholipids, distorting the phospholipid bilayer. Then, when liposomes containing baricitinib interact with the skin surface, baricitinib can easily be released from the liposome, and Transcutol molecules can increase the water solubility of baricitinib and facilitate its distribution towards the surface of the skin.

Different authors have demonstrated that, if the lipids are like those in the stratum corneum, more drugs will penetrate the skin [19]. It is worth mentioning that human skin contains CHOL and CER and disturbances in their levels cause disruption of the skin barrier function. Yet, harmonizing the CHOL and CER levels in the skin restores its barrier function [25]. Sinico and Fadda explained that a greater permeation and release could be produced when the liposomes are composed of lipids that are more similar to those of the skin [26]. This would explain the higher permeation of POPC:CHOL and POPC:CHOL:CER compared with liposome POPC without CHOL. The liposome POPC:CHOL:CER triplicated the results values of flux, permeability coefficient and theoretical plasma concentration in human steady state compared with the other studied liposomes (POPC and POPC:CHOL, see Table 3). Therefore, CER could be acting like a permeation enhancer. CERs have been considered the principal factor in the control of the skin barrier as the enhancer effect of CER analogues has been demonstrated in diverse studies [27]. Since the predicted plasma concentration at steady state did not reach therapeutic levels, it is likely that BNB only exerts a local effect on the skin [14].

Retention of BNB in the skin was not statistically different between POPC:CHOL and POPC:CHOL:CER, so both liposomes would be a good option in order to achieve a local effect of BNB because both liposomes reached values a hundred times higher than liposome POPC (Figure 5). Liposomes with CHOL and CER—which are the lipids found in the skin—were able to diffuse through the skin, thus creating a reservoir effect in the BNB. This achieved concentrations inside the skin higher than those obtained in the blood in oral therapy for AD treatment [28], considering the human skin density to be 1 g/mL [29].

The HET-CAM test showed no irritation effect caused by any of the three liposomes and, in reference to the modified Draize test, we observed a good Draize score for erythema and edema (Table 4). Liposome POPC effectively counteracted the impact of xylol on the skin and neither erythema nor edema were observed over the 3 h of the study. Xylol caused both reactions, erythema and edema, which were observed from the first assessment (after 15 min) and up to the end of the tolerance study, which was after 3 h. Liposomes POPC:CHOL and POP:CHOL:CER also effectively counteracted the edema caused by xylol. However, after 45 min of application, a slight erythema appeared in the areas where liposomes POPC:CHOL and POPC:CHOL:CER were tested. Nevertheless, this effect was more than 2-fold and 3-fold lower than the erythema caused by xylol. TEWL values were constant for all the liposomes with similar values to the negative control (within the range of 8–15 g/h·m2, which means a healthy value for rabbits), whereas the positive control showed a significant increase. The results are in accordance with those obtained in control rabbits, as observed by Babu M. Medi and Angela Anigbogu [30,31]. The skin hydration values were constant and followed the trend of the negative control, while the positive control showed a steady increase during the tolerance study. Finally, the histological study demonstrated that liposome POPC and POPC:CHOL avoided any damage to the tissue structures. Based on these promising results, further biochemical studies should be carried out to test the efficacy of these liposomal formulations on animal models of the disease, including mutant animals, before proceeding to clinical trials.

4. Materials and Methods

4.1. Materials

BNB, Ammonium Formate and POPC were purchased from Sigma–Aldrich (Madrid, Spain). Transcutol® P [Diethylene glycol monoethyl ether] was bought at Gattefossé (Barcelona, Spain). Fisher Chemical (Loughborough, UK) supplied the Acetonitrile. Finally, CHOL (ovine wool > 98%) and CER (bovine spinal cord ≥ 98%) were acquired at Avanti Polar Lipid Inc. (Alabaster, AL, USA). A microneedle roller (Currentbody, Barcelona, Spain) contains 540 titanium needles that are 0.25 mm long, corresponding to 72.3 microneedles/cm2.

BNB (C16H17N7O2S) is a pyrrolopyrimidine, the chemical structure of which is shown in the figure below, Figure 10, which has been obtained from PubChem, an open chemistry database at the National Institute of Health (NIH).

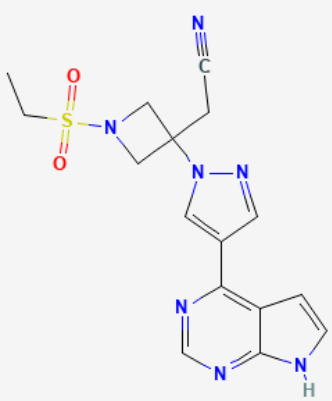

Figure 10. Chemical structure of BNB.

4.2. Biological Materials

The abdominal human skin (protocol code 93-01162 02/18 approved on 17 January 2020 by the 99 Bioethics Committee of SCIAS Hospital de Barcelona), was dermatomed to 400 µm thickness (Aesculap GA 630, Aesculap, Tuttligen, Germany). All the skin was subjected to a physical alteration with microneedles in order to simulate an AD skin by piercing the epidermis. Since the needles do not come into contact with the nerves or blood vessels, this technique is painless when performed on live animals.

4.3. Methods

4.3.1. Preparation of the Liposomes

Three different liposome formulations were prepared: (i) pure POPC liposomes, (ii) POPC:CHOL (0.8:0.2, mol/mol) liposomes and (iii) POPC:CHOL:CER (0.36:0.24:0.40, mol/mol/mol) liposomes.

All liposomes samples were elaborated in accordance with the methods published in other articles [32]. In short, to elaborate each liposome sample, we added 500 mg of BNB in a round bottom flask to the corresponding chloroform–methanol (2:1, v/v) lipid solutions to achieve the desired molar lipid concentration for each composition. Then, the mixture was sonicated for 10–15 s to make sure all BNB was dissolved. Following the removal of the solvent using a rotary evaporator, the thin lipid film was kept in a high vacuum overnight in the absence of light to ensure the absence of organic solvent traces. The thin films were rehydrated using a solution containing 10 mM TRIS·HCl ([tris(hydroxymethyl)aminomethane] 150 mM NaCl), and 5% (v/v) of Transcutol® P pH 7.40. Vigorous vortexing was performed for 5 cycles, at a temperature above that of the lipid mixture's transition, so as to obtain large multilamellar vesicles. The liposome size

was homogenized using an ultrasound bath with temperature control for 15 min. Finally, the liposomes were passed through a Sephadex® G50 column mounted in a 5 mL syringe and centrifuged at 1000 rpm for 10 s using a Rotanta 460R centrifuge (Andreas Hettich GmbH & Co. KG, DE, Tuttlingen, Germany) to eliminate non-encapsulated BNB.

4.3.2. Liposomes' Physicochemical Characterization

The physicochemical properties of the liposomes were analyzed using various parameters, including pH, vesicle size, polydispersity index, ZP and encapsulation efficiency. pH measurement was carried out, using a pH-meter micro pH 2001 (Crison Instruments SA, Alella, Spain), in triplicate. The Zetasizer Nano S (Malvern Instrument, Malvern, UK) was used to determine the liposomes size, PDI and ZP. All the physicochemical characteristics were determined in triplicate [33]. All the measures were analyzed by one-way ANOVA test followed by a Tukey's multiple comparison test. These measurements were repeated on samples stored for up to 1 month at 4 °C to assess the stability of the liposomes.

To study the EE percentage (EE%), the liposomes were broken down with Transcutol® P: Triton at 10% (8:1), so that they released the BNB, and quantified using HPLC (see Section 4.3.6). The comparison between the initial amount and the extracted amount gave the EE% (Equation (1)) [32]:

$$\boldsymbol{EE\%} = \frac{\boldsymbol{Q_f}}{\boldsymbol{Q_0}} \times \mathbf{100} \quad (1)$$

where Q_f is the total mass of BNB retained inside the liposomes and Q_0 is the total mass of BNB initially used to prepare the liposomes. Both quantities are expressed in mg.

4.3.3. In Vitro Drug Release Study

In order to investigate the release of the drug, we employed a dialysis membrane that had a molecular cut-off weight of 14,000 Da (Sigma–Aldrich, Madrid, Spain) in Franz-type diffusion cells. These cells had a diffusion area of 0.64 cm2 and a receptor chamber of 4.9 mL (Crown Glass Company, Inc., Jersey City, NJ, USA) [34,35]. Prior to use, the membrane was hydrated in methanol:water (1:1) for 24 h and then washed before being set in the Franz diffusion cells. The receptor medium used was Transcutol® P which was stirred at 500 r.p.m. to keep sink conditions. The experiment was conducted at 32 °C by means of a thermostatic water bath. An amount of 500 µL of formulation was added to the donor compartment; five replicates per each liposome were included. During the experiment, samples of 200 µL were collected at specific time intervals and, in order to maintain a constant volume in the cells, Transcutol® P was added after each sample collection. The collected samples were analyzed by a validated HPLC-fluorescence method, as described in Section 4.3.6. The cumulative amounts of BNB released from each liposomal formulation were plotted over time, and the data were analyzed by different kinetic models to describe the drug release profile. The determination coefficient (r2) was used to assess the goodness of fit [36].

Moreover, some non-modelestic parameters were calculated to compare different release profiles. These estimated parameters were the MRT of BNB from the formulation, the AUC representing the amount of BNB that was released from the formulation [37] and the efficiency (E) as the percentage of BNB released from the initial formulation.

4.3.4. Ex Vivo Permeation Study

The permeation studies were conducted using Franz diffusion cells with a surface area measuring 0.64 cm2 and a receptor chamber of 4.9 mL. The altered abdominal human skin was placed between the donor and the receptor compartments [34,35]. The receptor medium was Transcutol® P. Amounts of 500 µL of each liposome was put on the donor compartment. Samples of 200 µL were taken over 25 h and replaced by Transctuol® P after every sampling time. We analyzed the samples using the validated HPLC-fluorescence method (see Section 4.3.6).

Three permeation parameters of each liposome were calculated: flux (Jss, μg/h), permeability coefficient (Kp, cm/h) and theoretical predicted plasma concentration in human steady state applied to a 10 cm2 surface (Css, ng/mL). Flux is the slope calculated with the aligned points in the permeation profile [35]. The permeability coefficient was obtained by the following equation:

$$Kp = \frac{Jss}{C_0 \cdot A} \quad (2)$$

where C_0 (μg/mL) is the initial concentration of BNB in the liposome and $\boldsymbol{A}$ is the surface of the diffusion area (cm²) [34].

Css was calculated by the equation detailed below:

$$C_{ss} = \frac{Jss \cdot TSA}{Clp \cdot A} \quad (3)$$

where *Jss* (μg/h) is the flux, TSA (cm²) is the theoretical surface area of application, *Clp* (ml/min) is the human plasma clearance of BNB and *A* (cm²) is the diffusion area of the Franz cells [34]. The area of application considered was 10 cm².

After completing the permeation study, we removed all tissues from the diffusion cells and washed away any liposomes remaining on the surface with distilled water. Then, we extracted the BNB that was retained in the permeation area of the tissue, cutting it, weighing it and immersing it in 1 mL of Transcutol® P. The sample was then sonicated for 10 min using an ultrasonic water bath [33]. The final step was to analyze the Transcutol® P with the extracted BNB using HPLC. We calculated the retained BNB in the tissues (Q_{ret}) using Equation (4) and the results were stated, normalized by the weight of the tissue and the diffusion area (0.64 cm²) and multiplied by the recuperation of the drug:

$$\boldsymbol{Q_{ret} = \frac{Q_{ext}}{W \times A} \times \frac{100}{R}} \quad (4)$$

In this equation, Q_{ext} represents the quantity of drug extracted from the tissue and is measured in μg, *W* denotes the weight of the tissue in grams, while *A* is the diffusion area in cm². Finally, *R* represents the proportion of BNB that is recovered in each tissue [35].

4.3.5. Baricitinib Determination by HPLC

The measurement of BNB in each sample was carried out using high-performance liquid chromatography (HPLC) equipped with a fluorescence detector. The HPLC system consisted of a Chromatograph Waters Alliance 2695 and a Fluorescence Jasco FP-1520 detector that operated at an excitation wavelength of 310 nm and an emission wavelength of 390 nm. The chromatographic column was a Symmetry C18 (4.6 × 75 mm, 3.5 μm) and the mobile phase was Ammonium Formate 10 mM pH 7.4 (75:25 *v*/*v*); the flux was 1 mL/min and the volume of injection was 10 μL. The validated range for the quantification of BNB was from 0.03 to 1 μg/mL.

4.3.6. Tolerance Study and Histological Analysis

Liposomes were also evaluated by a modified Draize skin test to study the effect on induced erythema and edema with xylol to simulate atopic skin. We used non-anesthetized New Zealand healthy rabbits (Harlan, Barcelona, Spain). They were cared for in accordance with the standard conditions, receiving food and water ad libitum. The objective was to detect the possible signs of damage on altered skin as indicated by the level of erythema and edema [38,39]. The studies were conducted under a protocol in accordance with the Mexican Official Norm for Animal Care and Handling (NOM-062-ZOO-1999).

To obtain an ARS, we used microneedles so as to compromise the skin barrier function on the rabbits' backs. This was carried out one day after having measured their basal values and having shaved them. The animals were divided into different groups: the negative control group which only underwent microneedles; the positive control

group which, in addition to the microneedles, received xylol to induce skin irritation; 3 other groups which received microneedles, plus xylol, plus one of the liposomes. Next, we applied 0.5 mL of xylol to all the rabbits minus the negative control (which also did not have liposomes). The positive control received microneedles plus xylol.

The responses were recorded at 15 min, 45 min and 3 h 30 min. At the same points in time, the transepidermal water loss (TEWL) and skin hydration were measured. For the positive control, 0.5 mL of xylol was applied and evaluated at the same times as the liposomes. A visual scoring system was used to evaluate inflammation; this system classifies from 1 to 4 according to whether the erythema and edema were practically imperceptible or had reached a large area of exposure [40]: 0 denotes no erythema and no edema, 1 denotes a little sign of erythema or edema, 2 denotes explicit erythema or slight edema, 3 denotes a moderate to severe erythema or edema and 4 refers to serious erythema (beet redness) through to the first signs of depth injuries or severe edema [41].

Xylol was used as an irritant component to induce allergic contact dermatitis (ACD), characterized by manifestations such as skin redness, swelling, warmth and itching and accompanied by dryness and flaking. Other articles, like those of Patricia L Nadworny et al. [42] or Liu Tang et al. [43], used dinitrochlorobenzene, or Paul L. Stanley et al. [44], who used 12-O-tetradecanoylphorbol-13-acetate (TPA).

TEWL is the amount of water that can diffuse through the skin stratum corneum per unit of time. The appropriate structure of intracellular lipids in the stratum corneum is one of the key factors in retaining transdermal water [45,46]. TEWL was measured by Tewameter (TEWL-Dermalab, Agaram Industries, India). An increment of this value means there is damage on the skin barrier [47]. The skin hydration was measured by a Corneometer (EnviroDerm, Ireland), which can quantify the amount of water within the corneum.

After monitoring the mentioned parameters for 3 h, the treated animal parts were histologically evaluated to assess the effect of the liposomes. To ensure this, the animals were euthanized with xylazine (Rompun® 20 mg/mL, Bayer Hispania, Sant Joan Despí, Spain) and ketamine (Imalgene® 100 mg/mL, Boehringer Ingelheim Animal Health España, Sant Cugat del Vallès, Spain). The mixture was injected via the right ear vein at 4 mg/kg [48]. After clinical death, the back skin was immediately excised, rinsed with PBS pH 7.4, and set overnight at room temperature in 4% buffered formaldehyde and subsequently embedded in paraffin wax. Transverse sections measuring 5 µm were stained with hematoxylin and eosin and then examined using a light microscope (Olympus BX41 and camera Olympus XC50) on blinded-coded samples to assess the histological structure [49].

Finally, a HET-CAM test was conducted to evaluate the potential risk of causing irritation to the eye after a periocular application. The HET-CAM test assesses the potential toxicity of formulations when applied to the CAM of a 10-day embryonated hen's egg (supplied by the G.A.L.L.S.A. farm, Tarragona, Spain). The CAM was observed for five minutes following application, with any reactions, such as bleeding (hemorrhage), blood vessel disintegration (coagulation) and protein denaturation (intra- and extra-vascular vessel lysis coagulation), being noted [18]. To this end, we applied 300µL of liposomes to the CAM and we waited 5 min to see if there had been any reaction working with the INVITTOX protocol [50]. The positive control used was a 0.1 N solution of NaOH, while the negative control was a solution containing 0.9% NaCl [50]. The IS was calculated, as described by Garrós et al., including 3 replicates per formulation [49].

5. Conclusions

Three liposomal formulations containing BNB, a Janus kinase inhibitor, were developed for the topical treatment of complement flare-ups in AD. The liposomes were prepared using three different lipids: POPC, CHOL and CER. The POPC:CHOL:CER formulation showed higher flux and permeation compared to the other formulations. However, there were no statistically significant differences in the retention concentration in the skin between POPC:CHOL and POPC:CHOL:CER. These formulations also showed that they retained higher amounts of BNB than liposome POPC; this may be due to them having a longer effect. However, further biomedical investigations should be carried out. The formulations did not demonstrate any irritant effect in the HET-CAM test, and the liposomes POPC and POPC:CHOL did not cause any structural alteration according to the histological analysis.

Author Contributions: Conceptualization, Ò.D., M.M. and A.C.C.; methodology, Ò.D., M.M. and H.C.; validation, M.M. and H.C.; formal analysis, N.G.; investigation, N.G., M.J.R.-L., N.B. and R.M.-M.; resources, Ò.D., M.M., A.C.C. and M.J.R.-L.; data curation, P.B.-S., Ò.D. and M.M.; writing—original draft preparation, N.G. and P.B.-S.; writing—review and editing, P.B.-S. and M.M.; visualization, M.M.; supervision, A.C.C., M.M. and H.C.; project administration, M.M., A.C.C. and H.C.; funding acquisition, A.C.C., M.M. and H.C. All authors have read and agreed to the published version of the manuscript.

Funding: This research received no external funding.

Institutional Review Board Statement: The protocol used to carry out the studies was in accordance with the Mexican Official Norm for Animal Care and Handing (NOM-062-ZOO-1999) and with the approval of the Academic Committee of Ethics of the Vivarium of the Autonomous University of the Morelos State of Mexico, number 0122013. Moreover, the experiments were carried out in agreement with the guidelines stated in the protocol "Principles of Laboratory Animal Care" (publication 214/97 of 30 July).

Informed Consent Statement: Not applicable.

Data Availability Statement: The data presented in this study are available on request from the corresponding author.

Acknowledgments: The authors would like to thank Pol Alegret and Alexander Parra-Coca for their excellent technical support. We also thank Harry Paul for revising the English language.

Conflicts of Interest: The authors declare no conflict of interest. The funders had no role in the design of the study; in the collection, analyses, or interpretation of data; in the writing of the manuscript, or in the decision to publish the results.

References

1. Naseri, N.; Valizadeh, H.; Zakeri-Milani, P. Solid Lipid Nanoparticles and Nanostructured Lipid Carriers: Structure, Preparation and Application. *Tabriz Univ. Med. Sci.* **2015**, *5*, 305–313. https://doi.org/10.15171/apb.2015.043.
2. Bose, S.; Michniak-Kohn, B. Preparation and Characterization of Lipid Based Nanosystems for Topical Delivery of Quercetin. *Eur. J. Pharm. Sci.* **2013**, *48*, 442–452. https://doi.org/10.1016/J.EJPS.2012.12.005.
3. Sguizzato, M.; Esposito, E.; Cortesi, R.; Terrinoni, A. Molecular Sciences Lipid-Based Nanosystems as a Tool to Overcome Skin Barrier. *Int. J. Mol. Sci.* **2021**, *22*, 8319. https://doi.org/10.3390/ijms22158319.
4. Gregoriadis, G.; Florence, A.T. Liposomes in Drug Delivery. *Drugs* **1993**, *45*, 15–28. https://doi.org/10.2165/00003495-199345010-00003.
5. Coderch, L.; López, O.; De La Maza, A.; Parra, J.L. Ceramides and Skin Function. *Am. J. Clin. Derm.* **2003**, *4*, 107–129. https://doi.org/10.2165/00128071-200304020-00004.
6. Boncheva, M. The Physical Chemistry of the Stratum Corneum Lipids. *Int. J. Cosmet. Sci*. **2014**, 36, 505–515. https://doi.org/10.1111/ics.12162.
7. Danso, M.; Boiten, W.; van Drongelen, V.; Gmelig Meijling, K.; Gooris, G.; El Ghalbzouri, A.; Absalah, S.; Vreeken, R.; Kezic, S.; van Smeden, J.; et al. Altered Expression of Epidermal Lipid Bio-Synthesis Enzymes in Atopic Dermatitis Skin Is Accompanied by Changes in Stratum Corneum Lipid Composition. *J. Derm. Sci.* **2017**, *88*, 57–66. https://doi.org/10.1016/J.JDERMSCI.2017.05.005.

8. Elias, P.M. Lipid Abnormalities and Lipid-Based Repair Strategies in Atopic Dermatitis. *Biochim. Et Biophys. Acta. -Mol. Cell Biol. Lipids* **2014**, *1841*, 323–330. https://doi.org/10.1016/J.BBALIP.2013.10.001.
9. van Smeden, J.; Janssens, M.; Gooris, G.S.; Bouwstra, J.A. The Important Role of Stratum Corneum Lipids for the Cutaneous Barrier Function. *Biochim. Et Biophys. Acta. -Mol. Cell Biol. Lipids* **2014**, *1841*, 295–313. https://doi.org/10.1016/J.BBALIP.2013.11.006.
10. Dharmage, S.C.; Lowe, A.J.; Matheson, M.C.; Burgess, J.A.; Allen, K.J.; Abramson, M.J. Atopic Dermatitis and the Atopic March Revisited. *Allergy* **2014**, *69*, 17–27. https://doi.org/10.1111/all.12268.
11. Wollenberg, A.; Barbarot, S.; Bieber, T.; Christen-Zaech, S.; Deleuran, M.; Fink-Wagner, A.; Gieler, U.; Girolomoni, G.; Lau, S.; Muraro, A.; et al. Consensus-Based European Guidelines for Treatment of Atopic Eczema (Atopic Dermatitis) in Adults and Children: Part I. *J. Eur. Acad. Dermatol. Venereol*. **2018**, 32, 657–682.
12. Oranje, A.P. Practical Issues on Interpretation of Scoring Atopic Dermatitis: SCORAD Index, Objective SCORAD, Patient-Oriented SCORAD and Three-Item Severity Score. *Curr. Probl. Dermatol*. **2011**, 41, 149–155.
13. Jorgensen, S.C.J.; Tse, C.L.Y.; Burry, L.; Dresser, L.D. Baricitinib: A Review of Pharmacology, Safety, and Emerging Clinical Experience in COVID-19. *Pharmacother. J. Hum. Pharmacol. Drug. Ther.* **2020**, *40*, 843–856. https://doi.org/10.1002/phar.2438.
14. Committee for Medicinal Products for Human Use (CHMP). Olumiant-Assessment Report; Committee for Medicinal Products for Human Use (CHMP): London, UK, 2020.
15. Saeki, H.; Ohya, Y.; Furuta, J.; Arakawa, H.; Ichiyama, S.; Katsunuma, T.; Katoh, N.; Tanaka, A.; Tsunemi, Y.; Nakahara, T.; et al. Executive Summary: Japanese Guidelines for Atopic Dermatitis (ADGL) 2021. *Allergol. Int.* **2022**, 71, 448–458 https://doi.org/10.1016/j.alit.2022.06.009.
16. National Library of Medicine (US); National Center for Biotechnology Information PubChem Compound Summary for CID 5497103, 1-Palmitoyl-2-Oleoyl-Sn-Glycero-3-Phosphocholine. Available online: https://pubchem.ncbi.nlm.nih.gov/compound/1-Palmitoyl-2-oleoyl-sn-glycero-3-phosphocholine (accessed on 27 September 2022).
17. Jurecek, L.; Rajcigelova, T.; Kozarova, A.; Werner, T.; Vormann, J.; Kolisek, M. Beneficial Effects of an Alkaline Topical Treatment in Patients with Mild Atopic Dermatitis. *J. Cosmet. Derm.* **2021**, *20*, 2824–2831. https://doi.org/10.1111/jocd.13936.
18. Mallandrich, M.; Calpena, A.C.; Clares, B.; Parra, A.; García, M.L.; Soriano, J.L.; Fernández-Campos, F. Nano-Engineering of Ketorolac Tromethamine Platforms for Ocular Treatment of Inflammatory Disorders. *Nanomedicine* **2021**, *16*, 401–414. https://doi.org/10.2217/nnm-2020-0403.
19. González-Rodríguez, M.; Rabasco, A. Charged Liposomes as Carriers to Enhance the Permeation through the Skin. *Expert Opin. Drug. Deliv.* **2011**, *8*, 857–871. https://doi.org/10.1517/17425247.2011.574610.
20. Paranjpe, M.; Müller-Goymann, C.C. Nanoparticle-Mediated Pulmonary Drug Delivery: A Review. *Int. J. Mol. Sci.* **2014**, *15*, 5852–5873. https://doi.org/10.3390/IJMS15045852.
21. Schroeder, A.; Kost, J.; Barenholz, Y. Ultrasound, Liposomes, and Drug Delivery: Principles for Using Ultrasound to Control the Release of Drugs from Liposomes. *Chem. Phys. Lipids* **2009**, *162*, 1–16. https://doi.org/10.1016/J.CHEMPHYSLIP.2009.08.003.
22. Campos, F.F.; Calpena Campmany, A.C.; Delgado, G.R.; Serrano, O.L.; Naveros, B.C. Development and Characterization of a Novel Nystatin-Loaded Nanoemulsion for the Buccal Treatment of Candidosis: Ultrastructural Effects and Release Studies. *J. Pharm. Sci.* **2012**, *101*, 3739–3752. https://doi.org/10.1002/JPS.23249.
23. Domínguez-Villegas, V.; Clares-Naveros, B.; García-López, M.L.; Calpena-Campmany, A.C.; Bustos-Zagal, P.; Garduño-Ramírez, M.L. Development and Characterization of Two Nano-Structured Systems for Topical Application of Flavanones Isolated from Eysenhardtia Platycarpa. *Colloids. Surf. B Biointerfaces* **2014**, *116*, 183–192. https://doi.org/10.1016/j.colsurfb.2013.12.009.
24. D'Souza, S. A Review of In Vitro Drug Release Test Methods for Nano-Sized Dosage Forms. *Adv. Pharm.* **2014**, 2014, 1–12. https://doi.org/10.1155/2014/304757.
25. Pappas, A. Epidermal Surface Lipids. *Dermatoendocrinol* **2009**, *1*, 72–76. https://doi.org/10.4161/derm.1.2.7811.
26. Sinico, C.; Fadda, A.M. Vesicular Carriers for Dermal Drug Delivery. *Expert Opin. Drug. Deliv.* **2009**, *6*, 813–825. https://doi.org/10.1517/17425240903071029.
27. Chen, Y.; Quan, P.; Liu, X.; Wang, M.; Fang, L. Novel Chemical Permeation Enhancers for Transdermal Drug Delivery. *Asian J. Pharm. Sci.* **2014**, *9*, 51–64. https://doi.org/10.1016/J.AJPS.2014.01.001.
28. Shi, J.G.; Chen, X.; Lee, F.; Emm, T.; Scherle, P.A.; Lo, Y.; Punwani, N.; Williams, W.V.; Yeleswaram, S. The Pharmacokinetics, Pharmacodynamics, and Safety of Baricitinib, an Oral JAK 1/2 Inhibitor, in Healthy Volunteers. *J. Clin. Pharm.* **2014**, *54*, 1354–1361. https://doi.org/10.1002/jcph.354.
29. Rins, M.; Diez, I.; Calpena, A.C.; Obach, R. Skin Density in the Hairless Rat. Evidence of Regional Differences. *Eur. J. Drug. Metab. Pharm.* **1991**, *Spec No 3*, 456–457.
30. Medi, B.M.; Singh, J. Skin Targeted DNA Vaccine Delivery Using Electroporation in Rabbits: II. Safety. *Int. J. Pharm.* **2006**, *308*, 61–68. https://doi.org/10.1016/J.IJPHARM.2005.10.035.
31. Anigbogu, A.; Patil, S.; Singh, P.; Liu, P.; Dinh, S.; Maibach, H. An in Vivo Investigation of the Rabbit Skin Responses to Transdermal Iontophoresis. *Int. J. Pharm.* **2000**, *200*, 195–206. https://doi.org/10.1016/S0378-5173(00)00371-9.
32. Vázquez-González, M.L.; Botet-Carreras, A.; Domènech, Ò.; Teresa Montero, M.; Borrell, J.H. Planar Lipid Bilayers Formed from Thermodynamically-Optimized Liposomes as New Featured Carriers for Drug Delivery Systems through Human Skin. *Int. J. Pharm.* **2019**, *563*, 1–8. https://doi.org/10.1016/j.ijpharm.2019.03.052.

33. Moussaoui, S.E.; Abo-horan, I.; Halbaut, L.; Alonso, C.; Coderch, L.; Garduño-ramírez, M.L.; Clares, B.; Soriano, J.L.; Calpena, A.C.; Fernández-campos, F.; et al. Polymeric Nanoparticles and Chitosan Gel Loading Ketorolac Tromethamine to Alleviate Pain Associated with Condyloma Acuminata during the Pre- and Post-ablation. *Pharmaceutics* **2021**, *13*, 1784. https://doi.org/10.3390/pharmaceutics13111784.
34. Moussaoui, S.E.; Fernández-Campos, F.; Alonso, C.; Limón, D.; Halbaut, L.; Garduño-Ramirez, M.L.; Calpena, A.C.; Mallandrich, M. Topical Mucoadhesive Alginate-Based Hydrogel Loading Ketorolac for Pain Management after Pharmacotherapy, Ablation, or Surgical Removal in Condyloma Acuminata. *Gels* **2021**, *7*, 8. https://doi.org/10.3390/gels7010008.
35. Mallandrich, M.; Fernández-Campos, F.; Clares, B.; Halbaut, L.; Alonso, C.; Coderch, L.; Garduño-Ramírez, M.L.; Andrade, B.; del Pozo, A.; Lane, M.E.; et al. Developing Transdermal Applications of Ketorolac Tromethamine Entrapped in Stimuli Sensitive Block Copolymer Hydrogels. *Pharm. Res.* **2017**, *34*, 1728–1740. https://doi.org/10.1007/s11095-017-2181-8.
36. Kurakula, M.; Srinivas, C.; Kasturi, N.; Diwan, P. V Formulation and Evaluation of Prednisolone Proliposomal Gel for Effective Topical Pharmacotherapy. *Int. J. Pharm. Sci. Drug. Res.* **2012**, *4*, 35–43.
37. Pérez-González, N.; Bozal-De Febrer, N.; Calpena-Campmany, A.C.; Nardi-Ricart, A.; Rodríguez-Lagunas, M.J.; Morales-Molina, J.A.; Soriano-Ruiz, J.L.; Fernández-Campos, F.; Clares-Naveros, B.; Dinu, V. New Formulations Loading Caspofungin for Topical Therapy of Vulvovaginal Candidiasis. *Gel* **2021**, *7*, 259. https://doi.org/10.3390/gels7040259.
38. Lee, M.; Hwang, J.-H.; Lim, K.-M. Alternatives to In Vivo Draize Rabbit Eye and Skin Irritation Tests with a Focus on 3D Reconstructed Human Cornea—Like Epithelium and Epidermis Models. *Toxicol. Res.* **2017**, *33*, 191–203. https://doi.org/10.5487/TR.2017.33.3.191.
39. Gupta, P.K. Chapter 12-Toxicological Testing: In Vivo Systems. *In Fundamentals of Toxicology*; Academic Press: Cambridge, MA, USA, **2016**; pp. 131–150. https://doi.org/10.1016/B978-0-12-805426-0.00012-3.
40. Singh, S.; Singh, J. Dermal Toxicity and Microscopic Alterations by JP-8 Jet Fuel Components in vivo in Rabbit. *Env. Toxicol. Pharm.* **2004**, *16*, 153–161. https://doi.org/10.1016/J.ETAP.2003.12.001.
41. Mehanna, M.M.; Abla, K.K.; Elmaradny, H.A. Tailored Limonene-Based Nanosized Microemulsion: Formulation, Physicochemical Characterization and In Vivo Skin Irritation Assessment. *Adv. Pharm. Bull.* **2020**, *11*, 274–285. https://doi.org/10.34172/APB.2021.040.
42. Nadworny, P.L.; Wang, J.; Tredget, E.E.; Burrell, R.E. Anti-Inflammatory Activity of Nanocrystalline Silver-Derived Solutions in Porcine Contact Dermatitis. *J. Inflamm.* **2010**, *7*, 13. https://doi.org/10.1186/1476-9255-7-13.
43. Tang, L.; Cao, X.; Li, X.; Ding, H. Topical Application with Conjugated Linoleic Acid Ameliorates 2, 4-dinitrofluorobenzene-induced Atopic Dermatitis-like Lesions in BALB/c Mice. *Exp. Derm.* **2021**, *30*, 237–248. https://doi.org/10.1111/exd.14242.
44. Stanley, P.L.; Steiner, S.; Havens, M.; Tramposch, K.M. Mouse Skin Inflammation Induced by Multiple Topical Applications of 12-O-Tetradecanoylphorbol-13-Acetate. *Ski. Pharm. Physiol.* **1991**, *4*, 262–271. https://doi.org/10.1159/000210960.
45. Verdier-Sévrain, S.; Bonté, F. Skin Hydration: A Review on Its Molecular Mechanisms. *J. Cosmet. Derm.* **2007**, *6*, 75–82. https://doi.org/10.1111/j.1473-2165.2007.00300.x.
46. Alexander, H.; Brown, S.; Danby, S.; Flohr, C. Research Techniques Made Simple: Transepidermal Water Loss Measurement as a Research Tool. *J. Investig. Dermatol.* **2018**, *138*, 2295–2300.e1. https://doi.org/10.1016/j.jid.2018.09.001.
47. Netzlaff, F.; Kostka, K.H.; Lehr, C.M.; Schaefer, U.F. TEWL Measurements as a Routine Method for Evaluating the Integrity of Epidermis Sheets in Static Franz Type Diffusion Cells in Vitro. Limitations Shown by Transport Data Testing. *Eur. J. Pharm. Biopharm.* **2006**, *63*, 44–50. https://doi.org/10.1016/J.EJPB.2005.10.009.
48. Parra-Coca, A.; Boix-Montañés, A.; Calpena-Campmany, A.C.; Colom, H. In Vivo Pharmacokinetic Evaluation of Carprofen Delivery from Intra-Articular Nanoparticles in Rabbits: A Population Modelling Approach. *Res. Vet. Sci.* **2021**, *137*, 235–242. https://doi.org/10.1016/J.RVSC.2021.05.012.
49. Garrós, N.; Mallandrich, M.; Beirampour, N.; Mohammadi, R.; Domènech, Ò.; Rodríguez-Lagunas, M.J.; Clares, B.; Colom, H. Baricitinib Liposomes as a New Approach for the Treatment of Sjögren's Syndrome. *Pharmaceutics* **2022**, *14*, 1895 https://doi.org/10.3390/pharmaceutics14091895.
50. nteragency Coordinating Committee on the Validation of Alternative Methods (ICCVAM*). Test Method Protocol: Hen's Egg Test-Chorioallantoic Membrane (HET-CAM) Test Method*; Interagency Coordinating Committee on the Validation of Alternative Methods (ICCVAM): Bethesda, MD, USA, 2010.

Intrinsic permeation of baricitinib in human skin and selection of candidates as promoters: Two new HPLC validations

Núria Garrós, Helena Colom, Roya Mohammadi Mey Abadi, Negar Beirampour, Ana C. Calpena i Mireia Mallandrich.

Journal of Pharmaceutical and Biomedical Analysis, submitted Jan 31, 2024

Quartil Q2; factor d'impacte 3.571 l'any 2023.

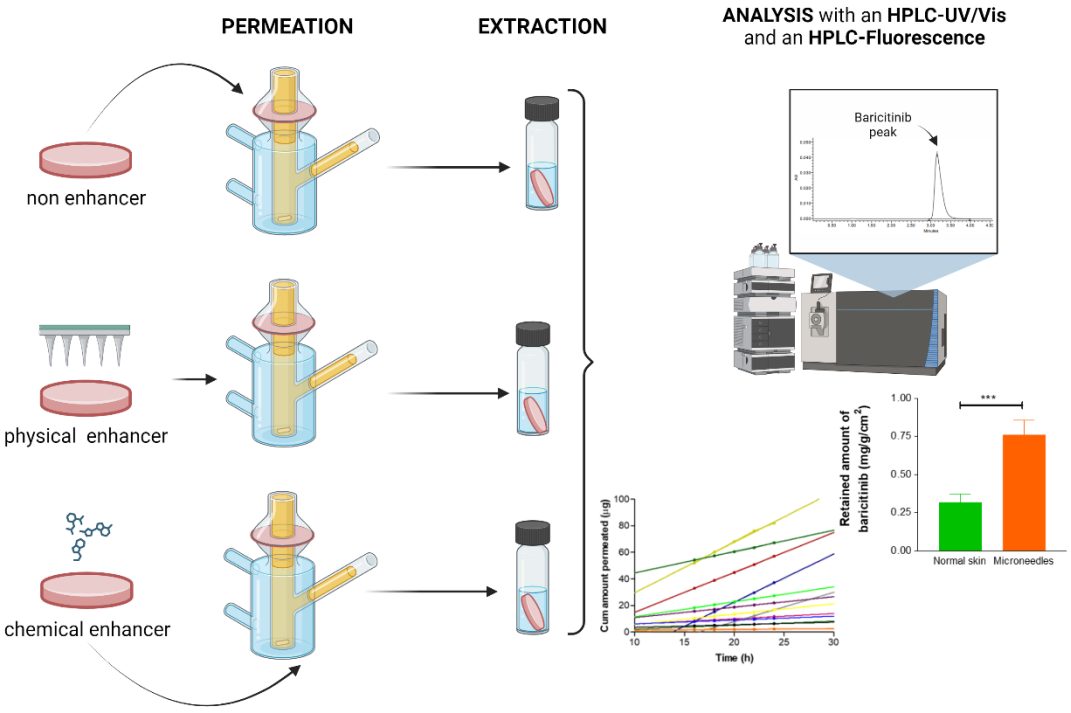

Enhancing Baricitinib Permeation for Topical Delivery with Microneedles and Chemical Enhancers and Raman Spectra Unveiled

Núria Garrós[1], Helena Colom[1,*], Roya Mohammadi Mey Abadi[1,2], Negar Beirampour[1], Majella E. Lane[3], Ana C. Calpena[1,2] and Mireia Mallandrich[1,2]

[1]Department of Pharmacy, Pharmaceutical Technology and Physical Chemistry, Faculty of Pharmacy and 6 Food Sciences, University of Barcelona, 08028 Barcelona, Spain; ngarroar50@alumnes.ub.edu (N.G.), hele-na.colom@ub.edu (H.C.), rmohammo31@alumnes.ub.edu (R.M.), nbeirabe7@alumnes.ub.edu (N.B.), acal-pena@ub.edu (A.C.C.), mireia.mallandrich@ub.edu (M.M.)
[2]Institute of Nanoscience and Nanotechnology, University of Barcelona. 645 Diagonal Avenue, 08028 Barcelona, Spain.
[3]Department of Pharmaceutics, UCL School of Pharmacy, London, UK.
*Correspondence: helena.colom@ub.edu (H.C.)

Abstract: This study investigates the potential of using the skin as a target for drug delivery, focusing on Baricitinib, an immunomodulator drug used for treating atopic dermatitis and rheumatoid arthritis. The skin's protective nature poses a challenge to drug diffusion, necessitating permeation enhancers. The research assesses intrinsic permeation of a saturated Baricitinib solution in Transcutol and examines its permeation through human skin at a concentration of 2 mg/mL. The study explores the impact of physical (titanium microneedles) and chemical permeation enhancers on Baricitinib's permeation. Confocal Raman Spectroscopy (CRS) and validated HPLC analytical methods, an HPLC-UV and an HPLC-fluorescence, are employed. For the first time Baricitinib Raman profile has been obtained. Microneedles enhance drug permeation and retention over 2-fold. Terpenes and fatty acids, especially menthol, significantly boost permeation (25-fold) and esters improve retention (3-fold). The findings suggest that percutaneous delivery of Baricitinib could be a promising alternative to oral administration.

Abbreviations: BNB, Baricitinib; DMSO, Dimethyl sulfoxide; PEG-400, Polyethylene glycol-400; AD, Atopic dermatitis; RA, Rheumatoid arthritis; AA, Alopecia areata; CRS; Confocal Raman Spectroscopy; FP, Fingerprint; HWN, High wavenumber.

Keywords: Baricitinib; HPLC-UV; Fluorescence; Skin, Permeation enhancer; Method validation.

1. Introduction

Baricitinib (BNB) is a small molecule (molecular weight (C16H17-N7O2S): 371.42 Da) (Figure 1), a Janus Kinase inhibitor with selectivity for JAK2 and JAK1. The JAK family components are the once which activate STATs causing hyperinflammation and chronic itch at skin among other symptoms using different neuronal cells, keratinocytes, and immunity cells on their way (Radi et al., 2021). This inhibition may reduce the proliferation of key immune cells and the cellular activation, resulting in a reduction of the inflammation. BNB has a low solubility in water (0.357 mg/mL) what difficult the formulation development, instead has a high solubility in organic solvents such us dimethyl sulfoxide (DMSO) and polyethylene glycol-400 (PEG-400) (Alshetaili, 2019; Anwer et al., 2022).

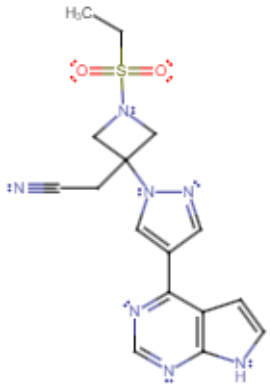

Figure 1. Structure of BNB obtained from the open database PubChem belonging to the National Institutes of Health (NIH).

BNB is used for the treatment of moderate-to-severe atopic dermatitis (AD), rheumatoid arthritis (RA), COVID-19 and recently has been approved as the treatment for sever alopecia areata (AA) in adults, and it is being studied for systemic lupus erythematosus (SLE) treatment (Committee for Medicinal Products for Human Use (CHMP), 2020; Markham, 2017; Wishart et al., 2023). It is available as oral administration tablets, the usual dose is 4 mg once a day, but this can be reduced to 2 mg once a day when the disease is under control (Committee for Medicinal Products for Human Use (CHMP), 2020). We want to focus on illness with skin manifestation, so it's been demonstrated orally administrated BNB can quickly improve skin pains as soon as after the first day starting the treatment (Thyssen et al., 2021).

AD is a widespread and persistent condition with a genetic predisposition, it is characterized by itching and inflammation of the skin. The usual treatment for AD is the use of topical glucocorticosteroids with systemic immunosuppressants but it has several adverse effects, topical corticosteroids can cause thinning of the skin, telangiectasis, and stretch mark; and immunosuppressant drugs make easy a Staphylococcus infection what force the coadministration with antibiotics (Oranje, 2011; Ring et al., 2012; Thomsen, 2014). RA is a systemic inflammatory autoimmune disease that attacks the joints, causing inflammation and damage. This can result in the gradual destruction of joints, including the loss of cartilage and erosion of nearby bone. To minimize inflammation in patients to prevent the accumulation of structural damage and maintain their functional abilities various types of drugs known as disease-modifying antirheumatic drugs (DMARDs) are used for this purpose but they don't stop the progression of structural damage (van der Heijde et al., 2022). One of the most used treatments is the combination of DMARDs with glucocorticoids to reduce long-term adverse effects. The potential negative effects range from a low chance of severe infections, or a potential higher risk of developing cancer become the most significant and concerning adverse events (Hsiao and Fraenkel, 2019). AA is a prevalent chronic autoimmune disorder that specifically affects tissues, leading to the loss of hair, the existing options for treating AA, including corticosteroids, immunomodulators, minoxidil, and contact immunotherapy, have limited effectiveness, and come with a significant chance of negative side effects and frequent relapses, particularly for individuals with severe AA (Zhou et al., 2021). And SLE is a multisystem autoimmune disease that frequently affects the skin (Wallace, 2014). The treatment of SLE often involves a combination therapy that includes high-dose glucocorticoids and immunosuppressive drugs (Tanaka, 2020), the morbidity and mortality associated with SLE are not solely a result of immune-mediated tissue damage, they

also arise from complications related to its treatments, including an elevated risk of accelerated coronary artery disease and increased susceptibility to infections (Fava and Petri, 2019).

The skin is an organ that covers the whole body, acting as a protective layer of the muscles, tissues, and organs beneath from UV radiation, mechanical stress, and exogenous pathogens and chemicals. It keeps the body temperature and prevents dehydration; it also has a sensory and immunological role (Fox et al., 2011). The skin is also a target for drug delivery either for local or systemic therapy. In the latter approach, the skin is an attractive alternative to the oral route because it overcomes the first-pass hepatic metabolism. Nevertheless, due to the protective function of the skin, the diffusion of drugs across the skin is usually hindered and requires the use of permeation enhancers. A high number of molecules have shown enhancer properties, and therefore they have been classified into different families (Figure 2): solvents, esters, fatty acids and alcohols, peptides, sugar and vitamin derivatives, lactams, terpenes, and amino acid derivatives (Kováčik et al., 2020).

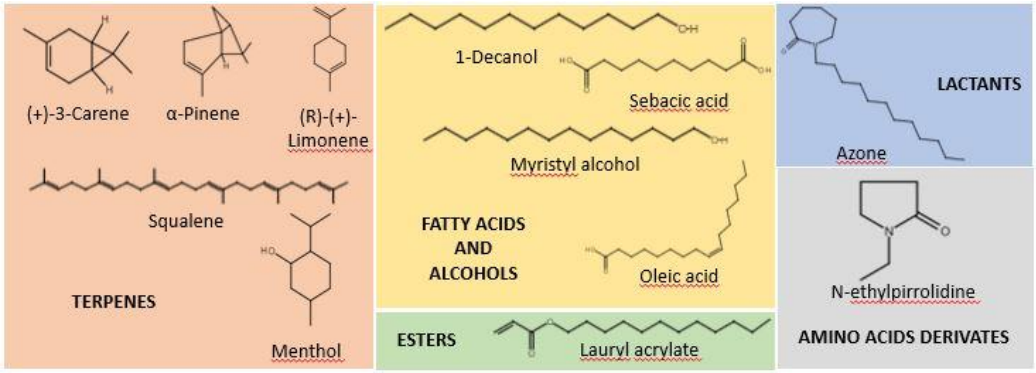

Figure 2. Some of the enhancers used in this work, classified into their corresponding families.

Azone was the first molecule specifically designed as a skin penetration enhancer. It has very good properties for enhancers and can help the permeations with a wide variety of drugs (Williams and Barry, 2012). Terpenes increase skin permeation by one or more mechanisms that interact with the lipids and/or keratin of the stratum corneum (Sapra et al., 2008). Saturated fat-ty acids with a length of around C10-C12 act joining a polar head group. In contrast, unsaturated chains longer than C18 disturb intracellular lipid packing and give increased permeation (Williams and Barry, 2012). Fatty alcohols disrupt the densely packed lipids which fill the extracellular spaces of SC. The most effective length seems to be the C10-C12 (Kanikkannan and Singh, n.d.). Pyrrolidines or amino acids derivates improve the permeation polar route by making diffusion more effective and reducing the nonpolar route (Southwell and Barry, 1983). Esters have the advantage of having a polar part and a nonpolar one. They are not the best enhancers in terms of promoting drug diffusion, but they are milder on the skin (Csóka et al., 2007). Not only do chemical permeation enhancers exist, but there are also physical enhancers, for instance, microneedles which act by inserting the drug directly into the stratum corneum increasing the drug flux, whereas chemical enhancers temporarily reduce skin resistance to enhance drug passage (Smith and Maibach, 2005).

Our goal for this work was to evaluate the impact of different permeation enhancers on the BNB's diffusion through human skin to achieve a localized effect in order to minimize the potential systemic issues associated with BNB. However, the information available on its oral

use indicates that as an immunosuppressant, it may increase the risk of infections, infestations, and hypercholesterolemia (Committee for Medicinal Products for Human Use (CHMP), 2020). Despite these risks, the benefit-risk ratio may still be beneficial for the patient. The studies published so far suggest that the benefits of using BNB may be superior to those of existing treatments (Bieber et al., 2022). To our knowledge, there have been no safety tests conducted on the topical use of BNB. As the vehicle for BNB, we selected Transcutol®, a glycol monoethyl ether, due to its high ability of solubilization and its safety profile that does not compromise the integrity of the skin structures unlike DMSO (Osborne and Musakhanian, 2018). Transcutol® has been previously used in cosmetics and oral and topical pharmaceutical formulations, according to studies made by Gattefossé undiluted Transcutol® caused no classifiable primary or cumulative skin irritation (Sullivan et al., 2014). For topical products, Transcutol® has been approved by the FDA concentrations up to 49,9% and the Good Manufacturing Practices in the USA endorses it since a 20 mg/kg concentration for dermal route and EMEA guidelines don't establish limits for Transcutol® in pharmaceutical products (Osborne and Musakhanian, 2018; Sullivan et al., 2014). Even so, Transcutol® in our project is used in a high concentration as a preliminary study so BNB has no solubility problem in the study of different enhancers (Mohammadi-Meyabadi et al., 2022). We have tested different types of enhancers: microneedle array as a physical enhancer to pierce stratum corneum (SC) and different chemical enhancers to modify the SC. Figure 2 shows the families of chemical enhancers we have considered for our study. The permeation and retention of BNB in skin studies need validated analytical methods to adequately quantify the drug in the tissue. To this end, Confocal Raman Spectroscopy (CRS) and high-performance liquid chromatographic (HPLC) were used. Raman spectroscopy imaging is noteworthy for its ability to analyze biomolecular information in samples. The process involves exciting the sample with visible or near-infrared laser light, leading to both elastic Rayleigh scattering and inelastic Raman scattering. The latter provides insights into the energy levels associated with molecular bond vibrations. Through spectral decomposition of the Raman signal, it becomes possible to probe and differentiate between active ingredients and endogenous skin components. Additionally, this analysis can unveil molecular modifications induced by actives on the skin. Raman spectra act as specific fingerprints, allowing for the identification and potential tracking of molecules within the skin, making it a valuable tool for studying cutaneous components and their interactions (Essendoubi et al., 2021).

CRS has been widely used in skin research, mainly as a qualitative technique that, as mentioned previously, allows you to differentiate the presence of the studied substance from among the other components of the skin. Recently, Caspers et al. reported a new application of CRS for the quantitative analysis of the amounts of compounds that penetrate the skin. The quantification of total skin uptake was performed by calculating the area under the depth profile curves (AUC) for the thickness of the stratum corneum (Caspers et al., 2019).

HPLC serves as an analytical method employed for the separation, identification, or quantification of individual components within a mixture. The separation process relies on the fundamental principle of column chromatography, and subsequent identification and quantification are achieved through spectroscopy techniques. We have validated two HPLC methods according to the International Conference on Harmonization (ICH) Q2A and ICH Q2B Guidelines for the quantification of BNB in Transcutol®P. One HPLC method used the UV detector for determining the drug extracted from the skin, and an HPLC with a fluorescence

detector was used for quantifying the drug in samples from the skin permeation tests, which needed a more sensitive method due to the lower concentration of BNB in these samples.

2. Materials and Methods

2.1. Materials

Transcutol®P [Diethylene glycol monoethyl ether] was bought at Gattefossé (Bacelona, Spain). Sigma-Aldrich (Madrid, Spain) supplied BNB and the permeation enhancers: Nonane, Lauryl acrylate, Squalene, Atone, Sebacic acid, (R)-(+)-Limnonene, α-Pinene, N-ethylpirrolidine, (+)-3-caren, 1-decanol, Myristic alcohol, Oleic acid, Menthol and Octanoic acid. BeautyBio GloPRO® roller microneedling for histological procedures were bought at Currentbody (Barcelona, Spain). Water Millipore MilliQ purification system (Millipore Corporation, Burlington, USA) was used to obtain ultrapure water for all experiments, and all the other chemical reagents used were of analytical grade.

2.2. Biological materials

Abdominal human skin (protocol code 93-01162 02/18 approved on 17/01/2020 by the Bioethics Committee of SCIAS Hospital de Barcelona), which was dermatomed to 400 µm thickness (Aesculap GA 630, Aesculap, Tuttligen, Germany).

2.3. Baricitinib solution preparation

A saturated solution of BNB was prepared by dissolving an excess of BNB in Transcutol®P and filtrating the leftovers with a 0.45 µm nylon filter. The saturated solution was used to assess the intrinsic permeation of BNB. Additionally, we prepared solutions of BNB at a concentration of 2 mg/mL with 5% of different enhancers, which are listed in Table 1.

2 mg/mL BNB solution was also included in the permeation study as the reference for evaluating the enhancement factor of the permeation enhancers. The concentration of 2 mg/mL has been chosen based on the daily oral dose currently available in the market as a reference. Since there is no data on BNB for topical application, we decided to start with this dose to assess its permeation capacity and safety in achieving a local effect.

Table 1. Permeation enhancers used in the study with their molecular formula, molecular mass, and CAS Register number.

Permeation enhancer	Molecular formula	Molecular Mass (g/mol)	CAS Register Number
Nonane	C_9H_{20}	128.26	111-84-2
Lauryl acrylate	$C_{15}O_2H_{28}$	240.38	2156-97-0
Squalene	$C_{30}H_{50}$	410.72	111-02-4
Azone	$C_{18}H_{35}NO$	281.5	59227-89-3
Sebacic acid	$C_{10}O_4H_{18}$	202.25	111-20-6
(R)-(+)-Limonene	$C_{10}H_{16}$	136.23	5989-27-5
α-Pinene	$C_{10}H_{16}$	136.23	80-56-8
N-ethylpirrolidine	C_4H_9N	71.12	123-75-1
(+)-3-caren	$C_{10}H_{16}$	136.23	498-15-7
1-Decanol	$C_{10}OH22$	158.28	112-30-1
Myristyl alcohol	$C_{14}OH_{30}$	214.39	112-72-1
Oleic acid	$C_{18}O_2H_{34}$	282.46	112-80-1
Menthol	$C_{10}OH_{20}$	156.27	89-78-1
Octanoic acid	$C_8O_2H_{16}$	144.21	124-07-2

CAS: Chemical Abstracts Service.

190 2.4. Ex vivo skin permeation test

191 The capacity of BNB to penetrate the skin and diffuse through it was evaluated by Franz
192 diffusion cells (Hanson Research, Chatsworth, CA, USA; Crown Glass Company, INC, NJ, USA).
193 The cells had a diffusion area of 2.54 cm^2 and a receptor compartment of 14 mL. The receptor
194 fluid was composed of Transcutol®P to maintain skin conditions. The experiment was
195 conducted at 32 ºC, and the receptor compartment was continuously stirred. To study the
196 intrinsic permeation of the drug, a saturated solution of BNB was tested on human skin
197 dermatomed at 400 µm. Both types of skin, healthy skin (non-treated) and skin treated with
198 microneedles were included. We used a roller with 540 titanium needles on 7.47 cm^2 (72.3
199 microneedles/cm^2) with a length of 0.25 mm to treat the skin by gently pressing the roller on
200 the skin surface. Both skin types were mounted on Franz cells and BNB saturated solution
201 was applied. Samples of 200 µL were taken and replaced afterwards with the same volume
202 of Transcutol®P at preestablished times over 24/30h. Table 2 describes the conditions used
203 in the ex vivo permeation tests.

204 Moreover, we tested different solutions of BNB 2 mg/mL with a chemical permeation
205 enhancer (Table 1). Aliquots of 600 µL of the BNB solution (either alone or with an enhancer)
206 were added to the skin. Samples of 200 µL were collected at different time points replacing
207 the same volume with fresh receptor fluid immediately after each sample collection to
208 maintain the cell volume constant throughout the test. The sampling time points and the
209 duration of the experiment for the intrinsic permeation and the chemical enhancers'
210 permeations were set based on previous experiments conducted during the method
211 development phase to obtain a meaningful sampling of the permeation profile. The tests
212 were conducted in triplicate.

213 The samples obtained in both tests were quantified by HPLC coupled to a fluorescence
214 detector, as described in section 2.8.

215 **Table 2.** Experimental conditions for the ex vivo skin permeation tests.

Condition	Description
Receptor fluid:	Transcutol®P
Cell volume:	14 mL
Diffusion area:	2.54 cm^2
Membrane:	Human skin
Thickness:	400 µm
Replicates:	5 replicates
Temperature:	32 ± 0.5 ºC
Stirring:	500 r.p.m.
Dose:	600 µL
Sample volume:	200 µL

216 2.5. Amount of drug retained in the skin.

217 We also investigated the amount of BNB retained in the skin [Qret (µg/g skin/cm^2)]. To this
218 end, the skin was removed from the diffusion cells after finishing the permeation test and
219 rinsed with distilled water. The area of the skin exposed to the permeation was cut out,
220 weighed, and the drug was extracted with 2 mL of Transcutol®P for 10 minutes using an
221 ultrasonic water-bath. The solvent was collected and quantified by HPLC prior filtration
222 (section 2.8). The Qret was determined per area and weight of skin (2.54 cm^2), and multiplied
223 by the recovery factor of the drug (equation 1):

$$Qret = Qext/(W \times A) \times 100/R \quad (1)$$

Where Qret is the amount of drug extracted from the skin, W is the weight of the skin, A is the diffusion area and R is the recovery (Cañadas-Enrich et al., 2018).

2.6. Biopharmaceutical parameter data analysis

The permeation profile was obtained from the cumulative permeated amounts of BNB versus time. The flux was determined considering the linear portion of the permeation profile by regression analysis (GraphPad Software Inc. version 5.0, San Diego, CA, USA) Software (Sanz et al., 2017). The resulting slope, corresponded to the flux, which is described in equation 2:

$$Jss = Q_t/(A \cdot t), \quad (2)$$

Where, Jss is the flux ($\mu g/h \cdot cm^2$) at the steady state; Qt is the amount of drug in the receptor fluid that diffused through the skin (µg); A is the cell diffusion area (cm^2); and t is the time that the receptor medium has been accepting the drug (h).

The permeability coefficient was calculated by the ratio of flux and initial concentration (equation 3):

$$Kp = Jss/C_0 \quad (3)$$

Where, Kp is the permeability coefficient expressed as cm/h; Jss is the flux, and C_0 corresponds to the initial concentration of drug applied expressed as µg/mL.

The predicted plasma concentration at the steady state in human was determined according to the equation 4:

$$Css = Jss \cdot A/[Cl_p], \quad (4)$$

Css (µg/mL) provided the predicted concentration of BNB in the plasma considering a hypothetical surface of application of 10 cm^2 (A), and the plasma clearance in humans (Clp) (Gómez-Segura et al., 2020) which was obtained from the literature, 9.42 L/h (CHMP, n.d.).

Css (µg/mL) provided the predicted concentration of BNB in the plasma considering a hypothetical surface of application of 10 cm^2 (A), and the plasma clearance in humans (Clp) (Gómez-Segura et al., 2020) which was obtained from the literature, 9.42 L/h (CHMP, n.d.).

The mean transit time (MTT) indicates the time in which the BNB crosses the skin. The MTT of BNB was calculated in the skin treated with enhancers and in non-treated skin in accordance with the equation 5 (Silva-Abreu et al., 2018):

$$MTT = V/(P_1 \times P_2 \times Ae) + 1/(2 \times P_2) \ , \quad (5)$$

where V is the volume of the donor compartment, P_1 is the partition coefficient, P_2 is the diffusion coefficient, and Ae is the diffusional area of the skin.

The partition coefficient (P_1) and the diffusion coefficient (P_2) were calculated using the following equations, equations 6 and 7 (Silva-Abreu et al., 2018):

$$Kp = P_1 \cdot P_2 \quad (6)$$

$$P_2 = 1/6 \cdot Tl \quad (7)$$

Tl is the lag time which was determined by extrapolating from the linear segment of the permeation profile to the x-axis (Gujjar and Banga, 2014).

And finally, the enhancement factor (EF) was calculated as the ratio of the permeability coefficient (Kp) of the enhancer and the non-treated skin (equation 8) (Shaikh et al., 2009):

$$EF = Kp\ enhancer/Kp\ (non\text{-}treated), \quad (8)$$

2.7. Confocal Raman profiling

The Raman analysis was performed using a Model 3510 SCA Skin Analyzer equipped with RiverICon version 3.0.130327 software from RiverD International B.V., Rotterdam, The Netherlands. The instrument was fitted with two near-infrared (NIR) lasers, emitting monochromatic light at 785 nm and 690 nm, respectively. Spectra were recorded in two regions: the fingerprint region (FP) (400–1800 cm^{-1}) and the high wavenumber region (HWN) (2500–4000 cm^{-1}).

Before the experiment, the instrument was calibrated using an external National Institute of Standards and Technology (NIST) glass calibration standard, as well as the instrument's internal Raman calibration standards, which included a neon lamp and a polymethylmethacrylate Raman sample. Calibration success was determined by meeting the built-in criteria in the software and achieving a signal-to-noise ratio above 30.

To obtain the Raman profile of BNB, ten frames were taken sequentially with a 30-second exposure time, and the average of these frames was calculated. Two different solutions were prepared using solvents. A 2% BNB solution in Transcutol and a 5% BNB solution in DMSO were prepared, along with DMSO and Transcutol blanks. The purpose of using these blanks was to remove the reference signals from the solvents, allowing us to isolate and analyse the signal specific to the drug.

Thus, vast majority of Raman spectroscopy uses a single wavelength like 785 nm and focuses on the FP region from 450 to 1750 cm^{-1}, which covers Raman signatures of many skin components including natural moisturizing factor (NMF), ceramide, uranic acid, etc. However, the HWN region (2800–3800 cm^{-1}) containing prominent Raman peaks of water and methyl groups is also critical in tissue hydration (Zhang et al., 2021).

2.8. Validation of the analytical methods

Due to the wide concentration range of the samples obtained in the ex vivo permeation study and the drug extraction from the skin, two analytical methods by high performance liquid chromatography (HPLC) for the quantification of BNB were validated: HPLC-UV for samples whose concentrations were within the range 2.5 - 40 µg/mL, and HPLC-Fluorescence for those samples ranging within the concentrations of 0.063 to 1 µg/mL. The HPLC-UV consisted of a Waters 1525 pump and a 2487 UV-VIS detector (Waters, Milford, USA) at a wavelength of 310 nm, and the HPLC coupled to a fluorescence detector (HPLC-F) consisted of a Chromatograph Waters Alliance 2695 and a Fluorescence Jasco FP-1520 detector at an Ex-wavelength of 310 nm and an EM wavelength of 390 nm. The mobile phase consisted of Ammonium Formate 10 mM pH 7: ACN (75:25 v/v) under isocratic elution at a flow rate of 1 mL/min in a Symmetry C18 column (4.6 x 75 mm, 3.5 µm) for both methods, and the injection volume for both methods was 10 µL.

The calibration curves for both analytical methods were prepared by diluting BNB in Transcutol®P starting from a stock solution of 60 µg/mL of BNB in Transcutol®P. Below we list the concentration of the working standard solutions:

- HPLC-F curve: 0.063, 0.125, 0.25, 0.5 and 1 µg/mL;
- HPLC-UV curve: 2.5, 5, 10, 20 and 40 µg/mL.

Empower 3 software (Waters, Milford, USA) was used to process the data. The validation of the methods was performed as described in the ICH Q2A and ICH Q2B Guidelines (ICH Expert Working Group, 2005), in terms of, precision, accuracy, linearity, sensitivity and specificity.

2.8.1. Linearity

Five calibration curves at 5 concentration levels were prepared to evaluate the linearity of both methods. The correlation coefficient (r^2) of the calibration curves was calculated by linear regression analysis, and the response factor for each calibration curve was evaluated, by one-way analysis of variance (ANOVA).

2.8.2. Accuracy and Precision

The inter-day precision of both methods was determined with five calibration curves prepared on different days by two different researchers and the relative standard deviation (%RSD) indicated the precision at each concentration level.

The accuracy was assessed by calculating the percentage of relative error (%RE) of the estimated concentration to the nominal one, at each concentration level (Equation 9):

$$\%RE=(C_0\text{-}Cn)/Cn \times 100, \quad (9)$$

where, C_0 is the observed concentration and Cn is the nominal concentration.

2.8.3. Sensitivity and specificity

The limits of detection (LOD) and quantification (LOQ) led to stablish the sensibility of the methods. The LOD and LOQ were calculated starting from the relationship between the standard deviation of the response and the slope of the calibration curve. Equation 10 and Equation 11 describe the estimation of LOD and LOQ, respectively:

$$LOD = [3.3\ s/p], \quad (10)$$

$$LOQ = [10\ s/p] \quad (11)$$

where, s is the standard deviation of the response, and p is the slope of the calibration curve.

The specificity was evaluated as the absence of any peaks interfering at the retention time of BNB in the chromatographic conditions.

2.9. Statistical analysis

Prism®, v. 5.00 software (GraphPad Software Inc., San Diego, CA, USA) was used for all statistical studies. The T-test was performed on the permeation with non-treated and treated skin with microneedles and ANOVA analysis was conducted on the permeation data regarding the chemical enhancers with statistical significance of $p<0.05$.

3. Results

3.1. Ex vivo skin permeation studies

Permeation studies investigated both the effect of physical promoters, such as microneedles, and the effect of chemical promoters.

333 3.1.1. Intrinsic permeation of baricitinib in human skin (non-treated and treated skin with
334 microneedles)

335 First, the intrinsic permeation study was performed using a saturated solution of BNB in
336 Transcutol®P on intact healthy skin and skin treated with microneedles as a physical
337 promoter. We present the results of the following study in Table 3, which shows us
338 permeation parameters such as the mean transit time in the skin (MTT, days) and the
339 enhancer factor (EF), and Figure 3, where we can observe the drug permeation profile in both
340 types of skin, its flux (Jss, µg/h·cm^2), the permeability coefficient of BNB to permeate each of
341 the skins (Kp, cm/h), and finally, the predicted plasma concentration at the steady-state in
342 human skin (Css, µg/mL).

343 **Table 3.** Biopharmaceutical parameters of BNB solutions with and without physical
344 penetration enhancer.

Parameter	Normal skin	Treated with microneedles
MTT (days)	93.8	31.2
EF	-	3.0

345 MTT = mean transit time in the skin; EF= enhancement factor.

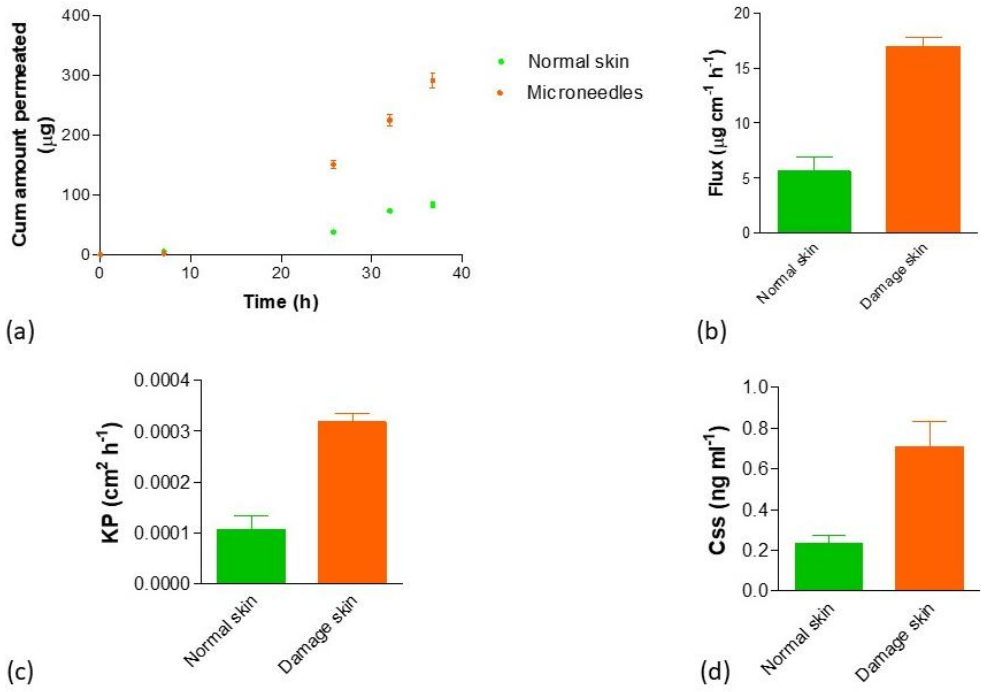

346

347 **Figure 3.** BNB permeation profile in normal and skin treated with microneedles: (a) BNB
348 cumulative amount permeated (µg) vs time (h); (b) BNB solutions flux (Jss; µg/h·cm^2); (c) The
349 permeability coefficient of BNB (Kp; cm/h); (d) Predicted plasma concentration of BNB at the
350 steady state in the plasma considering a hypothetical surface of application of 10 cm^2 (Css)
351 (ng/mL). Results are expressed by mean ± SD (n = 5). T-test analysis of variance with a
352 statistically significant difference: ** = $p < 0.01$; *** = $p < 0.0001$.

353 In all cases, the value of the studied parameters was higher in the skin treated with
354 microneedles compared to normal skin, with the amount permeated in the skin where we
355 used the physical enhancer being 2.5 times higher than the amount permeated in normal
356 skin.

3.1.2. Evaluation of Chemical enhancers on baricitinib's permeation through human skin

The impact of the chemical enhancers was assessed by a permeation study using a 2mg/mL solution of BNB in Transcutol®P with different chemical enhancers on intact healthy skin The permeation profile of BNB with the tested enhancers and without enhancer is presented in Figure 4, the Jss (μg/h·cm^2) is depicted in Figure 5 and Table 4 shows the rest of the permeation parameters: Kp (cm/h), Css (μg/mL), the MTT (days) and the EF for each penetration enhancer. A solution at the same concentration of BNB was used as a control (Non E). See Table 4 for the equivalence of the enhancers code and their identity.

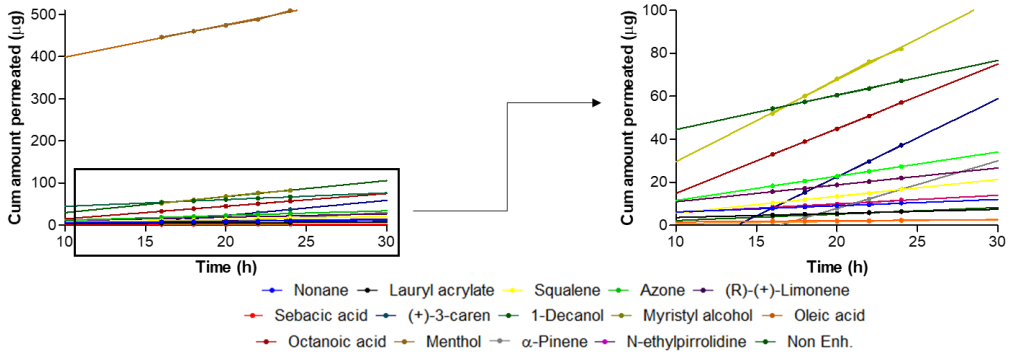

(a) **(b)**

Figure 4. BNB permeation profile: BNB cumulative amount permeated (μg) vs time (h): (a) Mean cumulative amount BNB permeated; (b) mean cumulative amount BNB permeated without M enhancer.

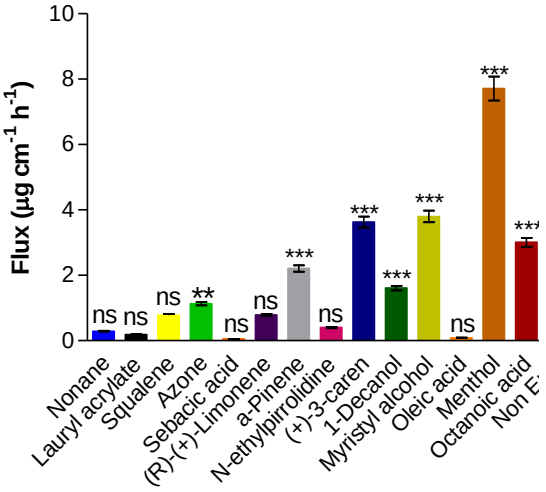

Figure 5. Flux of BNB obtained from the permeation of solutions with different enhancers and comparison to the plain solution without chemical enhancer. Results are expressed by mean ± SD (n = 5). ANOVA with Turkey's Multiple Comparison Test. Statistically significant difference between solutions vs no enhancer: ** = $p < 0.01$; *** = $p < 0.0001$.

Table 4. Biopharmaceutical parameters of BNB solutions with and without a penetration enhancer. Parameters presented are amount of BNB retained in the skin (Kp), predicted plasma concentration of BNB at the steady state in humans (Css), mean transit time in the skin (MTT) and enhancer factor (EF).

Permeation enhancer	Kp (x 10^{-4} cm/h)	Css (ng/mL)	MTT (days)	EF

Nonane	0.57±0.05	0.12±0.01	NA	0.97
Lauryl acrylate	0.37±0.03	0.08±0.01	NA	0.63
Squalene	1.54±0.16	0.33±0.02	64.1	2.59
Azone	2.22±0.23	0.47±0.05	NA	3.73
Sebacic acid	0.10±0.01	0.02±0.00	NA	0.17
(R)-(+)-Limonene	1.55±0.15	0.33±0.03	NA	2.61
α-Pinene	4.35±0.42	0.92±0.09	22.7	7.32
N-ethylpirrolidine	0.79±0.08	0.17±0.02	NA	1.33.
(+)-3-caren	7.14±0.74	1.51±0.16	13.8	12.02
1-Decanol	3.17±0.32	0.67±0.07	NA	5.33
Myristyl alcohol	7.49±0.78	1.59±0.17	13.2	12.60
Oleic acid	0.18±0.01	0.04±0.00	535.2	0.31
Menthol	15.18±1.60	3.22±0.34	NA	25.55
Octanoic acid	5.92±0.60	1.26±0.13	16.6	9.97
Non-Enhancer	0.59±0.06	0.13±0.01	165.7	-

Results are expressed by mean ± SD (n = 5).

Menthol by far achieves superior permeation compared to the other studied situations, followed by Myristyl alcohol and (+)-3-carene. Specifically, compared to permeation without using any chemical enhancer, they manage to multiply the permeation of BNB in the skin by 25, 12, and 12, respectively.

3.2. Amount of drug retained.

In both permeation studies, the potential drug retained in the skin was extracted for quantification purposes. The drug extracted from the skin was analyzed by UV HPLC and the amount of BNB retained in the skin was calculated starting from the concentration in the samples' results according to equation 1 in both experiments, the one executed with saturated solution and the ones with the 2 mg/mL solution.

3.2.1. Intrinsic permeation of baricitinib in human skin (non-treated vs. treated skin with microneedles)

The BNB retained in the skin after conducting the permeation study, both in non-treated skin and treated skin, is shown in Figure 6 and Table 5, skin treated with microneedles retained about 2.5-fold BNB more than non-treated skin.

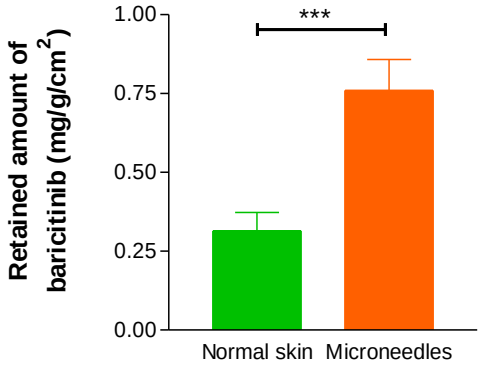

Figure 6. BNB amount retained in skin. Results are expressed as mean ± SD (n = 5). t-test analysis of variance. Statistically significant difference: *** = $p < 0.0001$.

Table 5. The amount of BNB retained in the skin is expressed as mg/g/cm^2 and the percentage of the amount spread at the beginning.

	Qret (mg/g/cm^2)	**% BNB retained (%/g skin)**

Non-treated skin	0.31±0.06	6.66±0.99
Treated skin with MN	0.76±0.09	16.08±1.90

Results are expressed by mean ± SD (n = 5). MN: microneedles.

3.2.2. Evaluation of the effect of chemical enhancers on baricitinib's permeation through skin

The BNB retained in the skin after conducting the permeation study with different chemical enhancers is shown in Figure 7. The enhancer which led to a higher retention of BNB in the skin was B (Lauryl acrylate). Table 6 shows the amount and percentage retained in the skin for each enhancer tested, as well as the drug amount retained in the skin with no enhancer.

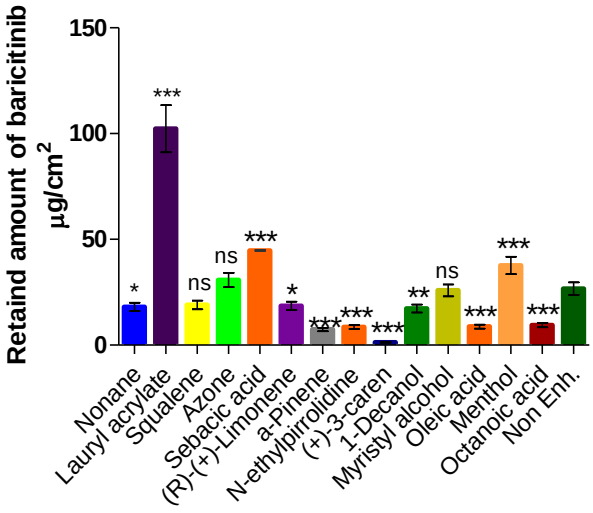

Figure 7. BNB amount retained in the skin treated with different permeation enhancers. Results are expressed as mean ± SD (n = 5). ANOVA with Turkey's Multiple Comparison Test. Statistically significant difference between solutions vs No enhancer: * = $p < 0.05$; ** = $p < 0.01$; *** = $p < 0.0001$.

Table 6. BNB amount retained in skin expressed as µg/cm^2 and %/g of BNB retained from the initial amount of seeding.

Code	Permeation enhancer	Qret (µg/cm^2)	% BNB retained (%/g skin)
A	Nonane	1.04 ± 0.21	0.08 ± 0.01
B	Lauryl acrylate	5.91 ± 0.53	0.49 ± 0.04
C	Squalene	1.10 ± 0.13	0.09 ± 0.01
D	Azone	1.78 ± 0.12	0.14 ± 0.01
E	Sebacic acid	2.59 ± 0.22	0.21 ± 0.01
F	(R)-(+)-Limonene	1.07 ± 0.12	0.09 ± 0.01
G	α-Pinene	0.43 ± 0.02	0.03 ± 0.00
H	N-ethylpirrolidine	0.49 ± 0.35	0.04 ± 0.02
I	(+)-3-caren	0.08 ± 0.00	0.00 ± 0.00
J	1-Decanol	1.00 ± 0.09	0.08 ± 0.00
K	Myristyl alcohol	1.50 ± 0.12	0.12 ± 0.01
L	Oleic acid	0.51 ± 0.04	0.04 ± 0.00
M	Menthol	2.18 ± 0.19	0.18 ± 0.01
N	Octanoic acid	0.55 ± 0.06	0.05 ± 0.00
Non-E	-	1.55 ± 0.17	0.13 ± 0.01

Results are expressed as mean ± SD (n = 5).

3.3. Confocal Raman Profiling

The profile of the confocal spectrum of BNB is depicted in the following figure. We present the spectrum in the HWN range (2500-4000 cm^{-1}) and the FP region (400-1800 cm^{-1}).

Analyzing the spectra obtained from the Transcutol solution and the DMSO solution in Figure 8, we present the signal obtained with DMSO, as we observe that it exhibits higher quality and definition.

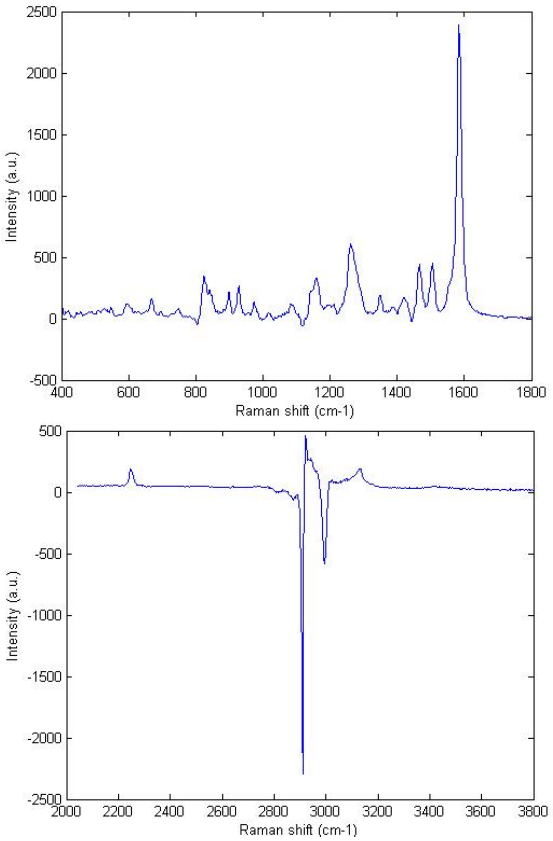

Figure 8. BNB spectrum based on the isolated signal attributed to BNB from the spectra of BNB solution on DMSO. Left: FP region and right: HWN region.

As we can see in Figure 8, BNB shows enhancement of vibrational modes around 1600 cm^{-1}, which can be indicative of the purine structure present in BNB. The band near 1200 cm^{-1} corresponds to the sulfone group. Finally, in the HWN, we observe a peak around 2810–2960 cm^{-1} that is associated with the C-CH_3 bonds.

3.4. Validation of analytical methods

Two validated methods were established for quantifying BNB in the collected samples. Due to the low concentration in ex vivo permeation test samples, an HPLC-fluorescence method was developed and validated. For higher concentration, samples obtained from skin extraction after permeation tests, an HPLC-UV method was utilized and validated. The results of both method validations are detailed in the subsequent sections.

3.4.1. HPLC-UV method

The parameters studied included linearity, accuracy, precision, specificity, and sensitivity. Figure 9 shows the calibration curves obtained; the r^2 values of each calibration curve were >0.999. The ANOVA showed no statistically significant differences between the response

factor obtained ($p > 0.05$) demonstrating that the method is linear within the concentration range of 2.5 - 40 µg/mL.

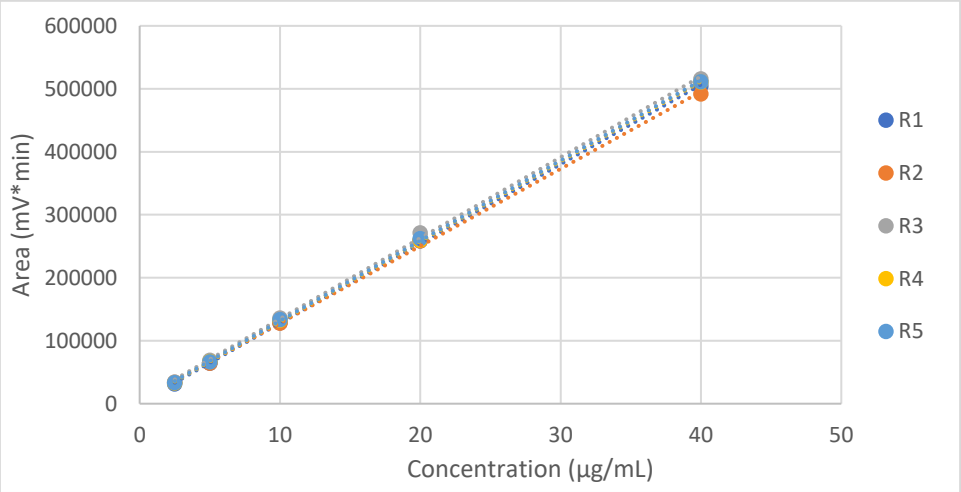

Figure 9. Linearity of the HPLC-UV method for the quantification of BNB within the concentration range of 2.5 - 40 µg/mL. The linearity was assessed by linear regression of the response (area) versus concentration from the standard working solutions by quintuplicated.

The accuracy and precision of the method were calculated as the percentage of the RE and the RSD, respectively. The data are shown in Table 7. The results of the %RE and %RSD are below 10% indicating that the method has enough precision and accuracy within the range 2.5 – 40 µg/mL, this criterium is based on the ICH Q2 and Q14 guidelines (Committee for Medicinal Products for Human Use, 2022; ICH Expert Working Group, 2005).

Table 7. Accuracy (%RE) and inter-day precision (%RSD) for BNB standard solutions. Estimated concentration results are expressed by mean ± SD (n = 5).

Concentration of the standard solution (µg/mL)	**Estimated Concentration (µg/mL)**	**%RE** (%)	**%RSD** (%)
2.50	2.28 ± 0.06	8.50	2.90
5.00	4.90 ±0.06	1.81	1.28
10.00	10.09 ± 0.06	-0.96	0.69
20.00	20.41 ± 0.22	-2.06	1.11
40.00	39.79 ± 0.09	0.51	0.24

The specificity of the analytical method was demonstrated because there was no interference of any other compound at the retention time of BNB (Figure 10). The retention time of BNB was 3.16 min.

The LOQ provided the sensitivity of the method. Both, the LOD and the LOQ, were calculated from the standard deviation of the response and the slope of the calibration curve of 2.5 - 40 µg/mL. According to equations 8 and 9, the LOD for BNB was established at 0.70 ± 0.29 µg/mL and the LOQ was established at 2.11 ± 0.31 µg/mL. These results indicate that the method is sensitive enough for the quantification of BNB in the samples from the drug extraction procedure.

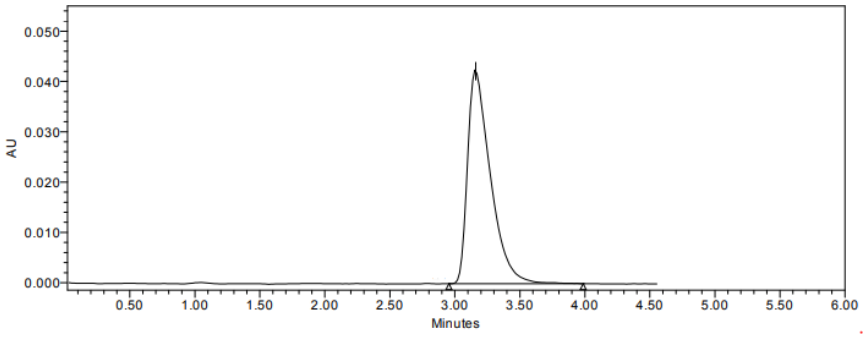

Figure 10. Chromatogram of BNB standard 40 µg/mL.

3.4.2. HPLC-fluorescence method

As in the HPLC-UV method, the parameters studied were linearity, accuracy, precision, specificity, and sensitivity. The r^2 values of each calibration curve were >0.999 as Figure 11 shows. The ANOVA showed no statistically significant differences between the response areas obtained (p = 0.05) demonstrating that the method is linear within the concentration range of 0.063 – 1.000 µg/mL.

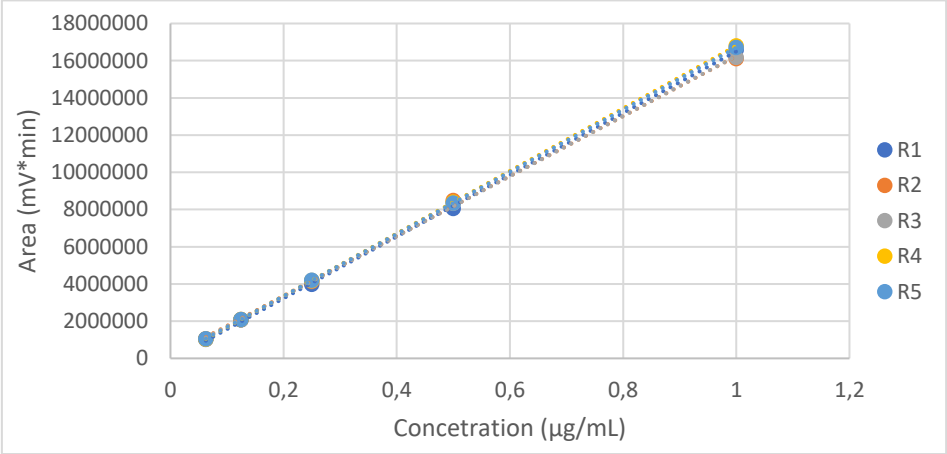

Figure 11. Linearity of the HPLC-F method for the quantification of BNB within the concentration range of 0.063 – 1.000 µg/mL. The linearity was assessed by linear regression of the response (area) versus concentration from the standard working solutions by quintuplicated.

The accuracy and precision of the method were obtained within the concentration range of 0.063 – 1.000 µg/mL. The results are shown in Table 8 expressed as percentages of the %RE and %RSD, respectively. These results show suitable precision and accuracy for the intended analysis (Committee for Medicinal Products for Human Use, 2022; ICH Expert Working Group, 2005).

Table 8. Accuracy and inter-day precision for BNB standard solutions. Estimated concentration results are expressed by mean ± SD (n = 5).

Concentration of the standard solution (µg/mL)	Estimated Concentration (µg/mL)	%RE (%)	%RSD (%)
0.063	0.06 ± 0.00	-1.31	4.08
0.125	0.12 ± 0.00	0.11	1.65
0.250	0.25 ± 0.00	-0.22	1.16
0.500	0.50 ± 0.01	0.82	2.22
1.000	1.00 ± 0.01	-0.23	0.63

The analytical method was considered specific because it demonstrated that there is no interference of any other compound at the retention time of BNB (Figure 12). The retention time of BNB was 3.16 min.

Figure 12. Chromatogram of BNB standard 0.25 µg/mL.

The LOD and LOQ were calculated within the concentration range 0.063 - 1 µg/mL, the LOD for BNB was established at 0.0116 ± 0.009 µg/mL and the LOQ was established at 0.040 ± 0.006 µg/mL. These results indicate that the method is sensitive enough for the determination of BNB in samples from the receptor fluid collected in the ex vivo permeation assays.

4. Discussion

In this work, we have investigated the use of different enhancers, both chemical and physical strategies to enhance BNB's availability in the skin. The receptor medium used in the permeation tests was glycol monoethyl ether (DEGEE), commercially known as Transcutol®P; we selected this solvent because of it is highly soluble and its safety profile is good and therefore it does not compromise the integrity of the skin structures (Osborne and Musakhanian, 2018).

For the first time, we were able to observe the BNB spectrum using this technique. The FP region is crucial for identifying and characterizing molecular structures, it contains unique vibrational modes associated with specific chemical bonds, allowing for the identification of functional groups and overall molecular structure. In drug analysis, the FP is often essential for confirming the identity of a particular drug compound. The HWNs associated with functional groups involving hydrogen atoms. It is important for studying hydrogen bonding, which can provide information about the molecular interactions and the solid-state structure of the sample. We initially employed the CR technique to explore the depth of BNB penetration into the skin. The signal strength proved insufficient for studying the low concentrations typical of our permeation and retention studies. The primary requirement for conducting measurements using CRS is that the molecule under examination must exhibit spectral characteristics of adequate intensity, allowing the signals to be distinguished from those originating from the skin components. This limitation was not due to the inefficiency

of the CRS technique but rather to the specific solution we aimed to use for our study which was not sufficient at the low concentrations we found the drug to overcome the various usual noises present in the measurement and surpass the signal from the pigskin. Consequently, we continued our analyses using the HPLC.

Solid metal microneedles were used to evaluate the permeation of BNB in human skin. As expected, the skin treated with microneedles showed an increased permeation of BNB. The use of microneedles causes an annular pathway that in-creases permeability. So, this is a strategy to consider in the topical delivery of BNB since microneedles are minimally invasive and painless due to their small size, as indicated by their name. Not only was the permeation enhanced by the microneedles, but also more of the drug was retained in the skin treated. This fact allows a depot effect that may improve the effectiveness of the treatment since a higher amount of the drug is deposited in the target organ. In a healthy adult who has been administered a multiple dose of 2 mg once a day, the Css is 5 ng/mL. This concentration is higher than the predicted Css that we achieve by administering a saturated solution of BNB on treated skin using microneedles (CHMP, 2020). With greater precision the maximum concentration (Cmax) reached when multiple doses of 2 mg are taken every 24 hours is 16.96 ng/mL and the minimum concentration of 3.57 ng/mL, so taking these data into account, we can consider that the saturated concentration of BNB does not reach the minimum concentration necessary to have a therapeutic effect (Shi et al., 2014).

Concerning the chemical permeation enhancers, menthol showed the greatest effect on BNB's permeation through human skin enhancing the permeation about 25-fold with respect to the non-enhancer (Wang and Meng, 2017). Myristyl alcohol, carene and octanoic acid followed the menthol effect in decreasing order. Menthol belongs to the terpenes class. These compounds have shown to increase the permeation of lipophilic drugs by disrupting the structure of the lipids in the SC or by interacting with the intracellular proteins or by increasing the partition coefficient of drug-co-solvent (Maibach and Wane Smith, 2005). Myristyl alcohol is a saturated fatty alcohol with 14 carbon atoms (C14). There are several studies on the impact of the length of the carbon chain of fatty acids on permeation enhancement, a number around C12 showed an optimal balance between the affinity to the skin and the partition coefficient, a shorter chain may be not lipophilic enough for the skin (for instance, octanoic acid) and longer chains may have high affinity to the stratum corneum lipids (Maibach and Wane Smith, 2005). Nevertheless, when evaluating the amount retained in the skin, it should be noted that lauryl acrylate showed the maximum effect although it had a low flux value. This enhancer offers good prospects as it restricts the drug's permeation yet retains the drug within the skin. While this might not suffice for a systemic effect, the retained drug in the tissue can effectively target the affected area of the skin (Shi et al., 2014). This targeted approach helps avoid the systemic side effects that often arise when the drug is taken orally.

To analyze the samples generated in the study, we developed and validated two new methods, an HPLC-UV method with isocratic elution which has the advantages of being faster and simpler than those already published in the literature (Gandhi and Kapoor, 2019; Hoang et al., 2021) for samples from the drug extraction from the skin. For those samples with lower drug concentration (receptor fluid from the permeation assays), a second HPLC method coupled to a fluorescence detector was developed. It was highly sensitive. To our knowledge, there are no publications dealing with any analytical fluorescence techniques for this drug.

In summary, microneedles improved the permeation and retention of the drug through and in the skin within a range of 2 to 3-fold. Terpenes and fatty acids had a higher impact on the BNB's permeation, particularly, menthol enhanced 25-fold BNB's permeation compared to a plain solution, and esters can multiply the retention of BNB in the skin up to 3 times. Hence, the percutaneous delivery of BNB is a promising alternative to the oral.

5. Conclusions

This study has evaluated the permeation of the drug with a saturated solution of BNB in Transcutol@P and the permeation capacity of the drug at the concentration level of 2 mg/mL. The effect of physical and chemical permeation enhancers on the BNB's permeation has also been examined.

The physical enhancer, which consisted of solid titanium microneedles to treat the skin before applying the saturated solution of BNB, led to a 2.5-fold enhanced permeation of BNB and the retention of the drug in the skin. And menthol as a chemical enhancer, increased 25-fold the permeation of BNB compared to a plain solution. In contrast, Lauryl acrylate showed a lower permeability coefficient than the plain solution of BNB, but a higher retention of the drug in the skin.

Additionally, a novel Raman spectrum of BNB has been published and two novel HPLC analytical methods for the determination of BNB in samples from the permeation assays and the drug extraction from the skin were validated, an HPLC-UV method and an HPLC-fluorescence method for the lower concentration samples. Both methods resulted to be specific, linear, precise, and accurate within the range 2.5 – 40 µg/mL for the HPLC-UV and 0.063 – 1 µg/mL for the HPLC-fluorescence.

Author Contributions: Conceptualization, A.C.C. and M.M.; methodology, A.C.C. and M.M.; software, A.C.C.; validation, A.C.C., M.M. and H.C.; formal analysis, A.C.C.; investigation, N.G., R.M. and N.B.; resources, A.C.C., M.M. and H.C.; data curation, A.C.C. and M.M.; writ-ing—original draft preparation, N.G..; writing—review and editing, A.C.C. and M.M.; visualiza-tion, M.M.; supervision, A.C.C., M.M. and H.C.; project administration, A.C.C., M.M. and H.C.; funding acquisition, A.C.C., M.M. and H.C. All authors have read and agreed to the published version of the manuscript.

Funding: This research received no external funding.

Institutional Review Board Statement: The study was conducted in accordance with the Decla-ration of Helsinki, and approved by the Bioethics Committee of SCIAS Hospital de Barcelona (protocol code 93-01162 02/18 approved on 17/01/2020.

Informed Consent Statement: Not applicable.

Data Availability Statement: The data presented in this study are available on request from the corresponding author. The data are not publicly available due to their being part of a Doctoral Thesis and it will be available once the Thesis has been published.

Acknowledgments: The authors would like to thank Rubèn Valle-Llop for his technical assistance, and Harry Paul for editing the English language.

Conflicts of Interest: The authors declare no conflict of interest.

References

Alshetaili, A.S., 2019. Solubility and Solution Thermodynamics of Baricitinib in Six Different Pharmaceutically Used Solvents at Different Temperatures. Zeitschrift für Physikalische Chemie 233, 1129–1144. https://doi.org/10.1515/zpch-2018-1323

Anwer, M.K., Ali, E.A., Iqbal, M., Ahmed, M.M., Aldawsari, M.F., Saqr, A. Al, Ansari, M.N., Aboudzadeh, M.A., 2022. Development of sustained release baricitinib loaded lipid-polymer hybrid nanoparticles with improved oral bioavailability. Molecules 27. https://doi.org/10.3390/molecules27010168

Bieber, T., Feist, E., Irvine, A.D., Harigai, M., Haladyj, E., Ball, S., Deberdt, W., Issa, M., Grond, S., Taylor, P.C., 2022. A Review of Safety Outcomes from Clinical Trials of Baricitinib in Rheumatology, Dermatology and COVID-19. Adv Ther 39, 4910–4960. https://doi.org/10.1007/s12325-022-02281-4

Cañadas-Enrich, C., Abrego, G., Alvarado, H.L., Calpena-Campmany, A.C., Boix-Montañes, A., 2018. Pranoprofen quantification in ex vivo corneal and scleral permeation samples: Analytical validation. J Pharm Biomed Anal 160, 109–118. https://doi.org/10.1016/j.jpba.2018.07.015

Caspers, P.J., Nico, C., Bakker Schut, T.C., de Sterke, J., Pudney, P.D.A., Curto, P.R., Illand, A., Puppels, G.J., 2019. Method to quantify the in vivo skin penetration of topically applied materials based on confocal Raman spectroscopy. Transl Biophotonics 1. https://doi.org/10.1002/tbio.201900004

CHMP, 2020. Assessment report: Olumiant. Amsterdam.

CHMP, n.d. Anexo I - Ficha Técnica o Resumen de las características del producto.

Committee for Medicinal Products for Human Use, 2022. ICH guideline Q14 on analytical procedure development.

Committee for Medicinal Products for Human Use (CHMP), 2020. Olumiant - Assesment report. London.

Csóka, G., Marton, S., Zelko, R., Otomo, N., Antal, I., 2007. Application of sucrose fatty acid esters in transdermal therapeutic systems. European Journal of Pharmaceutics and Biopharmaceutics 65, 233–237. https://doi.org/10.1016/j.ejpb.2006.07.009

Essendoubi, M., Alsamad, F., Noël, P., Meunier, M., Scandolera, A., Sandré, J., Manfait, M., Gobinet, C., Reynaud, R., Piot, O., 2021. Combining Raman imaging and MCR-ALS analysis for monitoring retinol permeation in human skin. Skin Research and Technology 27, 1100–1109. https://doi.org/10.1111/srt.13069

Fava, A., Petri, M., 2019. Systemic lupus erythematosus: Diagnosis and clinical management. J Autoimmun 96, 1–13. https://doi.org/10.1016/j.jaut.2018.11.001

Fox, L.T., Gerber, M., Plessis, J. Du, Hamman, J.H., 2011. Transdermal Drug Delivery Enhancement by Compounds of Natural Origin. Molecules 16, 10507–10540. https://doi.org/10.3390/molecules161210507

635 Gandhi, S.V., Kapoor, B.G., 2019. Development and Validation of UV Spectroscopic Method
636 for Estimation of Baricitinib. Journal of Drug Delivery and Therapeutics 9, 488–491.
637 https://doi.org/10.22270/jddt.v9i4-s.3230

638 Gómez-Segura, L., Parra, A., Calpena-Campmany, A.C., Gimeno, Á., de Aranda, I.G., Boix-
639 Montañes, A., 2020. Ex Vivo Permeation of Carprofen Vehiculated by PLGA Nanoparticles
640 through Porcine Mucous Membranes and Ophthalmic Tissues. Nanomaterials 2020, Vol. 10,
641 Page 355 10, 355. https://doi.org/10.3390/NANO10020355

642 Gujjar, M., Banga, A., 2014. Iontophoretic and Microneedle Mediated Transdermal Delivery
643 of Glycopyrrolate. Pharmaceutics 6, 663–671.
644 https://doi.org/10.3390/pharmaceutics6040663

645 Hoang, T.N., Pino, M., Boddapati, A.K., Viox, E.G., Starke, C.E., Upadhyay, A.A., Gumber, S.,
646 Nekorchuk, M., Busman-Sahay, K., Strongin, Z., Harper, J.L., Tharp, G.K., Pellegrini, K.L.,
647 Kirejczyk, S., Zandi, K., Tao, S., Horton, T.R., Beagle, E.N., Mahar, E.A., Lee, M.Y.H., Cohen, J.,
648 Jean, S.M., Wood, J.S., Connor-Stroud, F., Stammen, R.L., Delmas, O.M., Wang, S., Cooney,
649 K.A., Sayegh, M.N., Wang, L., Filev, P.D., Weiskopf, D., Silvestri, G., Waggoner, J., Piantadosi,
650 A., Kasturi, S.P., Al-Shakhshir, H., Ribeiro, S.P., Sekaly, R.P., Levit, R.D., Estes, J.D.,
651 Vanderford, T.H., Schinazi, R.F., Bosinger, S.E., Paiardini, M., 2021. Baricitinib treatment
652 resolves lower-airway macrophage inflammation and neutrophil recruitment in SARS-CoV-
653 2-infected rhesus macaques. Cell 184, 460-475.e21.
654 https://doi.org/10.1016/j.cell.2020.11.007

655 Hsiao, B., Fraenkel, L., 2019. Patient preferences for rheumatoid arthritis treatment. Curr
656 Opin Rheumatol 31, 256–263. https://doi.org/10.1097/BOR.0000000000000591

657 ICH Expert Working Group, 2005. ICH Harmonised Tripartite Guideline - Validation of
658 analytical procedures: text and methodology Q2(R1).

659 Kanikkannan, N., Singh, M., n.d. Skin permeation enhancement effect and skin irritation of
660 saturated fatty alcohols.

661 Kováčik, A., Kopečná, M., Vávrová, K., 2020. Permeation enhancers in transdermal drug
662 delivery: benefits and limitations. Expert Opin Drug Deliv.
663 https://doi.org/10.1080/17425247.2020.1713087

664 Maibach, H.I., Wane Smith, E. (Eds.), 2005. Percutanepus penetration enhancers, 2nd ed.
665 Taylor & Francis group.

666 Markham, A., 2017. Baricitinib: First Global Approval. Drugs 77, 697–704.
667 https://doi.org/10.1007/s40265-017-0723-3

668 Mohammadi-Meyabadi, R., Beirampour, N., Garrós, N., Alvarado, H.L., Limón, D., Silva-
669 Abreu, M., Calpena, A.C., Mallandrich, M., 2022. Assessing the Solubility of Baricitinib and
670 Drug Uptake in Different Tissues Using Absorption and Fluorescence Spectroscopies.
671 Pharmaceutics 14. https://doi.org/10.3390/pharmaceutics14122714

672 Oranje, A.P., 2011. Practical Issues on Interpretation of Scoring Atopic Dermatitis: SCORAD
673 Index, Objective SCORAD, Patient-Oriented SCORAD and Three-Item Severity Score. pp.
674 149–155. https://doi.org/10.1159/000323308

675 Osborne, D.W., Musakhanian, J., 2018. Skin Penetration and Permeation Properties of
676 Transcutol®—Neat or Diluted Mixtures. AAPS PharmSciTech.
677 https://doi.org/10.1208/s12249-018-1196-8

678 Radi, G., Simonetti, O., Rizzetto, G., Diotallevi, F., Molinelli, E., Offidani, A., 2021. Baricitinib:
679 The First Jak Inhibitor Approved in Europe for the Treatment of Moderate to Severe Atopic
680 Dermatitis in Adult Patients. Healthcare 9, 1575.
681 https://doi.org/10.3390/healthcare9111575

682 Ring, J., Alomar, A., Bieber, T., Deleuran, M., Fink-Wagner, -a, Gelmetti, C., Gieler, U.,
683 Lipozencic, J., Luger, --t, Oranje, A., Schä fer, T., Schwennesen, T., Seidenari, ---s, Simon, D.,
684 Stä nder, S., Stingl, G., Szalai, S., Szepietowski, ----jc, Taı, A., Werfel, T., Wollenberg, A.,
685 Darsow, -----u, NEURODERMITIS Bund, ---Deutscher, 2012. Guidelines for treatment of
686 atopic eczema (atopic dermatitis) Part II. Journal of the European Academy of Dermatology
687 and Venereology 26, 1176–1193. https://doi.org/10.1111/j.1468-3083.2012.04636.x

688 Sanz, R., Calpena, A.C., Mallandrich, M., Gimeno, Á., Halbaut, L., Clares, B., 2017.
689 Development of a buccal doxepin platform for pain in oral mucositis derived from head and
690 neck cancer treatment. European Journal of Pharmaceutics and Biopharmaceutics 117,
691 203–211. https://doi.org/10.1016/J.EJPB.2017.04.019

692 Sapra, B., Jain, S., Tiwary, A.K., 2008. Percutaneous permeation enhancement by terpenes:
693 Mechanistic view. AAPS Journal. https://doi.org/10.1208/s12248-008-9012-0

694 Shaikh, I., Jadhav, S., Jadhav, K., Kadam, V., Pisal, S., 2009. Aceclofenac Organogels: In Vitro
695 and In Vivo Characterization. Curr Drug Deliv 6, 1–7.
696 https://doi.org/10.2174/156720109787048320

697 Shi, J.G., Chen, X., Lee, F., Emm, T., Scherle, P.A., Lo, Y., Punwani, N., Williams, W. V.,
698 Yeleswaram, S., 2014. The pharmacokinetics, pharmacodynamics, and safety of baricitinib,
699 an oral JAK 1/2 inhibitor, in healthy volunteers. J Clin Pharmacol 54, 1354–1361.
700 https://doi.org/10.1002/jcph.354

701 Silva-Abreu, M., Carolina Espinoza, L., Halbaut, L., Espina, M., Luisa García, M., Cristina
702 Calpena, A., 2018. Comparative Study of Ex Vivo Transmucosal Permeation of Pioglitazone
703 Nanoparticles for the Treatment of Alzheimer's Disease.
704 https://doi.org/10.3390/polym10030316

705 Smith, E.W., Maibach, H.I. (Eds.), 2005. Percutaneous Penetration Enhancers. CRC Press.
706 https://doi.org/10.1201/9781420039207

707 Southwell, D., Barry, B.W., 1983. Penetration Enhancers for Human Skin: Mode of Action of
708 2-Pyrrolidone and Dimethylformamide on Partition and Diffusion of Model Compounds
709 Water, n-Alcohols, and Caffeine. Journal of Investigative Dermatology 80, 507–514.
710 https://doi.org/10.1111/1523-1747.ep12535090

711 Sullivan, D.W., Gad, S.C., Julien, M., 2014. A review of the nonclinical safety of Transcutol®,
712 a highly purified form of diethylene glycol monoethyl ether (DEGEE) used as a
713 pharmaceutical excipient. Food and Chemical Toxicology 72, 40–50.
714 https://doi.org/10.1016/j.fct.2014.06.028

715 Tanaka, Y., 2020. State-of-the-art treatment of systemic lupus erythematosus. Int J Rheum
716 Dis 23, 465–471. https://doi.org/10.1111/1756-185X.13817

717 Thomsen, S.F., 2014. Atopic Dermatitis: Natural History, Diagnosis, and Treatment. ISRN
718 Allergy 2014, 1–7. https://doi.org/10.1155/2014/354250

719 Thyssen, J.P., Buhl, T., Fernández-Peñas, P., Kabashima, K., Chen, S., Lu, N., DeLozier, A.M.,
720 Casillas, M., Ständer, S., 2021. Baricitinib Rapidly Improves Skin Pain Resulting in Improved
721 Quality of Life for Patients with Atopic Dermatitis: Analyses from BREEZE-AD1, 2, and 7.
722 Dermatol Ther (Heidelb) 11, 1599–1611. https://doi.org/10.1007/S13555-021-00577-
723 X/FIGURES/4

724 van der Heijde, D., Kartman, C.E., Xie, L., Beattie, S., Schlichting, D., Mo, D., Durez, P.,
725 Tanaka, Y., Fleischmann, R., 2022. Radiographic Progression of Structural Joint Damage
726 Over 5 Years of Baricitinib Treatment in Patients With Rheumatoid Arthritis: Results From
727 RA-BEYOND. J Rheumatol 49, 133–141. https://doi.org/10.3899/jrheum.210346

728 Wallace, D.J., 2014. Lupus: The Essential Clinician's Guide, 2nd ed. Oxford University Press,
729 New York.

730 Wang, H., Meng, F., 2017. The permeability enhancing mechanism of menthol on skin
731 lipids: a molecular dynamics simulation study. J Mol Model 23, 279.
732 https://doi.org/10.1007/s00894-017-3457-y

733 Williams, A.C., Barry, B.W., 2012. Penetration enhancers. Adv Drug Deliv Rev 64, 128–137.
734 https://doi.org/10.1016/j.addr.2012.09.032

735 Wishart, D.S., Feunang, Y.D., Guo, A.C., Lo, E.J., Marcu, A., 2023. Baricitinib [WWW
736 Document]. Drug Bank. URL https://go.drugbank.com/drugs/DB11817 (accessed 5.31.23).

737 Zhang, R., Bi, R., Ho Jun Hui, C., Rajarahm, P., Dinish, U.S., Olivo, M., 2021. A Portable
738 Ultrawideband Confocal Raman Spectroscopy System with a Handheld Probe for Skin
739 Studies. ACS Sens 6, 2960–2966. https://doi.org/10.1021/acssensors.1c00761

740 Zhou, C., Li, X., Wang, C., Zhang, J., 2021. Alopecia Areata: an Update on Etiopathogenesis,
741 Diagnosis, and Management. Clin Rev Allergy Immunol 61, 403–423.
742 https://doi.org/10.1007/s12016-021-08883-0

Mobility stays

3-month stay at the School of Pharmacy at the University College of London to continue learning new research techniques that will contribute positively to the preparation of my doctoral thesis.

31/07/2023

Certificate of Attendance at the School of Pharmacy, University College London
01 May – 31 July 2023

To whom it may concern,

It is my pleasure to provide a Certificate of Attendance for Miss Núria Garrós Aristizábal in relation to her work in the Skin Research Laboratory in the School of Pharmacy University College London, United Kingdom. Miss Núria Garrós Aristizábal attended the laboratory and performed a range of experimental work and activities from the period 01 May – 31 July 2023, a total of three months.

During her time in the Skin Research Laboratory, School of Pharmacy, University College London, Miss Núria Garrós Aristizábal undertook the following research activities:

(i) HPLC analysis
(ii) Confocal Raman spectroscopy analysis and profiling, and
(iii) Preliminary investigations of the skin permeation of baricitinib

Miss Núria Garrós Aristizábal worked extremely hard during her research visit and has demonstrated excellence and capability in a wide range of pharmaceutical research activities.

It was a pleasure for me to host Miss Núria Garrós Aristizábal in the Skin Research Laboratory and I look forward to continuing to collaborate with her in the coming years.

Yours sincerely,

Majella E. Lane

Majella E, Lane, Ph.D.
Associate Professor
Director
Skin Research Group

UCL School of Pharmacy
29-39 Brunswick Square, London WC1N 1AX
Tel: +44 (0)20 7753 5819
m.lane@ucl.ac.uk
www.ucl.ac.uk/pharmacy

Participation in congresses and conferences

- XV Congreso Sociedad Española de Farmacia Industrial y Galénica, Sevilla (Spain). December 2-4, 2021. Poster.
- Skin Forum 2022, Malmö (Sweden). June 21 and 22, 2022. Poster and Oral presentation.
- XIII Jornada de Recerca de la Facultat de Farmàcia i Ciències de l'Alimentació, Barcelona (Spain). October 19, 2022. Oral presentation.
- 6º Encuentro Internacional de Ciencias Farmacéuticas y Alimentarias, ECFA 2022, La Habana (Cuba). Novembre 23-25, 2022. Poster.
- Congreso IEEE Nano Perú 2022 - Tendencias en Nanociencias y Nanotecnología, online. Novembre 7-9, 2022. Poster.
- III Congrés AMIT-CAT – Dones en Nanociència i Nanotecnologia, Barcelona (Espanya). February 8, 2023. Oral presentation. Poster.
- ICSDISC 2023: 17. International Conference on Skin Disorders, Infections and Skin Care. London (Unite Kingdom). June 22 and 23, 2023. Oral presentation.
- Skin and Formulation, 6th Symposium - Current challenges in skin formulation. Nantes (France). October 2 and 3, 2023. Poster.

CHARACTERIZATION OF BARICITINIB LIPOSOMES FOR TOPICAL ADMINISTRATION

AUTORS Núria Garrós[1], Negar Beirampour[1], Roya Mohammadi[1], Pol Alegret[1], Óscar Domènech[1], Ana C. Calpena[1], Mireia Mallandrich[1], Helena Colom[1]

[1]Department of Pharmacy, Pharmaceutical Technology and Physical-chemistry, University of Barcelona, Avda. Joan XXIII, 08028 Barcelona, Spain.

INTRODUCTION

Autoimmune diseases are suffered by 3-5% of the population, some of them can affect the skin among other organs or only it[1]. The clinical manifestations in the skin are different but partly shared underlying immunological mechanism, unspecific cutaneous symptoms are usually exanthema, itching or scaling[2]. Most of the time, the topical adjuvant treatment for these cutaneous symptoms are corticoids but used during long time can produce some side effects[3].

PURPOSE

The aim of the work was to study liposomes of baricitinib for topical administration, an orally administrated, small-molecule, janus-associated kinase (JAK) inhibitor.

METHODS AND MATERIALS

Three different liposomes were elaborated containing different lipid composition: 1. POPC, 2. POPC:CHOL (8:2 mol/mol), and 3. POPC:CHOL:CER (36:24:40 mol/mol/mol). And the following issues were studied:

- Their size and polydispersity index (PDI) was determined by photon correlations spectroscopy (PCS) with a Zetasizer Nano ZS.
- Morphological examination of liposomes was performed using transmission electron microscopy (TEM).
- Permeation studies were performed with human skin from abdominal plastic surgery of healthy patients, using vertical amber glass Franz-type diffusion.

RESULTS AND DISCUSSION

The size of the liposomes was 86.0±1.4 nm and a PDI=0.120 for POPC; 53.5±0.9nm and a PDI=0.174 for POPC:CHOL; and 64.1±0.3 and a PDI=0.120 for POPC:CHOL:CER. Concerning the permeation, POPC:CHOL exhibited the highest cumulative permeated amount at 30h (22.40%); followed by POPC with 17% of Baricitinib permeated and finally, POPC:CHOL:CER which permeated 6% of the applied dose.

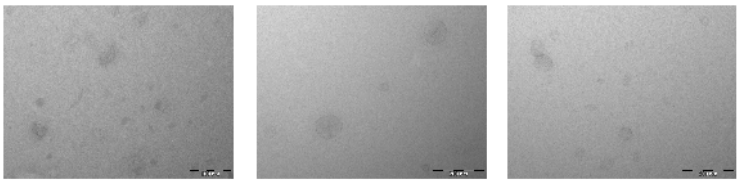

POPC POPC:CHOL POPC:CHOL:CER

Liposomes		Size (nm)	PDI	Zeta potential (mV)
POPC	blank	86,6 ± 1,6	0.091	11,7 ± 0,3
	+ baricitinib	86,0 ± 1,4	0.120	-14,2 ± 0,3
POPC:CHOL (8:2, mol/mol)	blank	79,8 ± 1,1	0.093	13,0 ± 1,1
	+ baricitinib	53,5 ± 0,9	0.174	13,2 ± 1,9
POPC:CHOL:CER (36,24, 40 mol/mol/mol)	blank	72,3 ± 1,4	0.135	0,87 ± 0,2
	+ baricitinib	64,1 ± 0,3	0.120	-16,3 ± 1,9

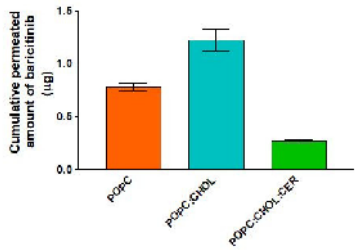

CONCLUSION

Liposomes could successfully be used as topical delivery carrier of baricitinib being an alternative for actual corticoids treatments.

REFERENCES

1. Karopka T, Fluck J, Mevissen HT, Glass Â. The Autoimmune disease database: A dynamically compiled literature-derived database. BMC Bioinformatics. 2006 Jun 27;7.
2. Sticherling M, Erfurt-Berge C. Autoimmune blistering diseases of the skin. Vol. 11, Autoimmunity Reviews. 2012. p. 226–30.
3. Personal of Mayo Clinic. Prednisona y otros corticoides. https://www.mayoclinic.org/es-es/steroids/art20045692. 2020

CERTIFICATE OF BEST PRESENTATION AWARD

ICSDISC 2023: XVII. International Conference on Skin Disorders, Infections and Skin Care
hereby certifies that

NÚRIA GARRÓS ARISTIZÁBAL

has presented an outstanding work entitled

Baricitinib Lipid-based Nanosystems as a Topical Alternative for Atopic Dermatitis Treatment
N. Garrós, P. Bustos, N. Beirampour, R. Mohammadi, M. Mallandrich, A.C. Calpena and H. Colom

LONDON, UNITED KINGDOM

JUNE 22-23, 2023